AN ABSTRACT OF THE THESIS OF

Scott Merrill Kent for the degree of Master of Science as a dual major in Civil Engineering and Forest Products presented on November 17, 1995. Title: Dynamic Behavior of Metal-Plate-Connected Wood Truss Joints.

Signature redacted for privacy. Signature redacted for privacy.

Abstract approved: _____ _____
Thomas H. Miller Rakesh Gupta

The objectives of this research were to evaluate the behavior of actual metal-plate-connected (MPC) tension-splice and heel wood truss joints under seismic loads from the Northridge earthquake (tension-splice joints only) and under loads from a large artificial earthquake (1.0 g's and 0.67 g's maximum horizontal and vertical accelerations, respectively). A proposed sequential phased displacement (SPD) loading standard was used to determine dynamic characteristics of MPC joints: energy dissipation, damping ratio and cyclic stiffness. A sinusoidal loading function was used to determine the effect of cyclic loading on the strength of MPC tension-splice and heel joints.

Joints were constructed from 2x4 in. nominal Douglas-fir. The size of the metal-plate-connectors for the tension-

splice and heel joints were 3x4 in. and 3x5 in., respectively.

Strength and stiffness of the MPC joints after the seismic and SPD loadings were compared to those properties in a control group of joints tested to failure under a static ramp load alone. Strength degradation was not observed in the tension-splice and heel joints as a result of the earthquake loading regimes. Stiffness degradation was observed in the heel joint as a result of the large artificial earthquake loads and in both the tension-splice and heel joints as a result of the SPD loading. The SPD loading regime did not affect the ultimate strength of the tension-splice joints, but did reduce the ultimate strength of the heel joints.

Dynamic properties, determined from the SPD loading, depended on the magnitude of displacement (displacement increases in amplitude with time). The damping ratio and energy dissipation tend to increase as the SPD loading progresses, whereas, the cyclic stiffness decreases. For design, damping ratios of 4.3% and 3.8% are recommended for the tension-splice and heel joints, respectively.

Cyclic loading can have a significant effect on the strength of MPC joints depending on the amplitude of the

cycles. Cycles with amplitudes greater than 20% of the mean ultimate strength (determined from the static loading control group) for the tension-splice joints and greater than 35% of the mean ultimate strength for the heel joints tend to reduce the strength.

Dynamic Behavior of Metal-Plate-Connected Wood Truss Joints

by

Scott M. Kent

A THESIS

submitted to

Oregon State University

in partial fulfillment of

the requirements for the

degree of

Master of Science in Civil Engineering and Forest Products

Completed November 17, 1995

Commencement June 1996

Master of Science thesis of Scott M. Kent presented on November 17, 1995

APPROVED:

Signature redacted for privacy.

Co-Major Professor, representing Civil Engineering

Signature redacted for privacy.

Co-Major Professor, representing Forest Products

Signature redacted for privacy.

Head of Department of Civil Engineering

Signature redacted for privacy.

Head of Department of Forest Products

Signature redacted for privacy.

Dean of Graduate School

I understand that my thesis will become part of the permanent collection of Oregon State University libraries. My signature below authorizes release of my thesis to any reader upon request.

Signature redacted for privacy.

Scott M. Kent

ACKNOWLEDGMENT

I wish to acknowledge the following for their contribution to this study:

- Alpine Engineered Products, Inc. for their donation of the metal-plate-connectors;

- Frank Lumber Company for their donation of lumber;

- Ken and Susan Kent, Jason Waggoner, and Mary Snoozy who provided support and an occasional helping hand.

DEDICATION

I wish to dedicate my work to the loving memory of my grandfather, Edward Daniel Keefe who was the best teacher, fisherman, captain, pilot, and astronaut I have ever known.

CONTRIBUTION OF AUTHORS

Dr. Rakesh Gupta and Dr. Thomas Miller were involved in the design of the experiment, analysis, and writing of each manuscript.

TABLE OF CONTENTS

TABLE OF CONTENTS (Continued)

TABLE OF CONTENTS (Continued)

TABLE OF CONTENTS (Continued)

LIST OF FIGURES

Figure Page

LIST OF FIGURES (Continued)

Figure Page

LIST OF FIGURES (Continued)

Figure Page

LIST OF FIGURES (Continued)

Figure Page

LIST OF FIGURES (Continued)

Figure Page

LIST OF FIGURES (Continued)

Figure Page

LIST OF TABLES

Dynamic Behavior of Metal-Plate-Connected Wood Truss Joints

1. Introduction

1.1 Background

Metal-plate-connected (MPC) wood trusses have widespread use in residential structures, apartments, commercial, and light industrial applications. Advantages of the system include the relative ease in fabrication and the low cost of creating complex roof geometries. This engineered product, although exposed to dynamic loadings from wind and earthquakes, is designed based predominately on the response to static loads.

Section 13.2.1 of the National Design Specification for Wood Construction (1991) provides general provisions for determining the design values for metal connector plates from physical testing. The lowest of two possible values is chosen as the design load: 1) one-third of the mean ultimate strength or 2) the load corresponding to 0.03 in. deflection, divided by 1.6. For the tension-splice and heel joints used in this study, one-third of the mean ultimate load controls, and is used as the design load. A one-third increase in allowable values is not included for earthquake loadings in this study.

The prevalence of MPC trusses in construction has not resulted in a widespread understanding of their behavior in

service, especially under seismic and high wind forces. Significant advances have been made in the area of modeling the earthquake behavior of timber shear walls and roof diaphragms in recent years, but research on the response of MPC joints to seismic forces has largely been ignored. The connections are primary factors controlling the response of the structural assembly; therefore, results from connection tests will continue to be significant in understanding the behavior of buildings during dynamic events.

This study will characterize structural behavior and failure modes of MPC joints under dynamic loading conditions, and determine if the ultimate capacity of MPC joints is affected by dynamic loads. Because wood structures rely on the mechanical connections to dissipate energy when subject to earthquake or wind loads, this is a necessary first step towards predicting truss joint behavior and subsequently predicting the behavior of a truss and a system of trusses under dynamic loads. This study is limited to two types of MPC joints: tension-splice and heel.

1.2 Objectives

The purpose of this study is not to determine allowable properties of MPC joints to be used in design, but to serve as a preliminary investigation into the behavior of MPC joints in response to a number of different dynamic loadings including earthquake simulations, a proposed standard sequential phased displacement loadings (Dolan 1994), and a cyclic loading.

The specific objectives of this research are as follows:

1. Evaluate the behavior of MPC joints under a static ramp load to serve as the control group. Sections 3.2.3.1 and 4.2.3.1 contain detailed descriptions of the test method for tension-splice joints and heel joints, respectively.

2. Evaluate the behavior of MPC joints under realistic earthquake loads (e.g. the Northridge earthquake and a large artificial earthquake). The key variables to be examined are post-earthquake strength, stiffness, and failure mode. Sections 3.2.3.3 and 3.2.3.4, and 4.2.3.3 describe in detail the test method for tension-splice joints and heel joints, respectively.

3. Determine the response of MPC joints to a proposed standard sequential phased displacement (SPD) loading (Dolan

1994). The SPD loading consists of incrementally increasing displacement controlled cycles to provide a more realistic response during a seismic event than normal fully reversed cyclic loading. From the SPD method, calculate dynamic characteristics: energy dissipation, equivalent viscous damping ratio, and cyclic stiffness. See sections 3.2.3.5 and 4.2.3.4 for detailed descriptions of the test method for tension-splice joints and heel joints, respectively.

4. Assess the effect of cyclic loading on the strength of MPC joints and investigate the relationship between amplitude of the cyclic load and post-cyclic loading strength. The cyclic loadings are examined as part of a preliminary investigation of wind loadings. A follow-up study will investigate the magnitude and number of cycles of actual wind events on MPC joints. Sections 3.2.3.6 and 4.2.3.5 contain detailed descriptions of the test method for tension-splice joints and heel joints, respectively.

5. Compare dynamic behavior to the static loading(control group) behavior of MPC joints.

2. Literature Review

2.1 Wood Structure Behavior Under Seismic Forces

Light-frame wood structures have historically shown varying response to seismic loads depending on the type of construction. Structures developing lateral load resistance using well-nailed plywood or oriented-strand-board shear walls and diaphragms have generally exhibited good performance. However, design attention needs to be given to anchorage between the walls and the foundation, location and aspect ratio of sheathed shear walls, and the number and frequency of openings in the diaphragm and shear wall systems. Also, various sub-structures need to be interconnected for adequate performance to be achieved under dynamic loads (Zacher 1994).

A study by Soltis (1983) conducted on the structural damage to wooden buildings in Anchorage, Alaska, after the earthquake (8.6 Richter magnitude) which occurred on March 27, 1964 in the Prince William Sound area showed that timber structures with well-nailed exterior shear walls demonstrated exceptional performance as a whole. Roof and floor systems also maintained load carrying ability even if the earth dropped away from one side of the structure due to small land slides. Damage to wood structures during the San Fernando earthquake of 1973 (6.6 Richter magnitude) was

extensive, usually due to the absence of adequate anchorage, shear walls, or non-symmetric shear wall geometry. Also, anchorage between the foundation and the first floor and connections between the roof system and the wall diaphragm were often visible points of failure.

Buchanan and Dean (1994) describe the ductility and behavior of various structural systems and connections under dynamic loads. Stiff, brittle structures tend to perform poorly under seismic forces because they do not allow for large displacements or have the capacity to absorb energy and sustain some damage without failure. The authors comment that MPC joints tend to fail at small deformations whereas nail plates and nailed connections can still carry load even at large deformations. Well-nailed shearwalls composed of plywood are very ductile and can resist large cyclic displacements with only a slight drop in load-carrying ability.

2.2 MPC Joint Behavior Under Static Loads

The structural performance of MPC joints has received extensive research attention in the last 20 years, but most of the research has focused on the performance of tensile joints under static axial loads. The evaluation of the performance of MPC joints under dynamic forces has received little attention. There is currently only one standard in

the U.S. (ASTM D1761-77) for the evaluation of the behavior (ultimate capacity, failure modes, etc.) of MPC joints which makes recommendations for testing the tension-splice joint under static axial loads only. These evaluations are inadequate for even non-earthquake type loadings, because actual joints (having different configurations) experience different loading (cyclic, combined, reversed) conditions in service.

MPC tension-splice joints were tested under static loads by Gupta and Gebremedhin (1990) to determine strength, stiffness, and failure modes. Nonlinear load-deflection curves were recorded for each joint. The joints were constructed using Southern pine No. 2 lumber and 3x4 in. 20-gauge metal plates. The tension-splice joints experienced a wood shearing failure as the corners of the plate pulled away from the surface of the wood at an average ultimate load of 6070 lb.

An interaction curve for combined axial tension and bending for MPC tension-splice joints was developed by Gupta (1994). Joints were manufactured from 2x4 in. Southern pine No. 2 lumber and 3x4 in. 20-gauge punched metal plates. Connection strength for the combined loading was evaluated under axial tensile loads with an eccentricity varying from 0.5 in. to 2.0 in. Groups of specimens loaded in pure bending and pure axial tension were tested as well. Bending

strength was determined by testing the tension-splice joint under third-point loads (loads applied perpendicular to the narrow face of the 2x4 in. member) and supported at each end of the member. For small applied moments (less than 30% of the average ultimate bending strength), the ultimate strength of tension-splice joints was relatively unaffected. However, large applied moments (greater than 30% of the average ultimate bending strength) significantly reduce axial strength.

2.3 Numerical Models for Static Loading Response of MPC Joints

Numerical and theoretical models have successfully been developed to analyze MPC joints subjected to static loads. Cramer et al. (1990) created a nonlinear finite-element model for tension and bending of MPC tension-splice joints. Three different types of elements were used to characterize the properties of the wood, metal-plate, and the wood/metal interface. The wood matrix was approximated by homogeneous, linear, continuous cubic elements and the punched metal plate was modeled using cubic elements with a discontinuous stress-strain curve to account for the elasto-plastic nature of steel. The nonlinear load-deflection curve for the wood/metal interface was approximated by nonlinear elastic springs using a curve fitting technique developed by Foschi

(1974) for nailed connections. The shape of the load-deflection curve for MPC tension-splice joints has a similar nonlinear shape to that of many types of nailed connections, therefore the curve fitting technique worked well. The nonlinear solution (Cramer et al. 1990) for nodal displacements was calculated numerically using a Newton-Raphson iteration procedure. Output from the finite-element model predicted ultimate bending moment capacities within 10% of experimental test data. Also, it was discovered that for large size plates, the assumption of equal tooth forces was not valid, which is in contrast to current design assumptions.

2.4 Wood Connection Behavior Under Cyclic Forces

Only a few studies on the fatigue properties of MPC joints were found (Sletteland et al. 1977, Tokuda et al. 1979, Hayashi et al. 1980, Dagher et al. 1991). In each of these studies, only the tensile joint was tested under repeated axial loads. In MPC wood trusses, other joints are also critical in the overall behavior of the truss. Evaluations from these previous studies are inadequate to determine behavior of MPC joints during earthquake loadings. In many parts of the United States, behavior of the joints during an earthquake must be considered when determining safe design loads.

In response to the demand for a standard to assess dynamic properties of wood connections, Dolan (1994) proposed the sequential phased displacement (SPD) loading. The purpose of the SPD loading is to provide a consistent method for the evaluation of dynamic properties such as equivalent viscous damping ratio, ductility, and cyclic stiffness.

Most light-frame wood structures have a natural frequency of vibration between 1.2 and 18 Hz (Foliente and Zacher 1994) which coincides with the dominant frequencies of many seismic events. To avoid dynamic amplifications, it is important that the structure respond as a highly damped system. To add to the somewhat limited energy dissipation provided by the structural members alone, connections can be effectively designed to increase the energy dissipation of the entire structure. Understanding the hysteresis behavior of wood joints is necessary to model the dynamic response of complex timber structural systems. A typical hysteresis curve for a wood connection has three general characteristics (Foliente and Zacher 1994): nonlinear, inelastic load-deflection curves, a continuing decrease in strength and stiffness as the cycles progress, and a pinched shape.

Emmerson and Fridley (1995) also studied the effect of cyclic loading on the strength of metal-plate-connected

joints. Six separate configurations were tested. The cyclic loading function consisted of three groups of 200 cycles oscillating between 20, 40, and 60 percent of the mean ultimate static load. Results were unavailable at the time of the writing of this paper.

3. Dynamic Behavior of Metal-Plate-Connected Tension-Splice Wood Truss Joints

3.1 Experimental Design

This study is to serve as a preliminary investigation into the effects of a variety of dynamic loads on metal-plate-connected tension-splice joints. The hypothesis being tested is that earthquake and cyclic loads decrease the strength and stiffness of metal plate connected (MPC) tension-splice joints. The different loadings are described in detail in section 3.2.3. The mean strength and stiffness of the tension-splice joints under each dynamic loading are compared to those from a control group (static ramp load, section 3.2.3.1). A t-test procedure, assuming equal variance, for comparing two sample means is used to analyze the strength and stiffness results. A two-sided p-value of 0.05 is chosen as the cutoff significance level. That is, if the statistical test indicates a two-sided p-value less than 0.05, then the conclusion of the test is that the means of the two populations are significantly different. Otherwise, if the p-value is greater than 0.05, there is not enough evidence to suggest that the means of the two populations are significantly different. The coefficient of variation (COV), defined as the standard deviation divided

by the mean and expressed as a percentage, is presented with the results to provide an indication of the variance. Table 3.1 lists the groups of tests examined in this study and provides sample sizes for each group. Table 5.1 summarizes the statistical results of the tests.

ASTM D2915-94 is used to estimate the required sample size, given an estimated COV, to determine the lower 5% exclusion limit with 95% confidence. Ten percent is a conservative estimate for the COV of MPC tension-splice joints (Gupta 1990). Using the procedure in ASTM D2915-94, a sample size of 18 is necessary for testing MPC tension-splice joints. This required sample size is much greater than the sample size used in this research; therefore, an accurate estimate of the allowable properties of MPC tension-splice joints is not possible. However, the purpose of this research is to determine how the dynamic loadings affect the mean strength and stiffness, not to determine the 5% lower exclusion limit.

There were a number of sources of variability in the fabrication and testing of the tension-splice joints. First, there were two batches of plates (discussed in section 3.2.1). This source of variability was addressed by only making strength and stiffness comparisons between a control group (static tests) and one of the various dynamic test groups with specimens fabricated using the same batch

Table 3.1: Tension-splice joint tests

Test	Plate Batch	Sample Size
Control Group (Static Ramp Load)	1	9
Control Group (Static Ramp Load)	2	9
Northridge Earthquake Simulation	1	10
Artificial Earthquake Simulation	2	9
Sequential Phased Displacement	1	8
Cyclic Loading	2	20

of plates. Second, there was natural variation in the wood. This variation was limited by using a single machine stress rated grade (1800f-1.6E) Douglas-fir. Third, the location of the hydraulic cylinder in the testing frame varied between tests. This was addressed by only making comparisons between groups of tests with similar hydraulic cylinder locations (section 3.2.2). Fourth, fabrication of the tension-splice joints was performed on three different presses: two of the presses were different universal testing machines, the other was a high pressure hydraulic press used to produce wood laminates.

Using different presses to fabricate the tension-splice joints should not have any affect on the strength or stiffness for a number of reasons. First, the author was responsible for the fabrication of all the tension-splice joints. Second, the plates were pressed into the wood at approximately the same rate for all of the presses (between 0.02 and 0.04 in./second). Third, the teeth were consistently pressed into the wood until the top of the plate was flush with the surface of the lumber on all of the joints. Fourth, care was taken to center each plate during the pressing operation.

3.2 Experimental Procedure

3.2.1 Materials

Test joints were fabricated from machine-stress rated Douglas-fir (1800f-1.6E) lumber which was conditioned at 70° F and 65% relative humidity to an equilibrium moisture content of approximately 14%. The tension-splice joints were connected using 20-gauge punched 3x4 in. metal plates, supplied by Alpine Engineered Products, Inc. (Pompano Beach, FL), which were pressed into the wood using a hydraulic press until the teeth were entirely embedded into the wood. Care was taken not to over-press or under-press the plates by visually inspecting the fabrication of each connection. After construction, the joints were placed into the environment room again for a minimum of seven days and a maximum of 28 days before testing to allow stress relaxation of the wood fibers near the connection, as recommended by Arbek (1979). Figure 3.1 is a photograph of a typical tension-splice joint used in this study.

Two different batches of the same type of plate were used in this study. The supply of 3x4 in. metal plates initially available, henceforth referred to as batch-1, was exhausted after completing the static tests, Northridge earthquake simulations, and the sequential phased displacement (SPD) loadings. New plates, batch-2, having

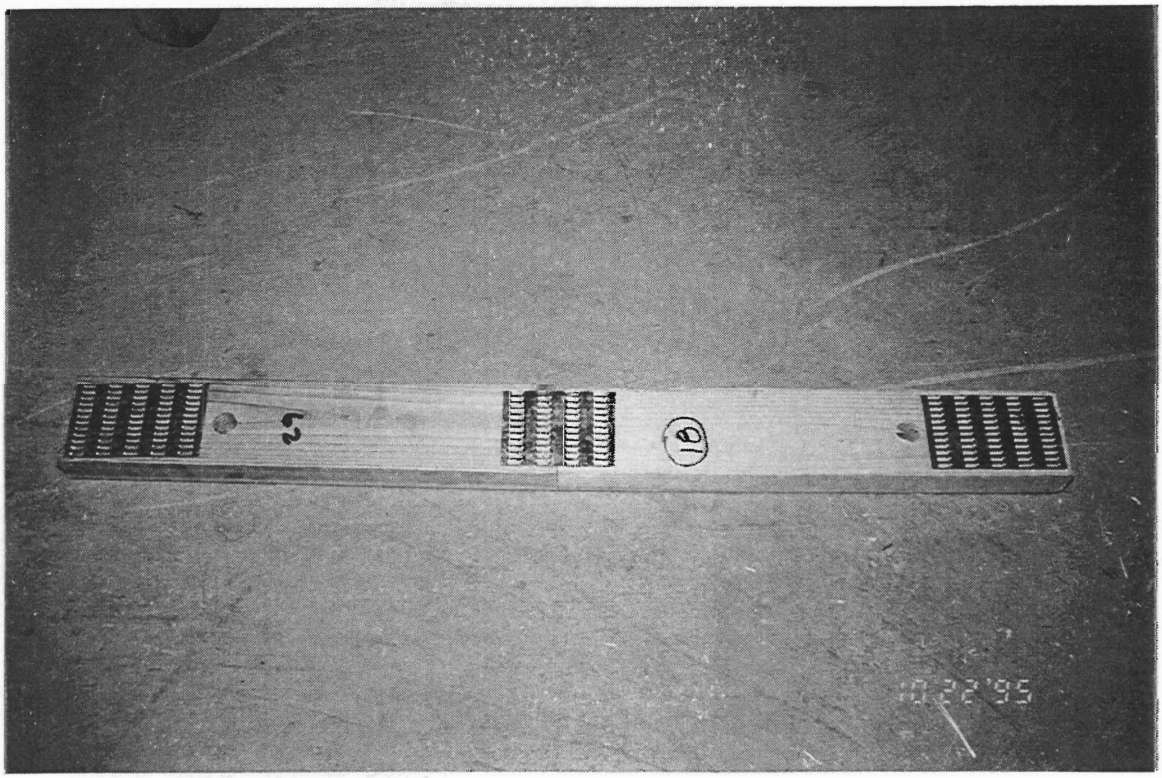

Figure 3.1: Photograph of a typical test joint used in the tension-splice study.

exactly the same tooth configuration as batch-1, were ordered from the same supplier. Figure 3.2 shows a photograph of the plates from the two batches. Table 3.2 lists characteristics of the metal-plate-connectors provided by Alpine Engineered Products, Inc. Actual batch-1 steel material properties are unavailable, therefore, a range of values for the properties expected for ASTM A446-89 Grade B steel is presented for the batch-1 properties.

There were two physical differences in the plates which could be seen visually. Batch-1 had very small zinc crystals, whereas batch-2 had larger, quite pronounced surface zinc crystals. Also, batch-1 tended to have a slightly rougher surface at the edge of the teeth than batch-2, consisting of small sharp barbs (less than 0.01 inches in length), most likely caused by the die during fabrication of the plate. These physical differences between the two types of plates themselves were considered unlikely to affect the strength during testing. It is also considered unlikely that the very small barbs noticed on the teeth on batch-1 plates caused significant damage to the surrounding wood fibers during fabrication.

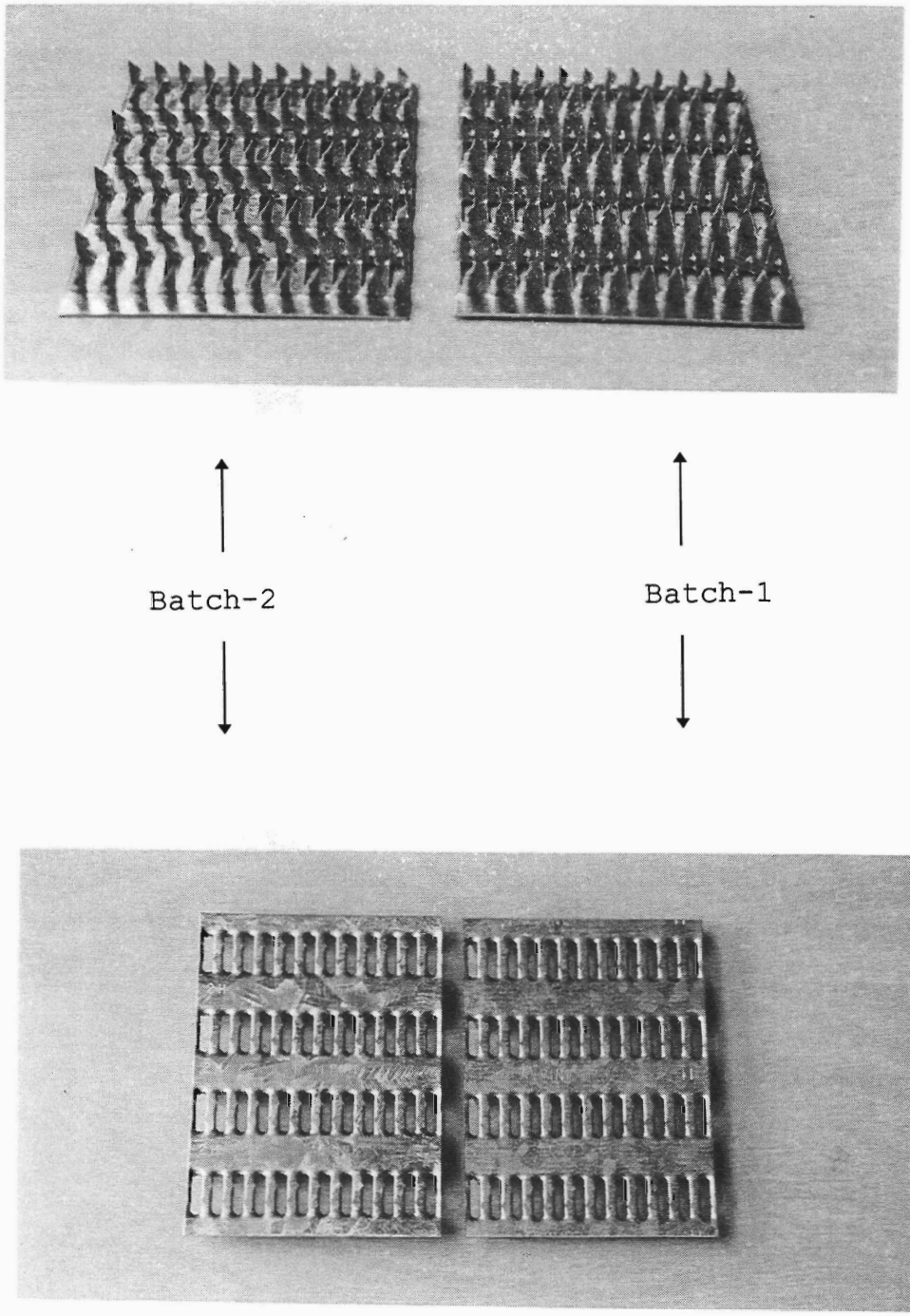

Figure 3.2: Photographic comparison of samples from the two batches of metal-plate-connectors used in this study.

Table 3.2: Physical properties of the metal-plate-connectors

Plate Properties Provided by Alpine Engineered Products, Inc.

Parameter	batch-1	batch-2
Yield Strength (ksi)	35-55[†]	51.5
Ultimate Strength (ksi)	53-62[†]	60.5
Percent Elongation at Failure (%)	25-39[†]	31.5
Thickness (in.)	0.036	0.036
Tooth Length (in.)	0.25	0.25
Tooth Width (in.)	0.12	0.12
Slot Length (in.)	0.25	0.25
Slot Width (in.)	0.12	0.12

[†] A range of values expected for the ASTM A446-89 Grade B steel used to fabricate the metal-plate connectors

3.2.2 Apparatus

A horizontal testing frame, developed by Gupta and Gebremedhin (1990), which allows for testing a range of joint configurations, and an 11,000 lb capacity Materials Testing System (MTS) dynamic hydraulic actuator were used to apply the loads to the joints. The specimen was positioned in the apparatus to minimize loading eccentricities. That is, the load was applied through the center-line of the tension-splice joints through 0.75 in. diameter pins. The use of the pins provided a pinned-end boundary condition at both ends of the tension-splice joints. Figure 3.3 shows the actuator position in the testing frame for the static tests (batch-1), Northridge earthquake simulations, and the SPD loadings. Figure 3.4 displays the actuator position for the static tests (batch-2), cyclic tests, and artificial earthquake simulations. The bolts shown in Figure 3.4 were placed to increase the overall stiffness of the testing frame.

Relative displacements between the two wood members were measured by two alternating-current, linearly-variable differential transducers (LVDTs) placed on either side of the tension-splice joint and held in place with a woven nylon strap. The LVDTs were supplied an input voltage of 5 volts and returned a signal which was linear within a 1 in. range.

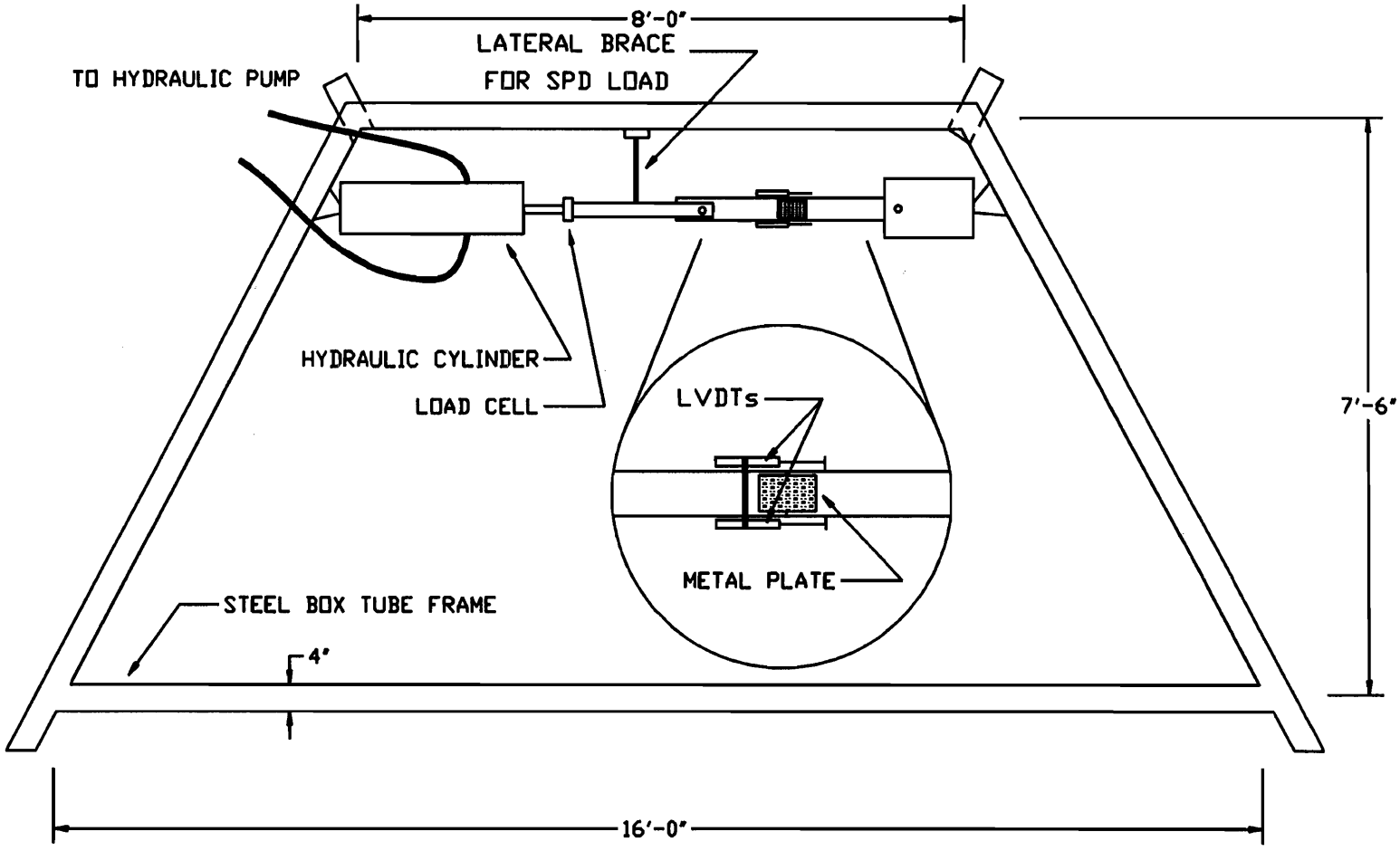

Figure 3.3: Testing setup during static (batch-1), Northridge earthquake, and SPD loadings.

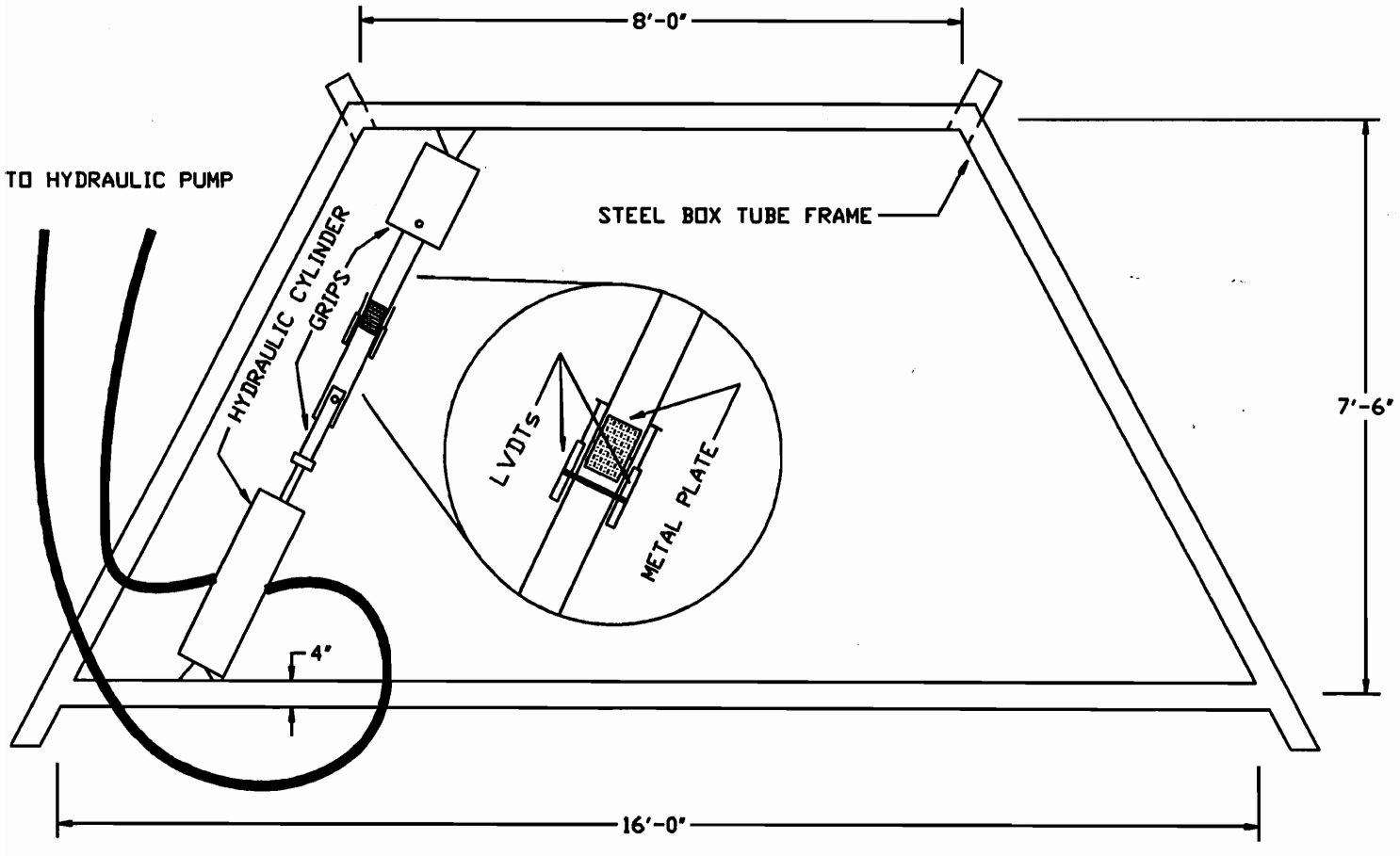

Figure 3.4: Testing setup during static (batch-2), artificial earthquake, and cyclic loadings

Axial load was measured by a load cell (25,000 lb capacity), which was placed between the hydraulic actuator and one end of the joint. The load cell was supplied with a 5 volt input.

The return voltages from the LVDTs and load cell were routed to an analog-to-digital card attached to a personal computer with an 80386 microprocessor and an 80387 math-coprocessor. The data acquisition/control software, Workbench PC 2.0 (Strawberry Tree, Inc.), controlled the feedback loops as well as the storage of data to the internal hard-drive. A schematic representation of the system is shown in Figure 3.5.

Application of virtually any type of load or deflection function, within the limits of the hydraulic system, can be accomplished in two ways. First, if the function can be simply described as a mathematical expression, the acquisition/control software is capable of generating a wide variety of mathematical functions. Second, if the loading is complex (such as an earthquake time-history), then the function can be digitized into a series of equal time-spaced inputs into a text file (the control program reads from the data file at a constant specified rate). The software reads each file entry at a specified rate and adjusts the feedback control of the hydraulic actuator. The system used in this

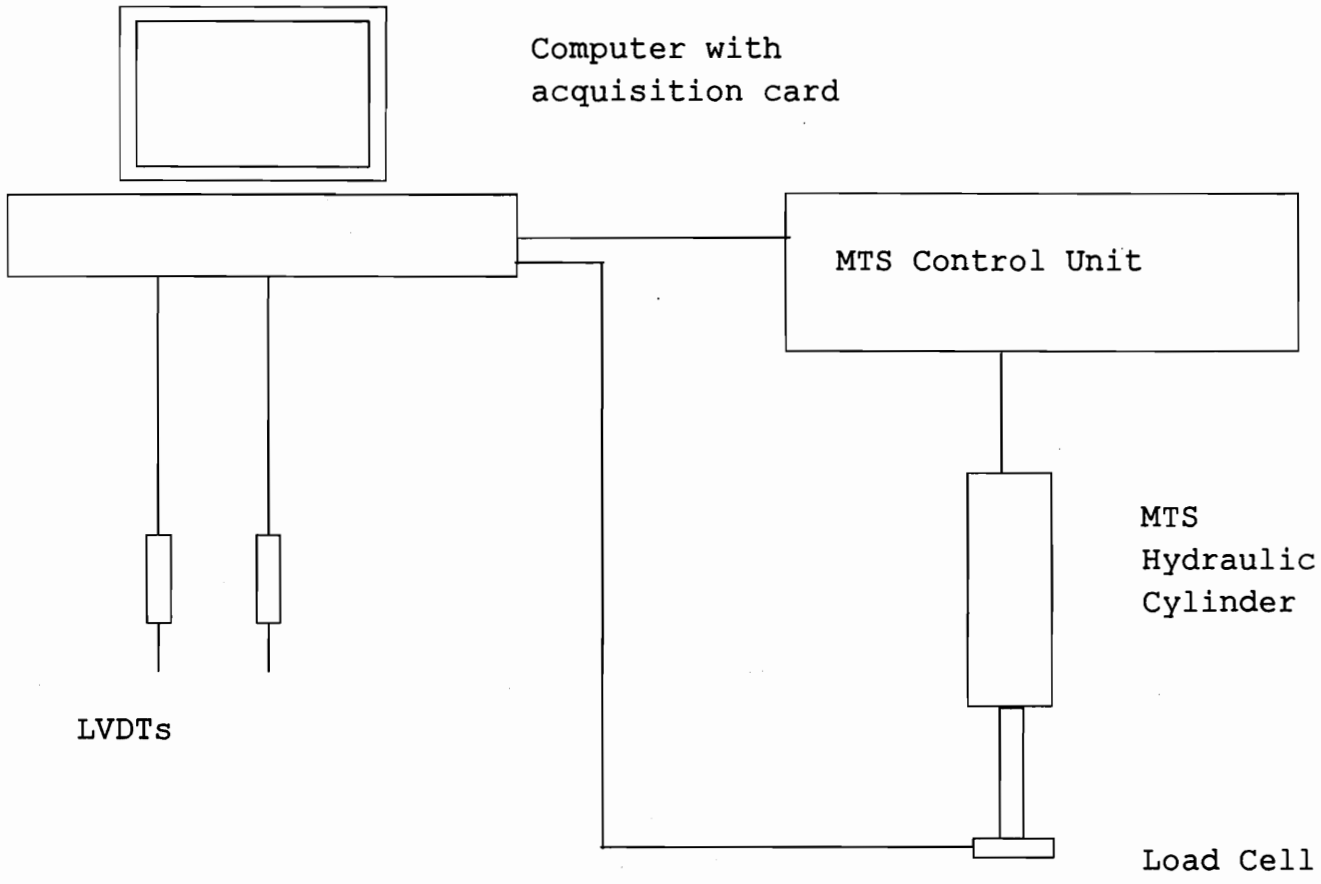

Figure 3.5: Schematic representation of the test system

study was capable of making feedback corrections (to both load and deflection) at a rate of 500 Hz.

3.2.3 Test Procedures

Tension-splice joint specimens were tested under five different loading conditions: 1) a static ramp load to serve as the control group (for two different batches of plates, batch-1 and batch-2), 2) a force time-history determined from a linear finite-element model (FEM) and based on a historic seismic event (Northridge earthquake), 3) an artificial force time-history (1.0 g's maximum horizontal acceleration and 0.67 g's maximum vertical acceleration) generated using WES-RASCAL (Silva 1987) in conjunction with the FEM, 4) a Sequential Phased Displacement (SPD) loading as proposed by Dolan (1994) to determine dynamic characteristics, and 5) a sinusoidal loading at different amplitude levels.

3.2.3.1 Static Tests

A linearly increasing tensile ramp load of 780 lb/min, controlled through a load-feedback loop, was applied axially to a group of nine tension-splice joints to cause failure in 8 to 10 min. A time-averaging algorithm, with an

incremental duration of 0.5 seconds, was used to smooth the voltage output from the load cell and the LVDTs.

3.2.3.2 Finite-element Modeling

A 30 ft span Fink truss, composed of nominal 2x4 in. Douglas-fir (modulus of elasticity of 1.6×10^6 psi), was modeled using a linear finite-element program (SAP90, Computers and Structures, Inc.) to estimate the response of the tension-splice joint to ground accelerations from: 1) the Northridge earthquake (Richter magnitude of 6.4) which occurred in California on January 17, 1994, and 2) an artificial earthquake time-history generated using WES-RASCAL (Silva 1987). Horizontal and vertical acceleration data for the Northridge earthquake were obtained from STA #24538 in Santa Monica, 15 miles from the epicenter. The first five modes were included in the analysis which contained 99.99% of the participating mass for the response in the horizontal direction. Figure 3.6 is a graphical representation of the finite-element model (FEM). Appendix A contains the SAP90 finite-element program input file.

The model is composed of linear beam elements connected by pinned joints, and is supported by horizontal and vertical springs connected to the heel joints. The web members are pinned at both ends. The top chord is continuous from the heel joint supports to the peak of the

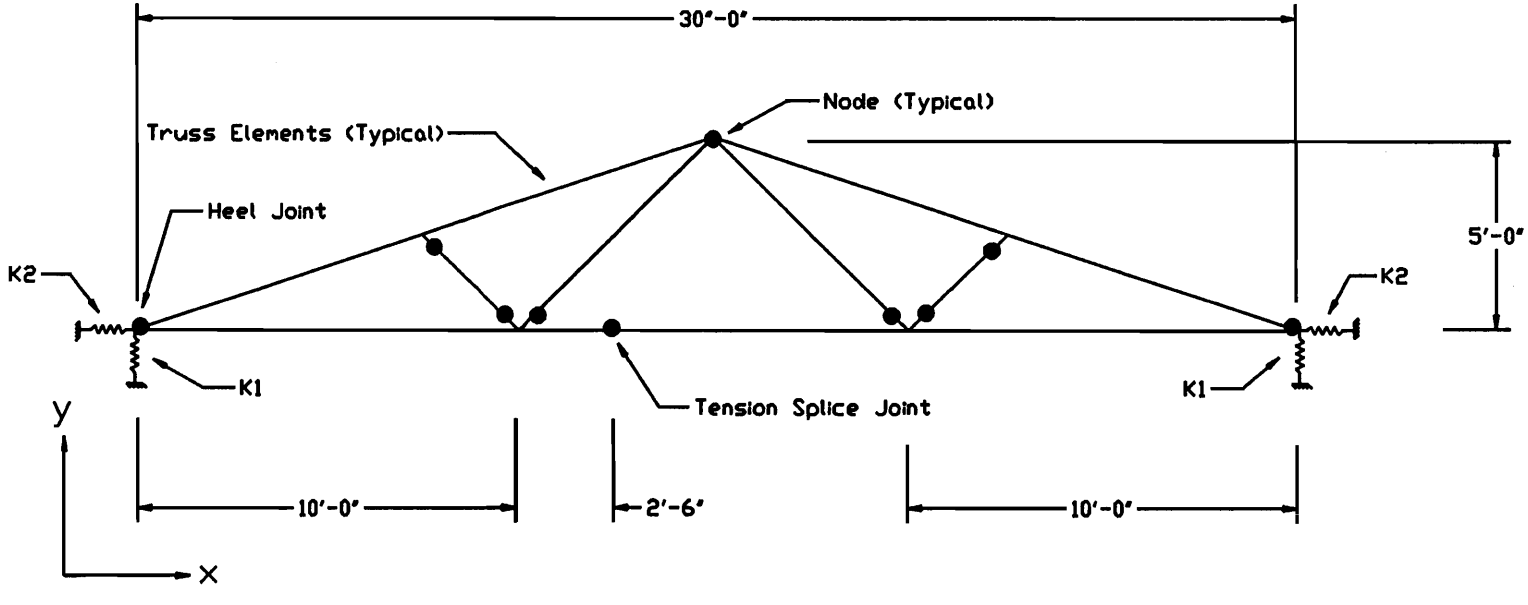

Figure 3.6: Finite element model of a typical metal-plate-connected truss

truss. The bottom chord is continuous from the heel joint supports to the tension splice joint.

The finite-element software (SAP90, Computer and Structures, Inc.) was only capable of accepting one damping coefficient to represent the system. Because the largest magnitude deflections during the earthquake simulation occurred at the supports (springs representing the bearing walls), a damping coefficient of 10%, typical of sheathed stud walls (Leiva 1994) was chosen to represent the entire system. The damping coefficient of 10% does not necessarily represent the damping associated with elongation (or contraction) of the truss members or the behavior at the connections.

The supporting springs simulate both the vertical stiffness (K1) and the out-of-plane (horizontal) stiffness (K2) of the bearing walls. The vertical (K2) and out-of-plane (horizontal, K2) stiffnesses are defined in the x-direction and y-direction, respectively, shown on Figure 3.6. However, during the literature survey, no information was found for the out-of-plane (horizontal) stiffness of walls applicable to this situation and an in-depth finite-element analysis was considered beyond the scope of this research. Also, this out-of-plane stiffness depends on a variety of factors such as the length of the bearing wall,

wall height, position of the truss along the wall, and type of construction. The approach used was to estimate the maximum possible out-of-plane support stiffness and then incrementally reduce that stiffness in the FEM to search for the worst-case response.

When compared to the trusses placed near the center of the bearing wall, it was assumed that the trusses placed nearest the end wall (running parallel to the trusses) would have the largest horizontal spring stiffness (K2). Experimental values obtained by Leiva (1994) on timber-framed shear walls suggest that 16 kips/in. is representative of the racking stiffness of a 30 ft long by 8 ft high wall. Once this maximum stiffness was established, the value was incrementally reduced in the FEM.

Investigation into the effect of vertical spring stiffness on the time history response of the model also was conducted. It was found that the model was not particularly sensitive to changes in the vertical spring stiffness.

Figures 3.7 and 3.8 display the maximum and minimum forces developed in the tension-splice joint during the Northridge earthquake simulation (both the horizontal and vertical components) for nominal 2x6 in. and 2x8 in. vertical support conditions, respectively. To construct Figures 3.7 and 3.8, two groups of simulations were run in the FEM with the equivalent of 2x6 in. and 2x8 in. vertical

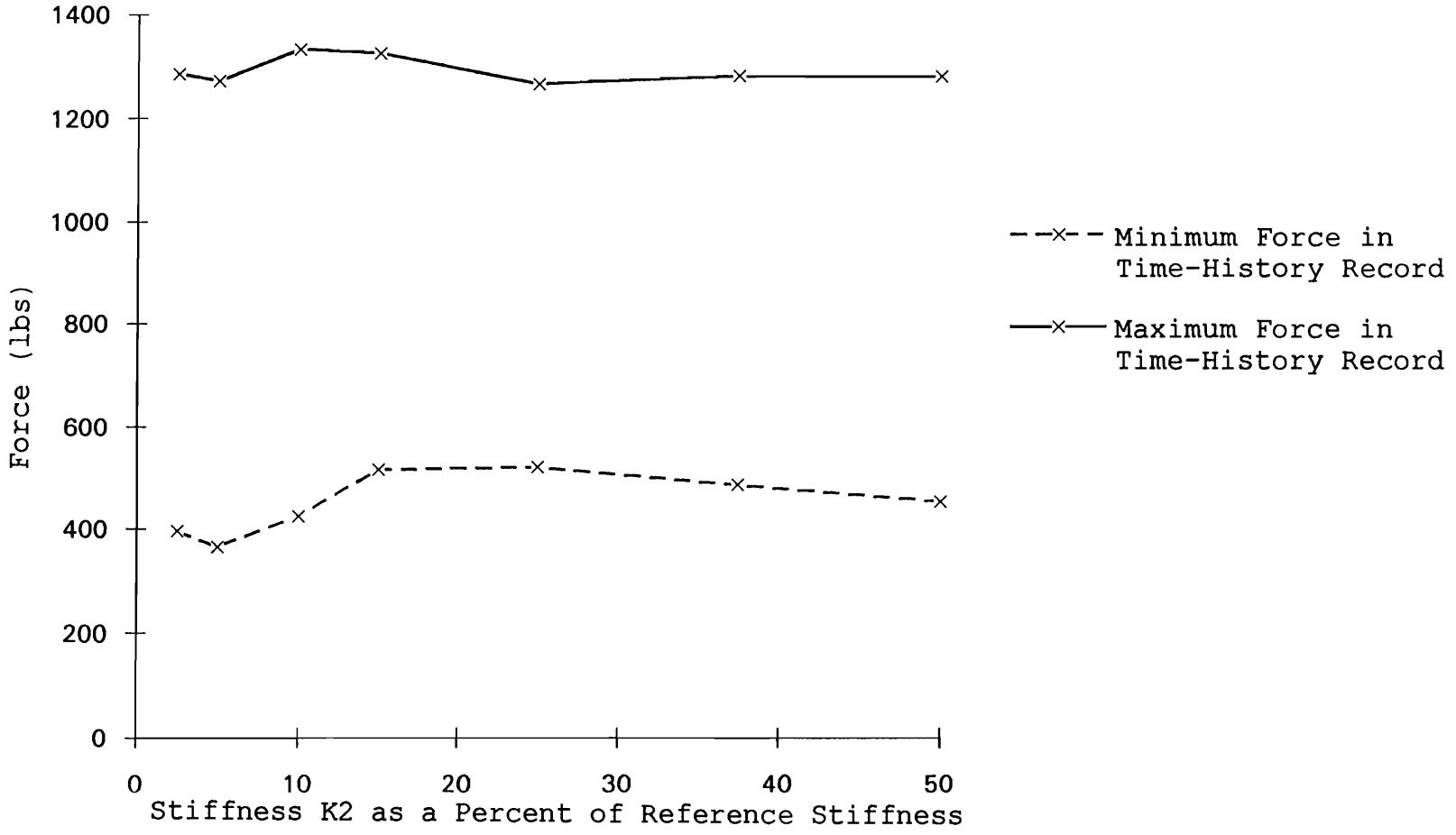

Figure 3.7: Maximum and minimum tensile forces developed in the tension-splice joint with nominal 2x6 in. cross section supports due to the Northridge earthquake (0.903g's and 0.232 g's horizontal and vertical peak accelerations, respectively) as a function of stiffness (K2)

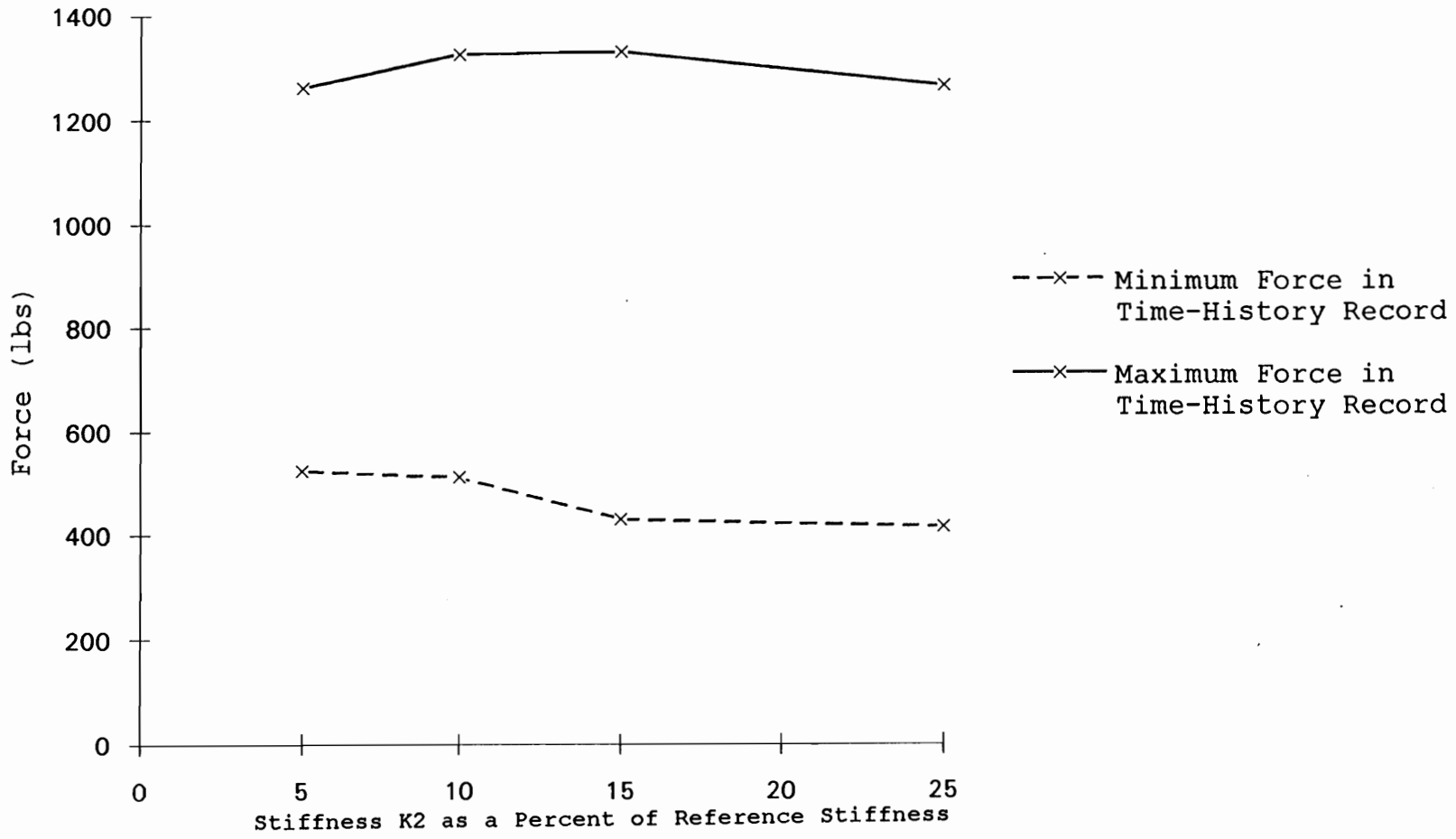

Figure 3.8: Maximum and minimum tensile forces developed in the tension-splice joint with nominal 2x8 in. cross section supports due to the Northridge earthquake (0.903g's and 0.232 g's horizontal and vertical peak accelerations, respectively) as a function of stiffness (K2)

supports and a varying horizontal support stiffness (from 2 to 50% of the reference stiffness of 16 kips/in.). The force levels between the 2x6 in. and 2x8 in. support cases vary by less than 100 lb. The final model included a horizontal spring stiffness equal to 10% of the reference value of 16 kips/in., or a spring stiffness of 0.80 kips/in. on either side of the truss. This horizontal spring stiffness maximized the model response in terms of the largest tensile force experienced in the tension-splice joint. The vertical spring stiffness selected for the final analysis was the equivalent of an 8 ft long, 2x6 in. Douglas-fir stud, which corresponded to approximately 140 kips/in. Axial stiffness of the studs was defined as K=AE/L where A=8.25 in^2, E=1.6x10^6 psi, and L=96 in.

The variables K1 and K2 (see Figure 3.6) are stiffnesses of the horizontal and vertical linear springs, respectively. The model is almost completely symmetrical with the exception of the tension-splice joint located in the bottom chord. This joint is placed 30 in. off center to model actual Fink truss construction (although the position of the tension-splice joint varies somewhat with different manufacturers). Pinned joints, which have no rotational restraint, are represented as dark circles.

Typical design dead loads for modern truss construction are 10 lb/ft^2 (including the weights of the top-chord,

sheathing, and roofing material) along the slope of the roof for the top chord and 10 lb/ft^2 (including the weight of the bottom chord, ceiling material, insulation, and permanent fixtures) along the bottom chord (Breyer 1993). At a truss spacing of 24 in. on-center, this corresponds to a uniformly distributed load of 20 lb/ft along the slope of the top chord and along the bottom chord. Self weight of the web members is estimated at 1.14 lb/ft (specific gravity of 0.50). Masses from the roof system and the truss members are lumped at the joints (nodes) for the dynamic analysis. Snow and wind loads were not included in the dynamic analysis for earthquake effects. To determine total design loads, the contribution of these other loads must, of course, be considered.

3.2.3.3 Northridge Earthquake Simulation (batch-1)

A group of ten tension-splice joints was subjected to a force time-history, to simulate the effects of the Northridge earthquake. A ramp load of 780 lb/min was first applied to the joints until the estimated dead load from the FEM of 900 lb was reached. The earthquake forces were then applied for a duration of 30 seconds, followed by a continuation of the ramp load until the joints failed. The earthquake force-time-history alone was not sufficient to fail the joints.

The 90 DEG (azimuth) horizontal component and the vertical component of the Northridge earthquake, shown in Figures 3.9 and 3.10, respectively, which had maximum accelerations of 0.903 g's and 0.232 g's, respectively, were analyzed separately to obtain the time-history response of the force at the tension-splice joint. The two components were then superimposed to obtain the combined response shown in Figure 3.11.

3.2.3.4 Artificial Earthquake Generation Using WES-RASCAL

The WES-RASCAL code (Silva 1987) is used to help assess seismic hazards in regions were strong motion data is scarce. This program has the ability to generate strong motion data by scaling specific parameters from small local seismic events, or weak motions. These weak motions provide the seismic wave characteristics used in the scaling process. The purpose of WES-RASCAL (Silva 1987) is not to predict the accelerogram of a future earthquake but to generate a time-history for a given magnitude event with realistic characteristics. WES-RASCAL (Silva 1987) is capable of generating an artificial time-history based on a target response spectrum; however, if a strictly theoretical approach is used to construct a time-history in this manner, the result may not simulate a realistic natural event. The variability of soil stratifications, interaction between

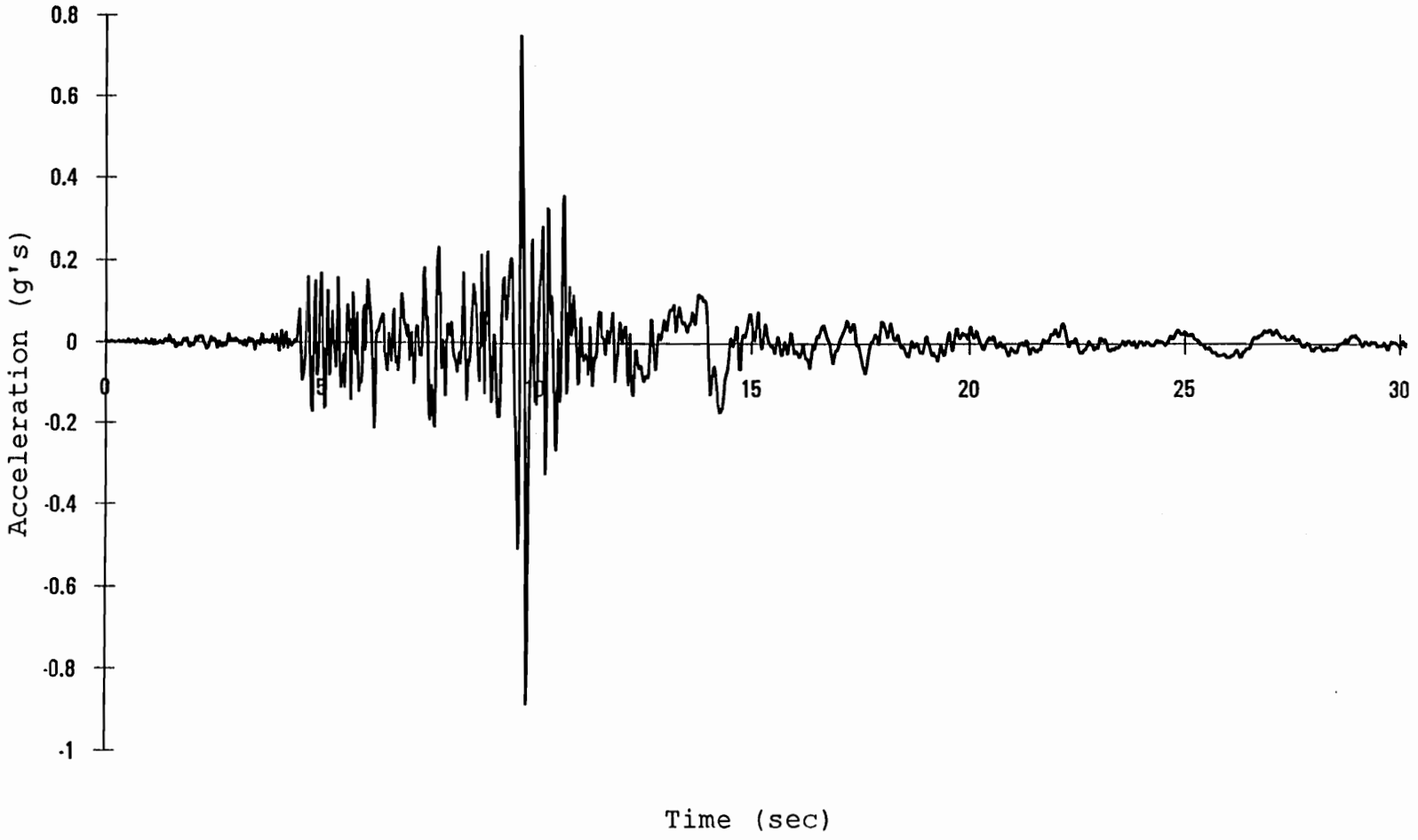

Figure 3.9: Horizontal ground acceleration during the Northridge earthquake

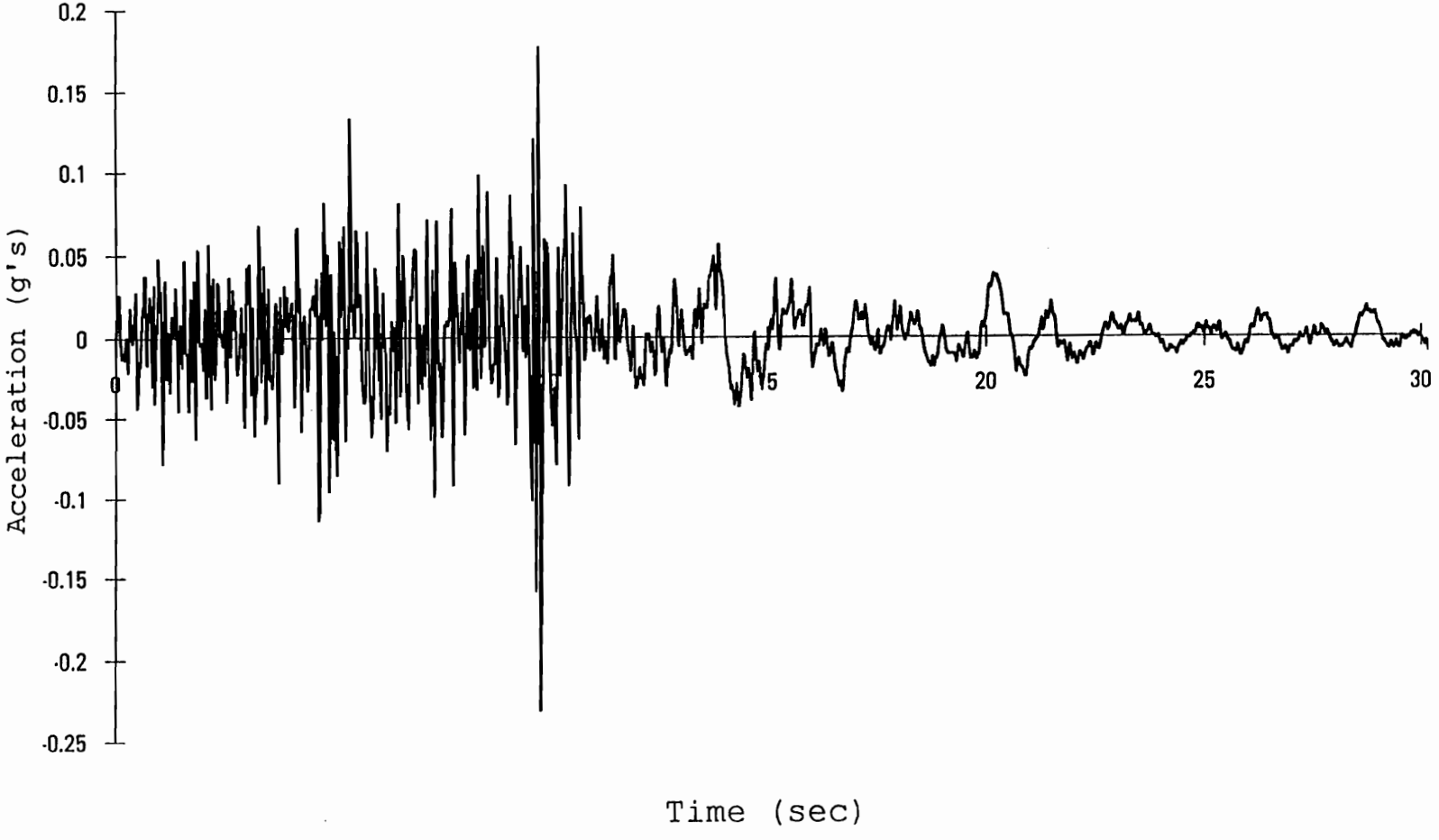

Figure 3.10: Vertical ground acceleration during the Northridge earthquake

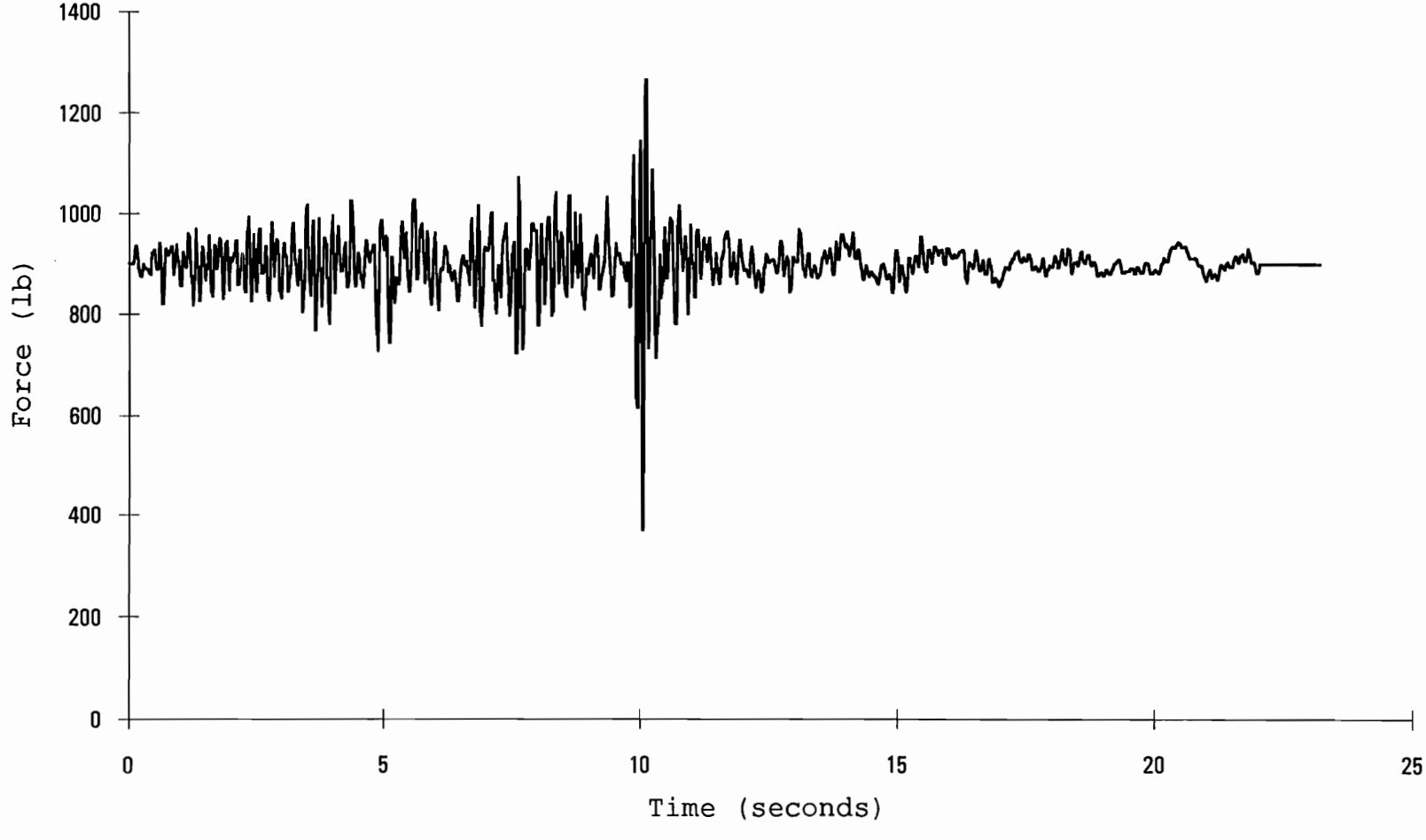

Figure 3.11: Combined response (target) of the tension-splice joint to the Northridge earthquake horizontal and vertical ground accelerations.

bedrock and soil, and a host of natural phenomena make the problem of developing a realistic accelerogram from a purely theoretical perspective nearly impossible. To address this problem, the program requires an input time-history from which it extracts specific phase characteristics from the Fourier amplitude spectrum. These phase characteristics are then applied in generating the artificial time-history output. This approach allows the program to generate a realistic artificial acceleration time-history

Although the artificial acceleration time-history record has a response spectrum closely matching a target design response spectrum, other properties, such as displacement and energy input may be exaggerated (Naeim 1995). WES-RASCAL (Silva 1987) manipulates the displacement record before and after the integration of the acceleration record to produce a more realistic account of the displacements. However, the displacement record produced by WES-RASCAL (Silva 1987) still tends to be exaggerated (Naeim 1995) even after the corrections.

The input for WES-RASCAL (Silva 1987) includes the type of simulation (artificial time-history from a response spectrum, or peak acceleration, velocity, and displacement only) soil characteristics, epicenter location, filtering parameters, input time-history, target response spectrum, and scaling parameters. The artificial time-history

generated for this study uses propagation parameters for the Western United States, the design response spectrum provided in the Uniform Building Code (ICBO 1994), Northridge earthquake phase characteristics, a source depth of 6 miles, and a moment magnitude of 7.0. Typical filtering and amplification factors for the Western United States were applied. The input file parameters used to determine the artificial time-history incorporated in this study are shown in Appendix B.

Response spectrum matching, after 10 iterations, is shown in Figure 3.12. The dashed line represents the Uniform Building Code (ICBO 1994) target response spectrum for Zone 4 and soil type 3 conditions. The solid line is the response spectrum of the output artificial earthquake accelerations. For the purpose of this study, the match was considered satisfactory (by a visual inspection).

The 1994 Uniform Building Code (ICBO 1994) dynamic time-history analysis procedure was used to determine the design forces for the tension-splice joint. First, the response of the tension-splice joint to the artificial time-history was determined using the FEM. Then, the forces were scaled according to the guidelines in the Uniform Building Code (ICBO 1994), sections 1624-1631. The scaling procedure is shown in Appendix C. This procedure produced forces, shown in Figure 3.13, much less severe than those for the

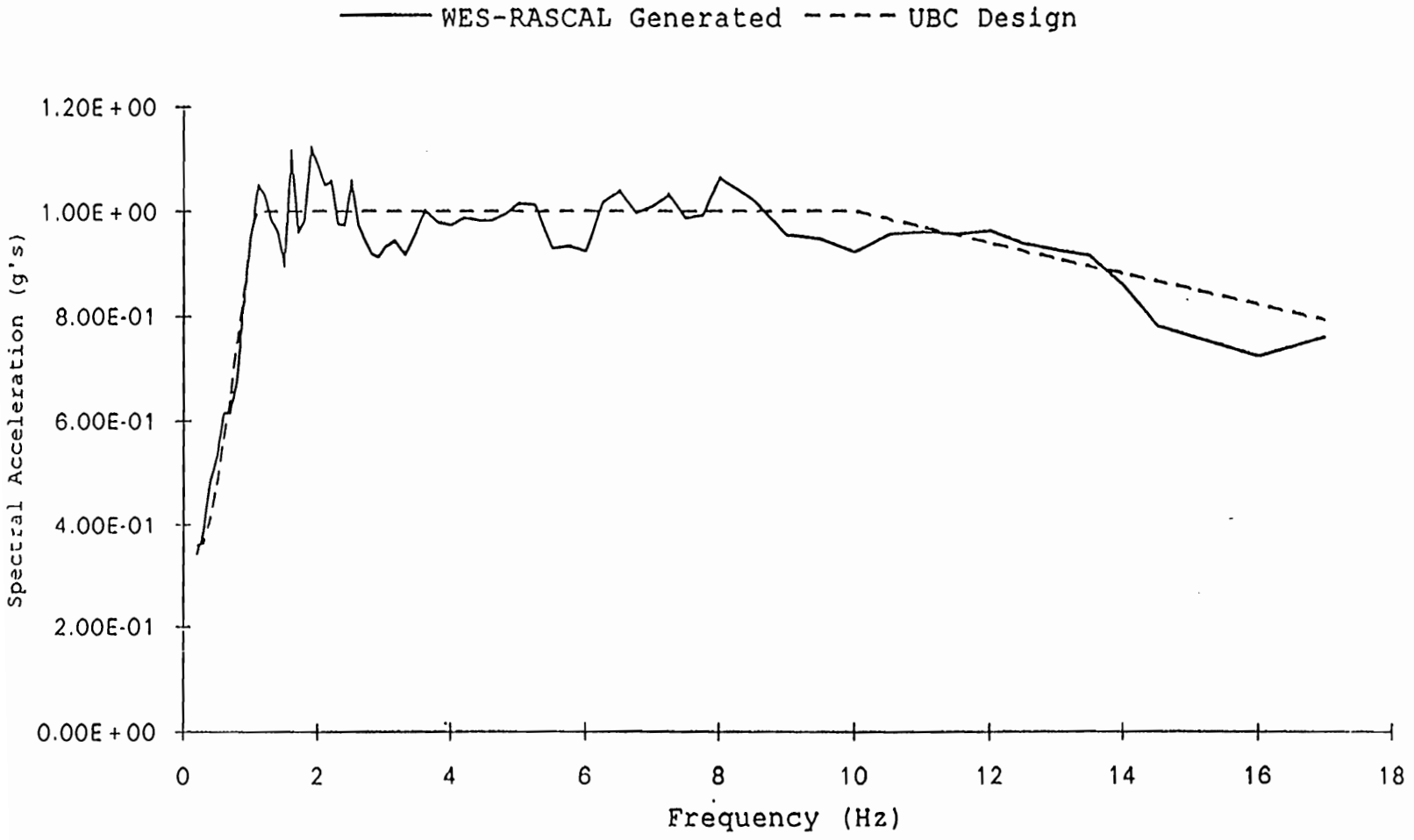

Figure 3.12: Comparison between the response spectra from WES-RASCAL and the Uniform Building Code (ICBO 1994).

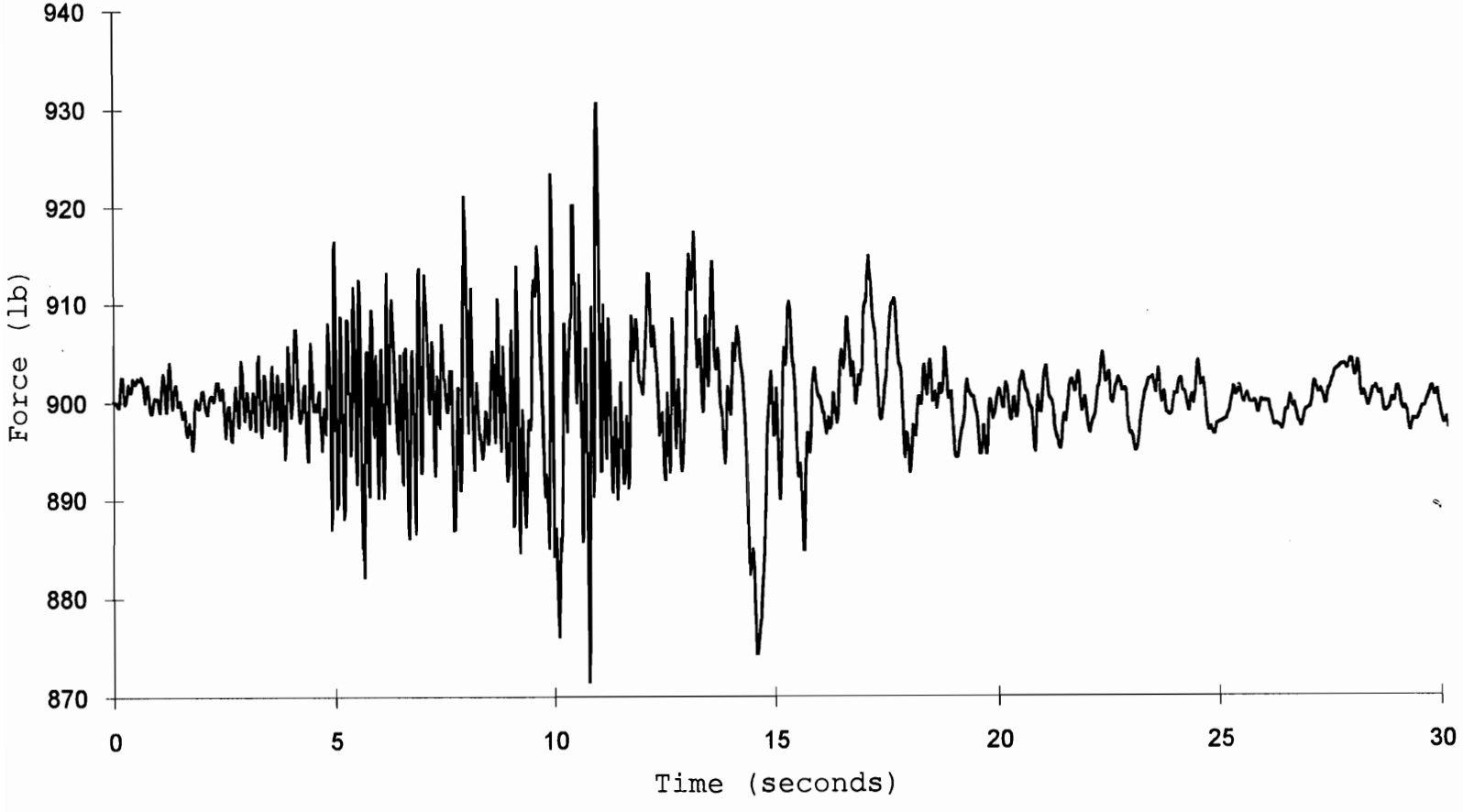

Figure 3.13: Earthquake design forces in the tension-splice joint during the artificial earthquake.

Northridge earthquake. Therefore, physical testing of tension-splice joints at this low force level was abandoned. Instead, the horizontal and vertical accelerations from the artificial earthquake time-history were scaled up for input into the FEM to simulate a very severe seismic event.

For horizontal accelerations, the artificial acceleration time-history was linearly scaled to a maximum horizontal acceleration of 1.0 g's. Similarly, for the vertical accelerations, the artificial accelerations were scaled to a maximum of 0.67 g's. The Uniform Building Code (ICBO 1994) seismic design section 1629.2 suggests scaling the maximum horizontal acceleration by 67% to estimate the maximum vertical acceleration. For this simulation, 67% of the horizontal ground acceleration time-history was used as the vertical ground acceleration time-history.

The horizontal and vertical artificial ground accelerations, shown in Figures 3.14 and 3.15, were applied separately to the FEM to determine the load response in the tension-splice for each direction (horizontal and vertical). Because the FEM was linear, the response to the horizontal and vertical ground accelerations were superimposed to obtain the combined response (additive effect of the horizontal and vertical accelerations). This procedure is very conservative in that the peaks of both the horizontal and vertical time-history records occur at the same point in

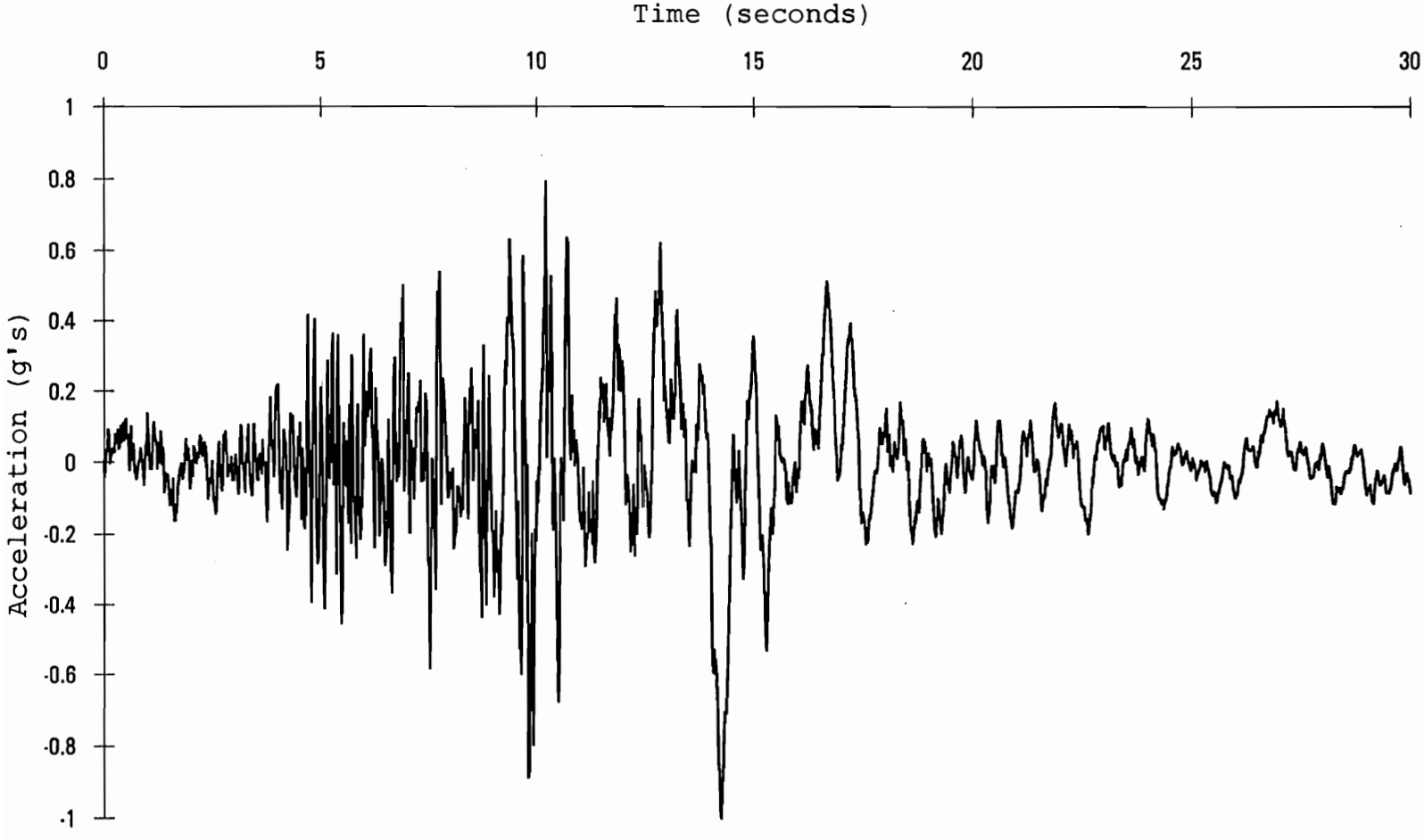

Figure 3.14: Horizontal ground acceleration (1.0 g maximum) during the artificial earthquake simulation

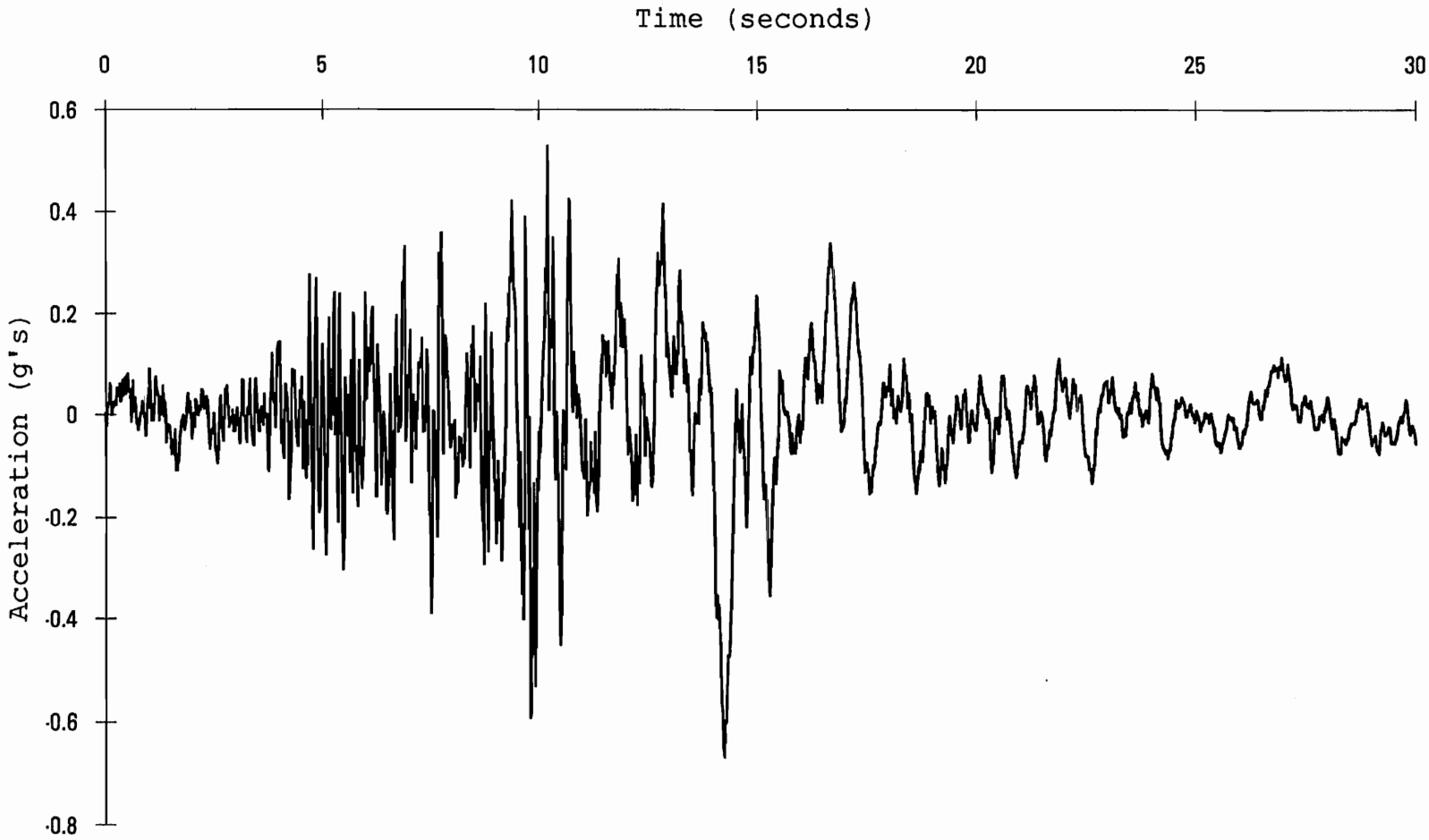

Figure 3.15: Vertical ground acceleration (0.67 g maximum) during the artificial earthquake simulation

time. An alternate method would be to develop a suite of independent horizontal and vertical acceleration time-histories using WES-RASCAL (Silva 1987) and combine them using the FEM to determine the possible range of maximum forces in the tension-splice joint.

The artificial earthquake loads were then applied to a set of nine real tension-splice joints in the laboratory. However, due to a load cell calibration error, the dead load applied to the joints was 800 lb rather than the desired 900 lb. The target forces applied to the tension-splice joints for the artificial earthquake simulation can be seen in Figure 3.16.

3.2.3.5 Sequential Phased Displacement (SPD) Loading (batch-1)

The proposed sequential phased displacement (SPD) method of Dolan (1994) was used to determine the dynamic properties of the MPC tension-splice joints, such as energy dissipation, damping ratio, and cyclic stiffness. The loading function combined fully reversed stabilizing cyclic displacements preceding degradation cycles at a frequency of 1 Hz, which approximates the expected response of a low-rise timber structure under a seismic or high wind event. The stabilizing and degradation cycles gradually increase, following the pattern shown in Figure 3.17, which

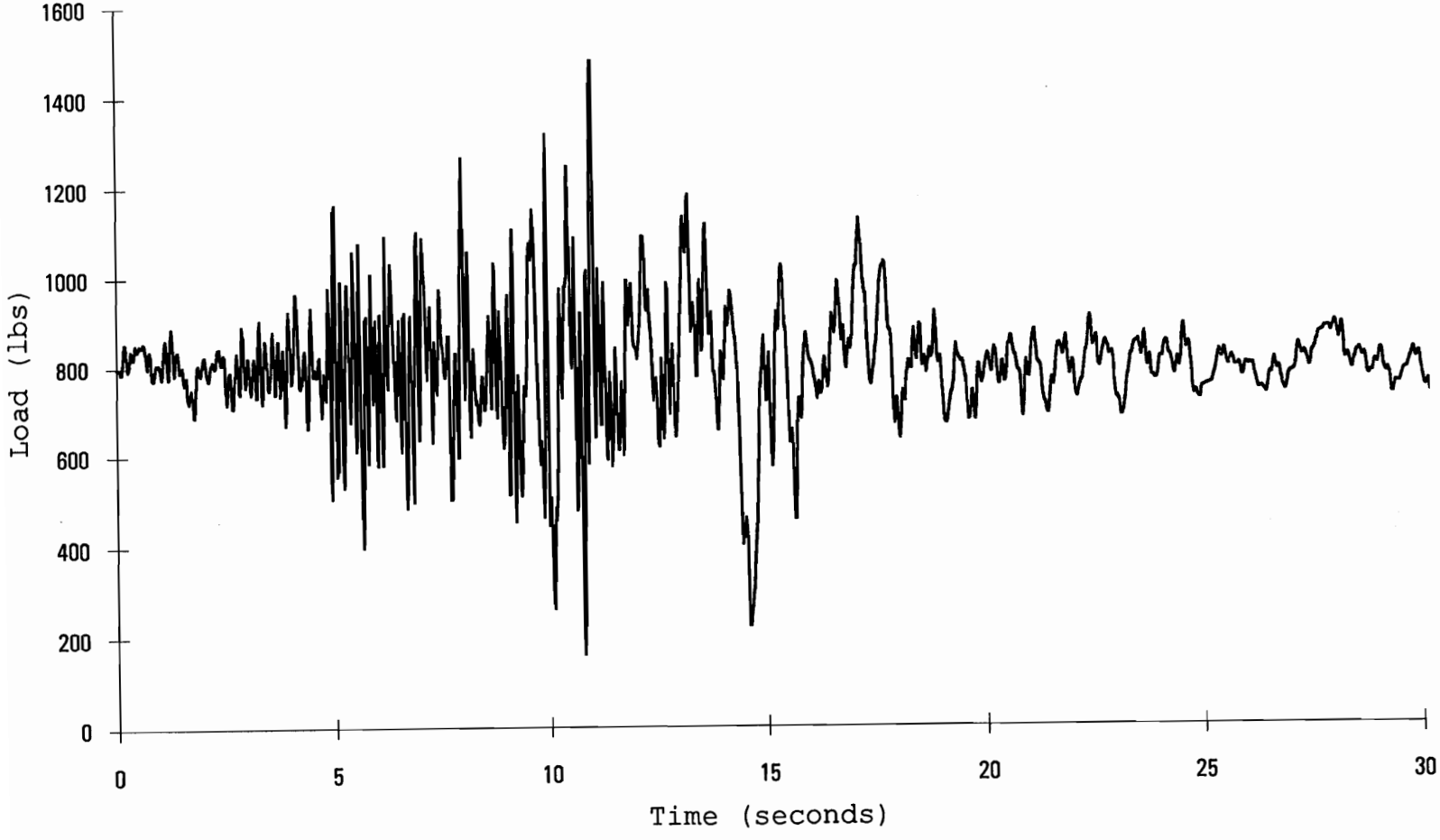

Figure 3.16: Target force-time-history applied to the tension-splice joint during the artificial earthquake simulation

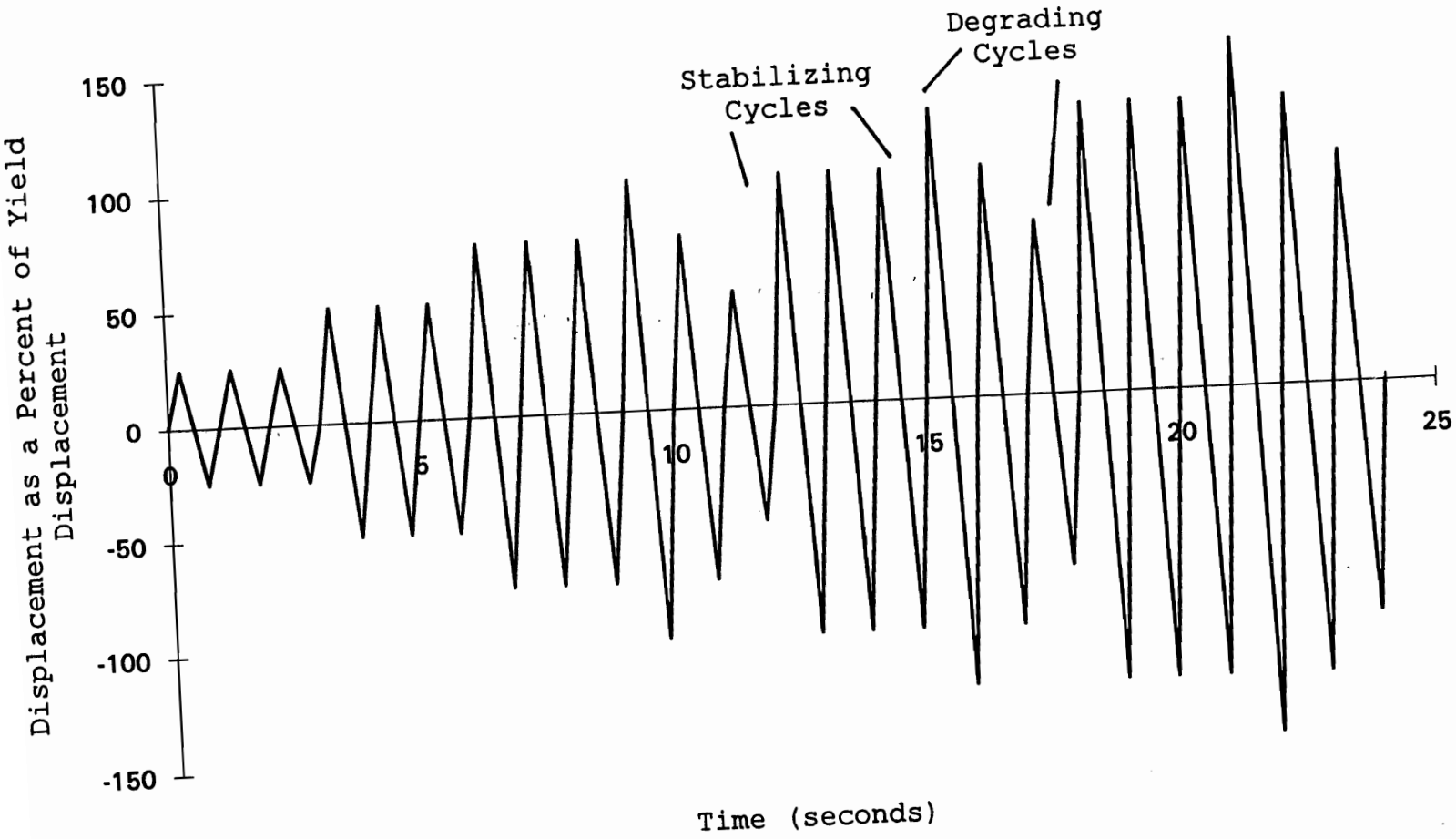

Figure 3.17: Sequential Phased Displacement loading (Dolan 1994).

graphically displays a typical SPD loading function proposed by Dolan (1994).

The SPD cycles are defined in terms of the yield displacement for the type of connection being studied. Because of the nonlinear load-deflection curves for MPC joints, a yield displacement (defined in section 3.3.1) of 0.006 in. (Appendix D) from the control group (batch-1), was used to scale the SPD cycles. Displacement control allows for a clear definition of the stabilized cycle from which dynamic properties are determined. The stabilized cycle is defined as the first cycle in the set of stabilizing cycles (see Figure 3.17) at which there is less than a 5% degradation from the maximum load in the previous cycle. The stabilized cycle is important because it provides a consistent location in the SPD loading for evaluating dynamic properties for comparison to other types of connections.

The rational of the SPD loading is that it better represents a seismic or wind event than a static ramp load or a simple cyclic loading function. Also, the use of the stabilized cycle allows for consistent calculations of the dynamic properties. The equivalent energy, elastic-plastic load-displacement curve provides a method so that comparisons of the dynamic properties between different materials and connection types can be made. Moreover, the

decay portion of the loading provides information on the lower bound of the hysteresis. If the connection has slack in it, the hysteresis can decrease to zero energy dissipation. Also, the increasing magnitude of the displacement phases can continue until failure, thus providing information on total ductility and capacity.

Although during wind or seismic events, the response of a structure contains a spectrum of frequencies, the 1 Hz frequency used in the SPD method makes for a more realistic dynamic simulation than a static ramp load to estimate dynamic properties. Also, hardware for a testing system capable of a 1 Hz frequency requires a smaller capital investment than a system capable of much higher frequencies. This allows the SPD method to be more readily adopted as a standard.

Under normal conditions, the tension-splice joint is not designed to resist compressive loads. An alternative to applying a fully reversed loading is to truncate the negative portion (causing compressive loads), shown in Figure 3.17, and apply only the positive displacements (in terms of the percent of yield displacement). However this alternate approach was not used in this first study to apply the SPD loading to tension-splice joints. It was decided to follow the proposed standard as closely as possible.

During the SPD tests, the compressive load limit for the hydraulic actuator of approximately 10,500 lb was reached before failure occurred in the joints. Therefore, the joints were subjected to a maximum of 120 cycles. Appendix D contains the number of SPD cycles applied to each joint. To prevent lateral movement of the hydraulic cylinder during testing, a brace was placed as shown in Figure 3.3. The compressive stiffness of the MPC tension-splice joints increased dramatically as the gap between the two wood members closed. Therefore, as the SPD test progressed, a much higher compressive load than tensile load was required to obtain the same magnitude deflection. Because of this, the actuator compressive load limit was reached before the joints could fail in tension. Therefore, it was decided to fail the joints under a ramp load of 780 lb/min to determine how the SPD loading affected the strength and stiffness of the MPC tension-splice joints. For those joints that did not reach the maximum capacity of the hydraulic actuator by 120-cycles, the test was manually stopped at this point so that all the joints would be subjected to approximately the same number of cycles. Appendix D shows the number of cycles applied to each joint.

3.2.3.6 Cyclic Testing (batch-2)

To determine the effect of cyclic loading at various amplitudes, a sinusoidal waveform with the baseline of the oscillations (centerline of the cycles) at 32% of the mean ultimate tensile strength (from the static loading control group, batch-2) were applied for 200 cycles at a frequency of 1 Hz to twenty tension-splice joints. First, the joint was loaded to 32% of the mean strength (0.32•6712 lb = 2148 lb, see Appendix D) at a load rate of 780 lb/min. Then, constant amplitude cycles (8.22, 12.3, 14.8, 15.6, 16.4, 18.1, 19.7, 20.6, and 24.7 percent of the mean strength) were applied at a frequency of 1 Hz for 200 seconds (total of 200 cycles) or until the joint failed. If the joint was still able to carry load after the cycles, the static ramp load was continued until failure. Figure 3.18 displays the cyclic loading function.

3.3 Test Results

3.3.1 General Results

Strength, specific gravity, and moisture content results for the tests in this study are shown in Appendix D (as well as strength, stiffness, deflection at maximum load, yield displacement, modulus of elasticity, number of growth rings per inch, grain orientation, late wood content,

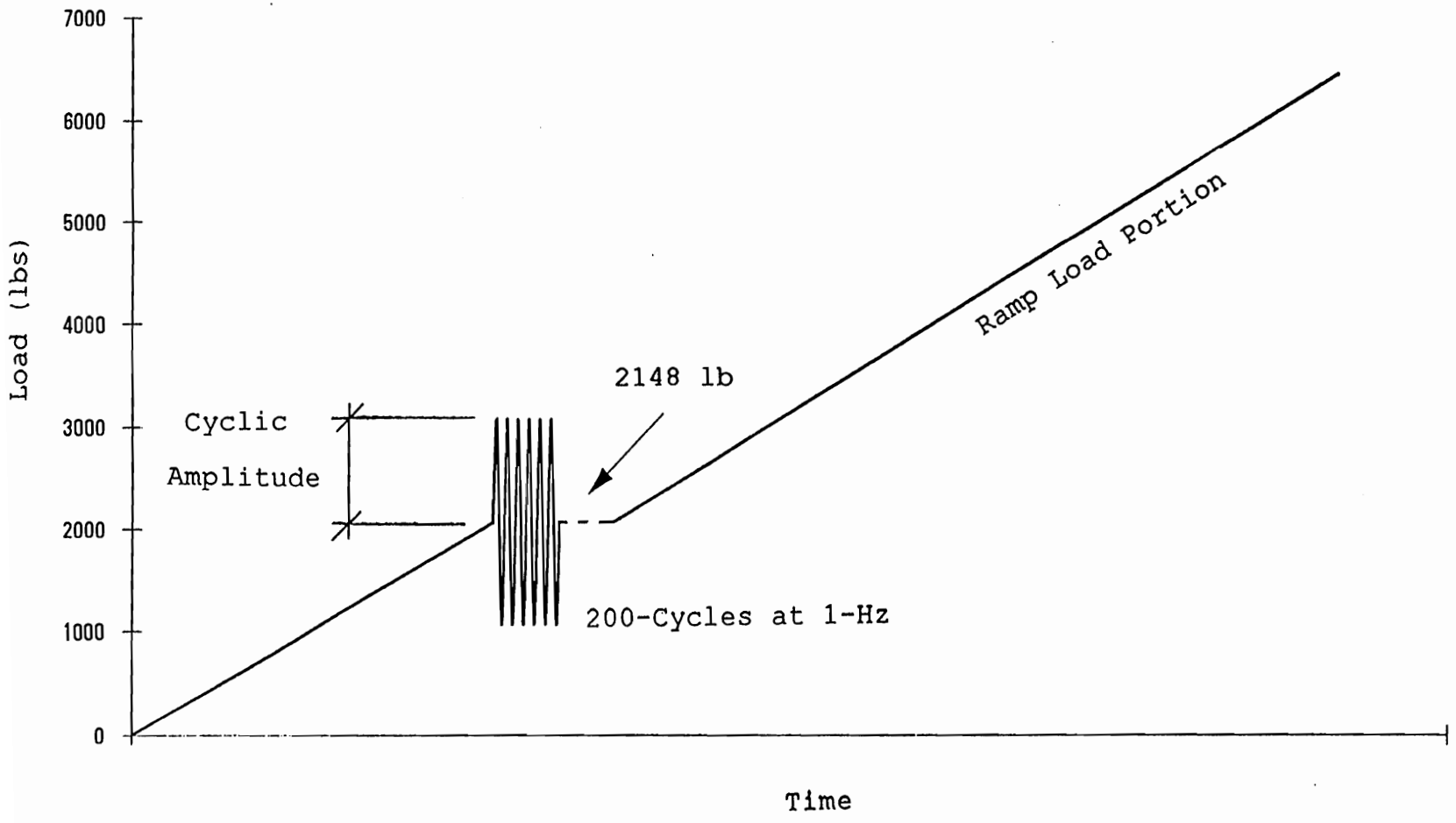

Figure 3.18: Cyclic loading function for tension-splice joints.

and failure mode) with their respective coefficients of variation (COV). A summary for each group of tests is shown in Table 3.3 Mean strength for the cyclic loading tests is not given in this table because of the strength dependence on the amplitude of the cycles.

Specific gravity and moisture content were measured according to ASTM D2395-93 (Method A, Volume by Measurement) and ASTM D4442-92 (Method A, Oven-Drying Primary), respectively. The modulus of elasticity of the wood used to construct the MPC tension-splice joints was measured using an E-computer (Metriguard, Model 390). The dominant failure mode of the tension-splice joints was tooth withdrawal, although there were three instances where the metal-plate-connector failed in tension (joint 7 of static batch-1 control group; joints 3 and 7 of the Northridge earthquake simulation, batch-1). The tooth withdrawal failure mode occurred as a result of the wood being crushed by the side of the tooth near the surface of the wood in conjunction with slight bending of the teeth. As the load increased, the back of the plate began to lift away from the surface of the wood causing the teeth in that area to become virtually ineffective in resisting load. Near the ultimate load, the wood fibers at the tooth-wood interface began to deform plastically due to the large loads transmitted by the metal-plate-connector through the teeth and into the wood. Figure

Table 3.3: Summary of the tension-splice joint test results

Test	Sample Size	Mean Strength (lb)	Mean Stiffness (x100,000 lb/in.)	Mean Specific Gravity
Control Group (batch-1)	9	7284	4.32	0.50
Control Group (batch-2)	9	6712	2.79	0.48
Northridge Earthquake Simulation	10	7569	3.99	0.50
Artificial Earthquake Simulation	9	6482	3.46	0.48
Sequential Phased Displacement	8	7189	1.89	0.50
Cyclic Loading	20	Varies*	Varies*	0.45

Test	Mean Moisture Content (%)	Mean Wood MOE ($x10^6$ psi)
Control Group (batch-1)	13.0	NA
Control Group (batch-2)	13.4	1.80
Northridge Earthquake Simulation	14.5	1.86
Artificial Earthquake Simulation	13.4	1.79
Sequential Phased Displacement	13.6	1.80
Cyclic Loading	12.6	1.76

NA: Not Available

* Depends on the cyclic amplitude

3.19 shows the dominant failure mode of tension-splice joints (tooth withdrawal). Gupta and Gebremedhin (1990) observed a similar failure mode in their study on MPC tension-splice joints.

The plate tension failure mode was uncommon in this study. If larger plates were used (greater than 3x4 in.), the average load per tooth would decrease due to the increased number of teeth resisting the load. This would tend to decrease the probability of a tooth withdrawal failure mode, as a result of the decreased load on a per-tooth basis. Plate-tension failures tend to occur at higher loads than tooth withdrawal failures because premature wood failures do not occur.

Because of the nonlinear shape of the load-deflection curves, which made it difficult to define a single valued stiffness, the yield point for each joint was defined at the design strength (one-third of the ultimate strength for that particular joint, National Design Specification for Wood Construction, 1991). To calculate the stiffness (secant stiffness), one-third of the ultimate strength of the joint was divided by the corresponding deflection. For the earthquake simulations (Northridge and artificial earthquakes), this point occurs after the loading.

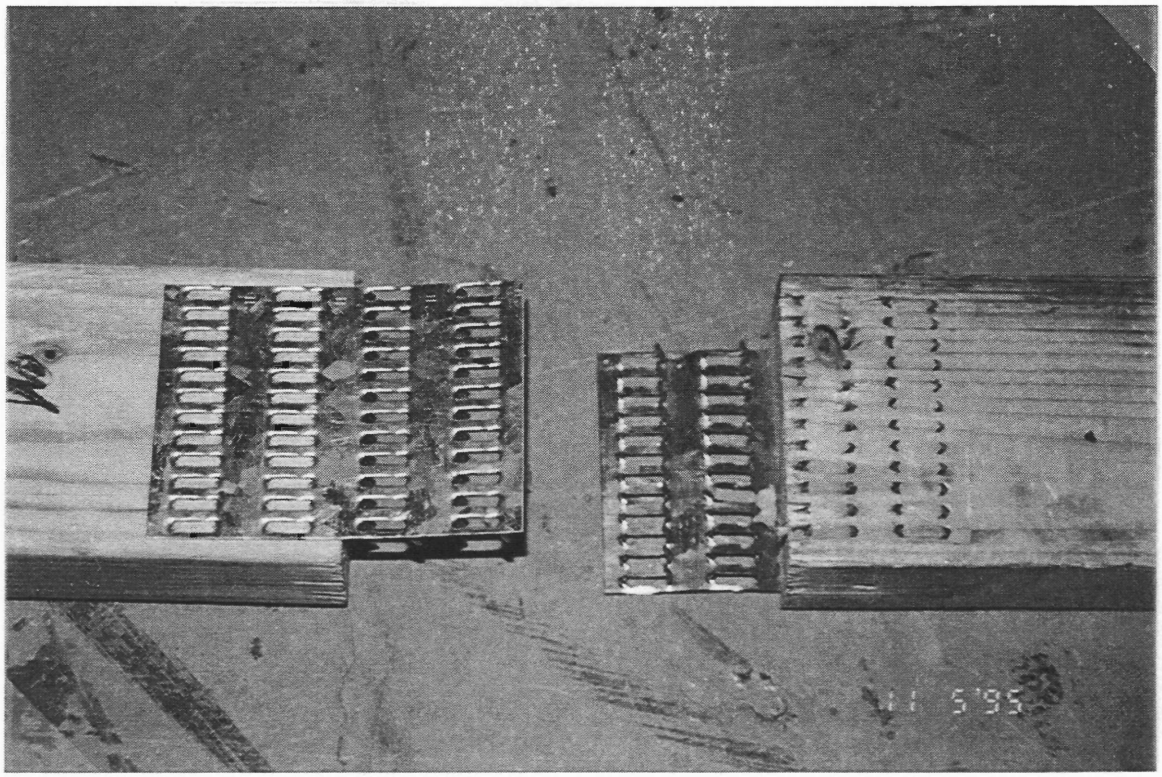

Figure 3.19: Dominant failure mode of the tension-splice joint.

3.3.2 Static Tests

3.3.2.1 Batch-1

The mean static strength of the control group for batch-1 was 7284 lb with a coefficient of variation (COV) of 6% (see Appendix D). The average yield displacement was 0.006 in. (Appendix D) The mean stiffness for the control group was 4.32×10^5 lb/in. with a COV of 16.1% (see Appendix D). Figure 3.20 shows a typical load-deflection curve during the static ramp load for batch-1 (for joint 4).

3.3.2.2 Batch-2

The mean static strength of the control group for batch-2 was 6712 lb with a COV of 8.06% (see Appendix D). The mean stiffness for batch-2 was 2.79×10^5 lb/in. with a COV of 14.4% (Appendix D). The average yield displacement was 0.008 in. (Appendix D). The failure mode for batch-2 was tooth-withdrawal with no instances of plate-tension failure. Figure 3.21 shows a typical load-deflection curve during the static ramp load for batch-2 (joint 8).

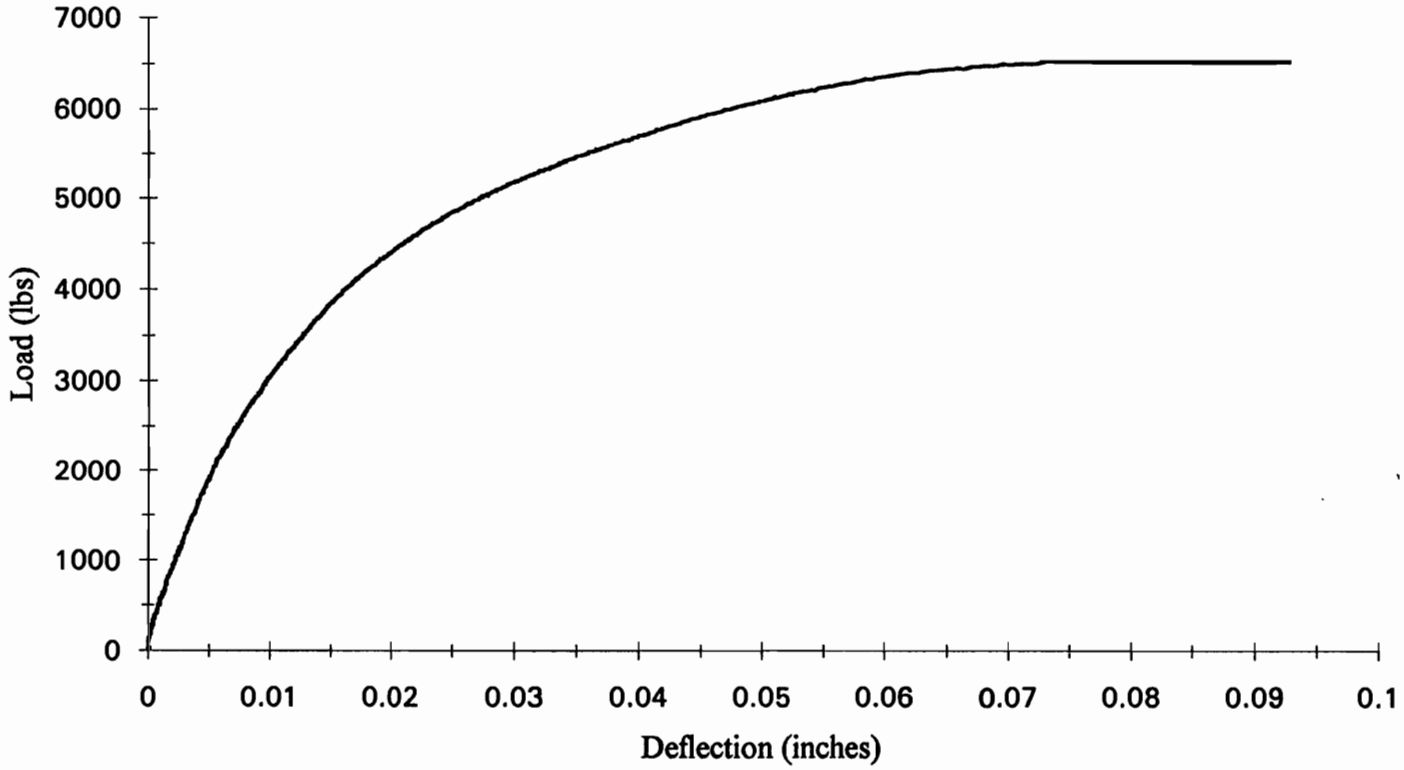

Figure 3.20: Typical load-deflection curve during the static ramp load (joint 4, batch-1)

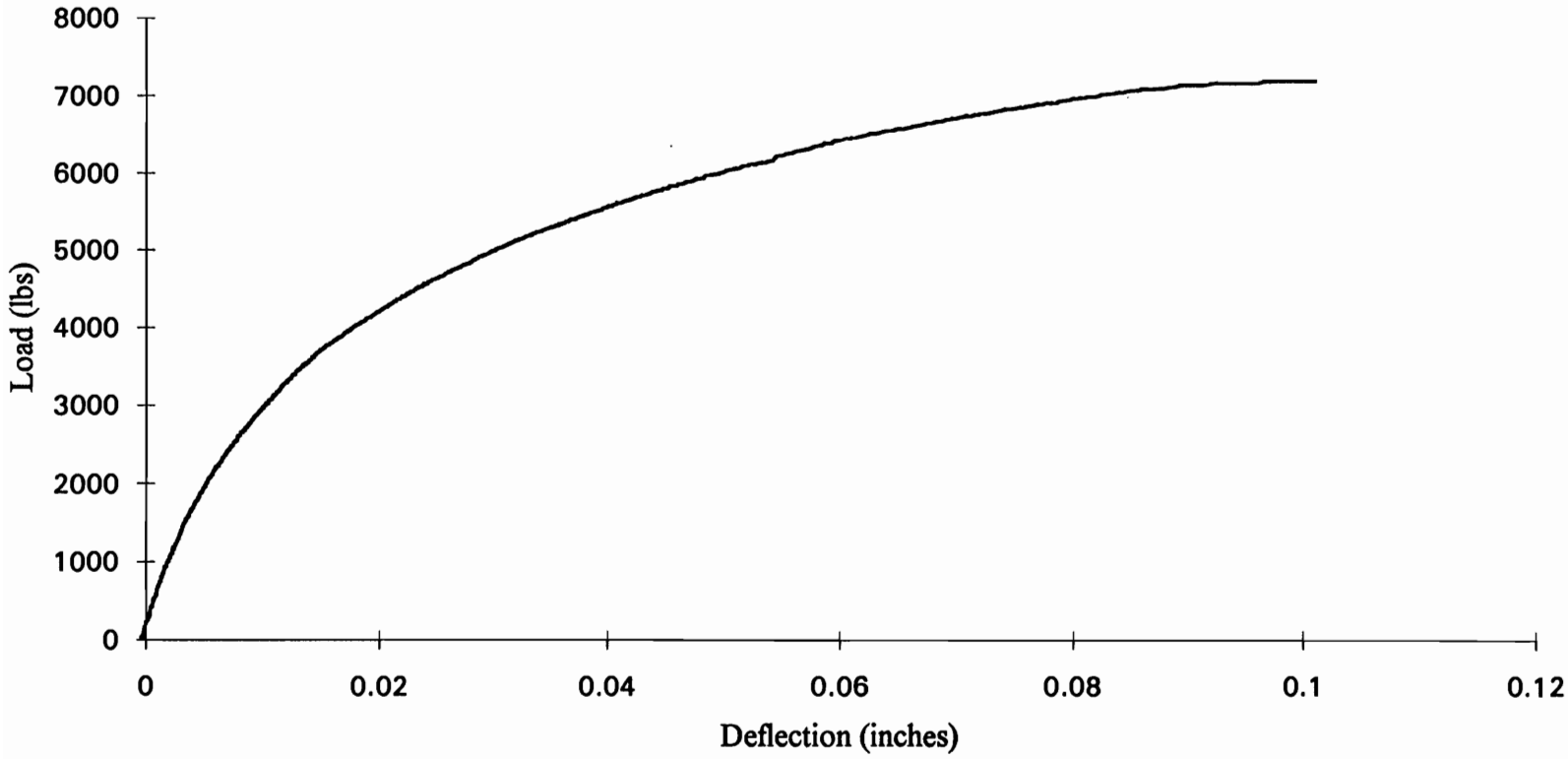

Figure 3.21: Typical load-deflection curve during the static ramp load (joint 8, batch-2)

3.3.2.3 Comparison of Static Tests

There is strong statistical evidence that the tension-splice joints constructed from the two different batches of plates have neither the same mean strength nor the same mean stiffness (two sided p-values of 0.025 and 0.007 for strength and stiffness comparisons, respectively, see section 3.1, and Table 5.1). Thus, the statistical evidence suggests that strength and stiffness comparisons should be made between joints fabricated from the same batch of metal plate connectors. To determine the strength and stiffness degradation, if any, caused by a particular earthquake or cyclic load, the statistical test should include the control group which was fabricated from the same batch of plates.

Specific gravity and moisture content values for the control groups using plates from batch-1 and batch-2 (Appendix D) cannot be statistically separated at the 0.05 level of significance (section 3.1). This evidence suggests that the differences in strength and stiffness between the two control groups are not due to differences in the wood. It is more likely that characteristics of the metal-plate-connectors themselves caused the differences in strength and stiffness between the static loading tests of the two different batches.

The fabrication of the tension-splice joints from the two batches of plates was similar. As stated in section

3.2.1, care was taken not to over-press or under-press the plates. Although the samples from batch-1 and batch-2 plates were fabricated using three different presses, there was no difference between the fabrication procedures. Also, recall the different locations of the hydraulic actuator during testing of the two control groups in the testing frame (section 3.1). Despite the different locations, the testing procedure, such as load rate and boundary conditions did not vary (section 3.2.2). Thus, the two control groups were assembled and tested under nearly identical conditions which themselves should not have influenced the strength or stiffness of the two control groups.

As shown in Figures 3.20 and 3.21, the load-deflection curves are nonlinear, which is typical of wood connections (Foschi 1974). The nonlinearity is due to a number of factors involving both the wood and the metal plate. The relative contributions from these different factors changes as the load increases. At lower load levels, the deflection can be attributed to the elastic response of the wood near the tooth-wood interface and the elastic response of the steel plate under tension. At higher load levels, the deflection is controlled by bending of the metal teeth and crushing of the wood at the tooth-wood interface.

3.3.3 Historic (Northridge) Earthquake Simulation (batch-1)

Analysis of the data suggests that the tension-splice joints did not degrade in either strength or stiffness when subjected to the Northridge earthquake time-history used in this simulation. The mean strength and stiffness of the joints (after being subjected to the earthquake loads), on application of the ramp load, were 7569 lb with a COV of 6.97% and 3.99×10^5 lb/in. with a COV of 14.1% (Appendix D), respectively.

A statistical comparison (section 3.1) of these results with the static loading control group (batch-1) suggested that the Northridge earthquake load time-history did not degrade the strength or stiffness of the tension-splice joints (two sided p-values of 0.78 and 0.28 for strength and stiffness degradation, respectively, see Table 5.1).

The lack of strength or stiffness degradation from the Northridge earthquake tests is not surprising. As shown in Figure 3.11, the maximum load developed in the tension-splice joint during the earthquake simulation (1234 lb) is only 17% of the average ultimate load for tension-splice joints (7284 lb, Appendix D, batch-1). Figure 3.22 shows a typical load-deflection curve including the earthquake time-history. A close-up of the earthquake portion of the curve is also shown in Figure 3.22. This close-up view shows how the joint responded to the earthquake loading. The data

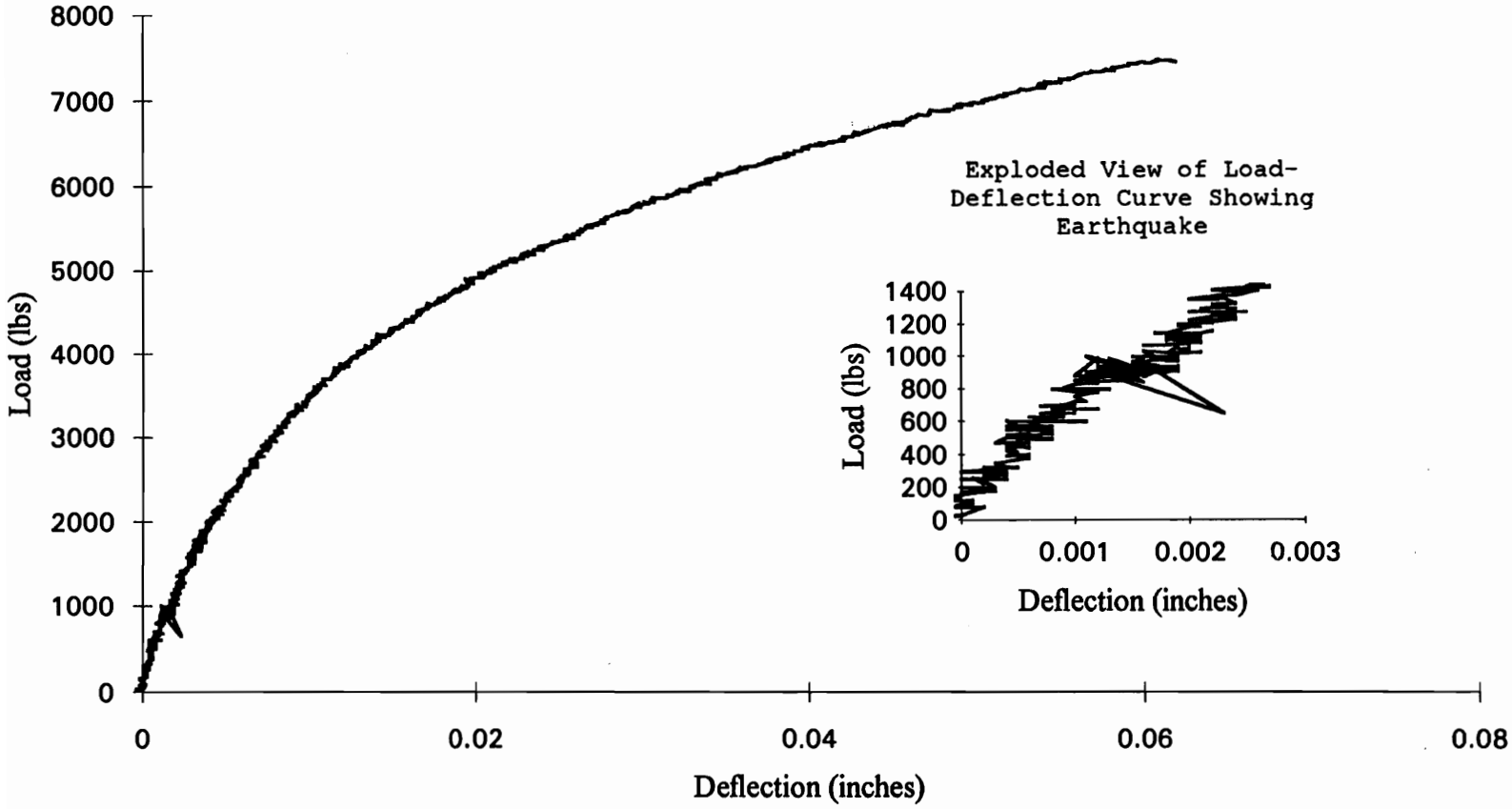

Figure 3.22: Typical load-deflection curve during the Northridge earthquake simulation (joint 6, batch-1)

acquisition rate was only 2 Hz which was not sufficient to completely define the load-deflection trace (a 50 Hz acquisition rate would be required).

Figure 3.23 shows a typical deflection-time curve (for joint 1) for the Northridge earthquake simulation. Figure 3.24 displays a close-up view of Figure 3.23 showing the earthquake portion of the test. Figures 3.23 and 3.24 show that the Northridge earthquake simulation has very little effect on the deflections of the joint. The earthquake time-history occurs between 70 and 100 seconds on Figures 3.23 and 3.24.

Figure 3.25 displays the Fourier amplitude spectrum of the target (forces derived from the FEM) and actual (forces measured during testing) force time-histories. This plot was developed using a Fast Fourier Transform (FFT) algorithm (Microsoft Excel, version 4.0a). The sampling rate of the data was 50 Hz for a duration of 30 seconds. However, only the first 20.48 seconds (the first 1024 data points) were used to calculate the FFT (the FFT procedure requires 2^n data points, where n is a positive integer). The magnitude of the complex output from the FFT was computed and plotted in the frequency domain up to the Nyquist frequency of 25 Hz. A moving linear-average filter (boxcar filter) with a band-width of 1 Hz was used to smooth the data.

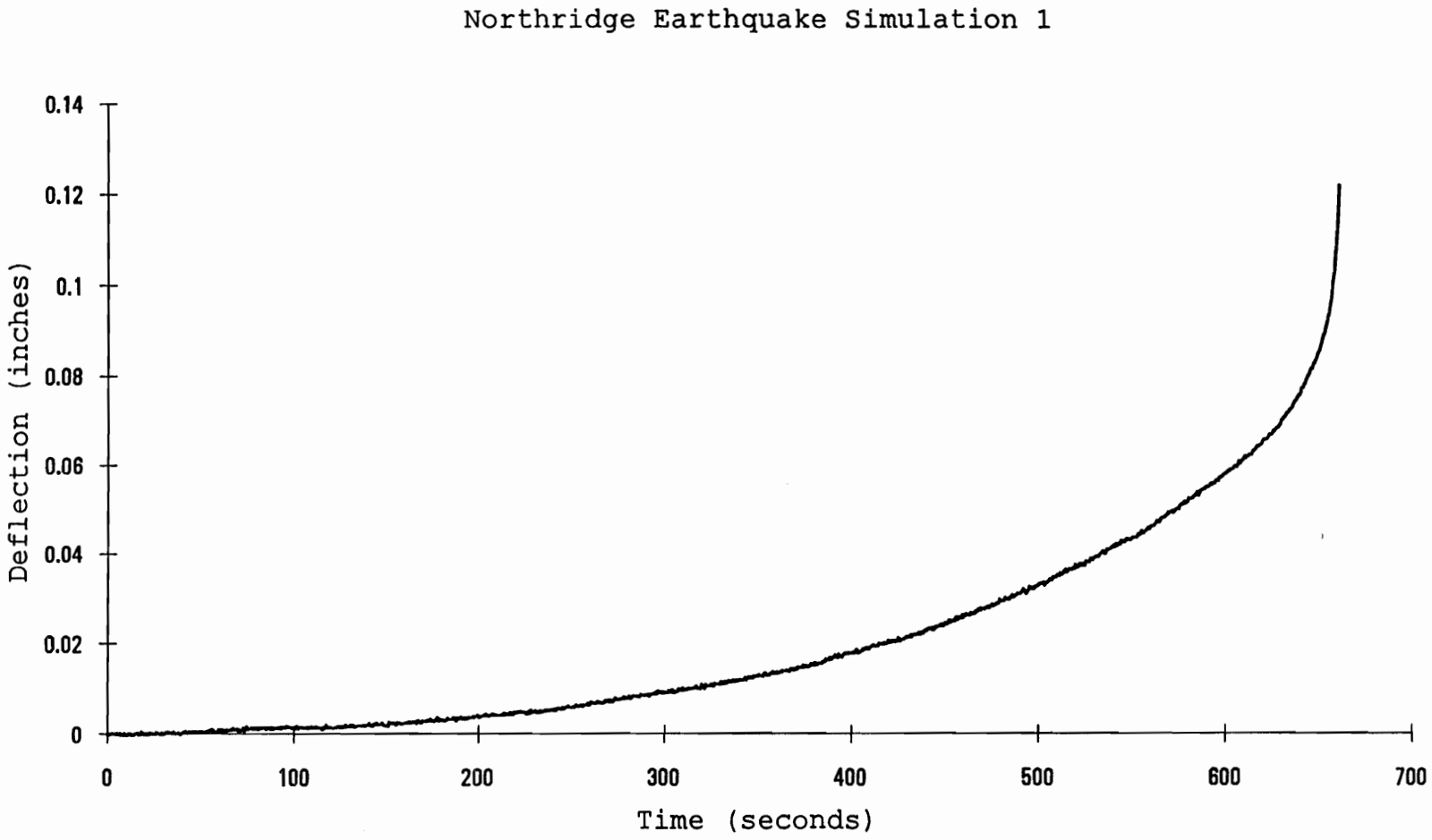

Figure 3.23: Deflection-time curve for the Northridge earthquake simulation (joint 1, batch-1)

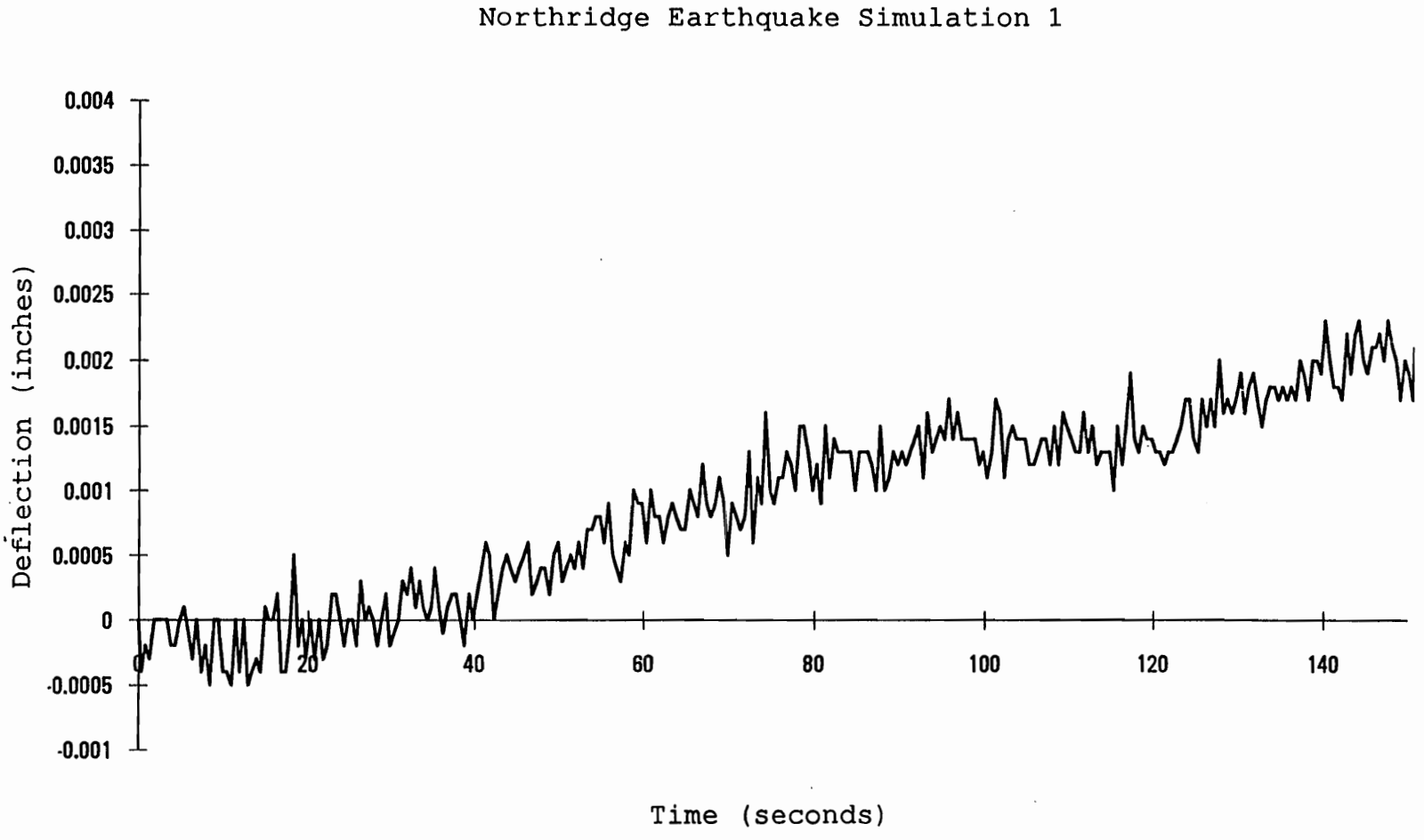

Figure 3.24: Close-up of the deflection-time curve for the Northridge earthquake simulation (joint 1, batch-1)

The "random" nature of the earthquake loads caused some loading control difficulties. First, the frequency components over 10 Hz were largely filtered out by the testing apparatus. As shown in Figure 3.25, the majority of the energy of the target force-time-history from the FEM is contained below 10 Hz. Therefore, the passive filtering by the hydraulic system should not significantly affect the results. Second, a small time lag of approximately 0.1 seconds occurred between the input to the hydraulic cylinder and the actual response of the hydraulic cylinder. Figure 3.26 displays how the testing apparatus responds to the force-time-history input during the most dynamic portion. The dashed line represents the target forces predicted for the tension-splice joint from the FEM. The solid line represents the actual measured forces applied to the tension-splice joints. The time lag, seen in Figure 3.26, does not significantly affect the results due to the fact that approximately the correct magnitudes of the loads are generally obtained, approximately 0.1 seconds behind their intended time.

To construct Figures 3.25 and 3.26, a pilot test joint, not included in the overall strength or stiffness results, was used to record the actual forces applied by the testing system during the earthquake simulation. To accurately record the force time-history for the pilot test tension-

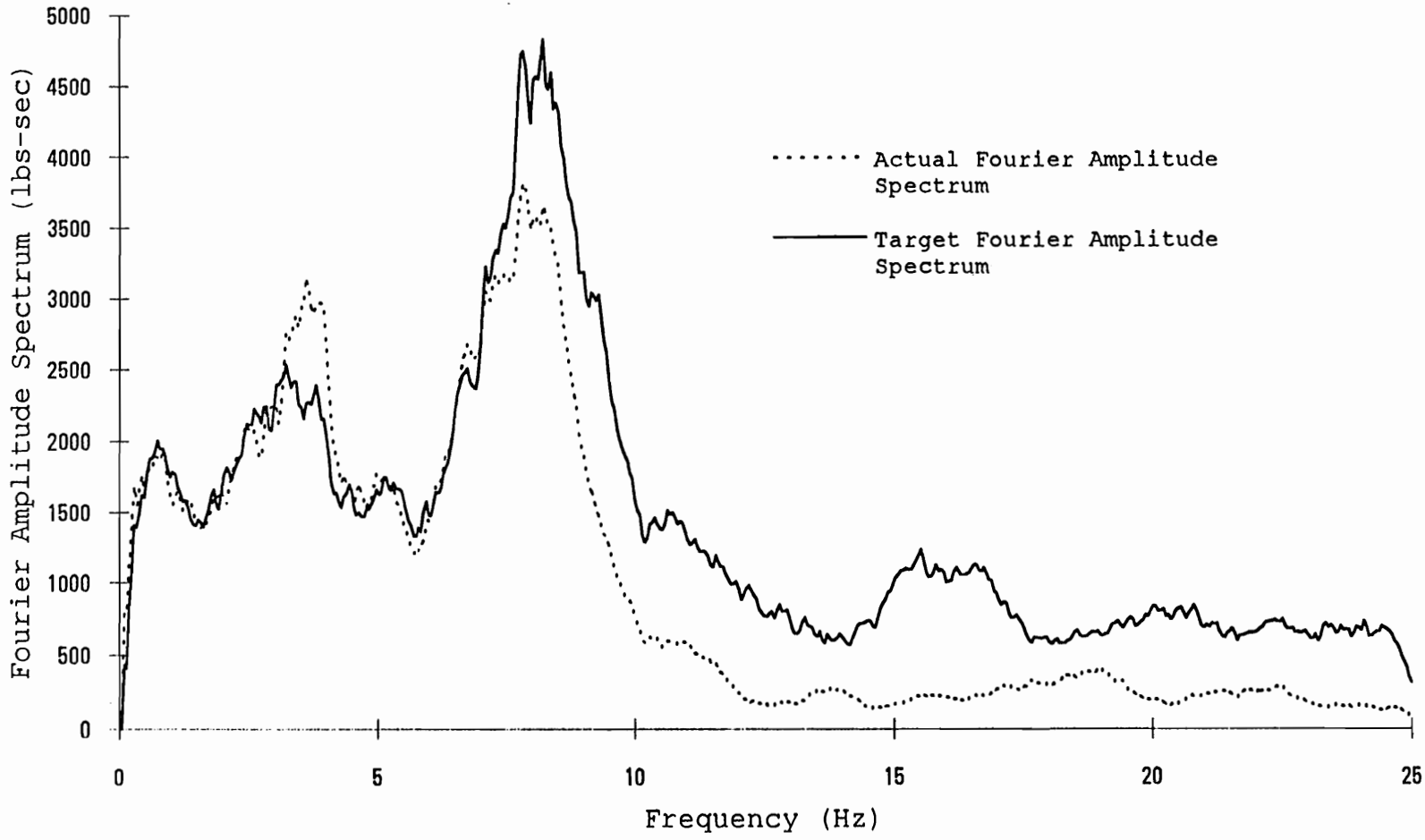

Figure 3.25: Fourier amplitude spectrum comparison between the target and actual forces during the Northridge earthquake simulation

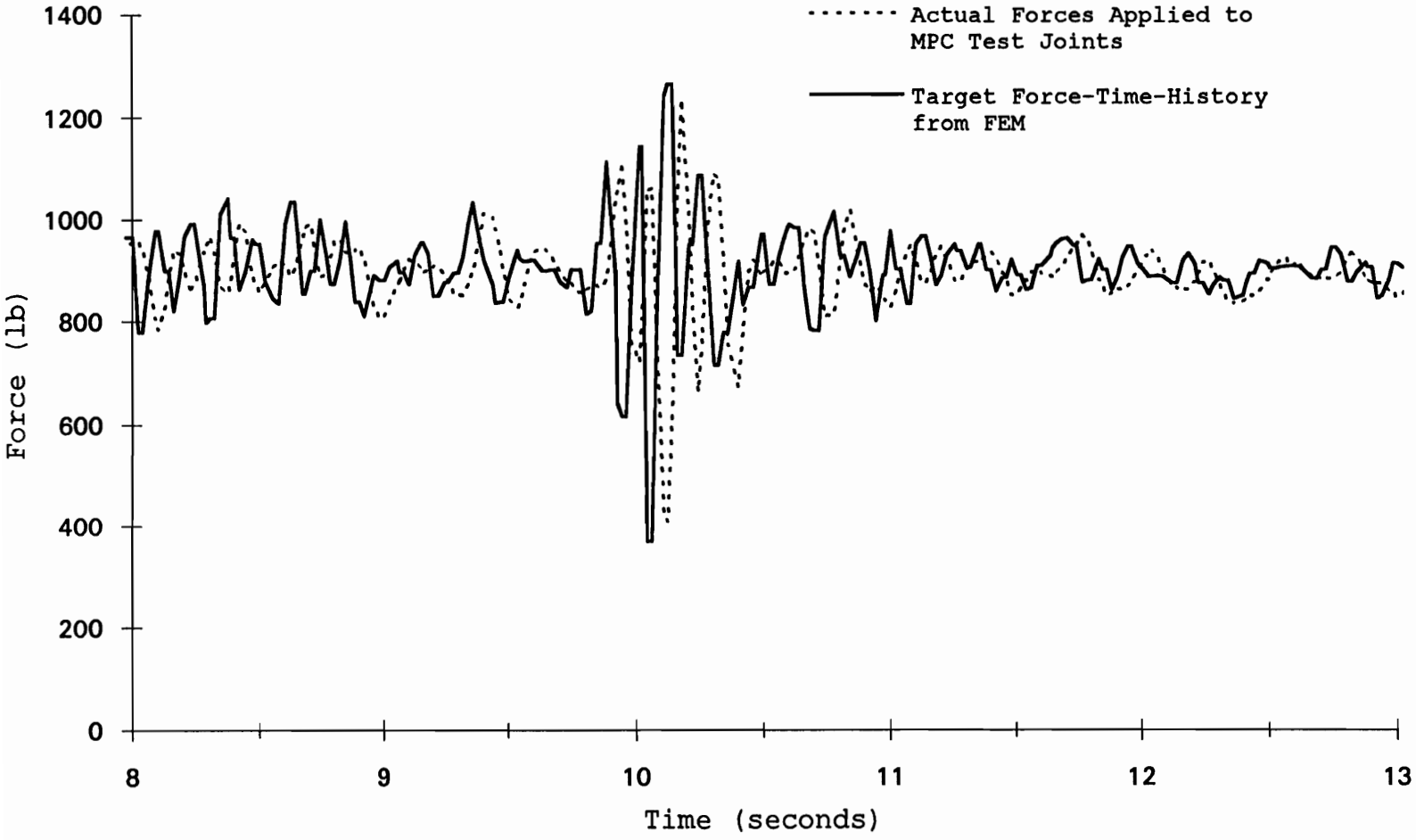

Figure 3.26: Target and actual forces during a portion of the Northridge earthquake loading

splice joint under the earthquake loading, a data acquisition rate of 50 Hz was used. However, using a 50 Hz data acquisition rate for the actual testing (which includes the ramp-load portion) far exceeded the memory capacity of the computer used for data acquisition. For actual testing, an acquisition rate of 2 Hz was used.

3.3.4 Artificial Earthquake Tests (batch-2)

The average strength and stiffness of the tension-splice joints after being subjected to the artificial earthquake load time-history were 6482 lb with a COV of 12.5% and 3.46×10^5 lb/in. with a COV of 15.1% (Appendix D), respectively. Strength and stiffness degradation did not occur as a result of the artificial earthquake when compared to the static strength for batch-2 plates (two sided p-values of 0.49 for strength degradation and 0.18 for stiffness degradation, respectively, see section 3.1 and Table 5.1).

Figure 3.27 shows a typical load-deflection curve (for joint 7) including the earthquake time-history. A close-up of the earthquake portion of the curve is also shown in Figure 3.27. This close-up view shows how the joint responded to the earthquake loading. The data acquisition rate was only 2 Hz which was not sufficient to completely

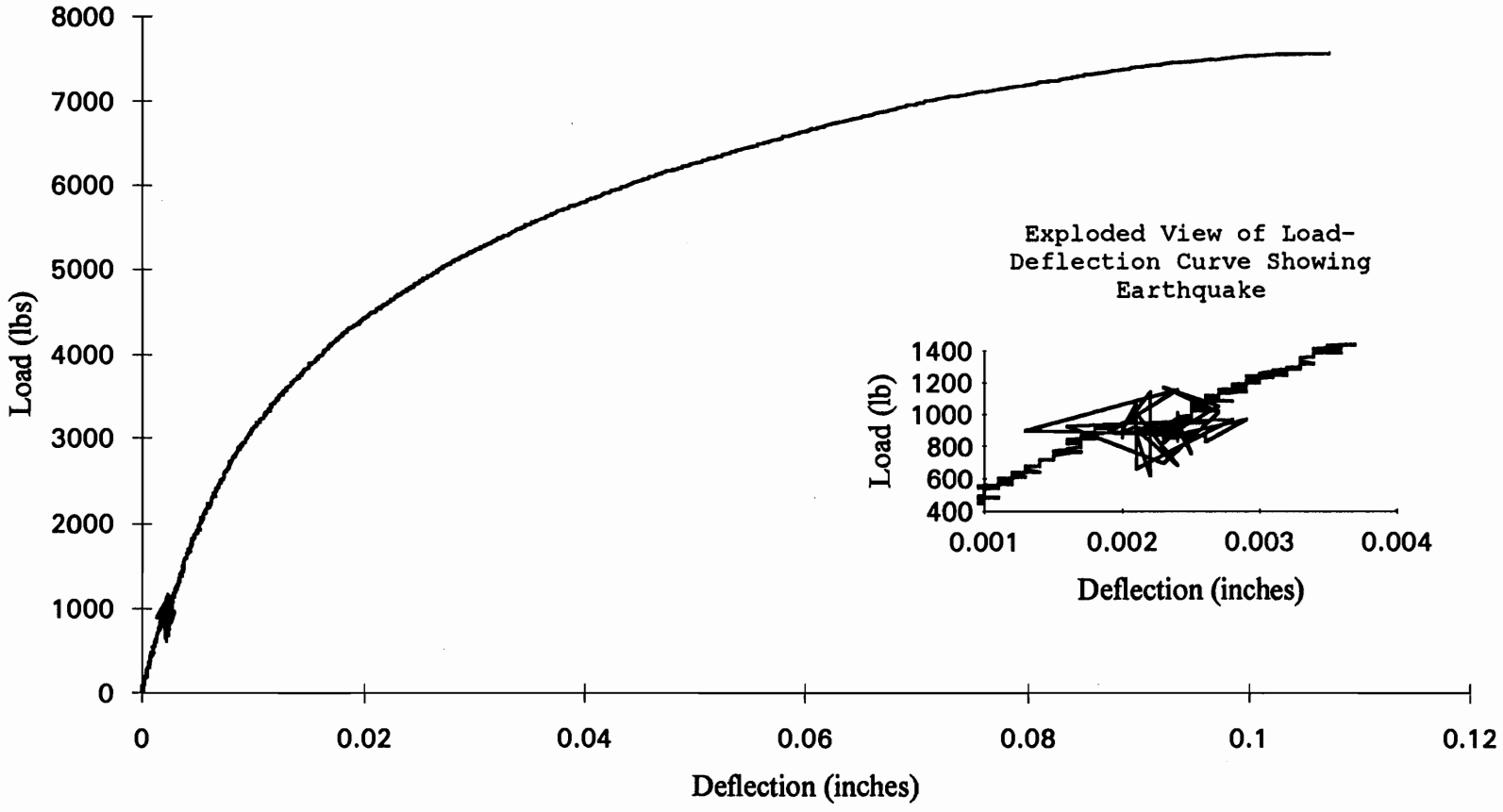

Figure 3.27: Typical load-deflection curve during the artificial earthquake simulation (joint 7, batch-2)

define the load-deflection trace (a 50 Hz acquisition rate would be required.

The absence of strength and stiffness degradation from the earthquake simulation tests can be explained. As shown in Figure 3.16, the maximum load developed in the tension-splice joint during the artificial earthquake simulation (1489 lb) is less than 22% of the average ultimate load for tension-splice joints (6712 lb for batch-2, Appendix D). Larger amplitude loads or repeated applications of the earthquake time-history may, however, cause strength degradation in tension-splice joints. But, the artificial earthquake ground accelerations were, by design, very large (1.0-g's maximum horizontal acceleration, 0.67-g's maximum vertical acceleration). Therefore, larger amplitude forces applied to a tension-splice joint are unlikely. Although, at this point, the effect of repeated applications of a large artificial earthquake time-history is unknown, it is possible that strength and/or stiffness degradation would occur.

Figure 3.28 shows the deflection-time curve (for joint 1 for the artificial earthquake simulation, batch-2). Figure 3.29 displays a close-up view of Figure 3.28 showing the earthquake portion of the test which occurs between 70 and 100 seconds. Figures 3.28 and 3.29 show that the artificial earthquake simulation has very little effect on

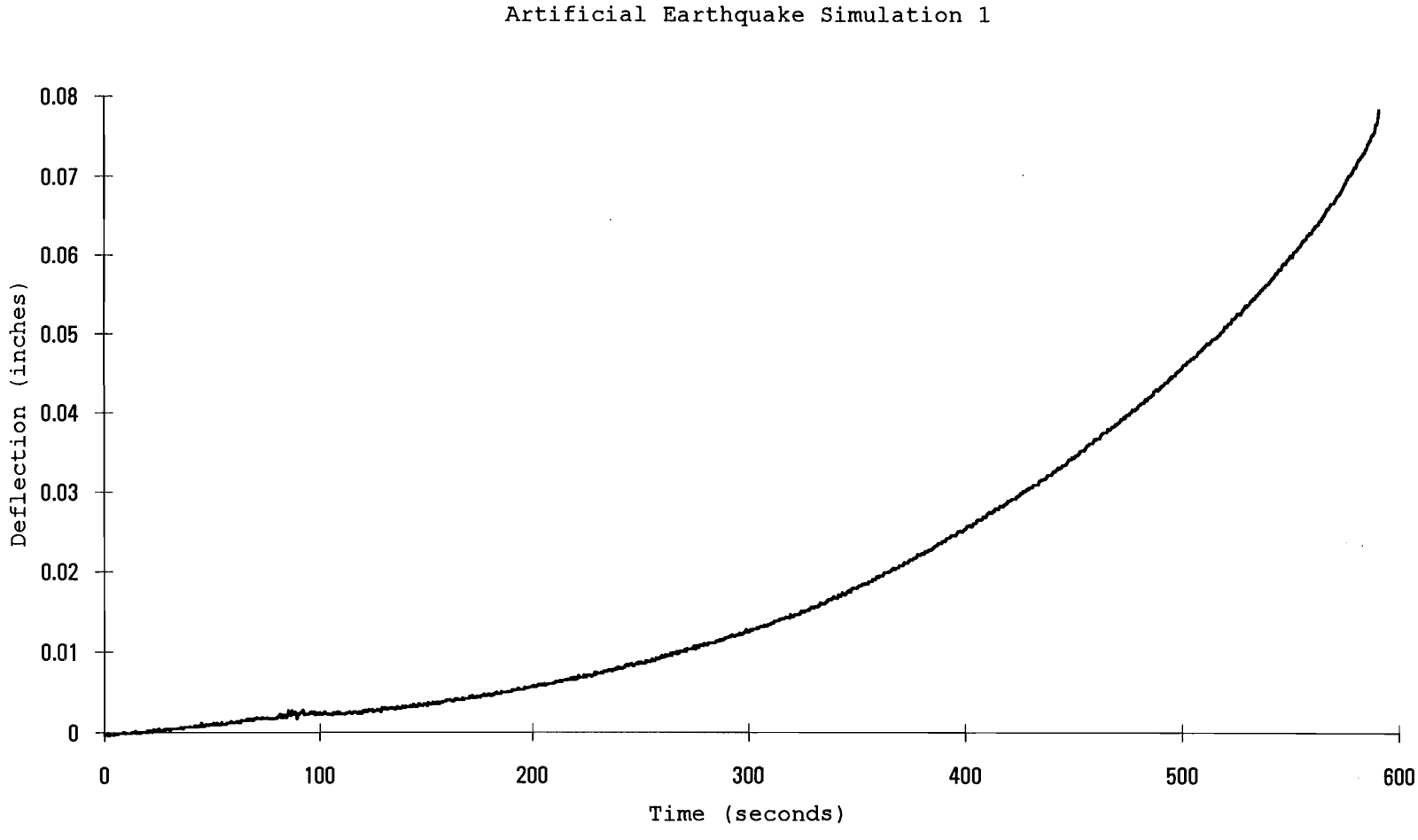

Figure 3.28: Deflection-time curve for the artificial earthquake simulation (joint 1, batch-2)

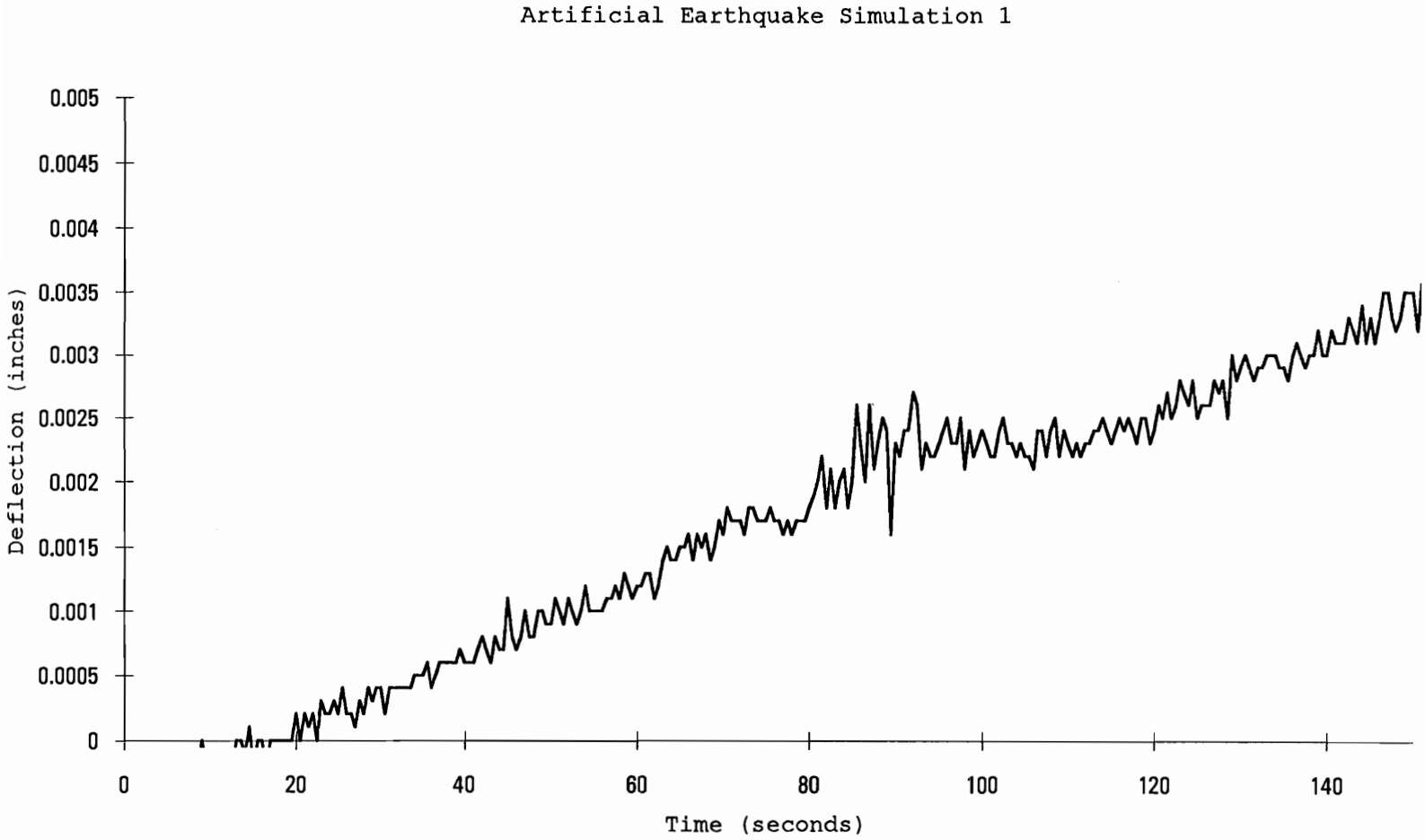

Figure 3.29: Close-up of the deflection-time curve for the artificial earthquake simulation (joint 1, batch-2)

the joint. Appendix E contains the deflection-time curves for all of the artificial earthquake simulation tests with their corresponding close-up views. In the close-up views, the white noise from the LVDTs can be seen as the deflection generally increases. The earthquake begins at approximately 70 seconds, after the first portion of the ramp load and ends at approximately 100 seconds, which is followed by the continuation of the static ramp load. Generally, the deflections tend to increase with time, corresponding to the increasing ramp load.

Figure 3.30 displays the Fourier amplitude spectrum of the target and actual force time-histories. This plot was constructed using the FFT (Microsoft Excel, version 4.0a) method as discussed for the Northridge earthquake loading in section 3.3.3. Figure 3.30 indicates that frequency control during the artificial earthquake simulation was superior to frequency control during the Northridge earthquake loading (by comparison to Figure 3.25). The actual Fourier amplitude spectrum tends to more closely follow the target Fourier amplitude spectrum. This is most likely due to the placement of the hydraulic actuator, grips, and specimen in a stiffer location in the testing frame as shown in Figure 3.4 (section 3.2.2).

Figure 3.31 displays both the target force time-history trace and the actual forces applied by the hydraulic

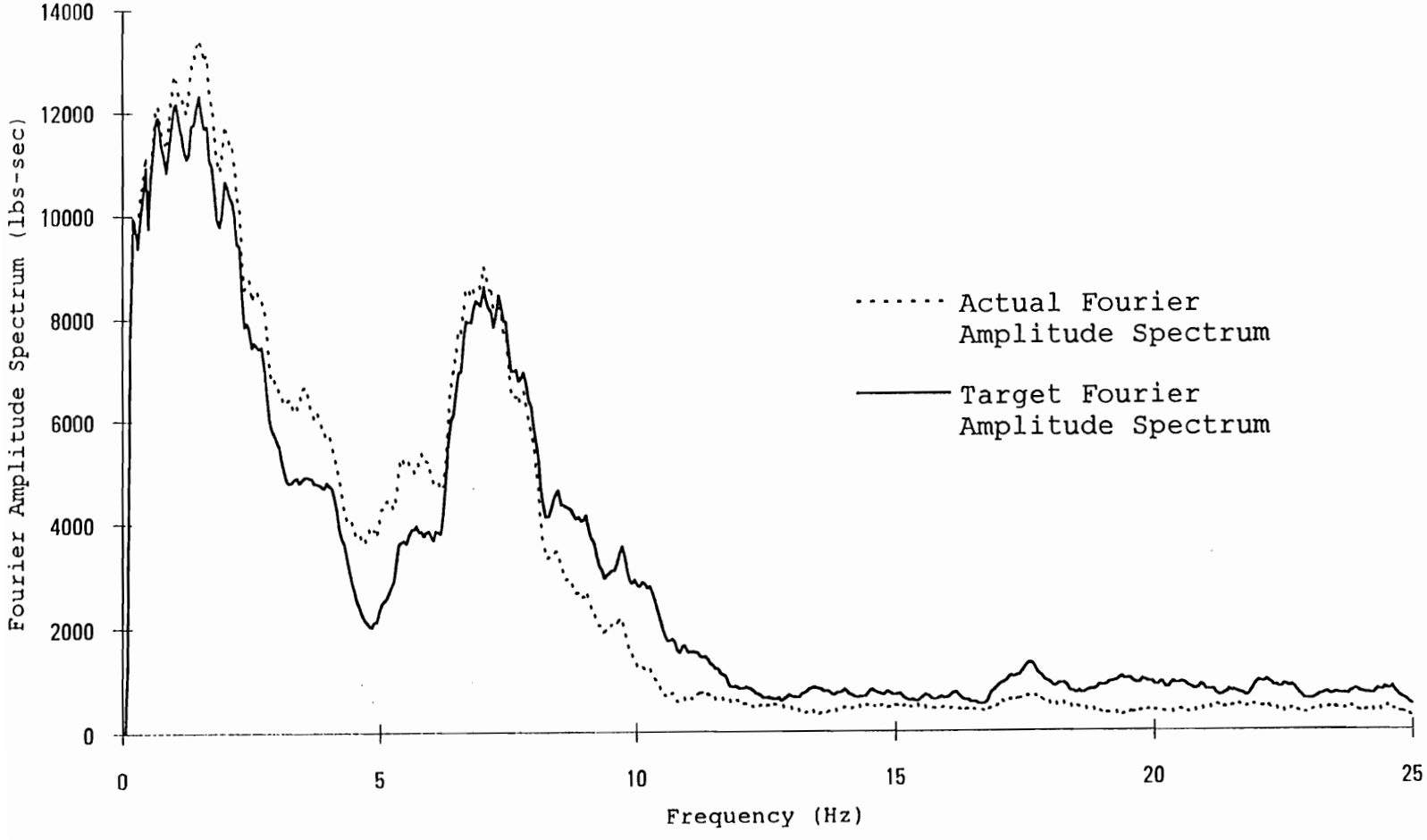

Figure 3.30: Fourier amplitude spectrum comparison between the target and actual forces during the artificial earthquake loading

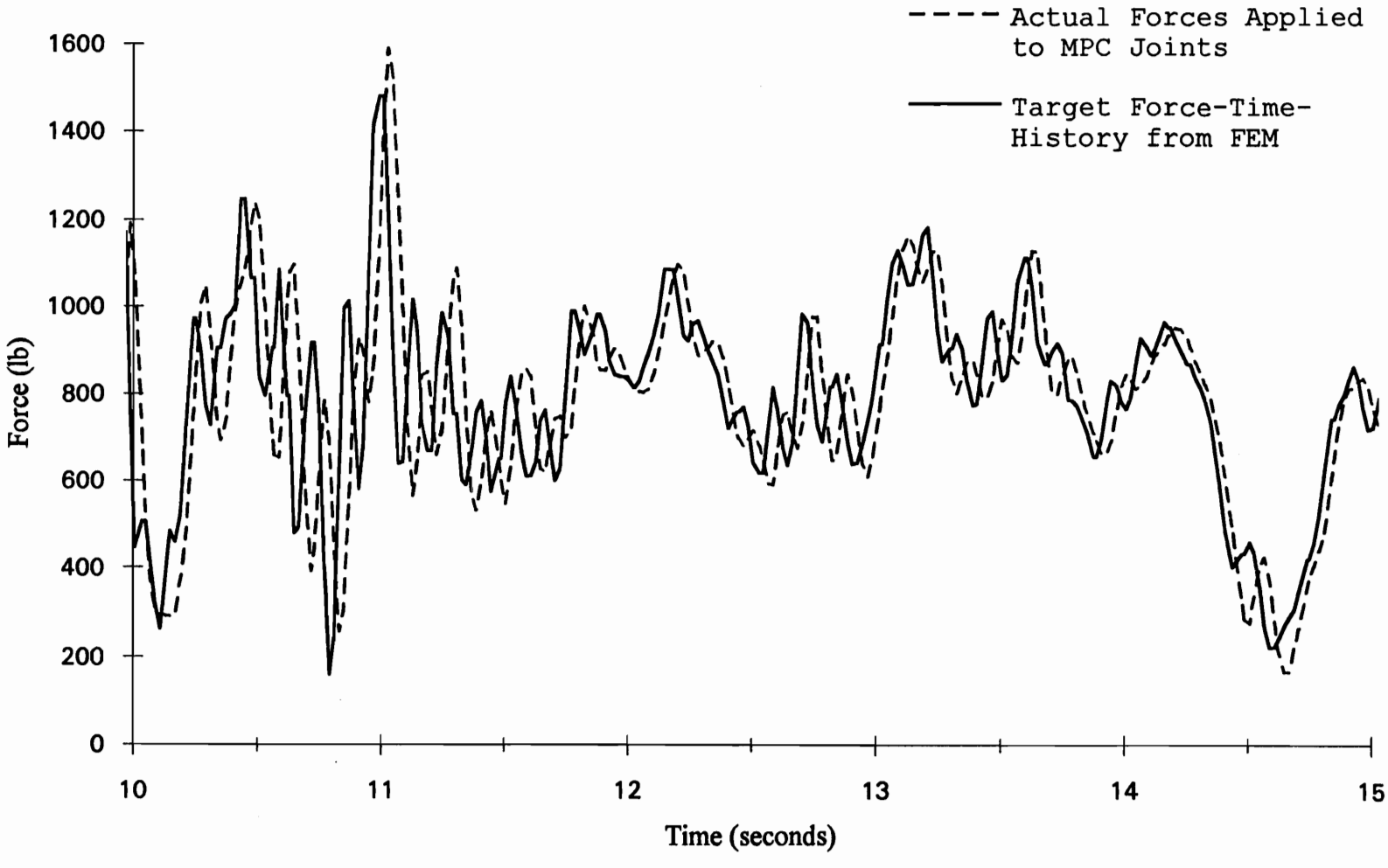

Figure 3.31: Target and actual forces during a portion of the artificial earthquake simulation

cylinder during a segment of the artificial earthquake simulation. The dashed line represents the desired forces predicted for the tension-splice joint from the FEM. The solid line represents the actual measured forces applied to the tension-splice joints. The time lag, seen in Figure 3.31, does not affect the results due to the fact that approximately the correct magnitudes of the loads are generally obtained, although approximately 0.1 seconds behind their intended time.

To construct Figures 3.30 and 3.31, a pilot test joint, not included in the overall strength or stiffness results, was used to record the actual forces applied by the testing system during the earthquake simulation. To accurately record the force time-history for the pilot test tension-splice joint under the earthquake loading, a data acquisition rate of 50 Hz was used. However, using a 50 Hz data acquisition rate for the actual testing (which includes the ramp-load portion) far exceeded the memory capacity of the computer used for data acquisition. For actual testing, an acquisition rate of 2 Hz was used.

3.3.5 Sequential Phased Displacement (SPD) Loading (batch-1)

The average strength and stiffness of the tension-splice joints subjected to the SPD loading and then failed under a static ramp load were 7189 lb with a COV of 4.87% and 1.89×10^5 lb/in. with a COV of 13.7% (Appendix D), respectively, where the stiffness was as defined in section 3.3.1. A statistical analysis (section 3.1, and Table 5.1), compared with the static loading control group from batch-1, indicates that the SPD loading did not significantly reduce the mean strength of the tension-splice joints (two sided p-value of 0.63); however, stiffness degradation did occur as a result of the SPD loading (two sided p-value=0.000).

Control difficulties were also encountered during the SPD tests. The difference between the maximum tensile load and the maximum compressive load in each cycle could approach as much as 14,000 lb. This difference required a loading rate of 28,000 lb/sec, which appeared to be near the maximum capabilities of the testing system. The effect of operating near the limits of the hydraulic system was a significant decrease in control. Also, the deflection feed-back loop was controlled by linearly-variable differential transducers (LVDTs) which had an approximate resolution of 0.0007 in. A higher resolution would be preferred to tighten the control of the deflection feed-back loop when working with such stiff connections.

Appendix F contains plots of the deflection-time and load-time curves for the tension-splice joints during the SPD loading. Generally, the compressive loads tend to increase at a higher rate than the tensile loads with time. This implies that the tension-splice joint is stiffer in compression than tension. Also, the deflection tends to be symmetrical during the test, following the prescribed sequential phased displacement loading (Figure 3.17). Large changes in the shape of the deflection curve (Appendix F, joint 2, and joint 6) may imply that a local failure has occurred in the wood.

Because the compressive loads on the tension-splice joints during the SPD loading were so large (up to 10500 lb), there was some out-of-plane movement of the joint. As the compressive load increased, the tension-splice joint tended to move downward slightly (less than 0.25 in). Therefore, a moment was created at the connection. Because there was no statistical evidence (section 3.1, and Table 5.1) of strength degradation as a result of the SPD loading, it can be assumed that the out-of-plane movement had no significant effect on the strength of the tension-splice joints.

The following dynamic properties, as defined by Dolan (1994), for tension-splice joints were evaluated using the SPD method: energy dissipation, equivalent viscous damping

ratio, and cyclic stiffness. These dynamic properties are described below and computed from individual hysteresis curves. Recall that the amplitudes of the cycles in the SPD loading are defined in terms of displacement as a percent of the yield displacement (determined from static tests for the type of connection and plate batch being studied). The dynamic properties of MPC tension-splice joints are then plotted against the deflection as a percent of the yield displacement. The percent of yield displacement is defined as the maximum displacement in the hysteresis curve being analyzed, divided by the yield displacement from the static loading control group (0.006 in, batch-1, Appendix D).

The hysteresis curve used in this study for calculation of the dynamic properties was not necessarily the stabilized hysteresis curve. The SPD method defines a stabilized cycle as one in the set of stabilizing cycles (defined in Figure 3.17) that has a load degradation of no more than 5% from the preceding cycle. Because of the control difficulties discussed above, it was not possible to impose this definition of a stabilized hysteresis curve to these tests on tension-splice joints. The testing system was able to control the deflections only within 4 to 7% of the target deflection. For example, if at a point during the SPD loading the deflection of the joint should have been 0.01 in, the actual deflection obtained from the testing system

would have been, on average, somewhere between 0.0093 in. and 0.017 in. Therefore, the third cycle in each set of stabilization cycles was arbitrarily used as the stabilized hysteresis curve to plot the hysteresis curve used for calculation of the dynamic properties. For nailed and bolted connections, only three stabilizing cycles are necessary to obtain a stabilized hysteresis curve (Dolan 1994). Henceforth, in this paper, the third cycle in the set of three stabilizing cycles is referred to as the stabilized cycle and is used to compute the dynamic properties.

Energy dissipation is the area enclosed by the load-deflection trace. Because tension-splice joints may behave differently in tension and compression, dynamic properties are calculated separately in this study for the two different load directions. Energy dissipation in tension (EA_t) is shown as the area confined by GAFCG (Figure 3.32). Similarly, the energy dissipation in compression (EA_c) is shown as the area confined by FDGCF. The energy input to the system follows the line, DCA. Therefore, the energy input in tension (EI_t) is shown as the cross-hatched area CAB. Also, the energy input in compression (EI_c) is shown as the cross-hatched area CDE.

The equivalent viscous damping ratio, or damping ratio, is a dimensionless parameter used to describe the resistance

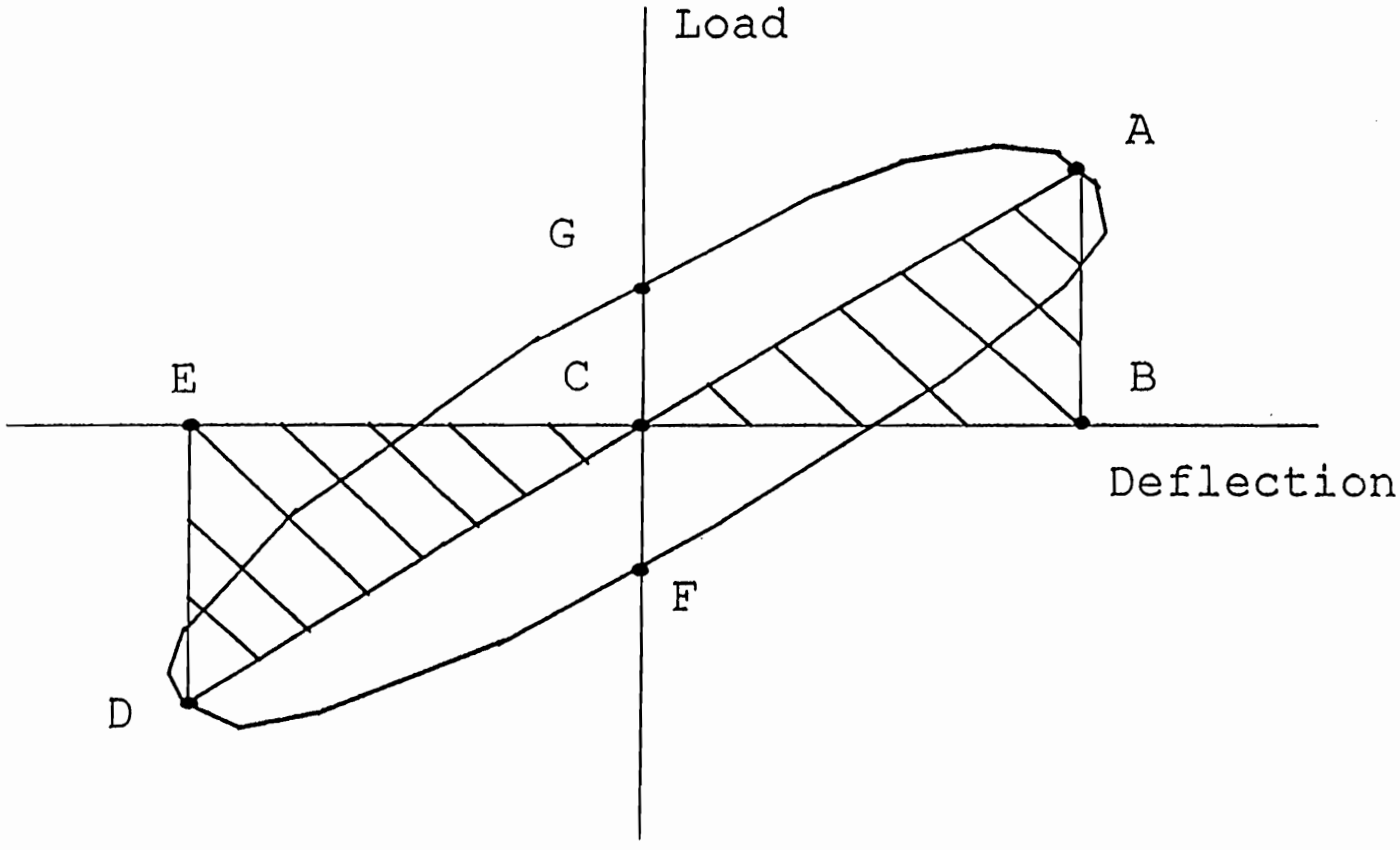

Figure 3.32: Hysteresis curve definitions (Dolan 1994).

to motion/deformation which is provided by friction in the connector and inelastic deformation (Breyer 1993). Under most circumstances, the damping ratio cannot be directly calculated from basic material properties and structure geometry, therefore, testing is required to determine this parameter for various systems.

With the above definitions of energy dissipation and energy input, the damping ratios for tension and compression, ξ_t and ξ_c, respectively, for any given cycle, may be approximated by the following formulas. Example calculations to determine the dynamic properties are presented in Appendix G.

$$\xi_t = EA_t/2\pi \cdot EI_t \quad \text{.....3.1}$$

$$\xi_c = EA_c/2\pi \cdot EI_c \quad \text{.....3.2}$$

A digitizing tablet (Calcomp Digitizer Products Division, Model No. 33120) was used to calculate the areas enclosed by the tensile and compressive regions of the hysteresis curves. Plots of the energy dissipation and damping ratio as functions of the displacement as a percent of yield displacement are shown in Figures 3.33 and 3.34, respectively.

Currently, there is no standard to determine a design level damping ratio from the SPD loading. For this study,

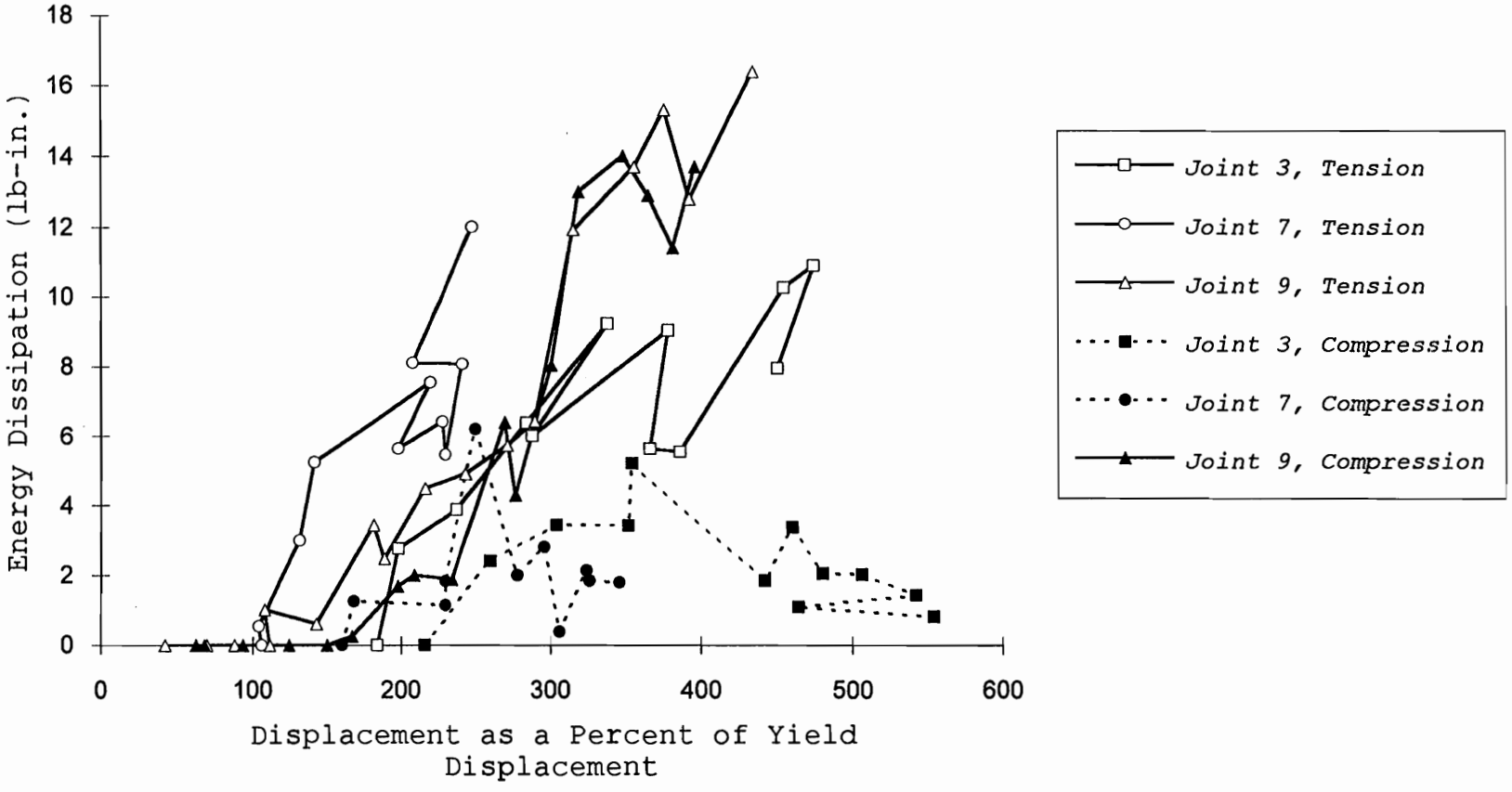

Figure 3.33: Energy dissipation of the tension-splice joints during the SPD loading

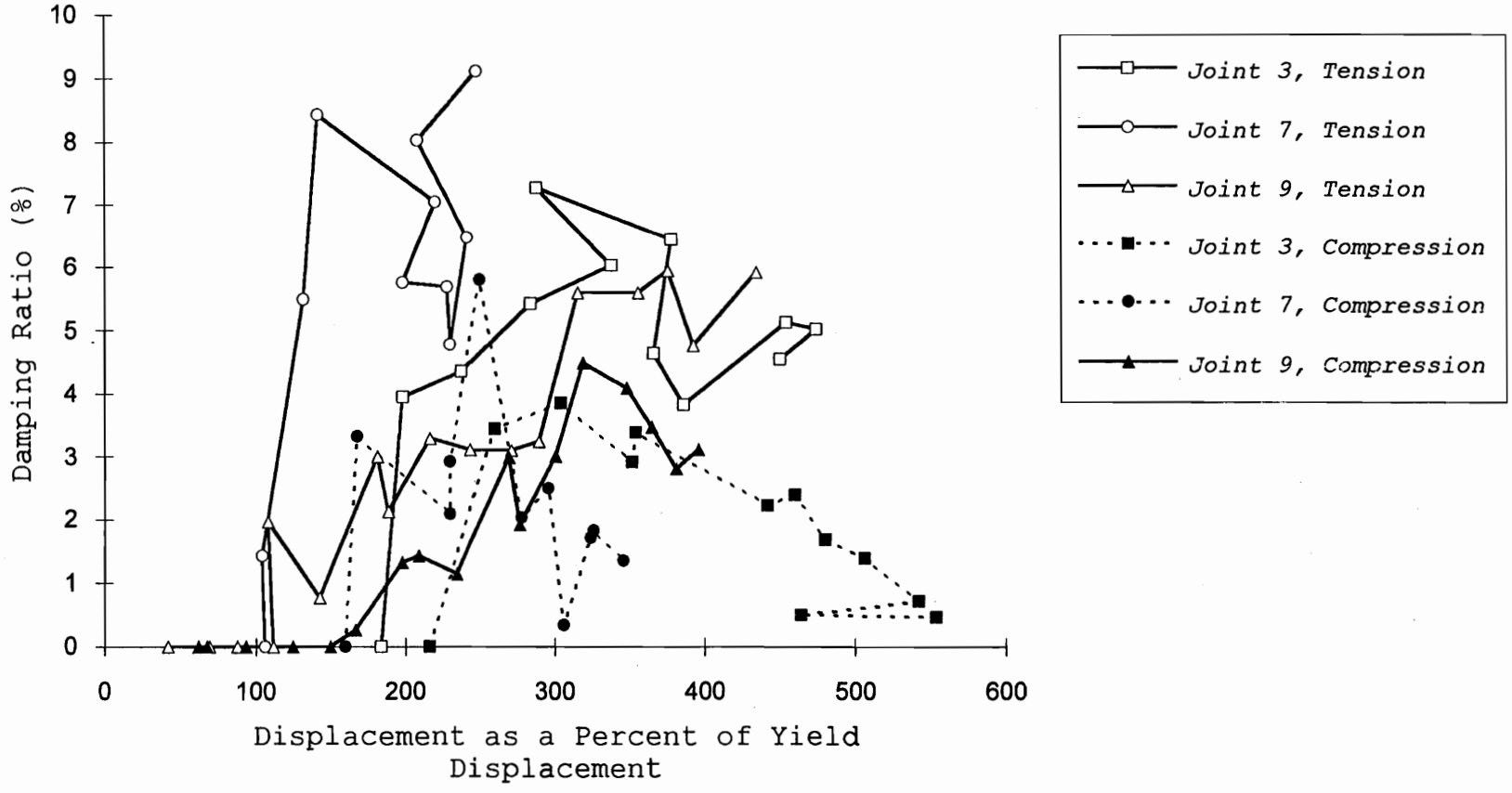

Figure 3.34: Damping ratio of the tension-splice joints during the SPD loading

it was decided to compute the damping ratio associated with the first stabilized hysteresis curve to have a maximum tensile load equal to, or exceeding, the design load for the tension-splice joint (approximately 33% of the average ultimate load, Appendix D, 0.33•7284=2404 lb.). Because tension-splice joints are not actually designed for compressive loads, only the damping ratio associated with tensile loads is presented. Table 3.4 displays a summary of the design damping ratio calculations from the SPD loading. Based on the above definition of design levels, a damping ratio of 4.3%, corresponding to the average of the damping ratio values presented in Table 3.4, is recommended for design. Because of the control difficulties, only three tests (joints 3,7, and 9) produced hysteresis curves from which the energy dissipation and damping ratio could be measured. In some cases, a more detailed examination of Figure 3.34 is suggested. Factors to consider are the number and amplitude of the cycles the tension-splice joint is expected to experience in service. It may be appropriate to select the damping ratio (from Figure 3.34) associated with the specific level of displacement expected for the joint in service.

Dolan (1994) defines the cyclic stiffness as the slope of a straight line drawn between the lower left of the hysteresis curve to the upper right of the hysteresis curve,

Table 3.4: Summary of the damping ratio calculations from the sequential phased displacement loading

Joint	Cycle Number	Energy Dissipation (lb-in.)	Damping Ratio (%)
3	50	3.45	5.49
7	43	6.38	5.43
9	29	1.03	1.97
Average	41	3.62	4.30

Note: See Appendix G for Sample Calculations for Joint 3

passing through the lowest and highest points. However, MPC tension-splice joints have different stiffnesses in the compressive and tensile directions; therefore in this paper, the definitions of cyclic stiffness for tension and compression are defined as the slopes of the lines CA and DC, respectively (Figure 3.32). A plot of the cyclic stiffness as a function of the displacement as a percent of yield displacement (0.006 in, defined from the static tests for batch-1, Appendix D) is shown in Figure 3.35. From this plot, it is clear that stiffness degradation does occur as the SPD loading progresses to greater displacement amplitudes. As the cycles progress (to a higher percent of yield displacement), less load on the joint is generally required to obtain a given deflection because of the accumulated damage in the wood fibers at the tooth-wood interface.

In tension, the above cyclic stiffness definition applies well because the tensile half of the hysteresis curve, or tension-half-cycle, remains relatively linear; however, as the SPD loading progresses, the compressive-half-cycle become increasingly nonlinear (increasing stiffness at higher loads, see Figures 3.37 and 3.38). This nonlinearity in the compression half-cycle is due to the closure of the gap between the two members of the joint. Figure 3.36 displays a typical plot of the axial load time-

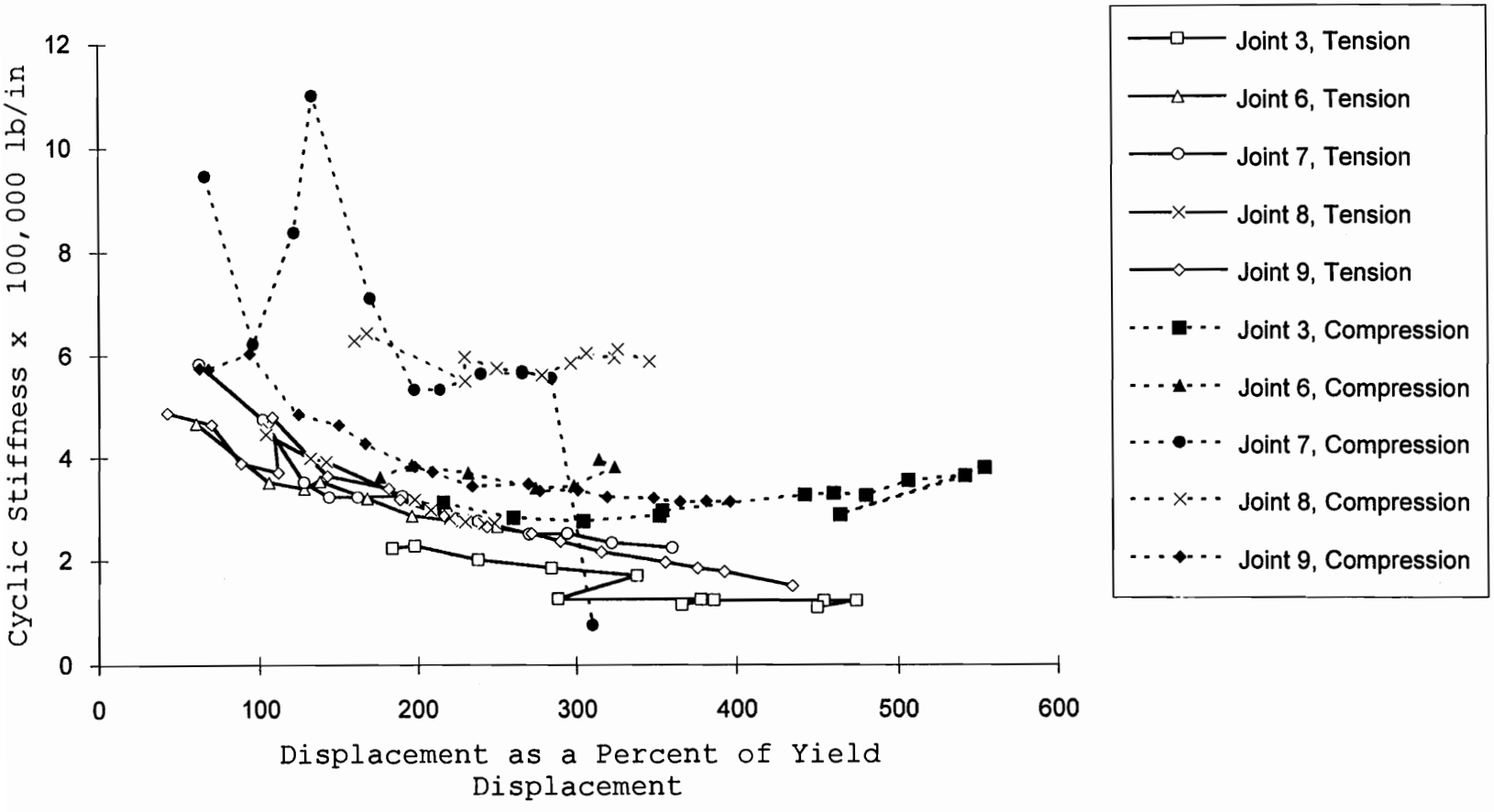

Figure 3.35: Cyclic stiffness of the tension-splice joints during the SPD loading

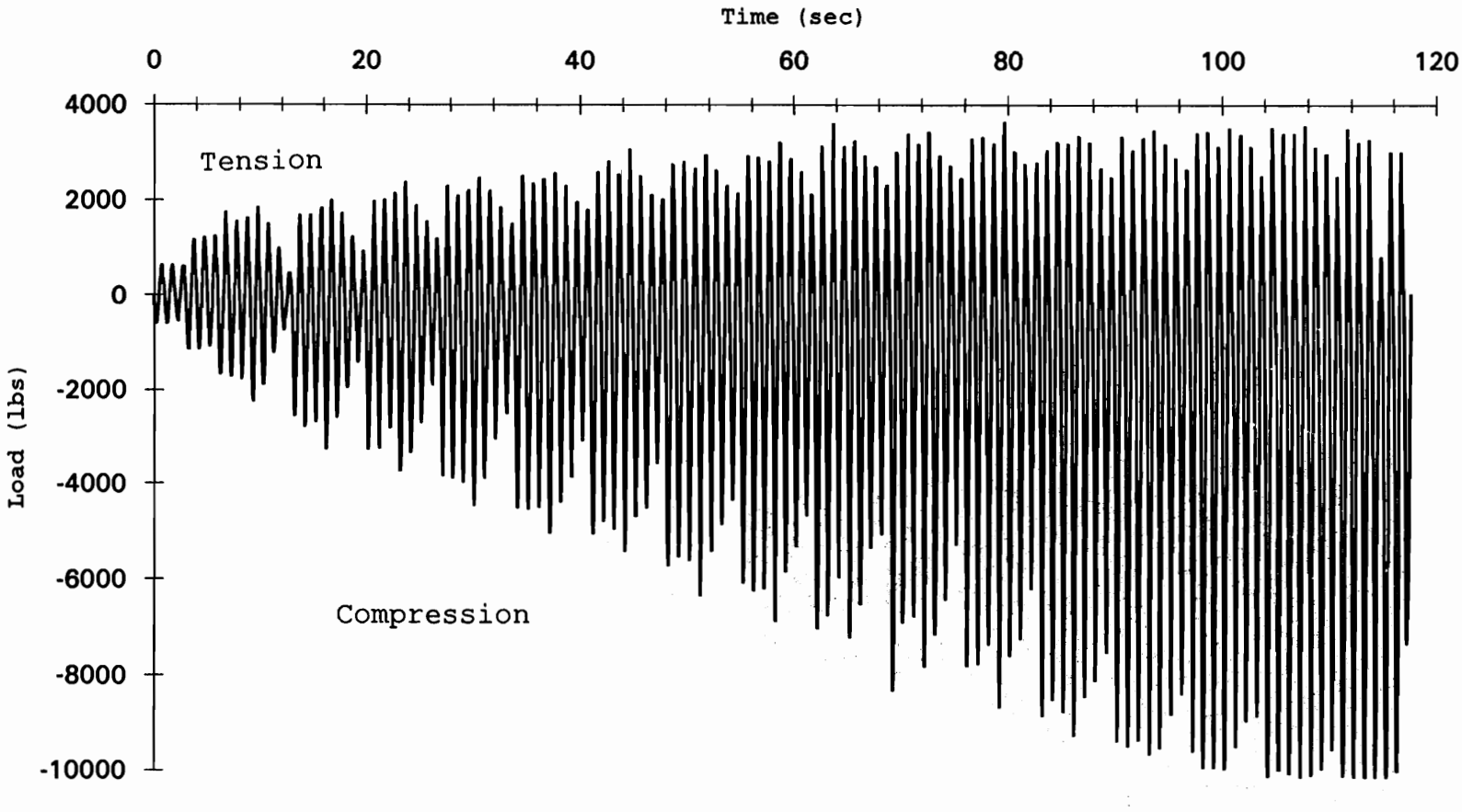

Figure 3.36: Typical load-time curve for the tension-splice joints during the SPD loading (joint 3, batch-1)

history for the tension-splice joint during the SPD loading (batch-1, joint 3). The tensile-side of the curve (positive loads) tends to level out as the SPD loading progresses. This is directly related to the decreasing stiffness of the connection (less load required to obtain the same deflection as the cycles progress). However, on the compressive-side of this plot, the compressive loads tend to be much larger than the tensile loads for any given cycle, especially towards the end of the test. This can be attributed to closure of the gap between the two members of the joint to the point where they are in direct contact.

Although Figures 3.33, 3.34, and 3.35 are quite variable, specific trends can be seen. The energy dissipation and damping ratio generally tends to increase with increasing percent of yield displacement during the SPD loading for the tension half-cycle; however, the compressive half-cycle does not show any clear increasing or decreasing trends. Cyclic stiffness generally tends to decrease with increasing displacement (as a percent of yield displacement) for both the tension and compression half-cycles. This implies that the connection is accumulating damage in the wood at the tooth-wood interface. The damaged wood fibers at the interface decrease the stiffness of the overall connection as they deform inelastically. It can be assumed that bending of the teeth and axial strain of the metal-

place-connector contribute somewhat to the deflection recorded by the LVDTs. However, because the teeth are embedded into the wood, the amount of bending is difficult to assess. At failure, though, slight bending of the teeth can be seen (see Figure 3.19). Also, strain gauges were not used to measure the complicated strain distribution in the metal-plate.

As the SPD loading progresses, the shapes of the hysteresis curves change. As shown in Figure 3.33, the energy dissipation generally increases with increasing displacement as a percent of yield displacement (for the tension-half cycle), which implies that the hysteresis curves are confining a larger area. Figure 3.37 shows a typical hysteresis curve (joint 3) at low load levels. Notice that very little area is confined by the curve. Figure 3.38 shows a typical hysteresis curve (joint 3) at a higher load level. The area confined by the curve has increased by 218% (from 3.45 lb-in. to 7.53 lb-in.).

3.3.6 Cyclic Loading Tests (batch-2)

The results of the cyclic loading tests are tabulated in Table 3.5 and plotted in Figure 3.39. The vertical axis of Figure 3.39 is the ratio of the maximum strength of the tension-splice joint under a static ramp load after completion of the 200-cycles to the average maximum strength

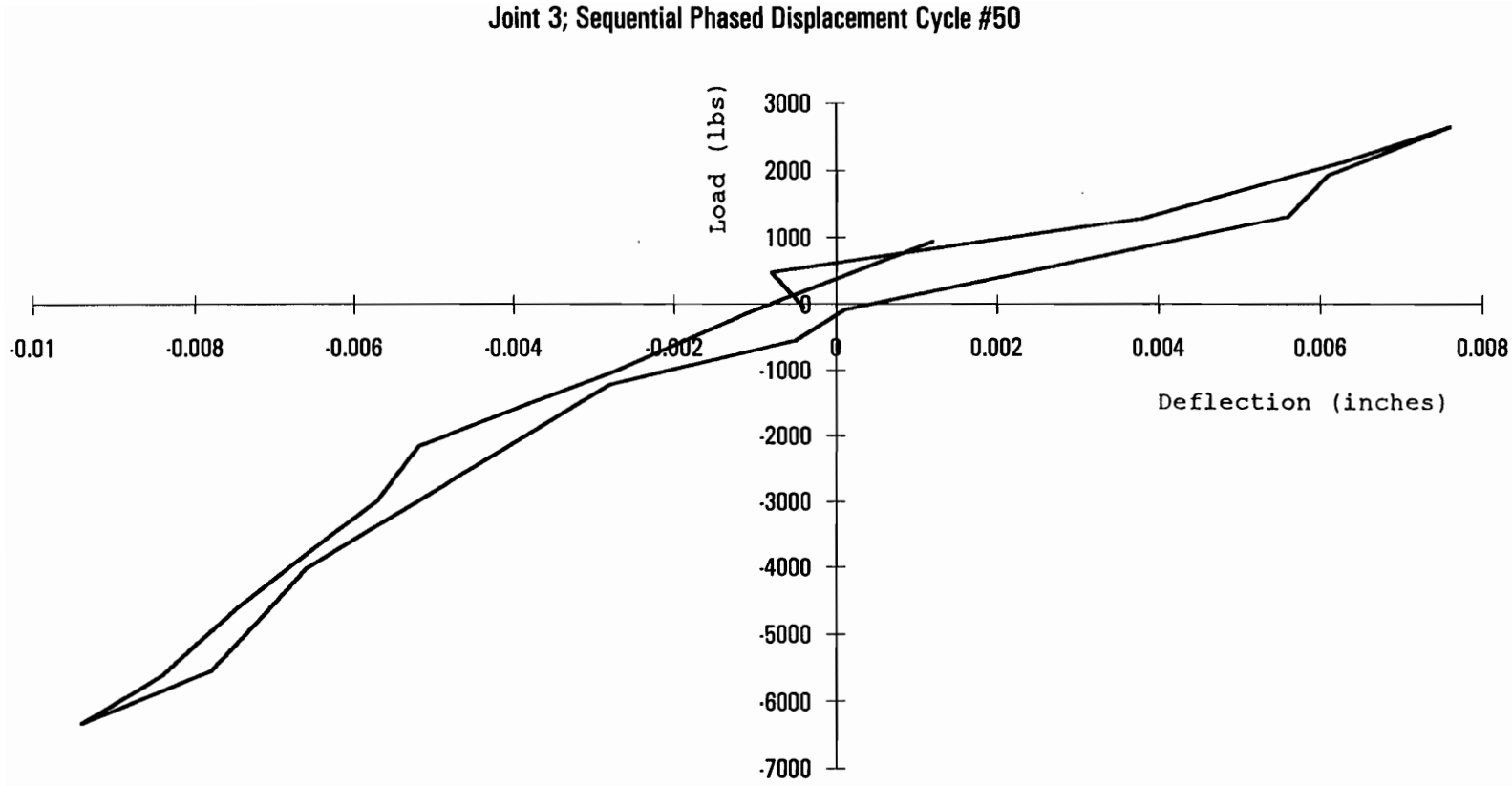

Figure 3.37: Hysteresis curve at a low load level during the SPD loading (joint 3, batch-1, cycle 50)

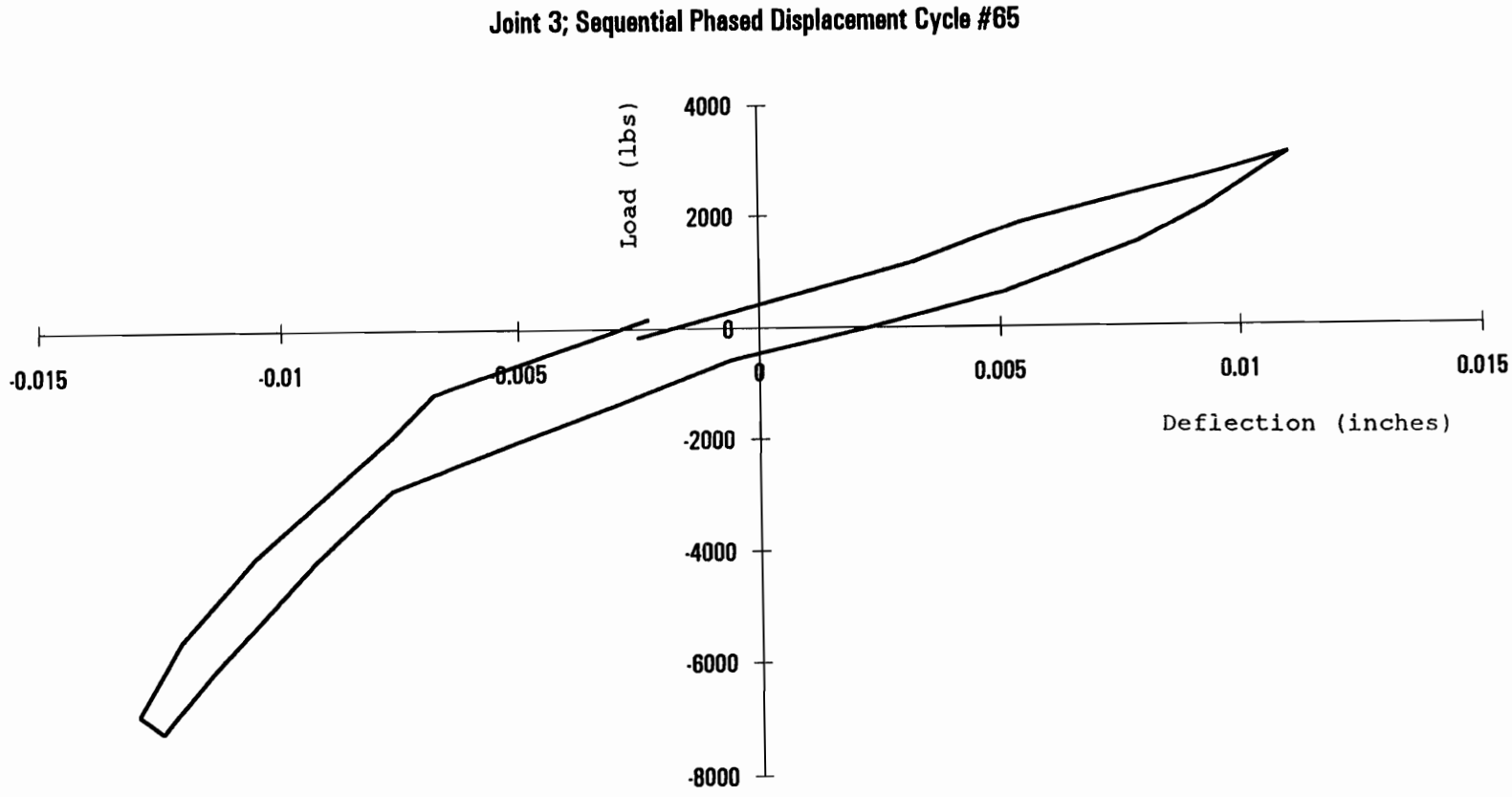

Figure 3.38: Hysteresis curve at a high load level during the SPD loading (joint 3, batch-1, cycle 65)

Table 3.5: Cyclic loading test results for tension-splice joints.

Test Number	Cyclic Amplitude (%)	Strength (lb)	Strength Ratio (1)
1	0.00	7428	1.11
2	0.00	6969	1.04
3	0.00	7034	1.05
4	0.00	6251	0.93
5	0.00	5840	0.87
6	0.00	6319	0.94
7	0.00	7192	1.07
8	0.00	6298	0.94
9	0.00	7074	1.05
10	8.22	5837	0.87
11	8.22	7930	1.18
12	8.22	4246	0.63
13	12.33	4208	0.63
14	12.33	3520	0.52
15	12.33	7549	1.12
16	14.80	7272	1.08
17	15.62	4479	0.67
18	16.44	6895	1.03
19	16.44	4647	0.69
20	18.08	0	0.00
21	18.08	0	0.00
22	18.08	6786	1.01
23	19.73	6660	0.99
24	19.73	0	0.00
25	19.73	0	0.00
26	20.55	0	0.00
27	20.55	0	0.00
28	20.55	0	0.00
29	24.66	0	0.00

(1) Actual Strength/Static Strength; Static Strength Average of tests 1-9 alone = 6712 lb (Appendix D)

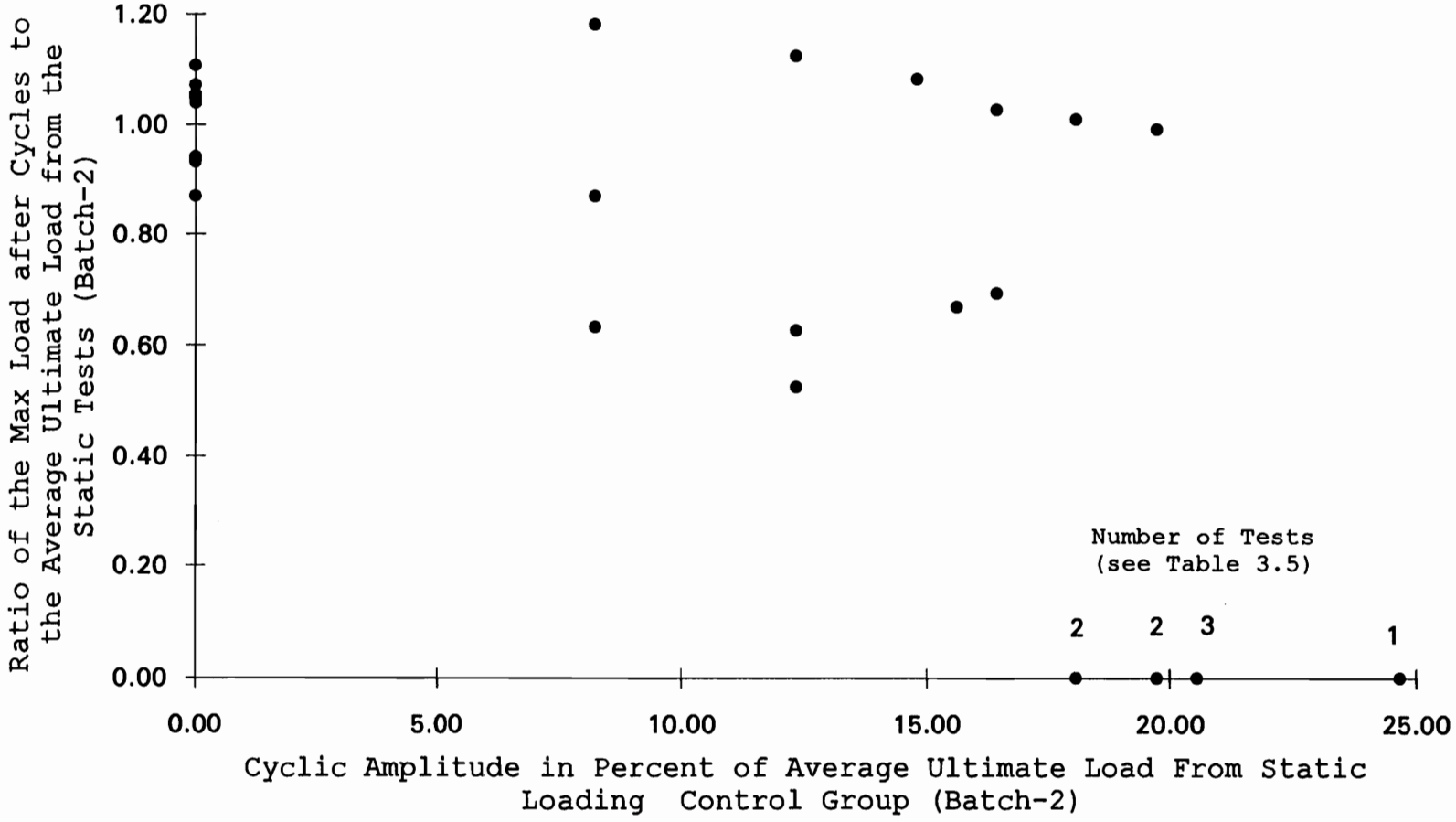

Figure 3.39: Cyclic loading test results

of the static loading control group (strength ratio) for batch-2. The horizontal axis (cyclic amplitude) is the amplitude of the cycles divided by the average maximum strength of the static loading control group for batch-2 (6712 lb, Appendix D) and expressed as a percentage (see Figure 3.18 for actual cyclic loading function). For a joint to be assigned a nonzero post-cyclic loading strength, it must be able to carry load after the conclusion of the 200-cycles. Joints which failed during the cyclic loading were assigned a zero strength ratio. The results for the static loading control group (batch-2) are plotted on Figure 3.39 at zero percent cyclic amplitude.

There appears to be a distinct threshold between 20 and 23% cyclic amplitude where tension-splice joints are no longer able to survive the entire set of cycles. Note that Chapter 5 contains further discussion and the implications for design of the cyclic loading results.

4. Dynamic Behavior of Metal-Plate-Connected Heel Wood Truss Joints

4.1 Experimental Design

This study is to serve as a preliminary investigation into the effects of a variety of dynamic loads on metal-plate-connected heel joints. The hypothesis being tested is that earthquake and cyclic loads decrease the strength and stiffness of metal plate connected (MPC) heel joints. The different loadings are described in detail in section 4.2. The mean strength and stiffness of the heel joints under each dynamic loading are compared to those from a control group (static ramp load, section 4.2.3.1). A t-test procedure, assuming equal variance, for comparing two sample means is used to analyze the strength and stiffness results. A two-sided p-value of 0.05 is chosen as the cutoff significance level. That is, if the statistical test indicates a two-sided p-value less than 0.05, then the conclusion of the test is that the means of the two populations are significantly different. Otherwise, if the p-value is greater than 0.05, there is not enough evidence to suggest that the means of the two populations are significantly different. The coefficient of variation (COV), defined as the standard deviation divided by the mean and expressed as a percentage, is presented with the results

to provide an indication of the variance. Table 4.1 lists the groups of tests examined in this study and provides the sample size for each group. Table 5.1 summarizes the statistical results of the tests.

ASTM D2915-94 is used to estimate the required sample size, given an estimated COV, to determine the lower 5% exclusion limit with 95% confidence. Ten percent is a conservative estimate for the COV of MPC heel joints (Gupta 1990). Using the procedure in ASTM D2915-94, a sample size of 18 is necessary for testing MPC heel joints. This required sample size is much greater than the sample size used in this research; therefore, an accurate estimate of the allowable properties of MPC heel joints is not possible. However, the purpose of this research is to determine how the dynamic loadings affect the mean strength and stiffness, not to determine the 5% lower exclusion limit.

There were a number of potential sources of variability the fabrication and testing of the heel joints. A single machine stress rated wood grade (1800f-1.6E) and a single batch of metal-place-connectors were used to fabricate the plates (section 4.2.1). The heel joint specimens were all tested in the same location in the testing frame (section 4.2.2). Moisture content was controlled by use of an environmental conditioning room. All the joints were fabricated using the same press (high pressure hydraulic

Table 4.1: Heel joint tests

Test	Sample Size
Control Group (Static Ramp Load)	9
Artificial Earthquake Simulation	10
Sequential Phased Displacement	9
Cyclic Loading	25

press used to produce wood laminates). The location of the plate on the heel joint was carefully controlled (see Figure 4.1). A source of variation which was difficult to control was the deflection of the test frame as loads were applied to the top chord of the heel joint. As the testing frame deformed (less than 0.75 inches at 6000 lb compressive load in the top chord), the direction of the load applied to the top chord of the heel joint may not have been perfectly aligned along the axis of the top chord due to a small rotation of the support. This alignment difficulty may have resulted in a moment being applied through the top chord of the heel joint, thereby contributing to the variability in the moment-rotation curves (discussed in section 4.3.2).

4.2 Experimental Procedure

4.2.1 Materials

Test joints were fabricated from machine-stress rated Douglas-fir (1800f-1.6E) lumber which was conditioned at 70° F and 65% relative humidity to an equilibrium moisture content of approximately 14%. The heel joints were connected using 20-gauge punched 3x5 in. metal plates, supplied by Alpine Engineered Products Inc. (Pompano Beach, FL), which were pressed into the wood using a hydraulic press (between 0.02 and 0.04 in./second) until the teeth were entirely embedded into the wood surface. Care was taken

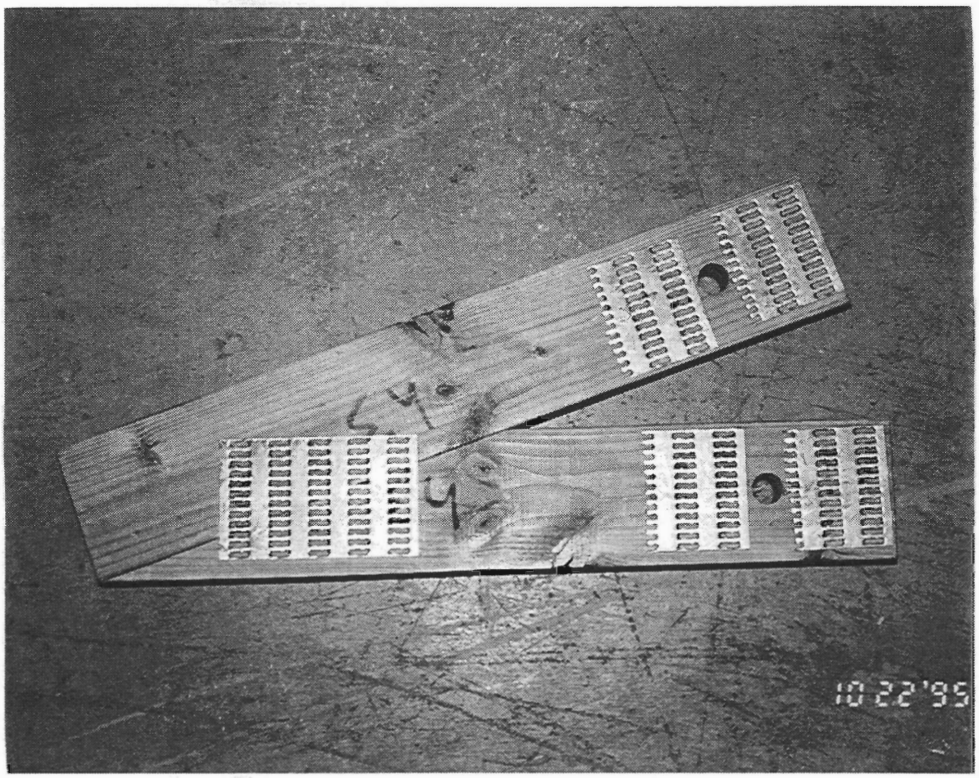

Figure 4.1: Photograph of a typical heel joint used in this study.

were entirely embedded into the wood surface. Care was taken not to over-press or under-press the plates by visually inspecting the fabrication of each connection. After construction, the joints were placed into the environment room again for a minimum of seven days and a maximum of 28 days before testing to allow stress relaxation of the wood fibers near the connection, as recommended by Arbek (1979). Figure 4.1 displays a photograph of a typical heel joint used in this study. Table 4.2 lists the physical characteristics of the metal plate connectors (properties provided by Alpine Engineered Products, Inc.).

4.2.2 Apparatus

A horizontal testing frame, developed by Gupta and Gebremedhin (1990), which allows for testing a versatile range of joint configurations, and an 11,000 lb capacity Materials Testing System (MTS) dynamic hydraulic actuator were used to apply the loads to the joints. Load was applied to the top chord of the heel joint through a 0.75 in. diameter pin which allowed for unrestrained rotation. Also, the bottom chord of the heel joint was attached to the grips through a 0.75 in. diameter pin. The pins were placed through a hole which was drilled through the centerline of the top and bottom chords, 2.63 in. and 3.25 in. from the end, respectively (see Figure 4.1). The specimen was

Table 4.2: Physical characteristics of the metal-plate-connectors

Plate Properties Provided by Alpine Engineered Products, Inc.

Parameter	Plate Property
Yield Strength (ksi)	51.5
Ultimate Strength (ksi)	60.5
Percent Elongation at Failure (%)	31.5
Thickness (in.)	0.036
Tooth Length (in.)	0.25
Tooth Width (in.)	0.12
Slot Length (in.)	0.25
Slot Width (in.)	0.12

positioned in the apparatus so that the load applied to the top chord of the heel joint was parallel to the axis of the top chord.

Relative displacements between the two wood members and rotation were measured by two alternating-current, linearly-variable differential transducers (LVDTs) placed as shown in Figure 4.2. The LVDTs were supplied an input voltage of 5-volts and returned a signal which was linear within a 1 in. range. Axial load was measured by two load cells (25,000 lb capacity) which were used to measure both the top and bottom chord loads. Each load cell was supplied with a 5-volt input.

The return voltages from the LVDTs and load cell were routed to an analog-to-digital card attached to a personal computer with an 80386 microprocessor and an 80387 math-coprocessor. The data acquisition/control software, Workbench PC 2.0 (Strawberry Tree, Inc.), controlled the feedback loops as well as the storage of data to the internal hard-drive.

A photograph of the LVDT placement is shown in Figure 4.3. The LVDT measuring rotation was securely connected to the bottom chord, and a reaction plate for the spring-loaded core is fastened to the top chord. The LVDT measuring axial movement of the top chord, relative to the bottom chord, was suspended over the top chord by a machined aluminum

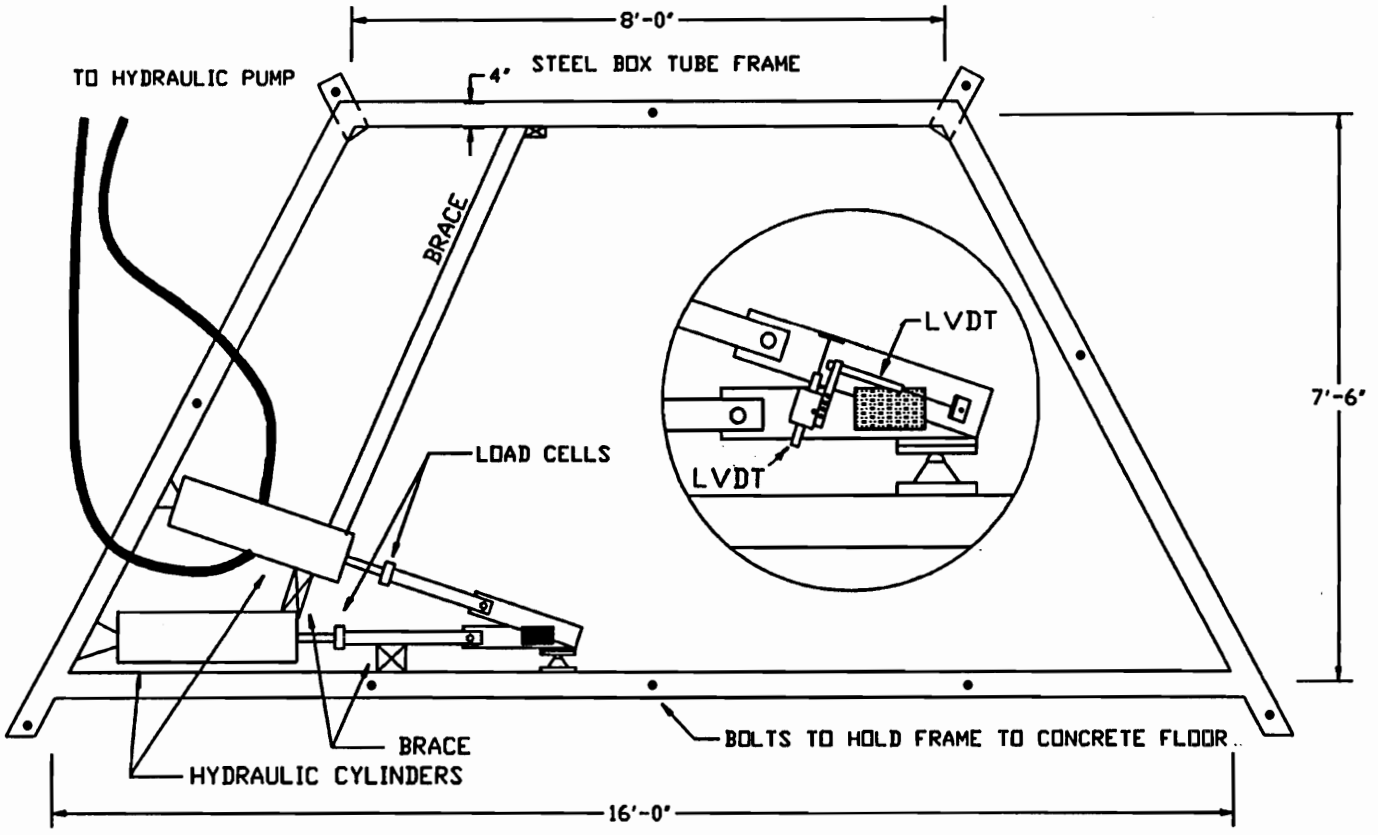

Figure 4.2: Testing setup used for the heel joint study.

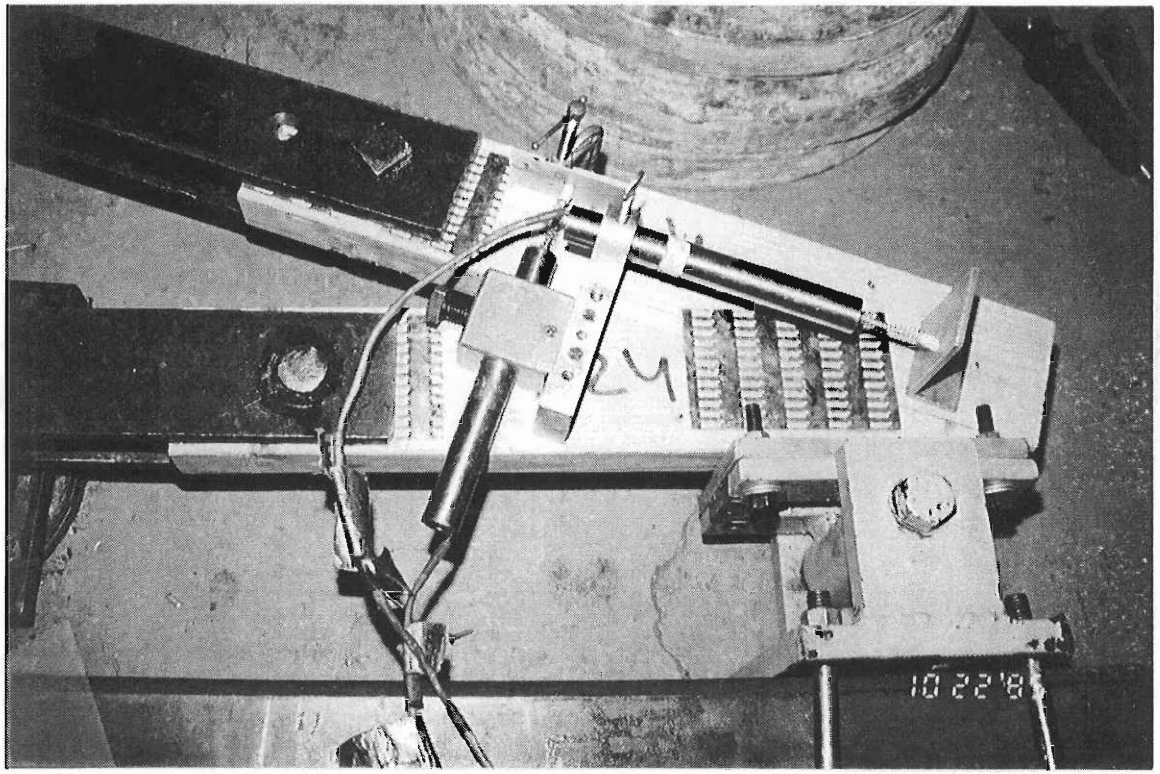

Figure 4.3: Photograph of the LVDT placement on the heel joints

connector, which was securely fastened to the bottom chord. The LVDT placement was intended to provide information about the relative movement of the top chord with respect to the bottom chord.

The two LVDTs shown in Figure 4.3 were used to measure the longitudinal deflection of the top chord relative to the bottom chord and rotation of the top chord in relation to the bottom chord of the heel joint. The LVDTs were placed in the same locations for all tests as shown in Figure 4.4 For the longitudinal deflection, a positive deflection corresponds to the response of the top chord to a compressive load (also defined as positive). A positive rotation implies that the acute angle between the top and bottom chord is increasing.

The support for the heel joint is shown in the lower right-hand corner of Figure 4.3. This support was designed to allow unrestrained rotation and lateral movement in the direction of the centerline axis of the bottom chord. The width of the support was 5.5 in. (6 in. nominal lumber) to simulate a typical bearing wall in a residential structure. With the use of three lag screws (used only in the sequential phased displacement tests) placed through a horizontal slot in the metal support and into the bottom chord, the support was able to restrain uplift caused by a tensile load in the top chord during the sequential phased

displacement (SPD) loading. Figure 4.4 shows how the lag screws were placed into the bottom chord of the heel joint. In applying the (SPD) loading to the heel joints, this restraint was essential because load reversals are developed which would cause the heel joint to lift off of the support (section 4.2.3.4).

As shown in Figure 4.2, the bottom chord of the heel joint was restrained using a hydraulic cylinder and a set of three braces. The cylinder was connected to the bottom chord of the heel joint through a 0.75 in. diameter pin which allowed unrestrained rotation. The purpose of the braces was to restrain movement of the hydraulic cylinders as the compressive loads were applied to the top chord. The hydraulic cylinder connected to the bottom chord was used essentially as a grip to hold the bottom chord in place while the loads were applied. Under dynamic loads (such as the artificial earthquake simulation, cyclic loading, and sequential phased displacement loading), the piston of the hydraulic cylinder was not completely restrained; a motion of less than 0.08 in. was observed. The support (shown in Figure 4.3), simulating the bearing wall, was designed to allow for this deflection. An oil lubricant was used to reduce friction at all points of movement around the support (between the wood and the steel support and around the contact areas between the steel support and the lag screws).

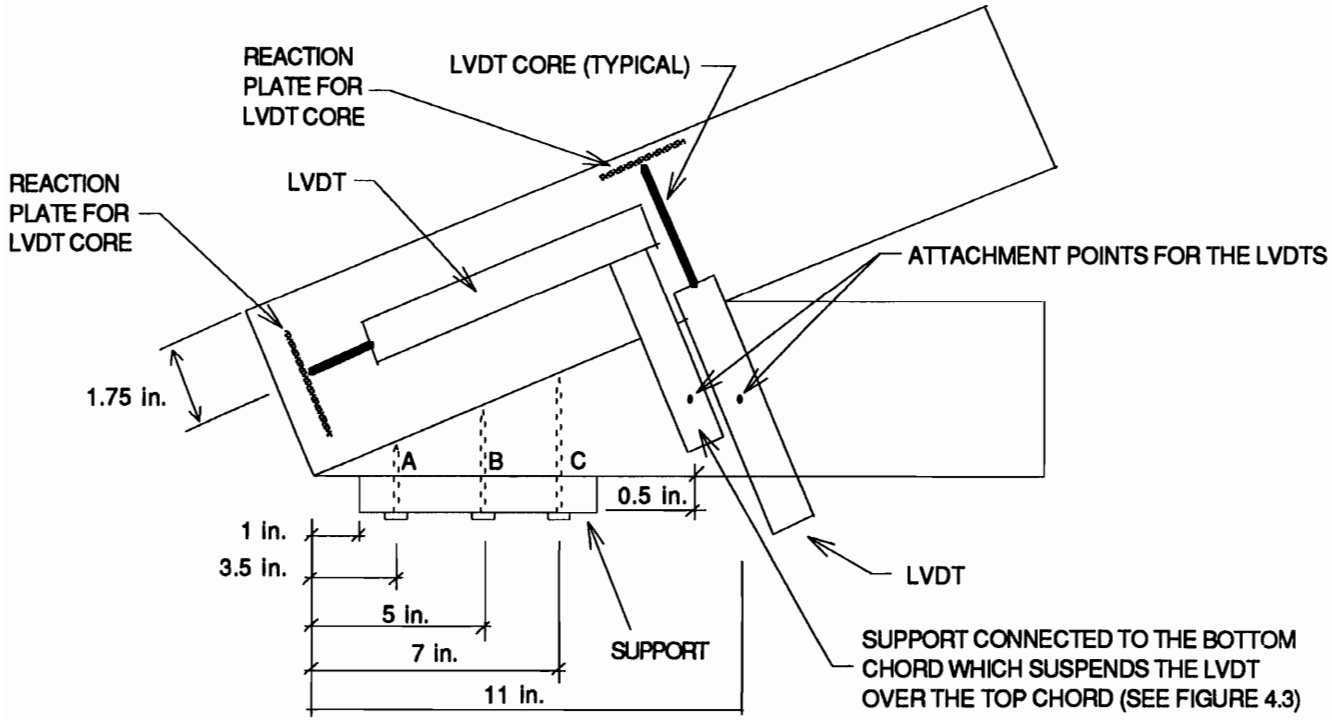

NOTES: A: 1.5 in. LONG LAG SCREW, 0.25 in. DIAMETER
B: 2.0 in. LONG LAG SCREW, 0.25 in. DIAMETER
C: 3.0 in. LONG LAG SCREW, 0.25 in. DIAMETER

Figure 4.4: LVDT and lag screw placement on the heel joint

Care was taken not to allow any oil near the metal-plate-connector. The "shock-absorber" effect that may have resulted from the small motions of the piston was accounted for in the design of the support (by providing the oil lubricant) and the fact that the load and deflections were measured between the grips and the joint. Thus, this did not influence the measurements of load or deflection.

Application of virtually any type of load or deflection function, within the limits of the hydraulic system, can be accomplished in two ways. First, if the function can be simply described as a mathematical function, the acquisition/control software is capable of generating a wide variety of mathematical functions. Second, if the loading is complex (such as an earthquake time-history), then the function can be digitized into a series of equal time spaced inputs into a text file (the control program reads from the data file at a constant specified rate). The software reads each file entry and adjusts the feedback control of the hydraulic actuator as necessary. The system used in this study was capable of making feedback corrections (to both load and deflection) at a rate of 500 Hz. A schematic representation of the system is shown in Figure 4.5.

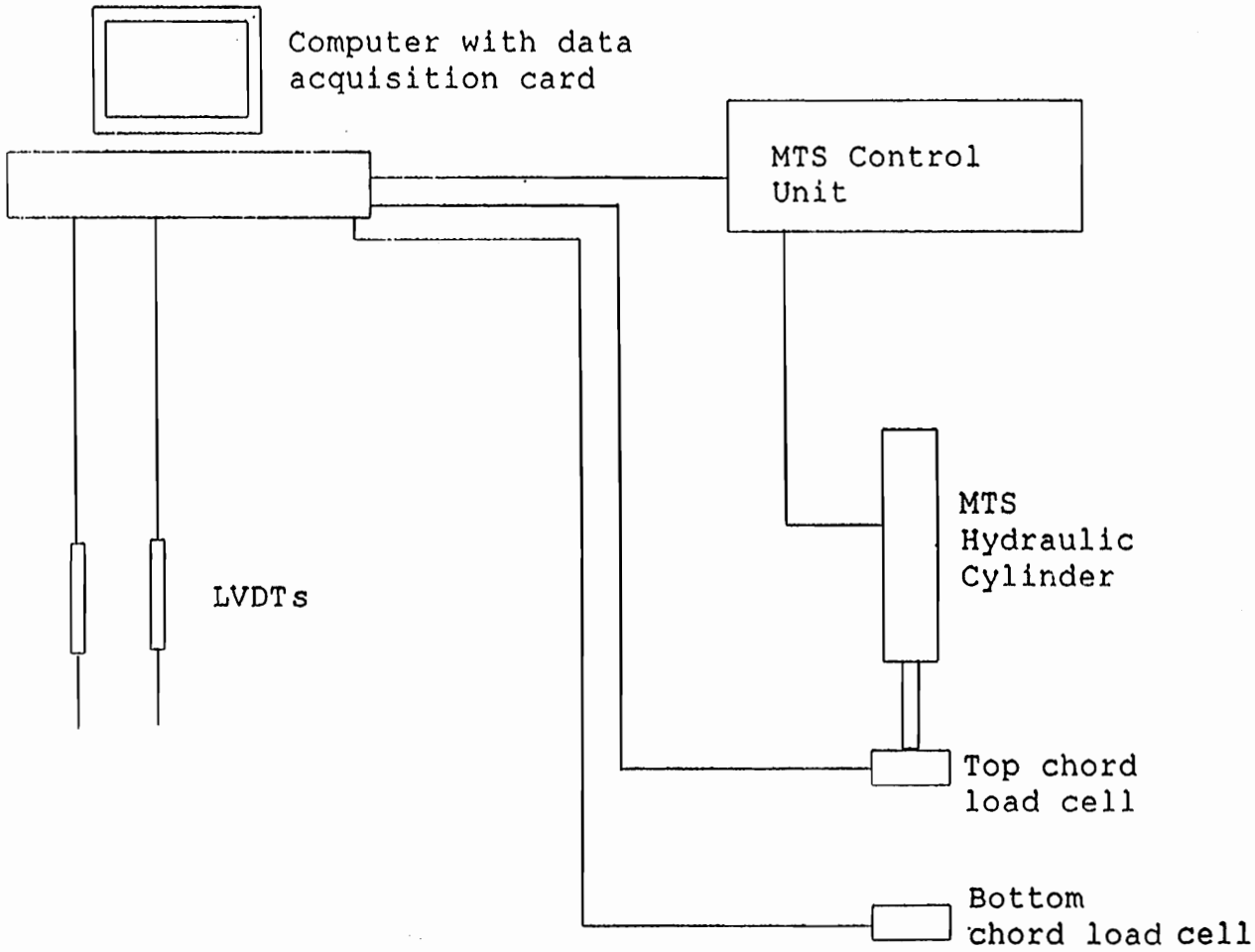

Figure 4.5: Schematic representation of the testing system

4.2.3 Test Procedures

Heel joint specimens were tested under four different loading conditions: 1) a static ramp loading to serve as the control group, 2) a force time-history determined from a linear finite-element model (FEM) and based on an artificial earthquake time-history (1.0 g's maximum horizontal acceleration and 0.67 g's maximum vertical acceleration) generated using WES-RASCAL (Silva 1987), 3) a sequential phased displacement (SPD) loading as proposed by Dolan (1994) to determine dynamic characteristics, and 4) a sinusoidal loading at different amplitude levels.

4.2.3.1 Static Tests

A linearly increasing tensile ramp load of 1200 lb/min, controlled through a load-feedback loop, was applied to the top chord of the heel joints to cause failure in 5 to 6 min.

4.2.3.2 Finite-element Modeling

A 30 ft span Fink truss, composed of nominal 2x4 in. Douglas-fir (modulus of elasticity of 1.6×10^6 psi), was modeled using a linear finite-element program (SAP90, Computers and Structures, Inc.) to estimate the response of the heel joint to ground accelerations from an artificial earthquake time-history (1.0 g's maximum horizontal

acceleration and 0.67 g's maximum vertical acceleration) generated using WES-RASCAL (Silva 1987). The first five modes were included in the analysis which contained 99.99% of the participating mass for the response in the horizontal direction. Figure 4.6 is a graphical representation of the finite-element model (FEM). Appendix H contains the SAP90 finite-element program input file.

The model is composed of linear beam elements connected by pinned joints, and supported by horizontal and vertical springs connected to the heel joints. The web members are pinned at both ends. The top chord is continuous from the heel joint supports to the peak of the truss. The bottom chord is continuous from the heel joint supports to the tension splice joint.

The finite-element software (SAP90, Computer and Structures, Inc.) was only capable of accepting one damping coefficient to represent the system. Because the largest magnitude deflections during the earthquake simulation occurred at the supports (springs representing the bearing walls), a damping coefficient of 10%, typical of sheathed stud walls (Leiva 1994) was chosen to represent the entire system. The damping coefficient of 10% does not necessarily represent the damping associated with elongation (or contraction) of the truss members or the behavior at the connections.

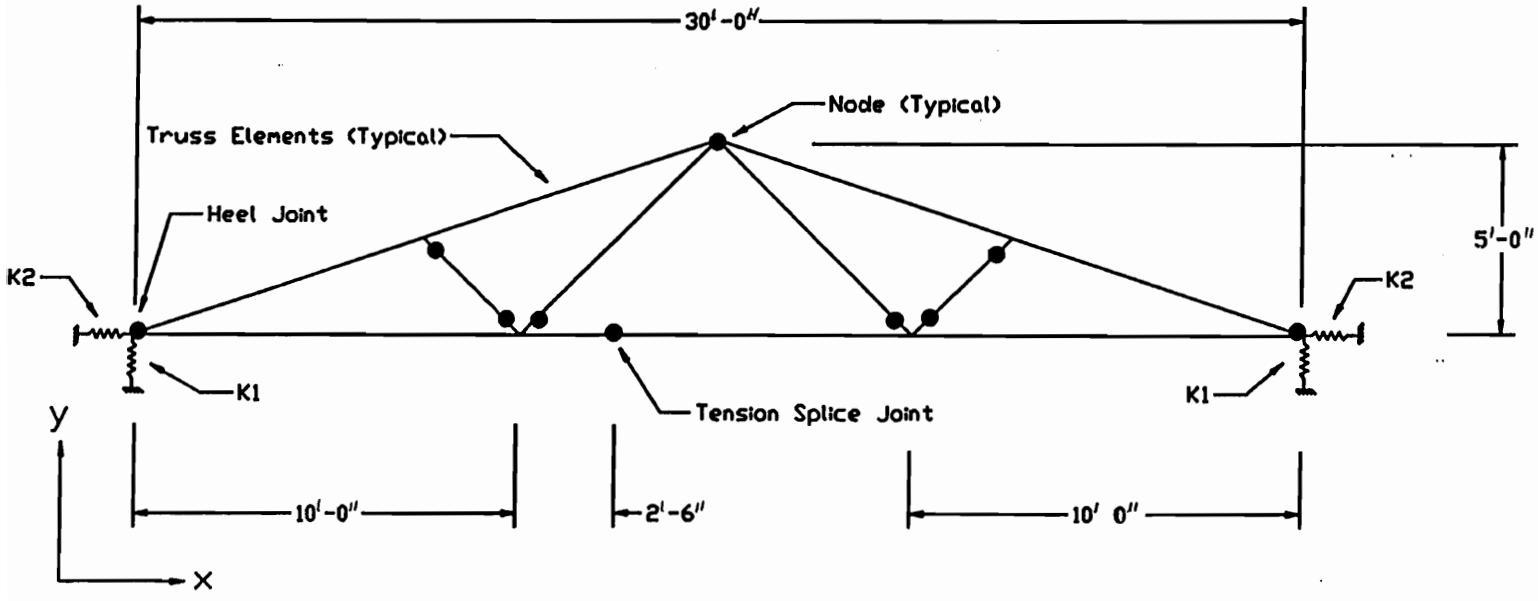

Figure 4.6: Finite element model of a typical metal-plate-connected truss

The supporting springs simulate both the vertical stiffness (K1) and the out-of-plane (horizontal) stiffness (K2) of the bearing walls. The vertical (K1) and out-of-plane (horizontal)stiffnesses (K2) are defined with respect to the x-direction and y-direction, respectively, shown on Figure 4.6. However, during the literature survey, no information was found for the out-of-plane stiffness of walls applicable to this situation and an in-depth finite-element analysis was considered beyond the scope of this research. Also, this out-of-plane stiffness depends on a variety of factors such as the length of the bearing wall, wall height, position of the truss along the wall, and type of construction. The approach used was to estimate the maximum possible out-of-plane support stiffness and then incrementally reduce that stiffness in the FEM to search for the worst-case response.

When compared to the trusses placed near the center of the bearing wall, it was assumed that the trusses placed nearest the end wall (running parallel to the trusses) would have the largest horizontal spring stiffness (K2). Experimental values obtained by Leiva (1994) on timber-framed shear walls suggest that 16 kips/in. is representative of the racking stiffness of a 30 ft long by 8 ft high wall. Once this maximum stiffness was established, the value was incrementally reduced in the FEM.

Previous research (Chapter 3) on MPC tension-splice joints examined the response to the Northridge earthquake ground accelerations (STA #24538 in Santa Monica, California) in the FEM to determine the stiffness of the supporting springs which maximized the forces in the tension-splice joint. Figure 4.7 displays the maximum and minimum compressive forces developed in the top chord of the heel joint in response to the Northridge earthquake accelerations (both horizontal and vertical accelerations superimposed) with varying out-of-plane spring stiffnesses (K2). As can be seen, the maximum and minimum compressive forces in the top chord are relatively insensitive to varying out-of-plane (K2) spring stiffnesses. It is assumed that this insensitive response also applies for the artificial earthquake simulation.

An identical version of the FEM used in the tension-splice joint study (chapter 3) was used in this study of heel-joints. The final model included a horizontal spring stiffness equal to 10% of the reference value, or a spring stiffness of 0.80-kips/in on either side of the truss. As discussed in chapter 3 (section 3.2.3.2), the member forces in the finite-element model were not sensitive to the vertical spring stiffness (K1). Therefore, to provide consistency between the tension-splice joint study (chapter 3) and the heel joint study (chapter 4), the same vertical

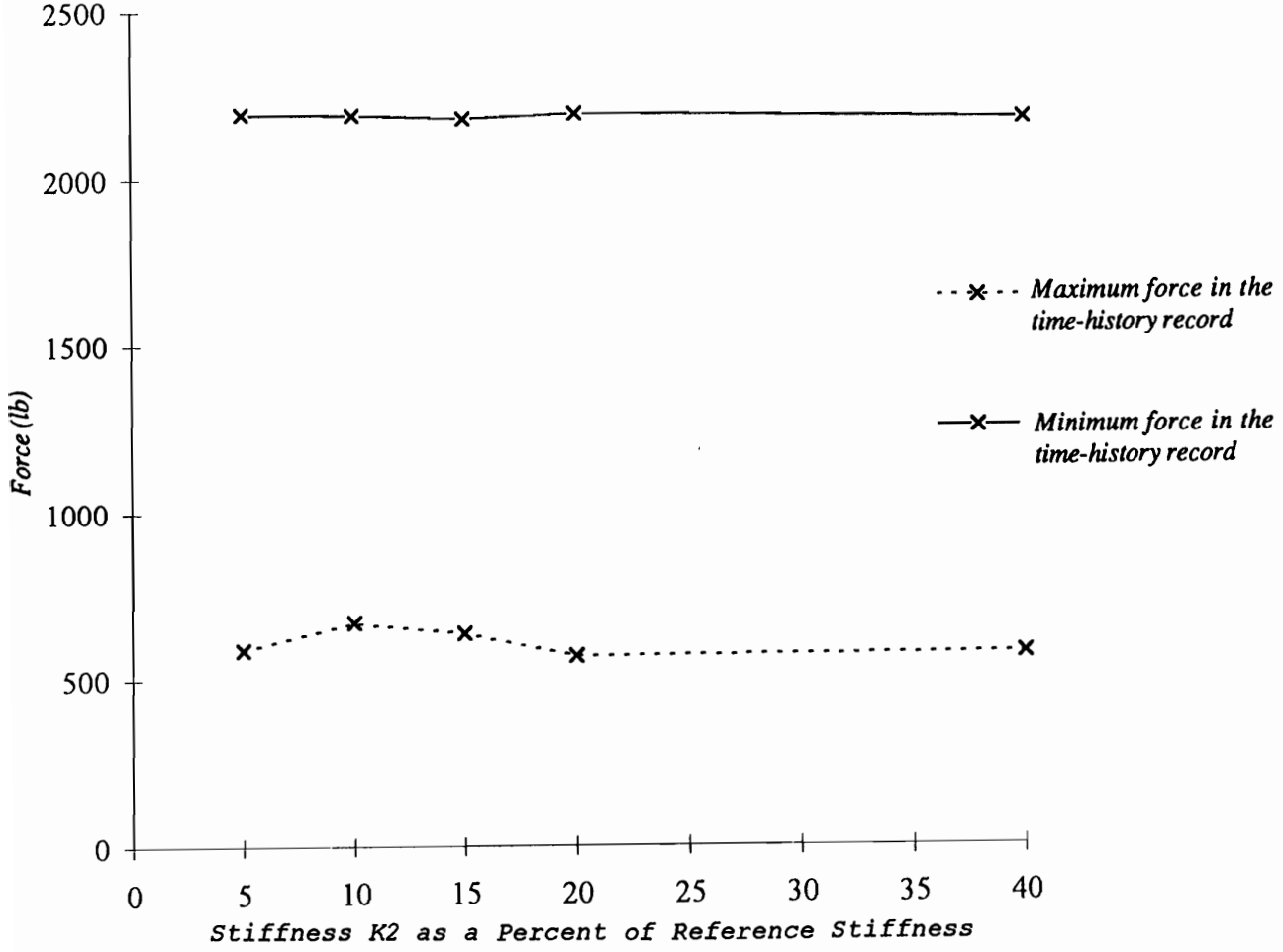

Figure 4.7 Maximum and minimum compressive forces developed in the top chord of the heel joint in response to the Northridge earthquake(0.903 g's and 0.232 g's horizontal and vertical peak accelerations, respectively) as a function of stiffness (K2)

spring stiffness (K2) was used in the finite-element model. The vertical spring stiffness selected for the final analysis was the equivalent of an 8-ft long 2x6 in. Douglas-fir stud, which corresponded to approximately 140-kips/in. Axial stiffness of the studs was defined as K=AE/L where $A=8.25$ in.^{2}, $E=1.6\text{x}10^6$ psi, and L=96 in.

The variables K1 and K2 (see Figure 4.6) are stiffnesses of the horizontal and vertical linear springs, respectively. The model is almost completely symmetrical with the exception of the tension-splice joint located in the bottom chord. This joint is placed 30 in. off center to model actual Fink truss construction (although the position of the tension-splice joint varies somewhat with different manufacturers). Pinned joints, which have no rotational restraint, are represented as dark circles.

Typical design dead loads for modern truss construction are 10 lb/ft^2 (including the weights of the top-chord, sheathing, and roofing material) along the slope of the roof for the top chord (not a horizontal projection) and 10 lb/ft^2 (including the weight of the bottom chord, ceiling material, insulation, and permanent fixtures) along the bottom chord (Breyer 1993). At a truss spacing of 24 in. on-center, this corresponds to a uniformly distributed load of 20 lb/ft along the slope of the top chord and along the bottom chord. Self weight of the web members is estimated

at 1.14 lb/ft (specific gravity of 0.50). Masses from the roof system and the truss members are lumped at the joints (nodes) for the dynamic analysis. Snow and wind loads were not included in the dynamic analysis for earthquake effects. To determine total design loads, the contribution of these other live loads must, of course, be considered.

4.2.3.3 Artificial Earthquake Generation Using WES-RASCAL

The WES-RASCAL code (Silva 1987) is used to help assess seismic hazards in regions were strong motion data is scarce. This program has the ability to generate strong motion data by scaling specific parameters from small local seismic events, or weak motions. These weak motions provide the seismic wave characteristics used in the scaling process. The purpose of WES-RASCAL (Silva 1987) is not to predict the accelerogram of a future earthquake but to generate a time-history for a given magnitude event with realistic characteristics. WES-RASCAL (Silva 1987) is capable of generating an artificial time-history based on a target response spectrum; however, if a strictly theoretical approach is used to construct a time-history in this manner, the result may not simulate a realistic natural event. The variability of soil stratifications, interaction between bedrock and soil, and a host of natural phenomena make the problem of developing a realistic accelerogram from a purely

theoretical perspective nearly impossible. To address this problem, the program requires an input time-history from which it extracts specific phase characteristics from the Fourier amplitude spectrum. These phase characteristics are then applied in generating the artificial time-history output. This approach allows the program to generate a realistic acceleration time-history.

Although the artificial acceleration time-history record has a response spectrum closely matching a target design response spectrum, other properties, such as displacement and energy input may be exaggerated (Naeim 1995). WES-RASCAL (Silva 1987) manipulates the displacement record before and after the integration of the acceleration record to produce a more realistic account of the displacements. However, the displacement record produced by WES-RASCAL (Silva 1987) still tends to be exaggerated (Naeim 1995) even after the corrections.

The input for WES-RASCAL (Silva 1987) includes the type of simulation (artificial time-history from a response spectrum, or peak acceleration, velocity, and displacement only) soil characteristics, epicenter location, filtering parameters, input time-history, target response spectrum, and scaling parameters. The artificial time-history generated for this study uses propagation parameters for the Western United States, the design response spectrum provided

in the Uniform Building Code (ICBO 1994), Northridge earthquake phase characteristics, a source depth of 6 miles, and a moment magnitude of 7.0. Typical filtering and amplification factors for the Western United States were applied. The input file parameters used to determine the artificial time-history incorporated in this study are shown in Appendix I.

Response spectrum matching, after 10 iterations, is shown in Figure 4.8. The dashed line represents the Uniform Building Code (ICBO 1994) target response spectrum for Zone 4 and soil type 3 conditions. The solid line is the response spectrum of the output artificial earthquake accelerations. For the purpose of this study, the match was considered satisfactory (by a visual comparison).

For horizontal accelerations, the artificial acceleration time-history was linearly scaled to a maximum horizontal acceleration of 1.0-g. Similarly, for the vertical accelerations, the artificial accelerations were scaled to a maximum of 0.67-g's. The Uniform Building Code (ICBO 1994) seismic design section 1629.2 suggests scaling the maximum horizontal acceleration by 67% to estimate the maximum vertical acceleration. For this simulation, 67% of the horizontal ground acceleration time-history was used as the vertical ground acceleration time-history. This procedure is very conservative in that the peaks of both the

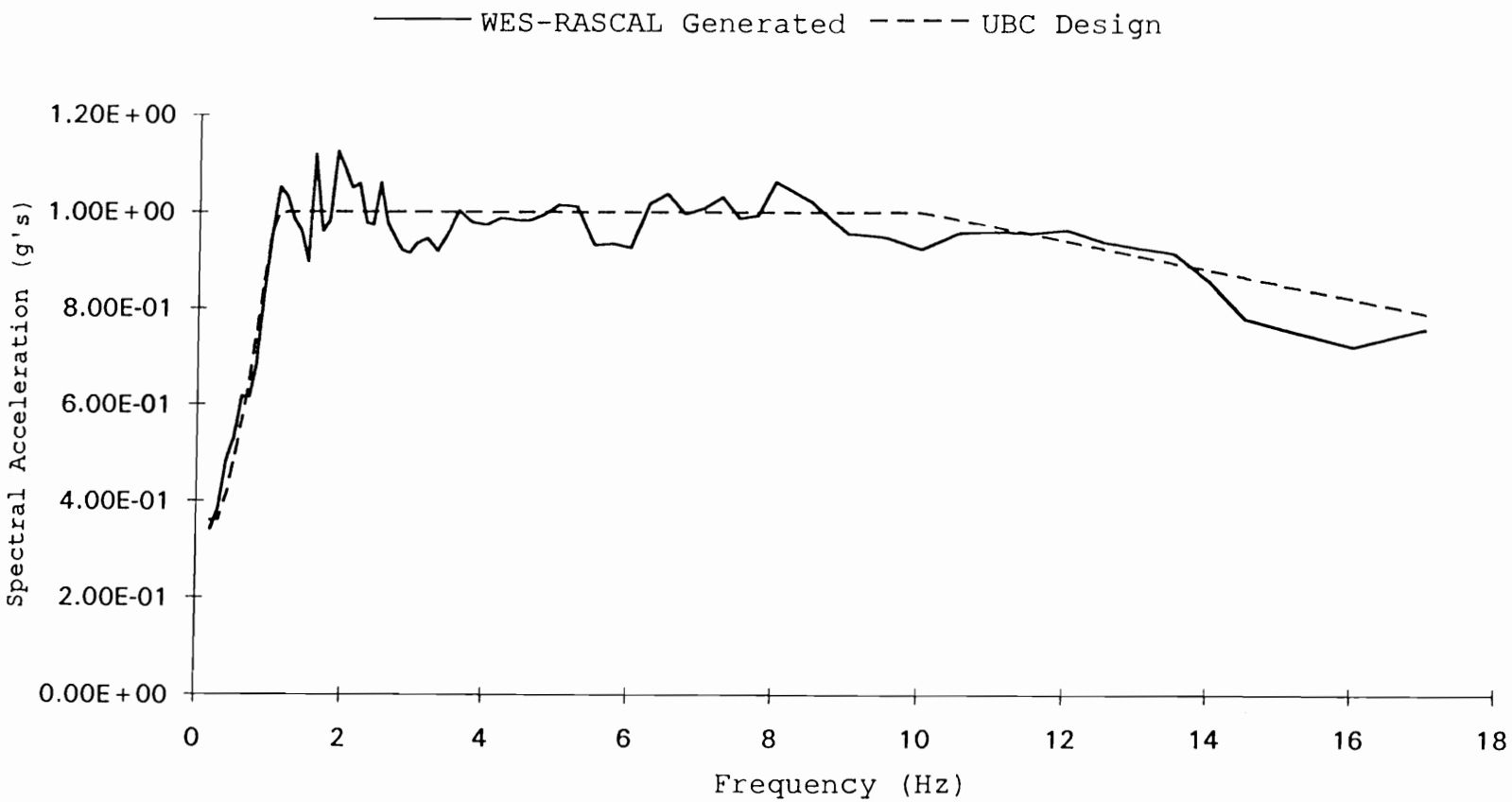

Figure 4.8: Comparison between the response spectra from WES-RASCAL and the Uniform Building Code (ICBO 1994)

horizontal and vertical time-history records occur at the same point in time. An alternate method would be to develop a suite of independent horizontal and vertical acceleration time-histories using WES-RASCAL (Silva 1987) and combine them using the FEM to determine the possible range of maximum forces in the heel joint.

The horizontal and vertical artificial ground accelerations, shown in Figures 4.9 and 4.10 were applied separately to the FEM to determine the load response in the heel joint for each direction (horizontal and vertical). Because the FEM was linear, the response to the horizontal and vertical ground accelerations were superimposed to obtain the combined response (additive effects of the horizontal and vertical accelerations). The loads were then applied to a set of ten actual heel joints in the laboratory. The target forces from the combined response of the horizontal and vertical artificial earthquake accelerations intended to be applied to the heel joints are shown in Figure 4.11.

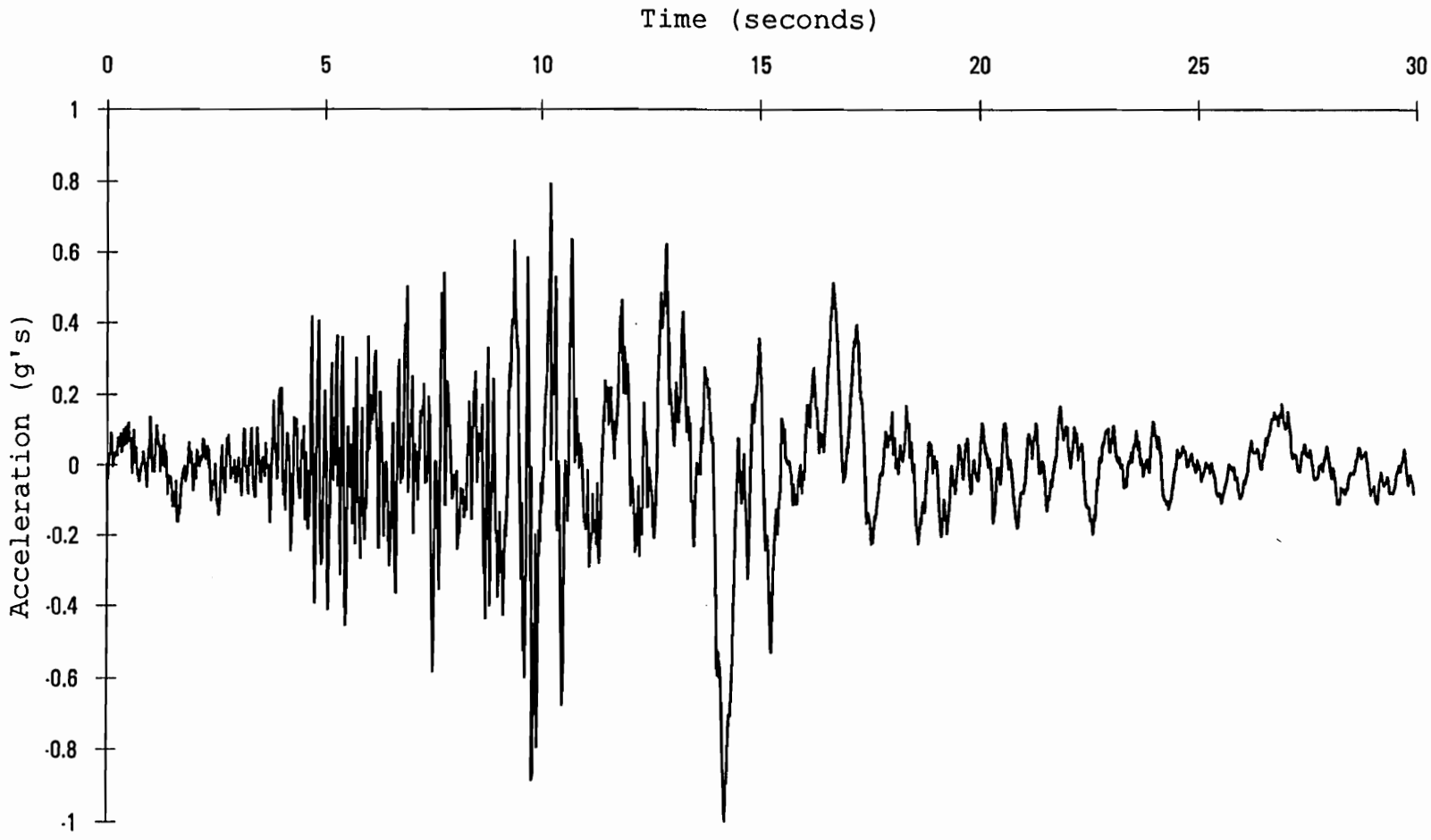

Figure 4.9: Horizontal ground acceleration (1.0 g maximum) during the artificial earthquake simulation

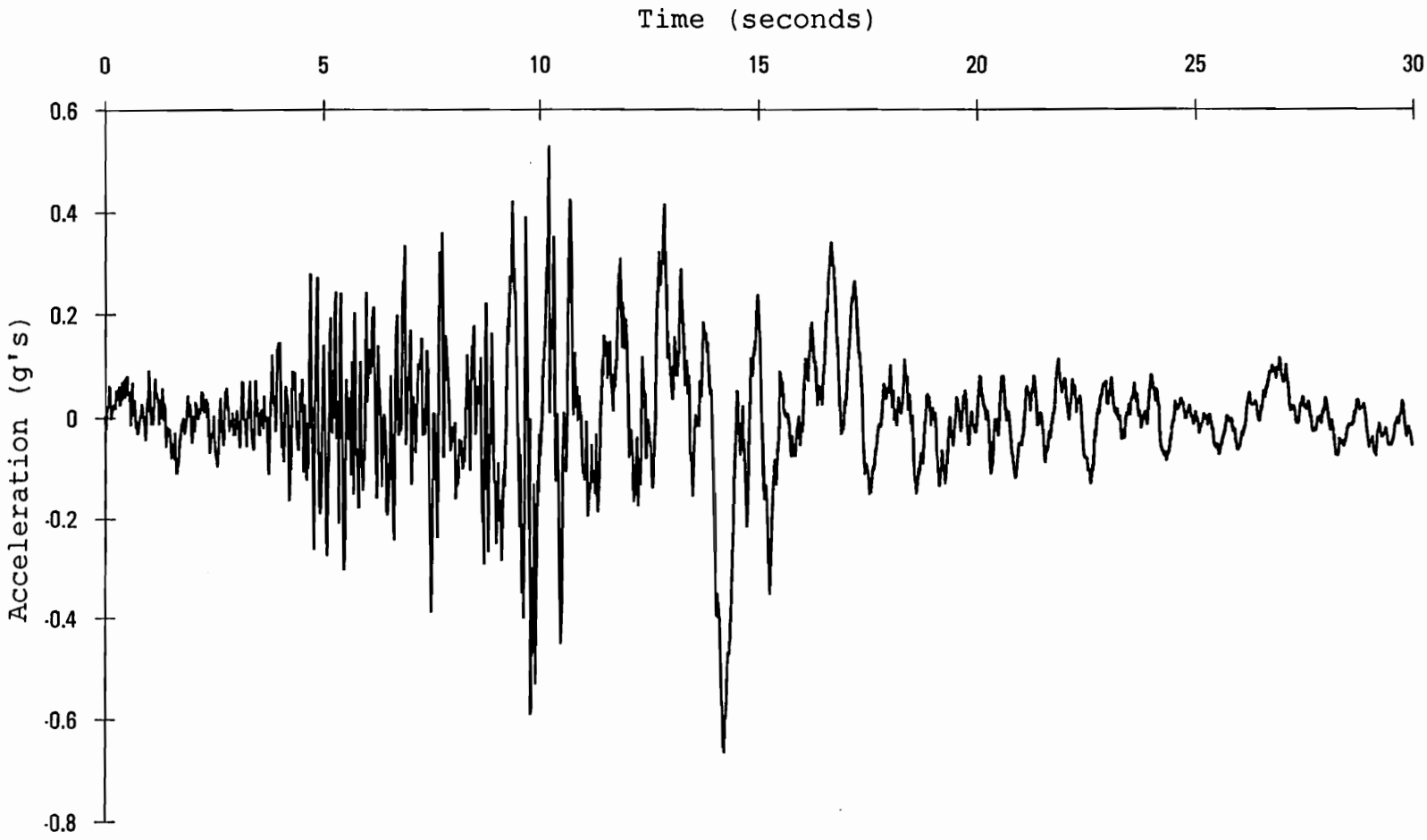

Figure 4.10: Vertical ground acceleration (0.67 g maximum) during the artificial earthquake simulation

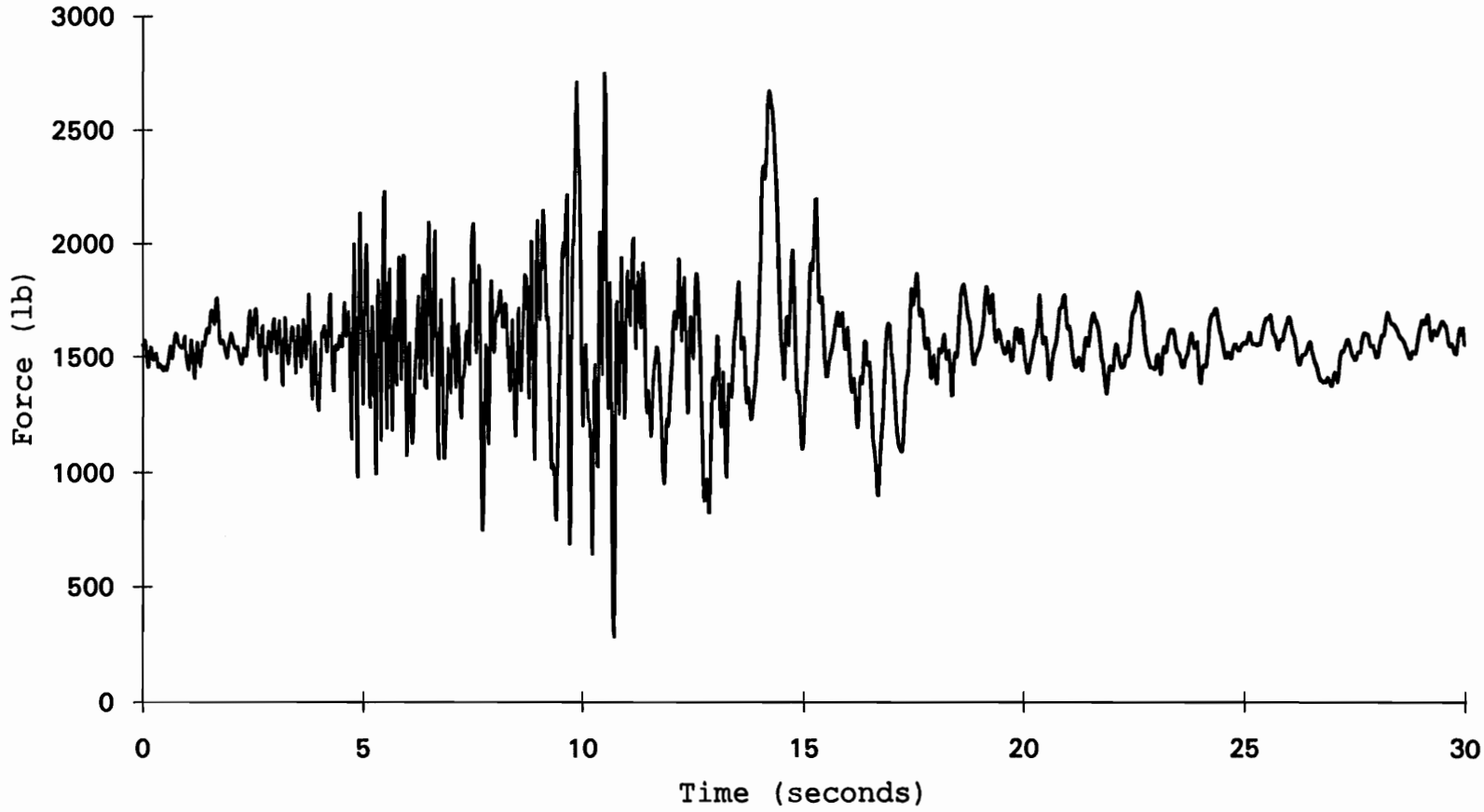

Figure 4.11: Combined (target) response of the top chord of the heel joint to the artificial earthquake horizontal and vertical ground accelerations

4.2.3.4 Sequential Phased Displacement (SPD) Loading

The proposed sequential phased displacement (SPD) method of Dolan (1994) was used to determine the dynamic properties of the MPC heel joints, such as energy dissipation, damping ratio, and cyclic stiffness. The loading function combined fully reversed stabilizing cyclic displacements preceding degradation cycles at a frequency of 1 Hz, which approximates the expected response of a low-rise timber structure under a seismic or high wind event. The stabilizing and degradation cycles gradually increase, following the pattern shown in Figure 4.12, which graphically displays a typical SPD loading function proposed by Dolan (1994).

The SPD cycles are defined in terms of the yield displacement for the type of connection being studied. Because of the nonlinear load-deflection curves for MPC joints, a yield displacement (defined in section 4.3.1) of 0.007 in. (Appendix J) from the control group (batch-1), was used to scale the SPD cycles. Displacement control allows for a clear definition of the stabilized cycle from which dynamic properties are determined. The stabilized cycle is defined as the first cycle in the set of stabilizing cycles (see Figure 4.12) at which there is less than a 5% degradation from the maximum load in the previous cycle. The stabilized cycle is important because it provides a

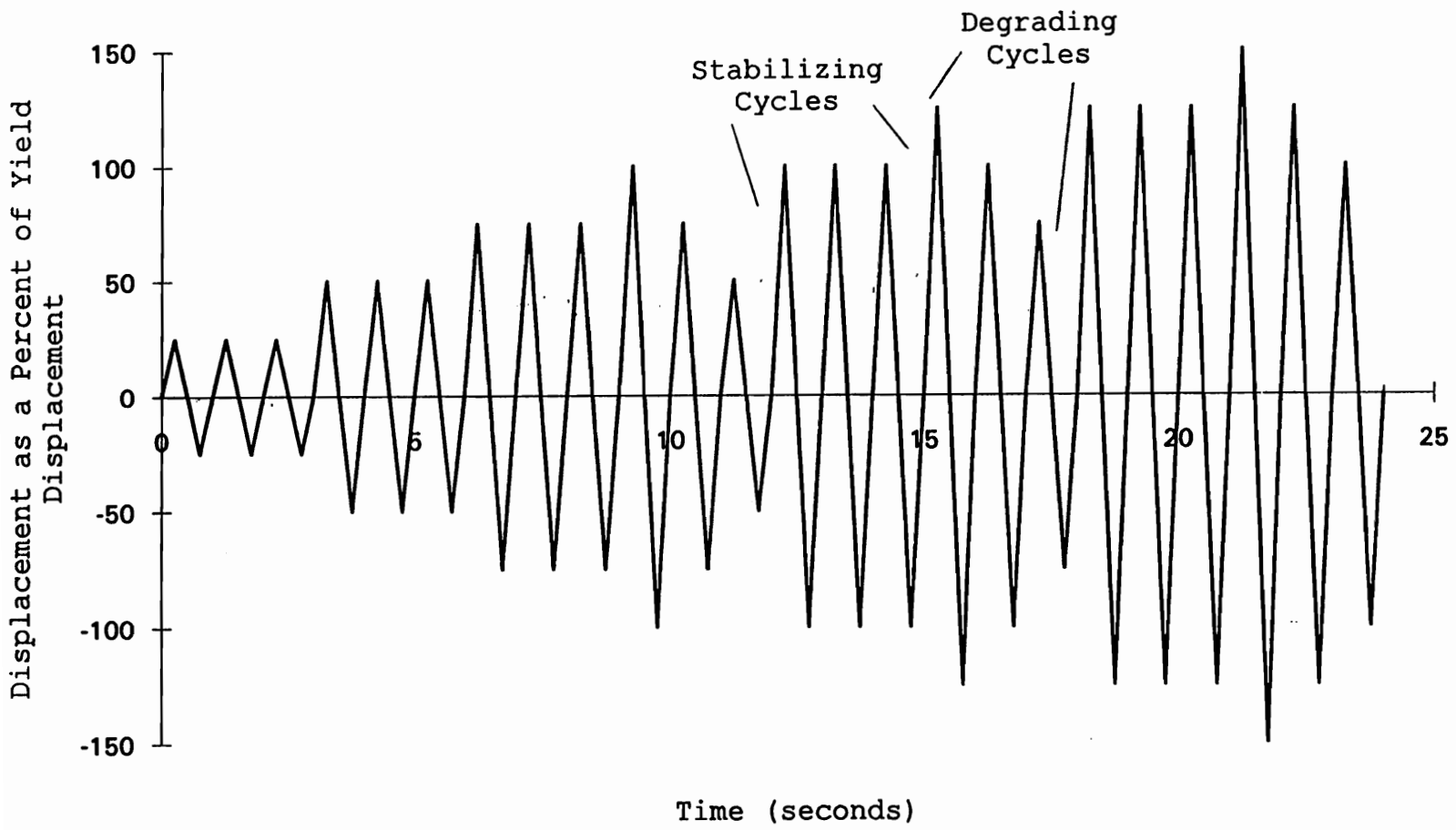

Figure 4.12: Sequential phased displacement loading (Dolan 1994)

consistent location in the SPD loading for evaluating dynamic properties for comparison to other types of connections.

The rational of the SPD loading is that it better represents a seismic or wind event than a static ramp load or a simple cyclic loading function. Also, the use of the stabilized cycle allows for consistent calculations of the dynamic properties. The equivalent energy, elastic-plastic load-displacement curve provides a method so that comparisons of the dynamic properties between different materials and connection types can be made. Moreover, the decay portion of the loading provides information on the lower bound of the hysteresis. If the connection has slack in it, the hysteresis can decrease to zero energy dissipation. Also, the increasing magnitude of the displacement phases can continue until failure, thus providing information on total ductility and capacity.

During previous testing of MPC tension-splice joints (chapter 3), the SPD function was limited to 120 cycles due to hydraulic capacity limitations. For consistency, the SPD loading was also limited to 120 cycles for testing of heel joints. The heel joints, after application of the SPD loading, were then failed under a ramp load of 1200 lb/min to determine how the SPD loading affected the strength and stiffness of the heel joints.

Under normal conditions, the heel joint is not designed to resist tensile loads. An alternative to applying a fully reversed loading is to truncate the negative portion (causing tensile loads), shown in Figure 4.12, and apply only the positive displacements (in terms of the percent of yield displacement). However this alternate approach was not used in this first study to apply the SPD loading to heel joints. It was decided to follow the proposed standard as closely as possible.

4.2.3.5 Cyclic Testing

To determine the effect of cyclic loading at various amplitudes, a sinusoidal waveform, with the baseline of the oscillations (center-line of the cycles) at 33% of the mean ultimate strength (from the static loading control group), were applied for 200 cycles at a frequency of 1 Hz to twenty-five heel joints. First, each joint was loaded to 33% of the mean strength (0.33 • 6211 lb = 2065 lb, Appendix J) at a load rate of 1200 lb/min. Then, constant amplitude cycles (at 5, 10, 15, 20, 25, 30, 33, 35, and 40% of the mean ultimate strength of the static loading control group of 6211 lb) were applied at a frequency of 1 Hz for 200 seconds or until the joint failed. If the joint was still able to carry load after the cycles, the static ramp load

was continued until failure. Figure 4.13 displays the cyclic loading function.

4.3 TEST RESULTS

4.3.1 General Results

Strength, specific gravity, and moisture content results for the tests in this study are shown in Appendix D (as well as maximum top chord load, axial stiffness, rotational stiffness, deflection at maximum load, rotation at maximum load, yield displacement, yield rotation, modulus of elasticity, number of growth rings per inch, grain orientation, late wood content, and failure mode) with their respective coefficients of variation (COV). Mean strength for the cyclic loading tests is not provided in this appendix because of the strength dependence on the cyclic amplitude of the cycles (defined in Figure 4.13).

Specific gravity and moisture content were measured according to ASTM D2395-93 (Method A, Volume by Measurement) and ASTM D4442-92 (Method A, Oven-Drying Primary), respectively. The modulus of elasticity of the wood used to construct the MPC heel joints was measured using an E-computer (Metriguard, Model 390). A summary of the test results is shown in Table 4.3.

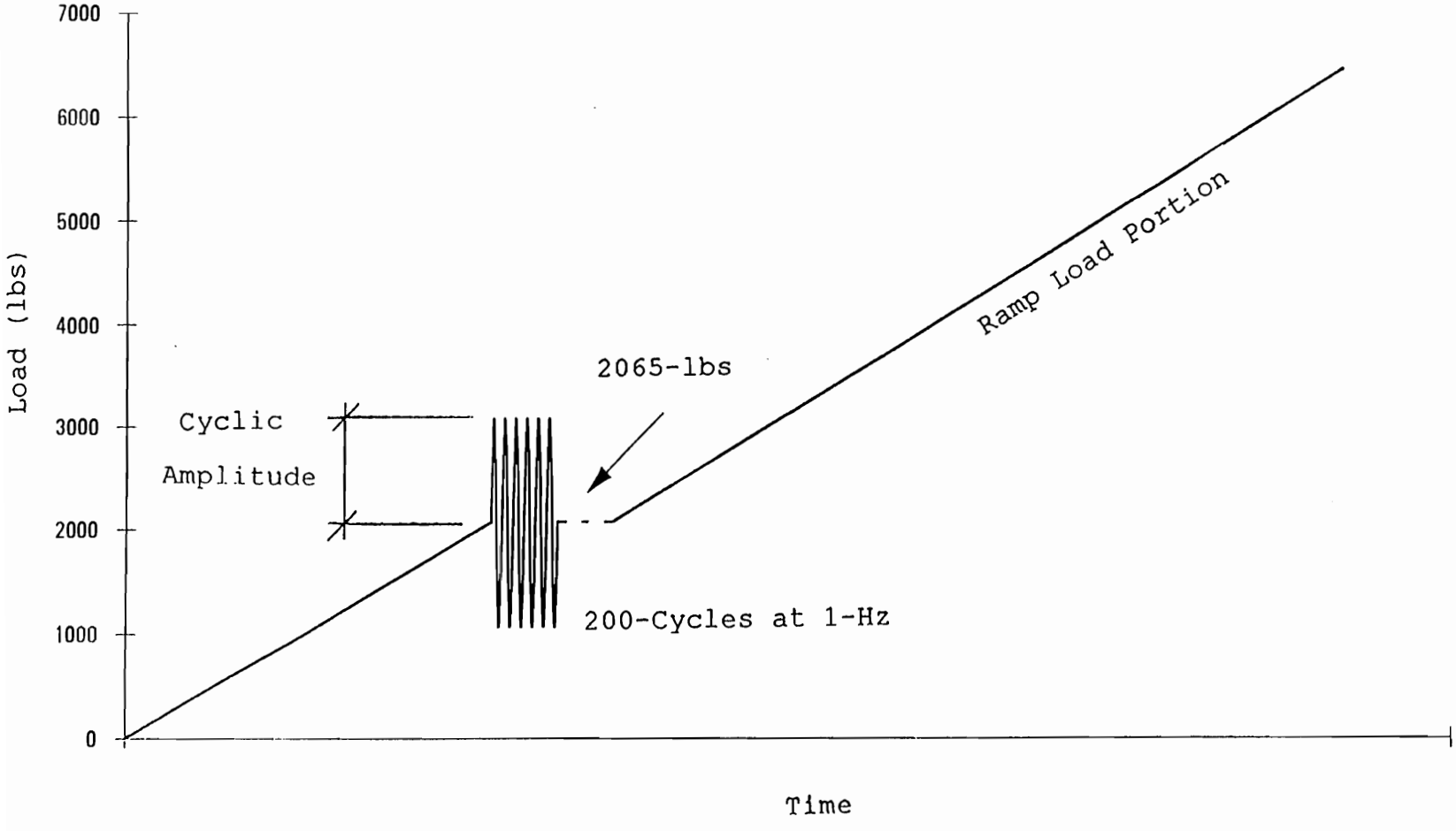

Figure 4.13: Cyclic loading function for the top chord of the heel joints

Table 4.3: Summary of the heel joint test results.

Test	Sample Size	Mean Strength (lb)	Mean Stiffness (x100,000 lb/in.)	Mean Rotational Stiffness (x100,000 lb-in./radian)
Control Group (Static Tests)	9	6211	3.58	52.1
Artificial Earthquake Simulation	10	6057	1.45	32.3
Sequential Phased Displacement	8	4185	1.36	84.0
Cyclic Loading	25	Varies*	Varies*	Varies*

* Depends on the cyclic amplitude

Test	Mean Specific Gravity	Mean Moisture Content (%)	Mean Wood MOE ($x10^6$ psi)
Control Group (Static Tests)	0.51	14.3	2.01
Artificial Earthquake Simulation	0.53	13.0	2.00
Sequential Phased Displacement	0.48	12.9	1.95
Cyclic Loading	0.51	12.7	2.09

Load-deflection and moment-rotation curves were analyzed to determine the axial and rotational stiffnesses, respectively. The load-deflection curve was based on the load in the top chord (compression defined as positive) and motion of the top chord parallel to its own axis (referred to in text as the top chord deflection). The construction of the moment-rotation curve was slightly more complicated. Moment was defined as the product of the applied load in the top chord and the perpendicular distance between the centerline of the top chord and the geometric center of the metal plate connector (1.75 in.). Figure 4.14 shows the geometry of the heel joint. As shown in Figure 4.14, the rotation angle can be calculated using Equation 4.1 (where 10.99 in. is the hypotenuse distance shown in Figure 4.14).

$$Rotation\ Angle\ (radians) = TAN^{-1}\left(\frac{LVDT\ Measurement\ (in)}{10.99in}\right) \quad \ldots\ldots\ldots 4.1$$

The dominant failure mode for the heel joints was tooth withdrawal. This mode occurred as a result of the wood being crushed by the side of the tooth near the surface of the wood in conjunction with slight bending of the teeth as the plate deformed in shear. As the load increased, the corners of the plate began to lift away from the surface of the wood causing the teeth in that area to become virtually ineffective in resisting load. In instances where the member failed near the grips (not near the metal plate

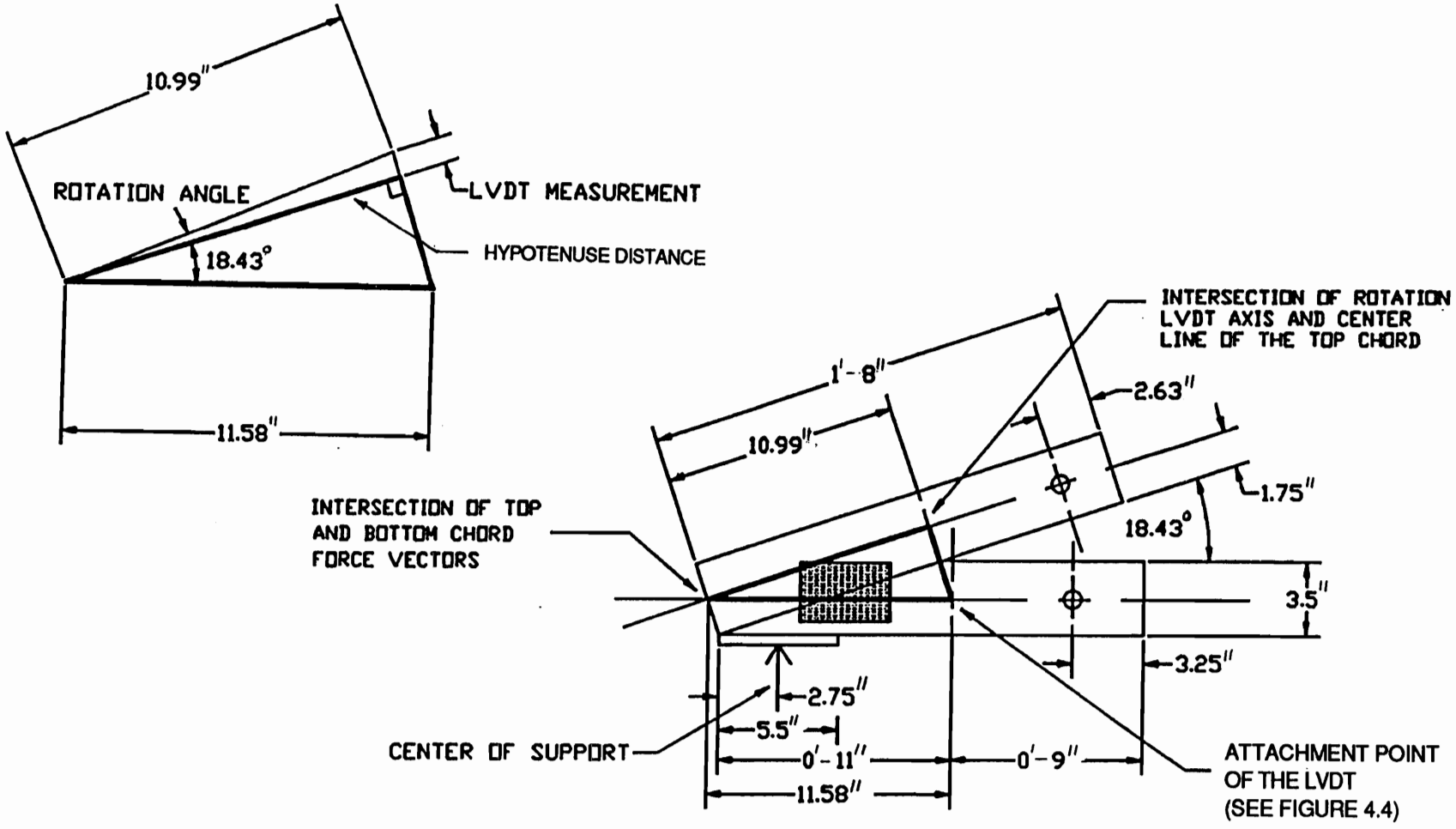

Figure 4.14: Detail of the heel joint geometry

connector) the results were discarded (one sample during the static loading control group and two samples during the sequential phased displacement loading). Figure 4.15 displays a typical heel joint failure mode. The large shear deformation of the plate is apparent. Gupta and Gebremedhin (1990) observed similar failures in their study on MPC heel joints.

The load-deflection and moment-rotation curves are nonlinear, which is typical of wood connections (Foschi 1974). The nonlinearity is due to a number of factors involving both the wood and the metal plate. The relative contributions of these factors changes as the load increases. At lower load levels, the deflection can be attributed to the elastic response of the wood near the tooth-wood interface and the elastic response of the steel plate under shear. As the load increases, the wood fibers begin to deform and crush near the tooth-wood interface. Also, the corners of the metal plate begin to lift away from the surface of the wood which causes the teeth near the corners to become less effective in resisting load. Near the ultimate load, the wood fibers at the tooth-wood interface begin to deform plastically due to the large loads transmitted from the metal-plate-connector, through the teeth, and into the wood. Furthermore, the metal-plate-

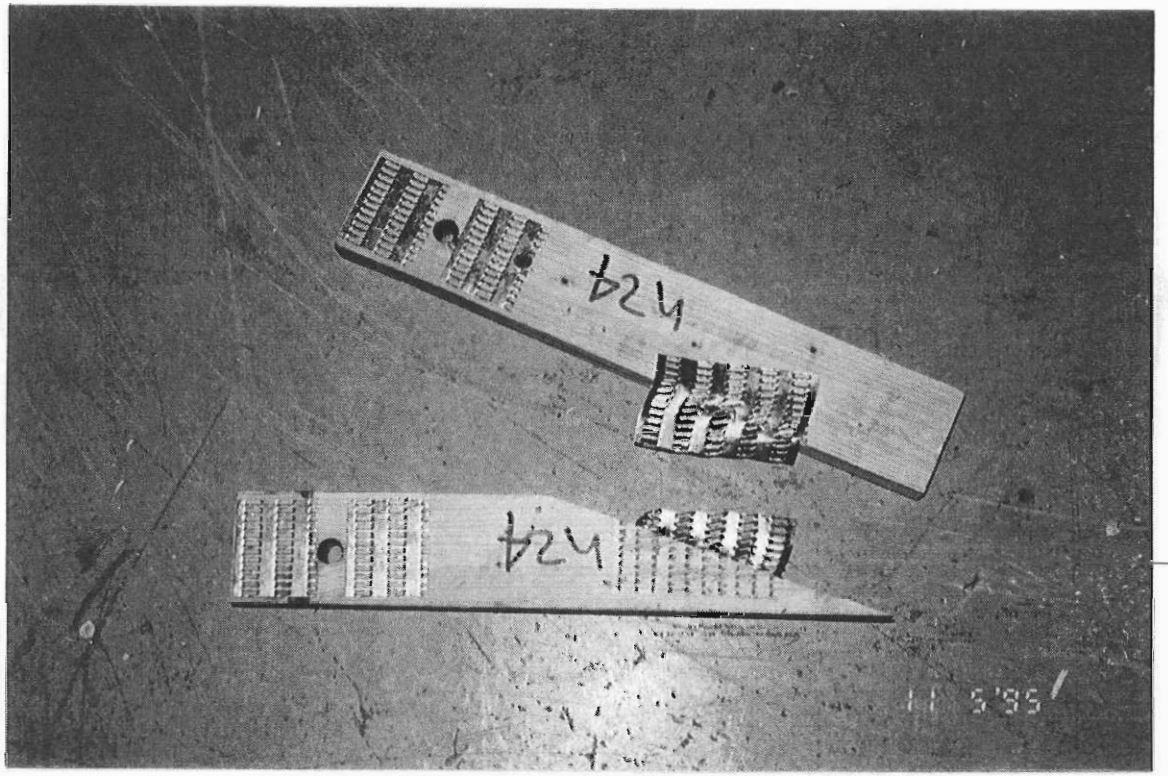

Figure 4.15: Photograph of the dominant failure mode for heel joints

connector experiences large inelastic shear deformations from the applied load (shown in Figure 4.15).

Because of the nonlinear shape of the load-deflection and moment-rotation curves, which caused difficulty in determining a single-valued stiffness, the yield points (for both deflection and rotation) were defined at the design load (one-third of the mean ultimate load, National Design Specification for Wood Construction 1991). The design load was based on the ultimate load in the top chord (or corresponding ultimate moment).

To calculate the axial stiffness for each joint (secant stiffness), one-third of the ultimate load on the top chord of the heel joint was divided by the corresponding deflection of the top chord with respect to the bottom chord at one-third of the ultimate strength. To calculate the rotational stiffness (secant stiffness), one-third of the ultimate moment (defined in section 4.3.1) for each joint was divided by the corresponding rotation (defined in equation 4.1) at one-third of the ultimate moment. For the artificial earthquake simulation, this point occurs after the loading. A rotational slip criteria was not considered in determining to design moment of the heel joints.

4.3.2 Static Tests

The mean strength for the static loading control group was 6211 lb (Appendix J) with a coefficient of variation (COV) of 6.92%. The mean axial stiffness of the top chord for the control group was 3.58×10^5 lb/in. with a COV of 60.9%. The mean rotational stiffness for the control group was 52.1×10^5 lb•in./rad with a COV of 54.4%. The yield points for axial deflection and rotation were at 0.007 in. and 0.0009 rad, respectively (Appendix J).

The shapes of the load-deflection and moment-rotation curves were rather inconsistent (Appendix K) Often, the LVDT measuring the deflection of the top chord did not register any motion until the load exceeded 1000 lb. This may be attributed to the joint experiencing initial rotation of the top chord with respect to the bottom chord, rather than pure deflection of the top chord. This situation caused the stiffness variation to be extremely high. Also, the shapes of the moment-rotation curves were very inconsistent. In some cases, the angle between the top and bottom chord decreased until a specific load, then began to increase, which was most likely due to a very slight eccentric alignment of the load, applied by the hydraulic cylinder, to the top chord (load not applied directly through the centerline of the top chord of the heel joint). The axial stiffness of the top chord ranged from a low of

1.80×10^5 lb/in. to a high of 8.94×10^5 lb/in. (Appendix J). The large COV's associated with the axial and rotational stiffnesses reflect the inconsistencies in the load-deflection and the moment-rotation curves. Appendix K contains the load-deflection and moment-rotation curves for the static loading control group.

Also, it is possible that the LVDT measuring axial deflection of the top chord was affected by the relative rotation of the top chord with respect to the bottom chord. If so, rotational movement of the top chord with respect to the bottom chord may have contributed to the deflection recorded by the LVDT measuring axial deflection of the top chord.

4.3.3 Artificial Earthquake Tests

The average strength (top chord ultimate load) of heel joints after being subjected to the artificial earthquake force time-history was 6057 lb with a COV of 7.62% (Appendix J). The average post-earthquake loading axial and rotational stiffnesses (defined in section 4.3.1) were 1.45×10^5 lb/in. with a COV of 54.3% and 32.3×10^5 lb•in/rad with a COV of 68%, respectively. (Appendix J). Figure 4.16 shows a typical top chord load-deflection curve including the earthquake time-history portion (for joint 1). A close-up of the earthquake portion of the curve is also shown in

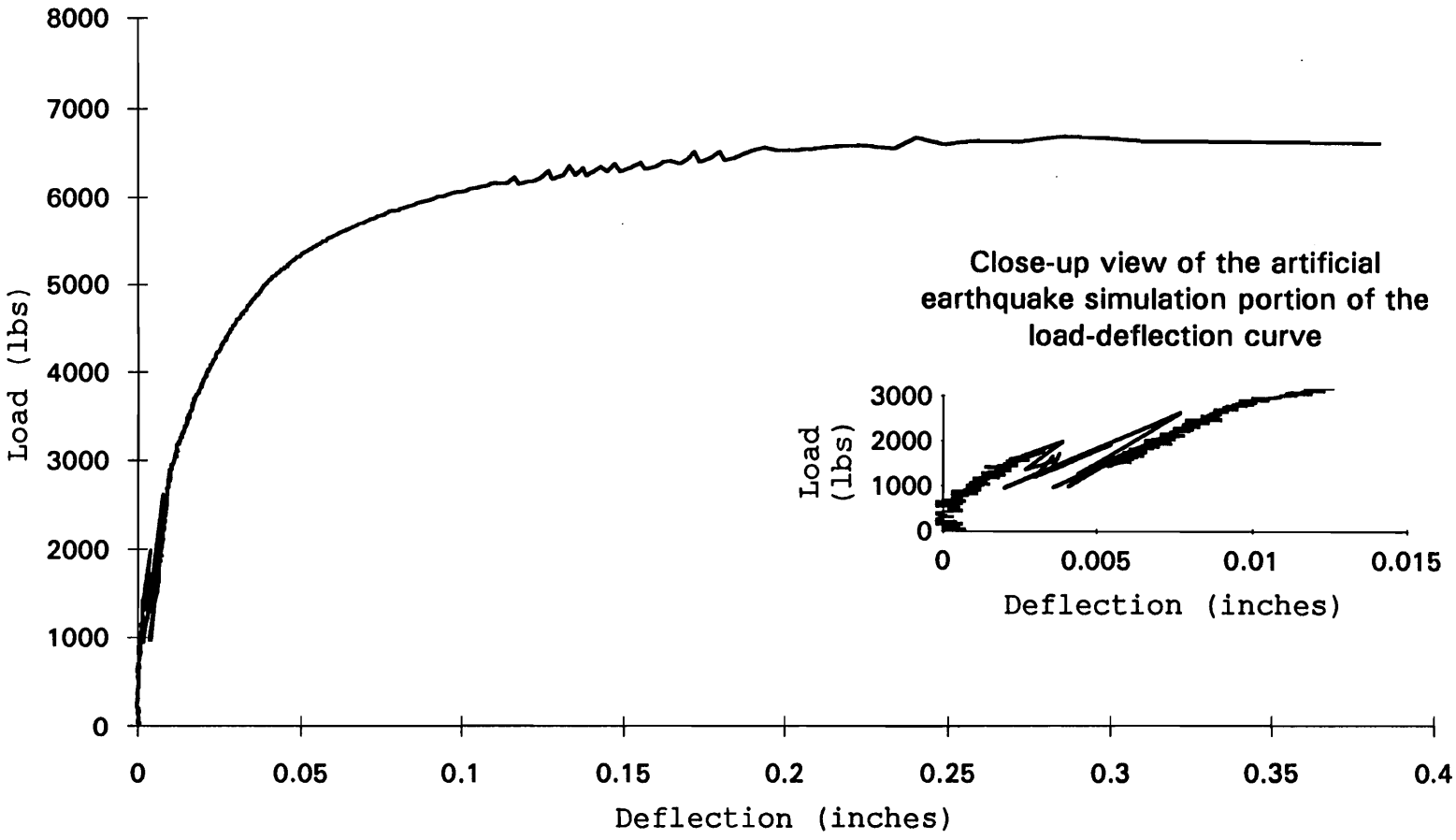

Figure 4.16: Typical top chord load-deflection curve including the earthquake time-history (joint 1)

Figure 4.16. This close-up view shows how the joint responded to the earthquake loading. The data acquisition rate was only 2 Hz, which was not sufficient to completely define the load-deflection trace (a 100 Hz acquisition rate would be required.

Figure 4.17 shows a typical top chord deflection-time curve for the artificial earthquake simulation (for joint 1). Figure 4.18 displays a close-up view of Figure 4.17 showing the earthquake portion of the test. Figure 4.18 shows that the artificial earthquake simulation has a pronounced effect on the axial deflection experienced in the heel joints. This can be seen in the permanent deflection caused by the earthquake time-history. Appendix L contains all of the axial deflection-time curves for the artificial earthquake simulation. There is a large amount of variability in the shapes of these curves for the same reasons as discussed for the static loading control group for the load-deflection and moment-rotation curves (section 4.3.2). The effect of the artificial earthquake occurs between 80 and 110 seconds in Figure 4.17, 4.18, and Appendix L.

No significant strength or rotational stiffness degradation occurred as a result of the artificial earthquake time history (two sided p-values of 0.46 and 0.15 for strength and rotational stiffness, respectively).

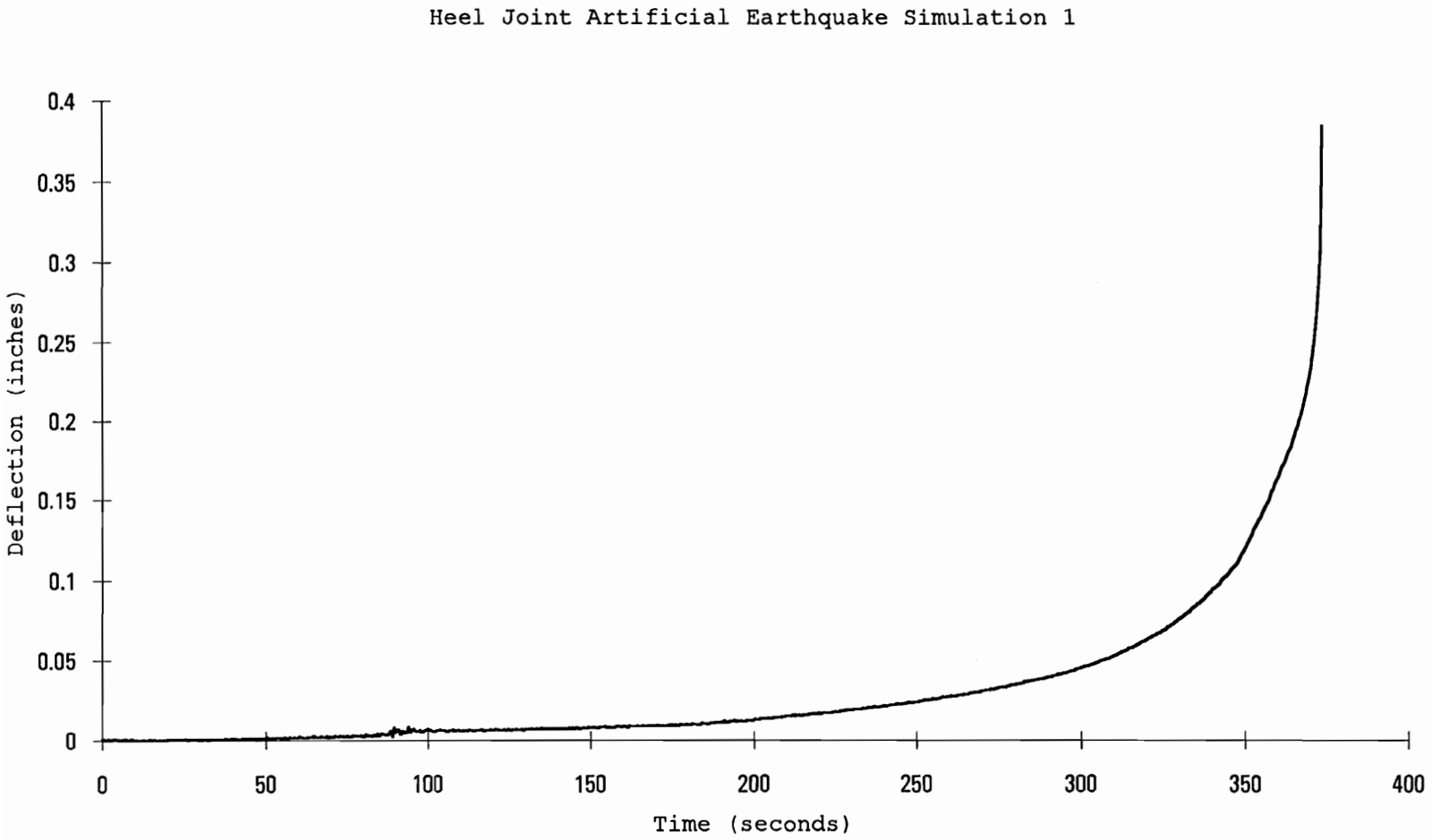

Figure 4.17: Typical top chord deflection-time curve for the artificial earthquake simulation (joint 1)

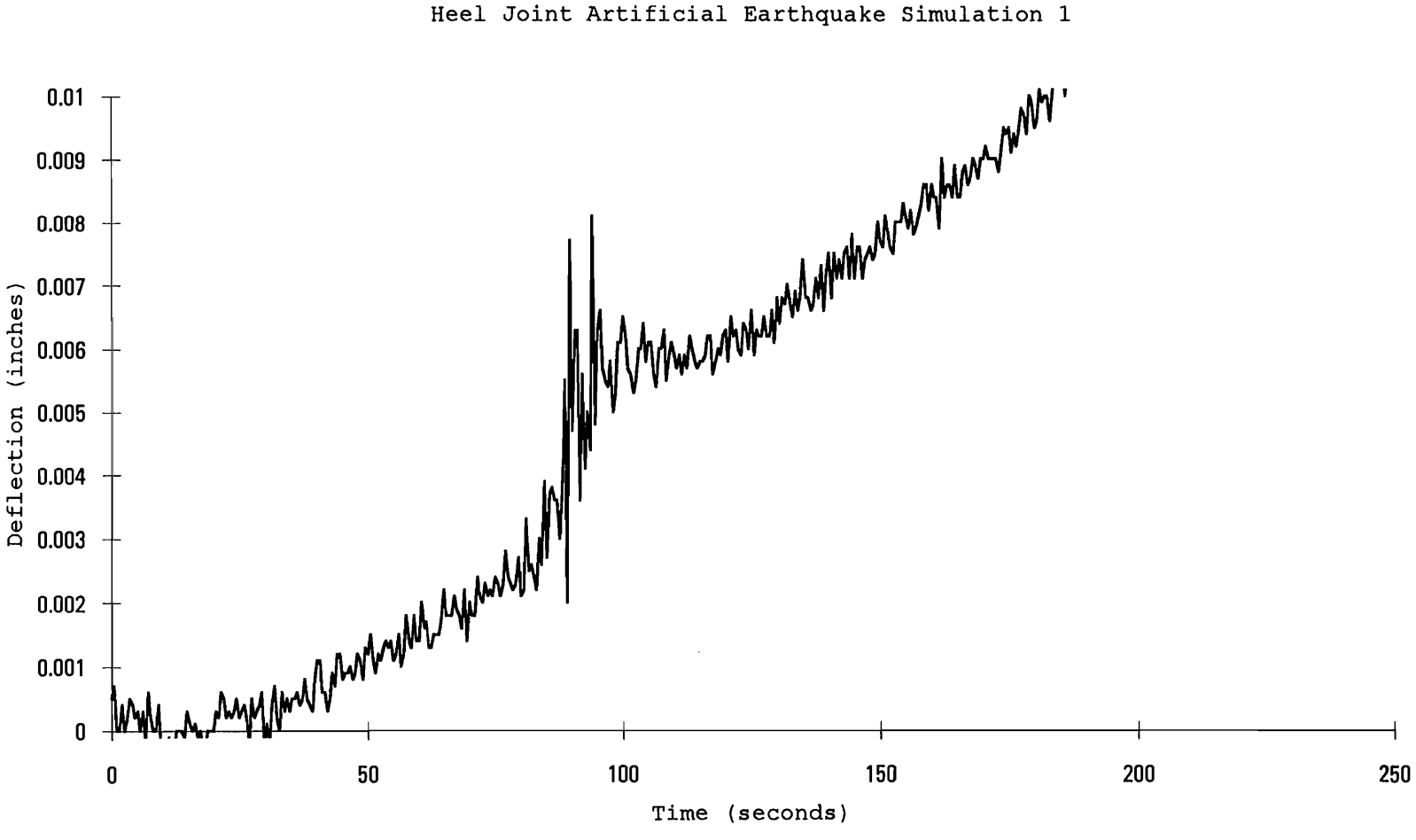

Figure 4.18: Close-up of a typical top chord deflection-time curve for the artificial earthquake simulation (joint 1)

However, axial stiffness was reduced as a result of the artificial earthquake time-history (two sided p-value of 0.003, see section 4.1 and Table 5.1).

Figure 4.19 displays a comparison of the Fourier amplitude spectra of the target and actual load time-histories for the top chord of the heel joint. This plot was developed using a Fast Fourier Transform (FFT) algorithm (Microsoft Excel, version 4.0a). The sampling rate of the data was 50 Hz for a duration of 30 seconds. However, only the first 20.48 seconds (1024 data points) were used to calculate the FFT. The FFT procedure requires 2^n data points, where n is a positive integer. The magnitude of the complex output from the FFT was computed and plotted in the frequency domain up to the Nyquist frequency of 25 Hz. A moving linear-average filter (boxcar filter) with a band-width of 1 Hz was used to smooth the data.

The "random" nature of the earthquake loads caused some loading control difficulties. First, the frequency components over 10 Hz were largely filtered out by the testing apparatus. As shown in Figure 4.19, the majority of the energy of the load time-history from the FEM response is contained below 10 Hz. Therefore, the passive filtering by the hydraulic system should not significantly affect the results. Second, a small time lag occurs between the input to the hydraulic system and the response, as shown in Figure

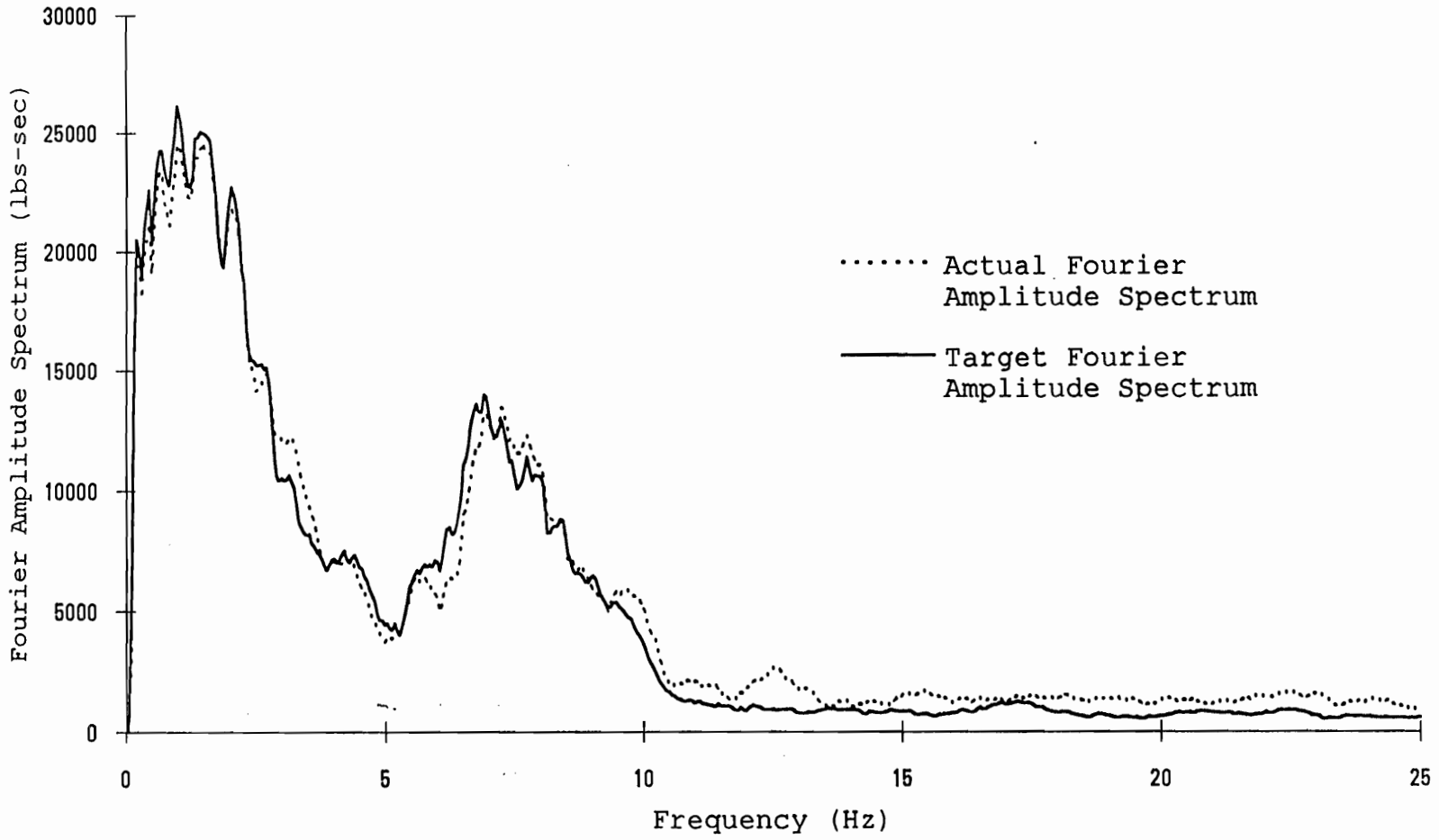

Figure 4.19: Fourier amplitude spectrum of the target and actual force time-histories for the top chord of the heel joint

4.20. Approximately the correct magnitudes of the loads are generally obtained, although approximately 0.1 seconds behind the intended time.

To construct Figures 4.19 and 4.20, a pilot test joint, not included in the strength or stiffness results, was used to record the actual loads applied by the testing system during the earthquake simulation. To accurately record the force-time-history of the pilot test heel joint to the earthquake loading, a data acquisition rate of 50 Hz was used. However, using a 50 Hz data acquisition rate for the actual testing (which includes the ramp-load portion) far exceeded the memory capacity of the computer used for data acquisition. For actual testing, an acquisition rate of 2 Hz was used.

4.3.4 Sequential Phased Displacement (SPD) Loading

The average strength (ultimate top chord load) of the heel joints subjected to the SPD loading and then failed under a static ramp load was 4185 lb with a COV of 15.8%. The average top chord axial and rotational stiffnesses were 1.36×10^5 lb/in. with a COV of 56.9% and 84.0×10^5 lb•in/rad with a COV of 69.3%, respectively (Appendix J). A statistical analysis (see section 4.1 and Table 5.1) indicated that the SPD loading significantly reduced the mean strength and axial stiffness of the heel joints (two

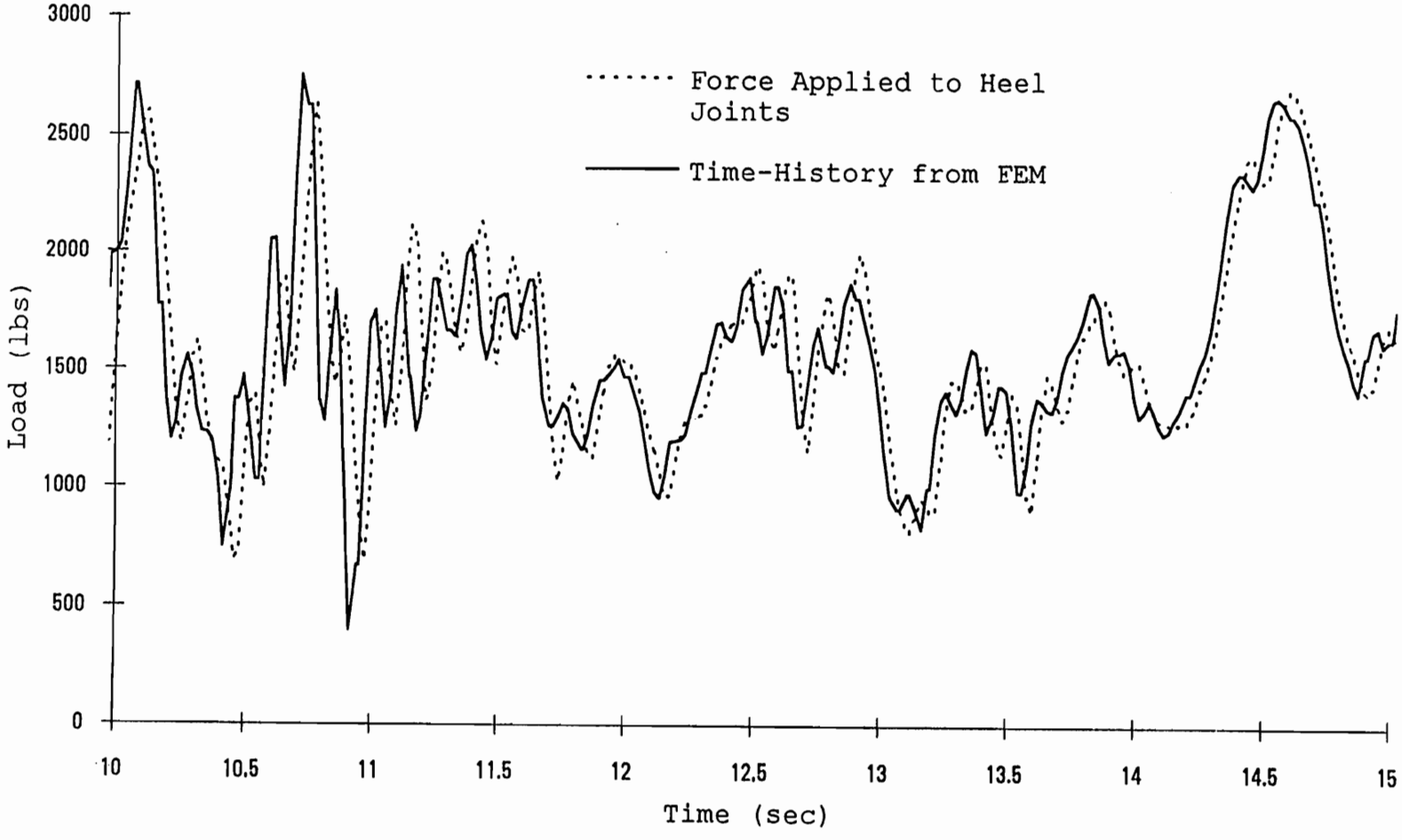

Figure 4.20: Target and actual top chord force-time response during a portion of the artificial earthquake time-history

sided p-values of 0.000 and 0.004 for strength and axial stiffness, respectively). However, significant rotational stiffness degradation did not occur as a result of the SPD loading (two sided p-value of 0.190).

Control difficulties were encountered during the SPD tests. The deflection feed-back loop was controlled by LVDTs which had an approximate resolution of 0.0007 in. A higher resolution deflection measurement system would be preferred to tighten the control of the deflection feed-back loop when working with such stiff connections.

The following dynamic properties, as defined by Dolan (1994), were evaluated for heel joints using the SPD method: energy dissipation, equivalent viscous damping ratio, and cyclic stiffness. These dynamic properties are described below and computed from individual hysteresis curves. Recall that the amplitude of the cycles in the SPD loading is defined in terms of the displacement of the top chord as a percent of the yield displacement (determined from static tests for the type of connection being studied). The dynamic properties of MPC heel joints calculated from this study are plotted against the deflection as a percent of the yield displacement. The deflection as a percent of the yield displacement is defined as the maximum displacement in the cycle being analyzed, divided by the top chord axial

yield displacement (0.007 in, section 4.3.1) determined from the static tests.

The hysteresis curve used in this study for calculation of the dynamic properties was not necessarily the stabilized hysteresis curve. The SPD method defines a stabilized cycle as one in the set of the stabilizing cycles (defined in Figure 4.12) that has a load degradation of no more than 5% from the preceding cycle. Because of the control difficulties discussed above, it was not possible to impose this definition of a stabilized hysteresis curve to these tests on heel joints. The testing system was able to control the deflections only within 4 to 7% of the target deflection. For example, if at a point during the SPD loading the deflection of the joint should have been 0.01 in, the actual deflection obtained from the testing system would have been, on average, somewhere between 0.0093 in. and 0.017 in. Therefore, the third cycle in each set of stabilization cycles was arbitrarily used as the stabilized hysteresis curve used for calculation of the dynamic properties. For most nailed and bolted connections, only three stabilizing cycles are necessary to obtain a stabilized hysteresis curve (Dolan 1994). Henceforth, in this paper, the third cycle in the set of three stabilizing cycles is referred to as the stabilized cycle and is used to compute the dynamic properties.

Energy dissipation is the area enclosed by the load-deflection trace. Recall that compression of the top chord is defined as positive. Energy dissipation in compression of the top chord (EA_c) is shown as the area confined by GAFCG (Figure 4.21). Similarly, the energy dissipation in tension of the top chord (EA_t) is shown as the area confined by FDGCF. The energy input to the system follows the line, DCA. Therefore, the energy input in compression (EI_t) is shown as the cross-hatched area CAB. Also, the energy input in tension (EI_c) is shown as the cross-hatched area CDE.

The damping ratios for the tension and compression half-cycles, ξ_t and ξ_c respectively, for any given half-cycle may be approximated by equations 4.2 and 4.3. The equivalent viscous damping ratio, or damping ratio, is a dimensionless parameter used to describe the resistance to motion/deformation which is provided by friction in the connector and inelastic deformation (Breyer 1993). Under most circumstances, the damping ratio cannot be directly calculated from basic material properties and structure geometry, therefore, testing is required to determine this parameter for various systems.

With the above definitions of energy dissipation and energy input, the damping ratios for tension and compression, ξ_t and ξ_C, respectively, for any given cycle may be approximated by Equations 4.2 and 4.3, respectively.

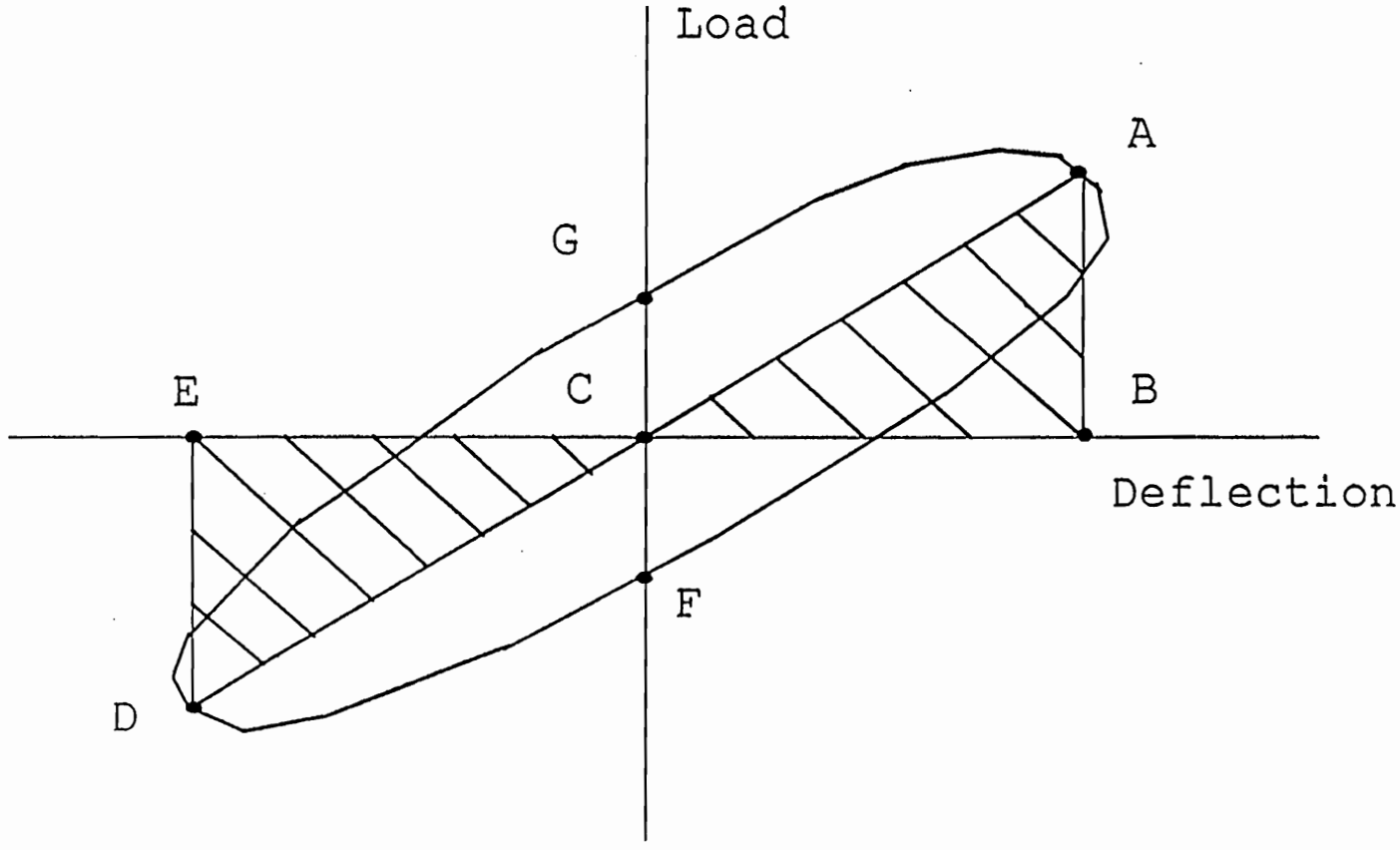

Figure 4.21: Hysteresis curve definitions (Dolan 1994)

Example calculations to determine the dynamic properties are presented in Appendix M.

$$\xi_t = EA_t/2\pi \cdot EI_t \quad \text{.....4.2}$$

$$\xi_C = EA_c/2\pi \cdot EI_c \quad \text{.....4.3}$$

A digitizing tablet (Calcomp Digitizer Products Division, Model No. 33120) was used to calculate the areas enclosed by the tension and compression regions of the hysteresis curves. Plots of the energy dissipation and damping ratio as functions of displacement are shown in Figures 4.22 and 4.23, respectively.

Dolan (1994) defined the cyclic stiffness as the slope of a straight line drawn between the lower left of the hysteresis curve to the upper right of the hysteresis curve, passing through the lowest and highest points curve (not necessarily passing through the origin). However, because the stiffness associated with compression in the top chord may be different than the stiffness associated with tension in the top chord, cyclic stiffnesses for compressive and tensile loads are defined as the slopes of the lines CA and DC, respectively (Figure 4.21). Figure 4.24 shows a plot of the cyclic stiffness during the SPD loading as a function of displacement.

Currently, there is no standard to determine a design level damping ratio from the SPD loading. For this study,

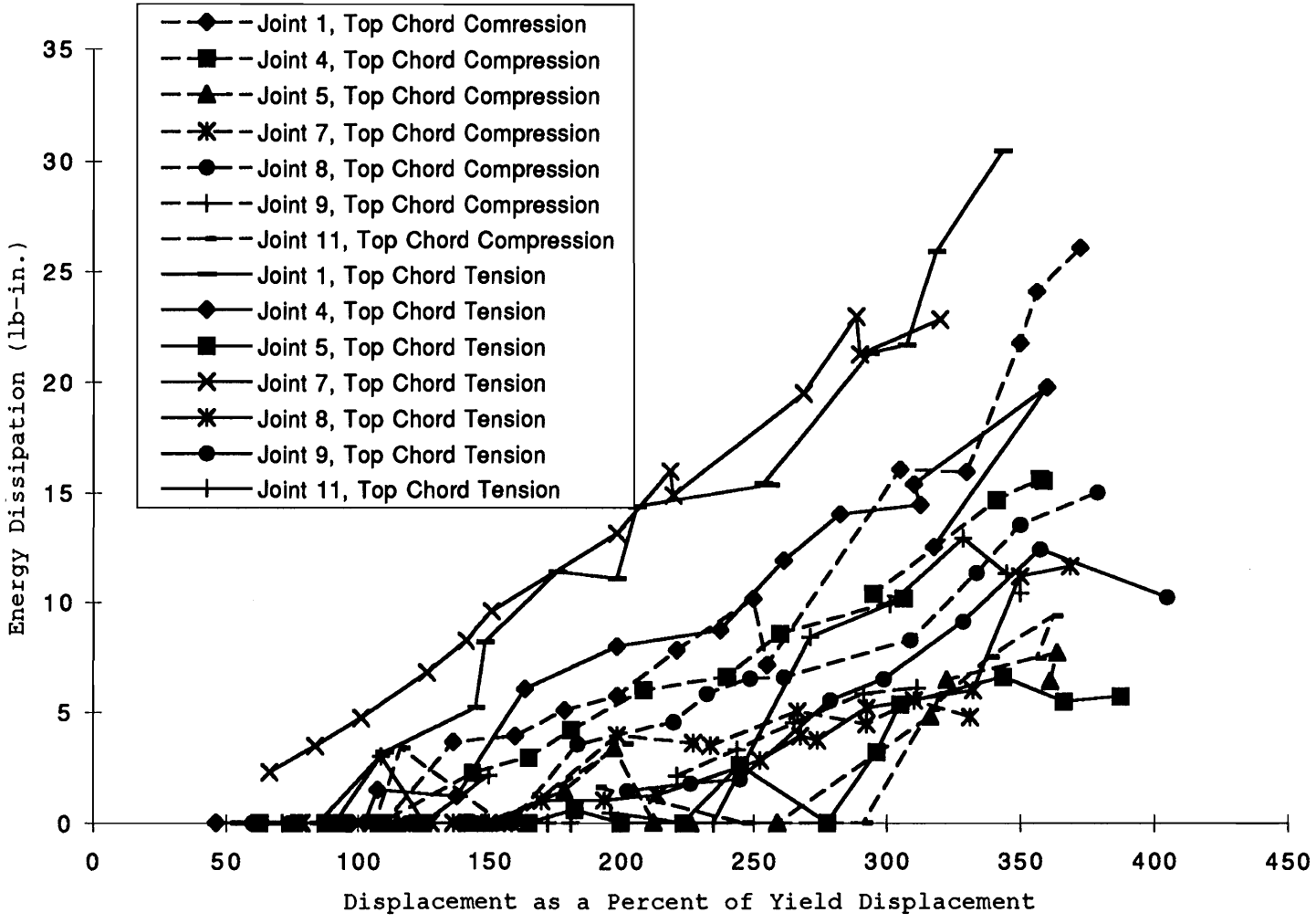

Figure 4.22: Energy dissipation of the heel joints during the sequential phased displacement loading

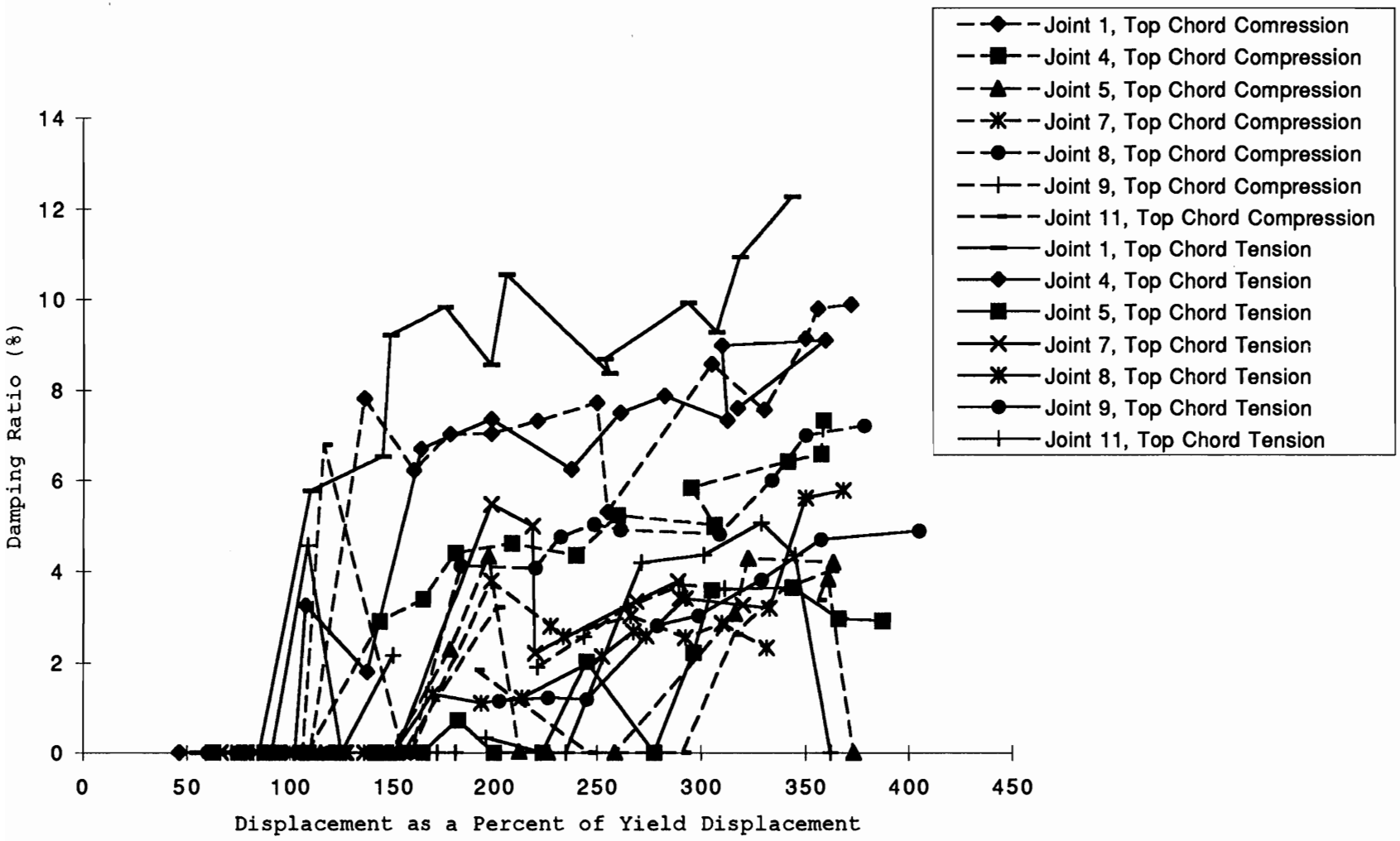

Figure 4.23: Damping ratio of the heel joints during the sequential phased displacement loading

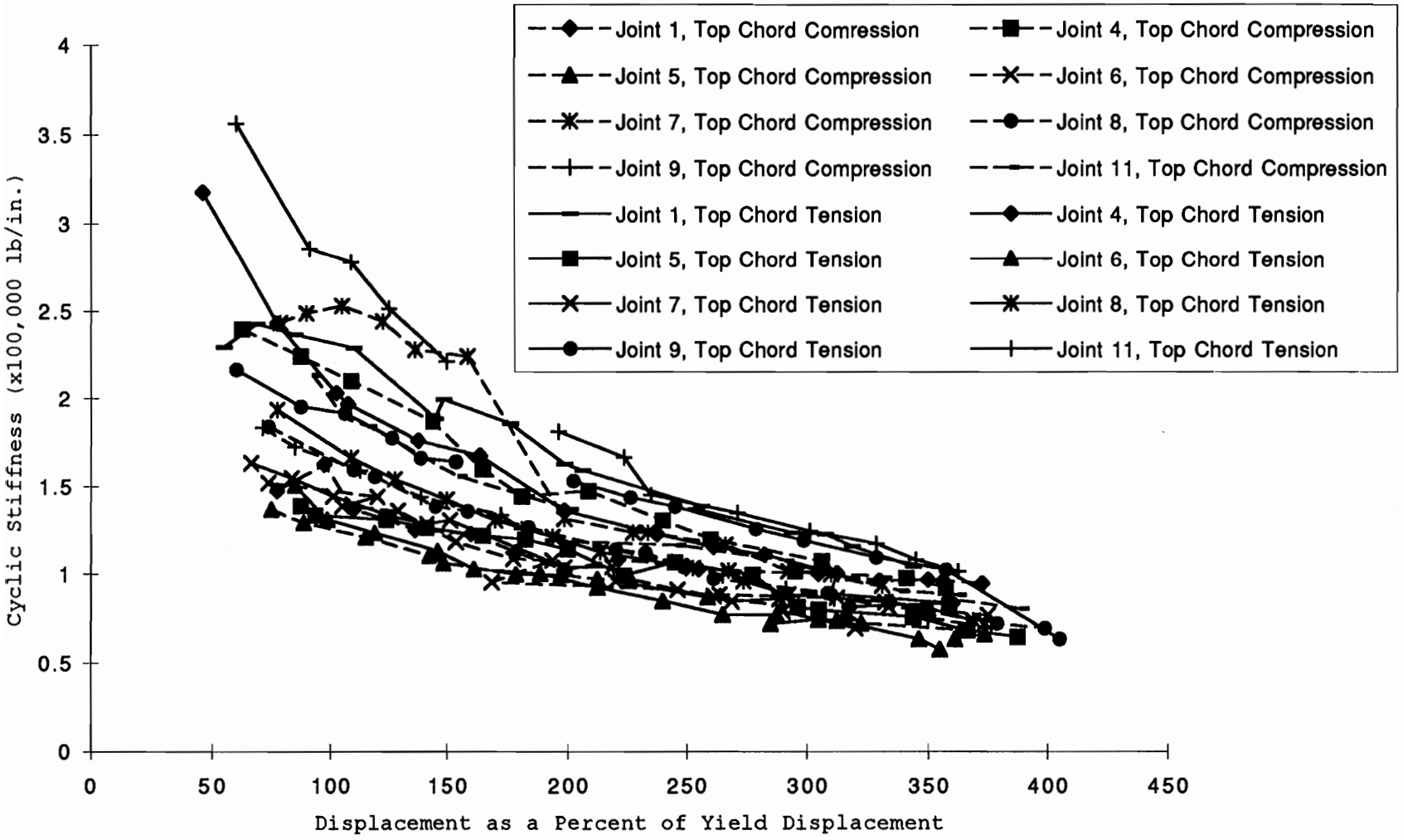

Figure 4.24 Cyclic stiffness of the heel joints during the sequential phased displacement loading

it was decided to compute the damping ratio associated with the first stabilized hysteresis curve to have a maximum compressive load in the top chord approximately equal to the design load (National Design Specification for Wood Construction, 1991) for the top chord of the heel joint (approximately 33% of the average ultimate load, Appendix J, 0.33•6211=2050 lb.). Because heel joints are not actually designed for tensile loads in the top chord, only the design level damping ratio associated with compressive loads in the top chord is presented. Table 4.4 displays a summary of the design damping ratio calculations from the SPD loading. Because of the control difficulties, only six tests (joints 1,4,5,8,9, and 11) produced hysteresis curves from which the energy dissipation and damping ratio could be measured. Based on the above definition of design levels, a damping ratio of 3.8%, corresponding to the average of the damping ratio values presented in Table 4.4, is recommended for design. In some cases, a more detailed examination of Figure 4.23 is suggested. Factors to consider are the number and amplitude of the cycles the heel joint is expected to experience in service. It may be appropriate to select the damping ratio (from Figure 4.23) associated with the specific level of displacement expected for the joint in service.

Table 4.4: Summary of the damping ratio calculations from the sequential phased displacement loading

Joint	Cycle Number	Energy Dissipation (lb-in.)	Damping Ratio (%)
1	92	15.9	7.55
4	36	2.26	2.91
5	85	5.46	3.07
8	57	4.53	4.08
9	64	2.12	1.90
11	50	3.58	3.21
Average	64	5.64	3.79

Note: See Appendix M for Sample Calculations for Joint 5

Although Figures 4.22, 4.23, 4.24 show a lot of variation between tests, specific trends can be seen. The energy dissipation and damping ratio both tend to increase initially, from 0 to 150% of the yield displacement, during the SPD loading. However, after 150% of the yield displacement, the damping ratio tends to level off, whereas the energy dissipation continues to increase. Cyclic stiffness clearly decreases with increasing displacement as a percent of yield displacement. This implies that the connection is accumulating damage at the tooth-wood interface. The damaged wood fibers at the interface decrease the stiffness of the overall connection as they dissipate energy due to inelastic deformation. Therefore, less load on the joint is required to obtain the same deflection. It can be assumed that bending of the teeth and shear deformation of the metal-place-connector also contribute to the deflection recorded by the LVDTs. However, because the teeth are embedded into the wood, the amount of bending is difficult to assess. At failure, though, slight bending of the teeth and shear deformation can be seen (see Figure 4.15). Also, strain gauges were not used to measure the complicated strain distribution in the metal-plate.

As the SPD loading progresses, the shapes of the hysteresis curves change. As shown in Figure 4.22, the

energy dissipation increases with increasing displacement as a percent of yield displacement, which implies that the hysteresis curves are confining a larger area. Figure 4.25 shows a typical hysteresis curve (for joint 5) at low load levels. Notice that very little area is confined by the curve. Figure 4.26 shows a typical hysteresis curve (joint 5) at a higher load level. The area confined by the curve has increased significantly due to the inelastic behavior of the damaged MPC joint.

The top chord load-time-history plots and deflection-time-history (for both axial deflection and rotation deflection) for each joint during the sequential phased displacement loading are displayed in Appendix N. The maximum load and top chord deflection for each cycle tends to increase with time; however, the deflection due to rotation-time curve is quite variable. The deflection due to rotation-time curve measures the response of the LVDT which is placed perpendicular to the top chord of the heel joint (see Figure 4.3) during the sequential phased displacement loading. The large amount of variation seen in the deflection due to rotation-time curve may be attributed to the natural variation of wood, especially the stiffness perpendicular to the grain, which is a primary factor resisting rotation. Also, the imperfect feed-back control also contributed to the variability of the curves in

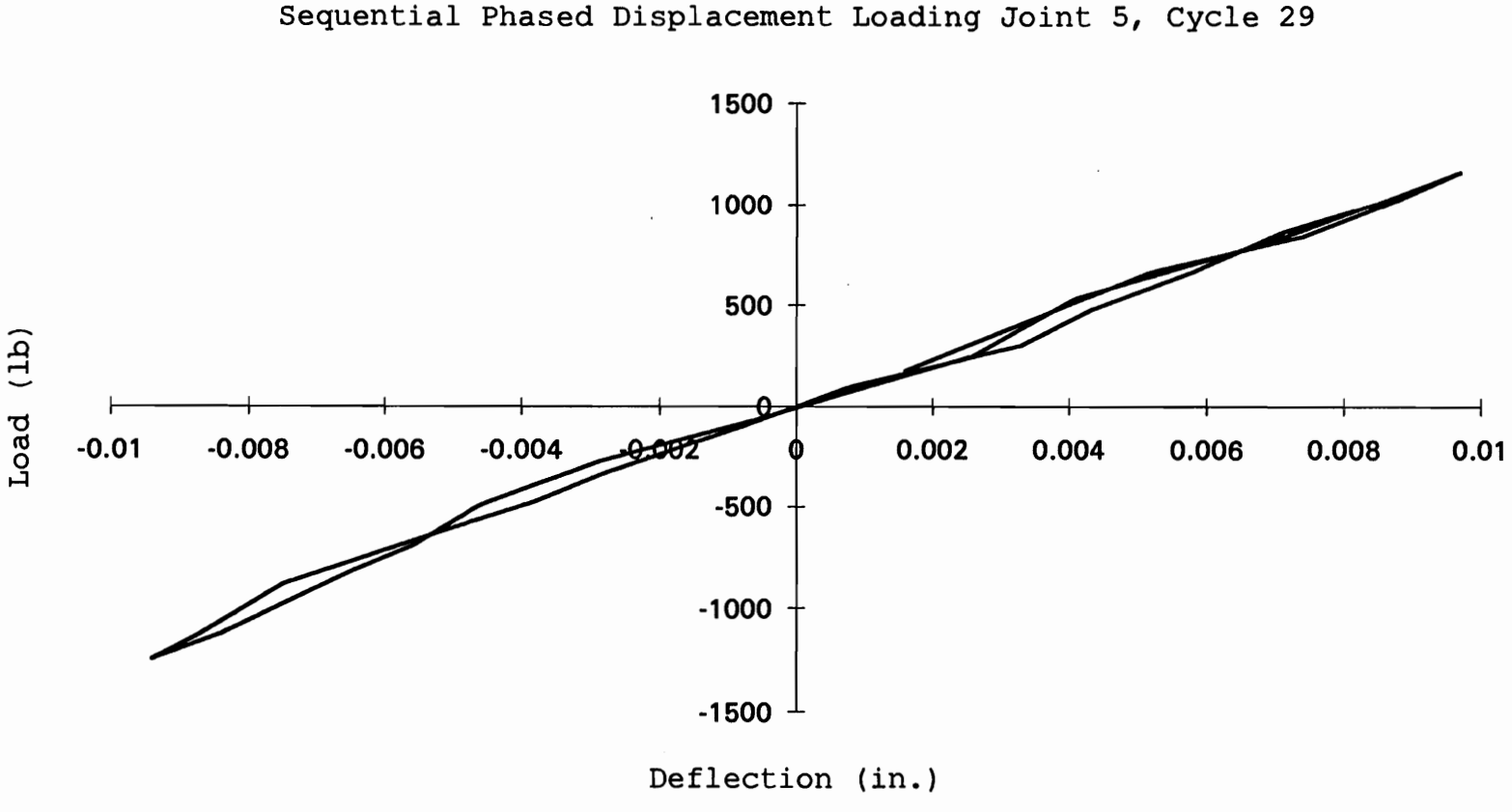

Figure 4.25: Typical hysteresis curve at low deflection levels (top chord load and deflection)

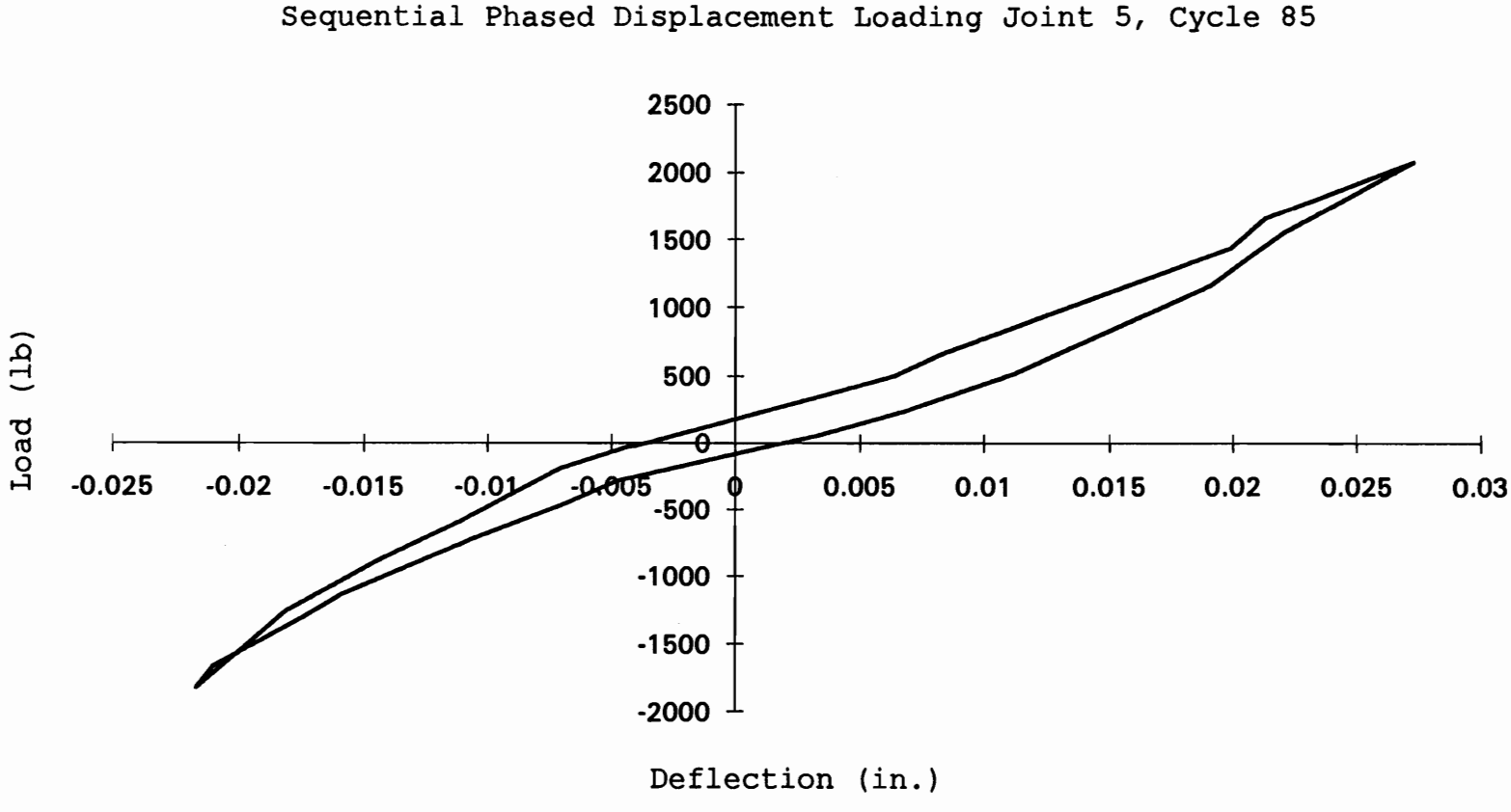

Figure 4.26 Typical hysteresis curve at high deflection levels (top chord load and deflection)

Appendix N. In Joint 2, after only 91 cycles, the lag screws withdrew from the bottom chord of the heel joint and therefore the sequential phased displacement portion of the test was terminated (the support could no longer resist a tensile load in the top chord). Joint 7 experienced a tension-perpendicular to the grain failure mode. This failure mode occurred due to the large perpendicular to grain stresses transmitted from the metal-plate-connector to the bottom chord when the top chord was in tension.

4.3.5 Cyclic Loading Tests

The results of the cyclic loading tests are tabulated in Table 4.5 and plotted in Figure 4.27. The vertical axis of Figure 4.27, strength ratio, is defined as the ratio of the maximum strength (ultimate top chord load) of the heel joint under a static ramp load after completion of the 200-cycles to the average maximum strength of the static loading control group (6211 lb, Appendix J). The horizontal axis is defined as the amplitude of the cycles (defined in Figure 4.13) divided by the average maximum strength (6211 lb, Appendix J) of the static loading control group and expressed as a percentage. For a joint to be assigned a nonzero post-cyclic strength ratio, it must be able to carry load after the conclusion of the 200-cycles. Joints which failed during the cyclic loading were assigned a zero

Table 4.5: Cyclic loading test results for heel joints.

Cyclic Amplitude	Test Number	Ultimate Top Chord Load (lb)	Strength Ratio (1)
0	static1	5619	0.90
0	static2	6436	1.04
0	static3	6161	0.99
0	static4	5865	0.94
0	static5	6540	1.05
0	static6	6369	1.03
0	static7	7001	1.13
0	static9	5773	0.93
0	static10	6134	0.99
5	5-1 †	5059	0.81
5	5-2	5520	0.89
5	5-3	6459	1.04
10	10-1	4681	0.75
10	10-2	6426	1.03
10	10-3	6722	1.08
15	15-1	5363	0.86
15	15-2	5983	0.96
15	15-3	5362	0.86
20	20-1	6617	1.07
20	20-2	5710	0.92
25	25-1	5750	0.93
25	25-2	6502	1.05
30	30-1	4095	0.66
30	30-2	4731	0.76
30	30-3	6705	1.08
33	33-1	5208	0.84
33	33-2	5599	0.90
33	33-3	6200	1.00
35	35-1	5307	0.85
35	35-2	0	0.00
35	35-3	0	0.00
40	40-1	0	0.00
40	40-2	0	0.00
40	40-3	0	0.00

(1) Actual strength divided by the mean static strength; static strength = 6211 lb (Appendix J)

† Cyclic Amplitude in Percent - Test Number

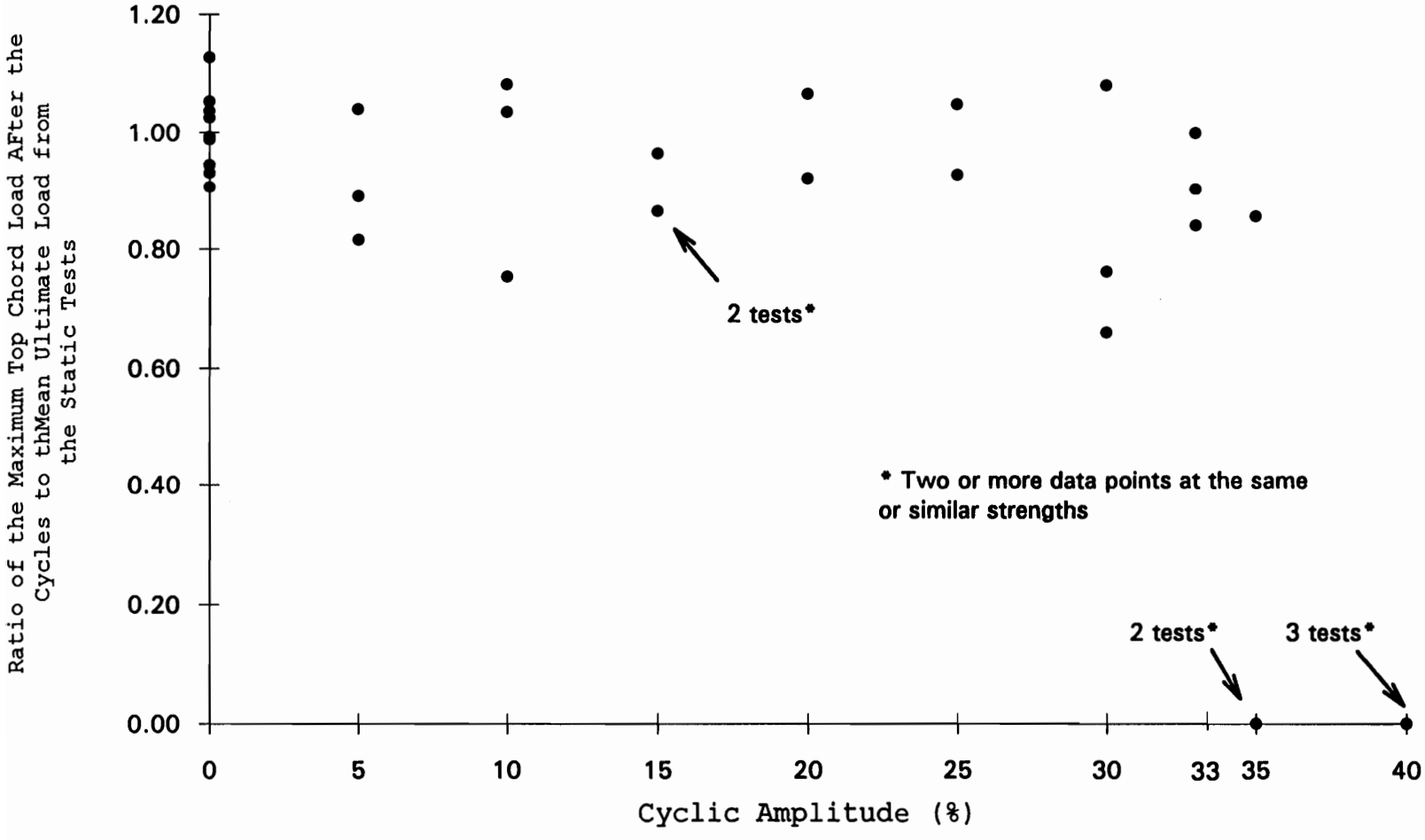

Figure 4.27: Cyclic loading test results

strength ratio. A threshold appears to exist at approximately 35% cyclic amplitude where heel joints are no longer able to survive the entire set of cycles. Chapter 5 contains further discussion and the implications for design of the cyclic loading results.

5. Conclusions

Metal-plate-connected (MPC) tension-splice and heel joints exhibit nonlinear load-deflection and moment-rotation (observed for heel joints only) behavior under static ramp loads. The application of load-controlled ramp loads (700 lb/min and 1200 lb/min for tension-splice and heel joints, respectively) causes complete and sudden failure with little warning. The most common failure mode for the MPC tension-splice and heel joints tested was tooth withdrawal. Tension-splice joints can also experience a plate-tension failure mode (not a wood failure).

The horizontal and vertical accelerations from the Northridge earthquake and those from an artificial earthquake (1.0 g's and 0.67 g's peak horizontal and vertical accelerations, respectively) developed using WES-RASCAL (Silva 1987) were applied as base accelerations to a finite-element model of a 30 ft span Fink truss. The predicted forces in the tension-splice joint from the finite-element model of the truss (for both of these earthquake simulations) are below the design load (one-third of the mean ultimate strength, National Design Specification for Wood Construction, 1991) (by 16% for the Northridge earthquake simulation and 6% for the artificial earthquake simulation). However, the maximum load predicted from the

finite-element model for the top chord of the heel joint during the artificial earthquake (1.0 g's and 0.67 g's peak horizontal and vertical accelerations, respectively) is 44% of the mean ultimate load from the static loading control group which exceeds the design load (33% of the mean ultimate load from the static loading control group, National Design Specification for Wood Construction 1991).

The effect of multi-event earthquake loadings applied to MPC joints is unknown at this point. In this study, strength and stiffness effects after only one earthquake were analyzed. From the cyclic tests, it is evident that caution should be applied when using metal-plate-connected joints in situations where cyclic loading is prevalent, such as in high wind areas, bridges, and floors. Although the cyclic loadings investigated in this study loaded the MPC joints beyond their design range (one-third of the mean ultimate strength, National Design Specification for Wood Construction, 1991), it is possible that lower level cyclic loads (less than the design load) may also have an effect on the strength after a large number of cycles. An example of this can be seen from fatigue testing of MPC tension-splice joints (Hayashi et al., 1980), where failure occurred in joints which were cycled numerous times (greater than 10,000 cycles) at low load levels.

A summary of the statistical results is shown in Figure 5.1 and Table 5.1. Figure 5.1 displays groups of tests with statistically equivalent strength and stiffness for the tension-splice and heel joint tests. Table 5.1 displays the two sided p-values for the tension-splice and heel joints for strength and stiffness comparisons between the dynamic tests and their corresponding static loading control group.

5.1 Metal-Plate-Connected Tension-Splice Joints

The Northridge (0.903 g's maximum horizontal acceleration and 0.232 g's maximum vertical acceleration) and artificial earthquake (1.0 g's maximum horizontal acceleration and 0.67 g's maximum vertical acceleration) simulations caused no strength or stiffness degradation when compared to the control groups of static tests fabricated from similar plates. Because each earthquake was applied to the joints only once, the effect of cumulative earthquake loadings on the strength of the MPC tension-splice joints is unknown.

Dynamic properties of MPC tension-splice joints are shown to be dependent on the level of displacement in the Sequential Phased Displacement (SPD) loading. As the displacement increases, damage accumulates in the connection causing the damping ratio and energy dissipation to increase and the cyclic stiffness to decrease. For design, a damping

Table 5.1: Summary of two-sided p-values from a student's t-test.

Two Sided p-values from the Tension Splice Joint Tests*

Test	Strength	Stiffness
Control Group Batch-1 & Control Group Batch-2	0.025	0.007
Control Group Batch-1 & Sequential Phased Displacement Batch-1	0.630	0.000
Control Group Batch-1 & Northridge Earthquake Simulation Batch-2	0.780	0.280
Control Group Batch-2 & Artificial Earthquake Simulation Batch-2	0.490	0.180

* Determined from a two sample Student's t-test

Two Sided p-values from the Heel Joint Tests*

Test	Strength	Axial Stiffness	Rotational Stiffness
Control Group & Artificial Earthquake Simulation	0.46	0.003	0.150
Control Group & Sequential Phased Displacement	0	0.004	0.190

* Determined from a two sample Student's t-test

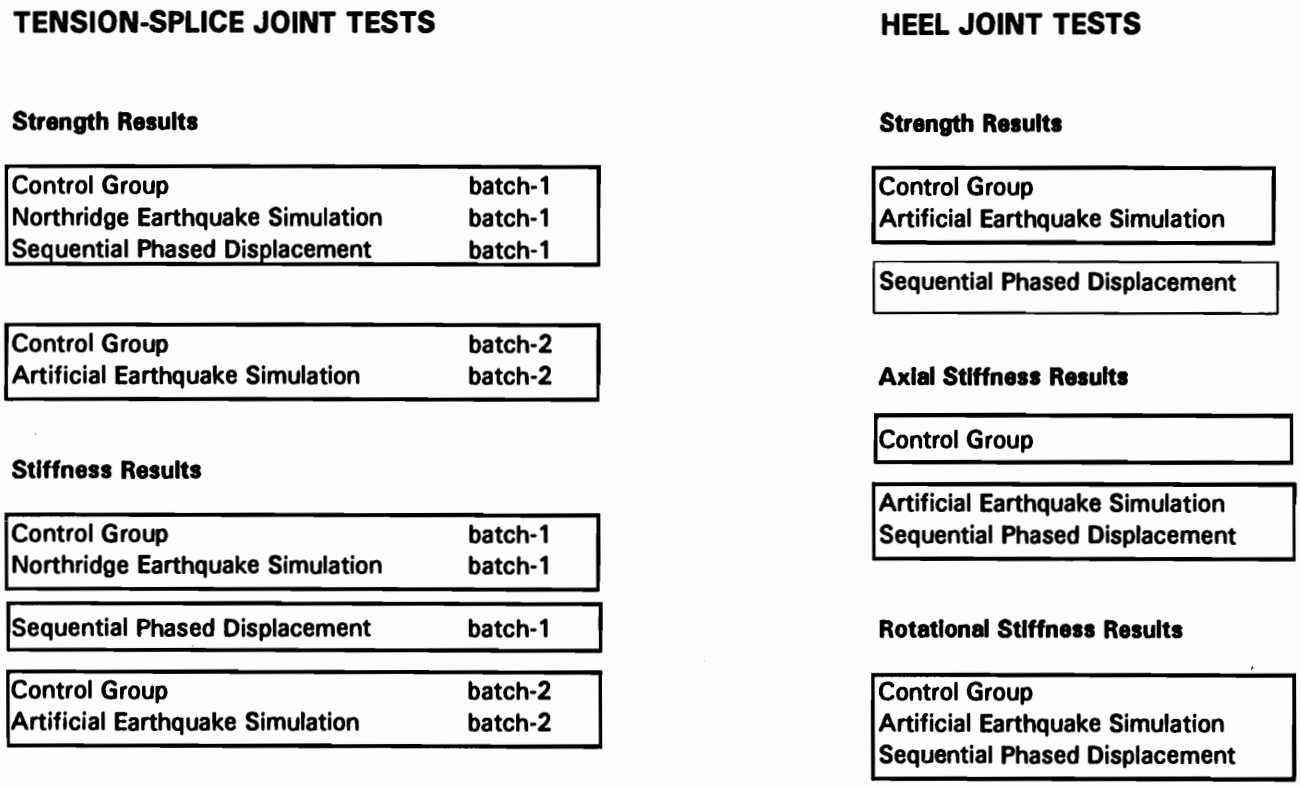

Figure 5.1: Summary of the statistical results for the tension-splice and heel joint testing

ratio of 4.3% is suggested for the tension-splice joint, based on the sequential phased displacement tests (section 3.3.4).

The cyclic loading, consisting of 200-cycles applied at a frequency of 1 Hz, used in this study has a significant effect on the strength of tension-splice joints. There appears to be a threshold between 20 and 23% cyclic amplitude (amplitude expressed as a percentage of the mean ultimate strength of the control group from batch-2, 6712 lb, Appendix D) beyond which the tension-splice joints cannot survive 200-cycles.

5.2 Metal-Plate-Connected Heel Joints

The artificial earthquake (1.0 g's maximum horizontal acceleration and 0.67 g's maximum vertical acceleration) simulation caused no strength (top chord ultimate load) degradation or rotational stiffness degradation when compared to the control group; however axial stiffness degradation was observed. Because each earthquake was applied to each joint only once, the effect of cumulative earthquake loadings on the strength of the MPC heel joints is unknown.

Dynamic properties of MPC heel joints are shown to be dependent on the level of displacement in the SPD loading. As the cycles progress, damage accumulates in the connection

causing the damping ratio and energy absorption to increase and the cyclic stiffness to decrease. For design, a damping ratio of 3.8% is suggested for the heel joint, based on the sequential phased displacement loading (section 4.3.4)

The cyclic loading examined in this study had a significant effect on the post-cyclic strength (top chord ultimate load) of heel joints. There appears to be a threshold at approximately 35% cyclic amplitude (amplitude expressed as a percentage of the mean ultimate strength of the control group, 6211 lb, Appendix J) beyond which the heel joints cannot survive 200 cycles.

5.3 Recommendations for Further Study

- Construct a finite-element model of a truss system which includes the effects of the finite stiffnesses of the MPC joints. The model should have the capability to include the damping ratios representative of each type of material and connection. The purpose of this model would be to better estimate truss member loads during a seismic or high wind event.
- Investigate more fully the support conditions (from the bearing walls) for the above finite-element model.
- Examine the impact of multiple earthquake loadings on the strength and stiffness of MPC joints because in some areas (California, for example) a structure can be

expected to experience more than one earthquake during its service life.

- Develop a testing system which is suited for high frequency stochastic loads. The system should be stiffer than the one used in this study and have a higher frequency feed-back control rate (greater than 500 Hz) for both load and deflection controlled input functions.
- Determine magnitude and number of cycles expected for realistic wind loadings of MPC truss joints. Investigate effects of these realistic wind loadings on strength and stiffness of MPC joints.

Bibliography

American Society for Testing and Materials. (1994). ASTM D1761-77: Standard Methods of Testing Mechanical Fasteners in Wood., D2395-93: Standard Test Methods for Specific Gravity of Wood and Wood-Base Materials., ASTM D4442-92: Standard Test Methods for Direct Moisture Content Measurement of Wood and Wood-Base Materials., ASTM D2915-94: Standard Practice for Evaluating Allowable Properties for Grades of Structural Lumber., Vol. 04.10. Philadelphia, PA.

Arbek, T. (1979). "The Effect of Time on Strength of Truss Plate Joints." Bachelor of Science of Forestry Thesis. Department of Civil Engineering, Carleton University. Ottawa, Canada.

Breyer, Donald E. (1993). "Design of Wood Structures." Third Edition. McGraw-Hill, Inc., New York, NY.

Buchanan, A. H., and Dean, J. A. (1994) "Practical Design of Timber Structures to Resist Earthquakes." Proceedings from the Pacific Timber Engineering Conference, Gold Coast Australia, pp 813-822.

Cramer, S. M., Shrestha, D., Fohrell, W. B. (1990). "Theoretical Consideration of Metal-Plate-Connected Wood-Splice Joints." Journal of Structural Engineering, Vol 116, No. 12, pp 3458-3473.

Dagher, H. J., Caccese, V., Hsu, Y., Wolfe, R. and Ritter, M. (1991). "Feasibility of Metal Connector Plates in Timber Bridges: Fatigue Study." Technical Report, Department of Civil Engineering, University of Maine, Orono, Maine.

Dolan, J. D. (1994). "Proposed Test Method for Dynamic Properties of Connections Assembled with Mechanical Fasteners." Journal of Testing and Evaluation 22(6), pp 542-547.

Emmerson, R., and Fridley, K.J. (1995). Forest products society annual meeting. Technical Poster presentation session. Portland, OR.

Foliente, G. C. and Zacher, E. G. (1994). "Performance Tests of Timber Structural Systems Under Seismic Loads." Proc. Research Needs Workshop on Analysis, Design and Testing of Timber Structures Under Seismic Loads. G. C. Foliente, ed., Forest Products Laboratory, University of California, Berkeley, CA.

Foschi, R. O. (1974). "Load-Slip Characteristics of Nails." Wood Science., 7(1), pp 69-76.

Gupta, R. (1994). "Metal-Plate Connected Tension Joints Under Different Loading Conditions." Wood and Fiber Science, 26(2), pp 212-222.

Gupta, R., Gebremedhin, K. G. (1990). "Destructive Testing of Metal-Plate-Connected Wood Truss Joints." Journal of Structural Engineering, American Society of Civil Engineering, 116(7), pp 1971-1982.

Hayashi, T., Sasaki, H., Masuda, M. (1980). "Fatigue Properties for Wood Butt Joints with Metal Plate Connectors." Forest Products Journal, 30(2), pp 49-54.

International Council of Building Officials (1994), Uniform Building Code, Vol. 2: Structural Engineering Design Provisions. Whittier, California.

Leiva, L. (1994). "Racking Behaviour of Timber-Framed Shear Walls." Proceedings from the Pacific Timber Engineering Conference, Gold Coast Australia.

Naeim, F., Lew, M. (1995). "On the Use of Design Spectrum Compatible Time Histories." *Earthquake Spectra*, Vol 11, No. 1, 111-127.

National Design Specification for Wood Construction (1991). National Forest Products Association, Washington, D.C.

Polensek, A., Schimel, B. D. (1988). "Analysis of Nonlinear Connection Systems in Wood Dwellings." Journal of Computing in Civil Engineering, 2(4), 365-379.

Silva, W. J., Lee, K. (1987). State-of-the-Art for Assessing Earthquake Hazards in the United States: WES-RASCAL Code for Synthesizing Earthquake Ground Motions. US Army Corps of Engineers, Miscellaneous Paper S-73-1, Report 24 of a series, Washington D.C.

Sletteland, N. T., Pratt, G. L., and Schuler, R. T. 1977. "Fatigue life of Metal Plate Connector Plates." ASAE Paper No. 77-4037. St. Joseph, MI.

Soltis, Lawrence A. (1983). "Performance of Low-Rise Timber Buildings Subjected to Seismic, Wind, and Snow loads. American Society of Civil Engineering Preprint 83-015. New York, NY.

Tokuda, M., Takeshita, M., and Sugiyama, H. (1979). "The Behaviors of Metal Plate Connector Joints Subjected to Repetitive Tension Force. J. Japan Wood Res. Soc., 25(6), pp 408-413.

Zacher, E. G. (1994). "Past Seismic Performance of Timber Buildings." Research Needs Workshop on Analysis, Design and Testing of Timber Structures Under Seismic Loads. G. C. Foliente, ed., Proc. Forest Products Laboratory, University of California, Berkeley, CA.

Appendices

Appendix A

Finite Element Model (SAP 90) Input File for Tension-Splice Joints

SAP90 Input file used for the dynamic analysis. Acceleration time-history data in a text file named motion.txt. Linear Model.

```
C SAO90 Input File
C Fink Truss, 4/12 pitch, 30-ft span
C 20 lbs/ft dead load on top and bottom
C chords.  Includes dead weight of web
C members.  Using 2x4 truss members
C E=1.6e6-psi
C Units are KIP INCHES
SYSTEM
 R=0  L=2  C=0  V=5  T=0.0001  P=0  W=0  Z=0
GRID
 XN=31    YN=3    ZN=14    OG=0                    // Defines the x,y, & z
 0 12 24 36 48 60 72 84                            // grid
96 108 120 132 144 156 168 180
 192 204 216 228 240 252 264 276
 288 300 312 324 336 348 360
 0 12 24
 0 12 24 36 48 60 72 84
 96 108 120 132 144 156
JOINTS                                             // Defines the location
 8    X=24 Y=12 Z=96                               // of the joints
 16   X=384 Y=12 Z=96
 100  X=114 Y=12 Z=126
 101  X=204 Y=12 Z=156
 102  X=294 Y=12 Z=126
 103  X=144 Y=12 Z=96
 104  X=264 Y=12 Z=96
 105  X=24 Y=12 Z=0
 106  X=384 Y=12 Z=0
 200  X=408 Y=12 Z=96
 201  X=0 Y=12 Z=96
 108  X=174 Y=12 Z=96

                                                   // Defines properties of
FRAME                                              // the materials
 NM=5 NL=0 NSEC=0 Z=-1
 1   A=8.25 J=0 I=20700,20700 AS=0,0 E=1600.1 G=0 W=0.00065001
M=1.6822E-006\
     TC=0
 2   A=5.256 J=0 I=5.34989,0.98496 AS=0,0 E=1600.07 G=0 W=0.001667\
     M=4.31333E-006 TC=0
 3   A=5.256 J=0 I=5.34989,0.98496 AS=0,0 E=1600.07 G=0 W=0.001667\
     M=4.31333E-006 TC=0
 4   A=5.256 J=0 I=5.34989,0.98496 AS=0,0 E=1600.07 G=0 W=9.479E-005\
     M=2.45319E-007 TC=0
 5   A=0.012 J=0 I=999999,999999 AS=0,0 E=1600.1 G=0 W=0 M=0 TC=0

                                                   // Places member between
                                                   // the joints

 1    8    100  M=2,2,1 LP=2,0 LR=1,0,0,1,0,1
 2    100  101  M=2,2,1 LP=2,0 LR=0,1,0,0,1,1
```

```
 3     101   102   M=2,2,1 LP=2,0 LR=1,0,0,1,0,1
 8     104   16    M=3,3,1 LP=2,0 LR=0,1,0,0,1,1
 9     100   103   M=4,4,1 LP=2,0 LR=1,1,0,1,1,1
 10    103   101   M=4,4,1 LP=2,0 LR=1,1,0,1,1,1
 11    101   104   M=4,4,1 LP=2,0 LR=1,1,0,1,1,1
 12    104   102   M=4,4,1 LP=2,0 LR=1,1,0,1,1,1
 13    201   8     M=5,5,1 LP=2,0 LR=1,1,0,1,1,1
 14    16    200   M=5,5,1 LP=2,0 LR=1,1,0,1,1,1
 4     102   16    M=2,2,1 LP=2,0 LR=0,1,0,0,1,0
 5     8     103   M=3,3,1 LP=2,0 LR=1,0,0,1,0,0
 6     103   108   M=3,3,1 LP=2,0 LR=0,1,0,0,1,0
 7     108   104   M=3,3,1 LP=2,0 LR=1,0,0,1,0,0
 20    8     105   M=1,1,1 LP=2,0 LR=1,1,0,1,1,1
 21    16    106   M=1,1,1 LP=2,0 LR=1,1,0,1,1,1

                                                  // Defines the location
                                                  // of the restraints
RESTRAINTS
 105   105   1     R=1,1,1,1,0,1
 106   106   1     R=1,1,1,1,0,1
 100   100   1     R=0,1,0,1,0,1
 103   103   1     R=0,1,0,1,0,1
 101   101   1     R=0,1,0,1,0,1
 104   104   1     R=0,1,0,1,0,1
 102   102   1     R=0,1,0,1,0,1
 200   200   1     R=1,1,1,1,1,1
 201   201   1     R=1,1,1,1,1,1
 108   108   1     R=0,1,0,1,0,1
 8     8     1     R=0,1,0,1,0,1
 16    16    1     R=0,1,0,1,0,1

TIMEH
 ATYPE=0 NSTEP=1500 DT=0.02 NF=1 NV=5 D=0.1
 NF=1 PRIN=0 NPL=1 NAM=motion.txt
 LC=-3 NF=1 S=483.4 AT=0 ANGLE=0


COMBO
 1     C=1,1
```

Appendix B

WES-RASCAL Input File for Tension-Splice Joints

WES-RASCAL input file used to create an artificial earthquake using the UBC (ICBO 1994) design response spectrum and the Northridge earthquake horizontal accelerations for the phase characteristics (NRINPUT.TXT).

Description	Real RASCAL input file
title	"WES : WUS : HALF-SPACE (M7, 5 % DAMPING, IV25VERT) : KEY5 = -1"
output file name	scotty8
site condition parameters	50.0 2.7 00.0 10.0 3.2
"	300.0 0.0 0.0 7
"	5.0 15.0 4 0.0
keys	0 1 0 0 -1 0
number of near-site amplification factors	5
frequency, amplification factors	0.1 1.023
"	.316 1.096
"	1.0 1.349
"	3.162 2.188
"	10.0 2.344
input time-history file name	NRINPUT.TXT
input time-history file format	3000 1 0.02 (1F9.6)
output time-history normalizing factors	-1.0 0.00 0.00
number of iterations	10 10
number of input response spectrum points	7
input response spectrum points (frequency, pseudo acceleration)	0.33 0.36
"	.5 0.48
"	.67 0.62
"	1 0.96
"	1.11 1
"	10 1
"	30 0.4
output time-history filtering parameters	23.0 5 0.10 -5

Appendix C

Design Load Calculations for Tension-Splice Joints

Procedure to scale the force-time-history output from the finite-element model artificial earthquake simulation to design level forces.

Compute base shear using the Uniform Building Code (ICBO 1994) procedure:

$$V_{static} = \frac{ZIC}{R_w} W$$ -UBC Equation 12-1

$$C = \frac{1.25\,S}{T^{2/3}}$$ -UBC Equation 12-2

where:

Z	=	0.4	-From UBC Table 23-I (Zone 4)
R_w	=	8	-From UBC Table 23-O (Bearing Wall System Type 1-A)
I	=	1.0	-From UBC Table 23-L (Standard Occupancy)
S	=	1.5	-From UBC Table 23-J (Soil S3, no soil information available)
W	=	1382 lb	-From the finite-element model (Total Dead Weight)

Compute the Structure Period using Method A of UBC section 1628.2.2

$$T = C_t (h_n)^{2/3}$$

Where

C_t = 0.020 (for timber structues)

h_n = 8 ft (height of bearing walls)

$$T = (0.020)(8\,ft)^{2/3} = 0.08\ seconds$$ -UBC Equation 28-3

$$C = \frac{1.25(1.5)}{0.08^{2/3}} = 10.1 > 2.75,$$ Therefore, C = 2.75

$$\frac{C}{R_W} = \frac{2.75}{8} = 0.344 > 0.075$$ Therefore acceptable

Compute the Base Shear

$$V_{static} = \frac{0.4(1.0)(2.75)}{8}(1382\ lb) = 190\ lb$$

The dynamic base shear ($V_{dynamic}$) is the combined maximum forces of the lateral supports of the Fink truss (one support at each end) during the artificial earthquake simulation. The first five modes are included in the dynamic analysis which includes 99.99% of the participating mass for the response in the horizontal direction. The UBC, section 1629.5.1, requires at least 90% of the participating mass of the sturcture be included in the dynamic analysis.

$V_{dynamic}$ = 2(1877 lb) = 3754 lb

Minumum design forces in the tension-splice joint for the artificial earthquake simulation are computed by scaling the finite-element output using the following ratio:

$$\frac{V_{static} \bullet 0.80}{V_{dynamic}} = \frac{(190\ lb)(0.80)}{3754\ lb} = 0.04$$ -UBC Section 1629.5.3

Therefore, the design level forces are approximately 4% of the forces calculated in the finite-element model for the artificial earthquake.

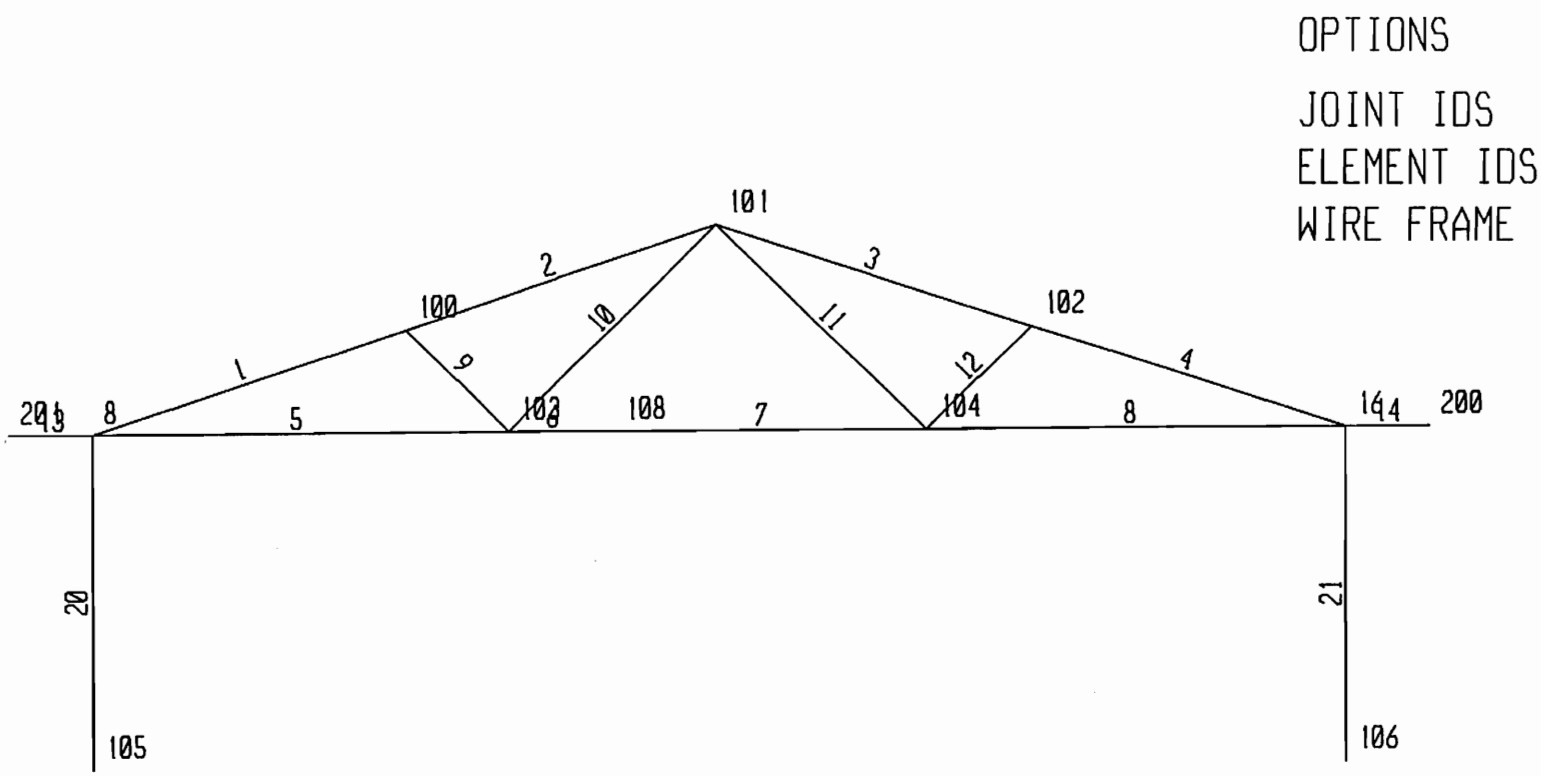

FINITE ELEMENT MODEL SHOWING NODE AND ELEMENT NUMBERING

Segments from the finite elment analysis output required to determine the design level forces in the truss members

R E A C T I O N S A N D A P P L I E D F O R C E S

LOAD COMBINATION 1 - FORCES "F"

JOINT	F(X)	
8	.0000	
16	.0000	
100	.0000	
101	.0000	
102	.0000	
103	.0000	
104	.0000	
105	.0000	
106	.0000	
108	.0000	
200	**-.1877**	<---- Base Shear at Left Support
201	**.1877**	<---- Base Shear at Right Support

P A R T I C I P A T I N G M A S S - (percent)

MODE	X-DIR	Y-DIR	Z-DIR	X-SUM	Y-SUM	Z-SUM
1	**99.998**	00.000	.000	99.998	00.000	.000
2	.000	00.000	16.874	99.999	00.000	16.874
3	.000	00.000	51.477	99.999	00.000	68.351
4	.001	00.000	.016	100.000	00.000	68.367
5	.000	00.000	.715	100.000	00.000	69.082

T O T A L W E I G H T S A N D M A S S E S

PROP	WEIGHT	
1	.1248	
2	.6326	
3	.6001	
4	.0241	
5	.0000	
TOTAL	**1.382**	<-------Total Structure Weight (kips)

Appendix D

Tension-Splice Joint Test Results

Tension-Splice Joints
Static (Batch-1)

Test Number	Strength (lb)	Stiffness (x 100,000-lb/in)	Moisture Content (%)	Deflection at Maximum Load (in.)	Yield Displacement (in.)	Failure Mode
1	7271	3.46	11.4	0.171	0.007	Tooth Withdrawal
2	6901	5.75	12.8	0.081	0.004	Tooth Withdrawal
3	7691	4.27	13.5	0.124	0.006	Tooth Withdrawal
4	6523	3.62	13.7	0.093	0.006	Tooth Withdrawal
5	7024	4.59	12.9	0.107	0.005	Tooth Withdrawal
6	7355	4.08	13.1	0.118	0.006	Tooth Withdrawal
7	7957	4.08	13.4	0.139	0.007	Plate Tension
9	7629	4.10	13.4	0.122	0.006	Tooth Withdrawal
10	7207	4.90	12.7	0.081	0.005	Tooth Withdrawal
Average	7284	4.32	13.0	0.115	0.006	--
COV (%)	6.03	16.1	5.4	25.1	16.0	--

Test Number	Specific Gravity	MOE (x 1,000,000-psi)	% Late Wood	Rings per inch	Grain Orientation
1	0.49	NA	10	6	Flat
2	0.50	NA	30	7	Flat
3	0.49	NA	20	9	Flat
4	0.48	NA	15	8	Flat
5	0.51	NA	20	8	Flat
6	0.54	NA	20	7	Flat
7	0.47	NA	20	10	Flat
9	0.49	NA	15	8	Flat
10	0.52	NA	25	7	Flat
Average	0.50	NA	19	8	--
COV (%)	3.93	NA	30	15	--

NA: Not Available

Flat: Flat-Sawn Lumber (Growth Rings Parallel to Wide Face of Lumber)

Quarter: Quarter-Sawn Lumber (Growth Rings Perpendicular to Wide Face of Lumber)

Both: Combination of Flat and Quarter-Sawn

Tension-Splice Joints
Static (Batch-2)

Test Number	Strength (lb)	Stiffness (x 100,000-lb/in)	Moisture Content (%)	Deflection at Maximum Load (in.)	Yield Displacement (in.)	Failure Mode
1	7428	2.460	13.5	0.093	0.010	Tooth Withdrawal
2	6969	2.445	13.2	0.100	0.010	Tooth Withdrawal
3	7034	2.494	13.9	0.125	0.009	Tooth Withdrawal
5	6251	3.256	12.2	0.089	0.006	Tooth Withdrawal
6	5840	2.596	13.6	0.091	0.008	Tooth Withdrawal
7	6319	2.478	13.6	0.067	0.009	Tooth Withdrawal
8	7192	3.525	13.8	0.101	0.007	Tooth Withdrawal
9	6298	2.762	12.9	0.088	0.008	Tooth Withdrawal
10	7074	3.062	13.8	0.114	0.008	Tooth Withdrawal
Average	6712	2.79	13.4	0.096	0.008	--
COV (%)	8.06	14.4	4.07	17.3	15.6	--

Test Number	Specific Gravity	MOE (x 1,000,000-psi)	% Late Wood	Rings per inch	Grain Orientation
1	0.49	1.65	NA	NA	NA
2	0.47	1.65	NA	NA	NA
3	0.47	1.88	NA	NA	NA
5	0.46	1.86	NA	NA	NA
6	0.46	1.77	NA	NA	NA
7	0.48	1.83	NA	NA	NA
8	0.48	NA	NA	NA	NA
9	0.47	1.86	NA	NA	NA
10	0.52	1.88	NA	NA	NA
Average	0.48	1.80	--	--	--
COV (%)	4.04	5.42	--	--	--

NA: Not Available

Flat: Flat-Sawn Lumber (Growth Rings Parallel to Wide Face of Lumber)

Quarter: Quarter-Sawn Lumber (Growth Rings Perpendicular to Wide Face of Lumber)

Both: Combination of Flat and Quarter-Sawn

Tension-Splice Joints

Northridge Earthquake Simulation (Batch-1)

Test Number	Strength (lb)	Stiffness (x 100,000-lb/in)	Moisture Content (%)	Deflection at Maximum Load (in.)	Yield Displacement (in.)	Failure Mode
1	7976	4.604	12.3	0.122	0.006	Tooth Withdrawal
2	7551	4.504	15.1	0.107	0.006	Tooth Withdrawal
3	8110	3.712	13.1	0.112	0.007	Plate Tension
4	6578	3.534	16.8	0.933	0.006	Tooth Withdrawal
5	7751	4.156	14.8	0.136	0.006	Tooth Withdrawal
6	7479	4.910	NA	0.062	0.005	Tooth Withdrawal
7	8254	3.422	12.6	0.093	0.008	Plate Tension
8	7836	3.210	13.2	0.103	0.008	Tooth Withdrawal
9	7106	4.168	16.3	0.104	0.006	Tooth Withdrawal
10	7048	3.721	16.4	0.078	0.006	Tooth Withdrawal
Average	7569	3.99	14.5	0.185	0.006	--
COV (%)	6.97	14.1	11.9	11.9	17.2	--

Test Number	Specific Gravity	MOE (x 1,000,000-psi)	% Late Wood	Rings per inch	Grain Orientation
1	0.47	1.99	15	6	Flat
2	0.59	2.07	25	6	Flat
3	0.48	1.59	15	5	Flat
4	0.56	2.07	25	6	Flat
5	0.47	1.99	20	6	Flat
6	NA	1.59	20	6	Flat
7	0.44	1.59	15	5	Flat
8	0.46	1.59	10	4	Flat
9	0.55	2.07	20	5	Flat
10	0.51	2.07	25	6	Flat
Average	0.50	1.86	19	6	--
COV (%)	10.1	11.9	13	14	--

NA: Not Available

Flat: Flat-Sawn Lumber (Growth Rings Parallel to Wide Face of Lumber)

Quarter: Quarter-Sawn Lumber (Growth Rings Perpendicular to Wide Face of Lumber)

Both: Combination of Flat and Quarter-Sawn

Tension-Splice Joints

Sequential Phased Displacement (Batch-1)

Test Number	Strength (lb)	Total Number of Cycles Applied	Stiffness (x 100,000-lb/in)	Moisture Content (%)	Deflection at Maximum Load (in.)	Yield Displacement (in.)
2	6915	94	1.568	13.9	0.074	0.0147
3	6970	118	1.904	13.8	0.099	0.0122
4	6708	81	1.761	13.3	0.071	0.0127
5	7280	76	2.379	13.2	0.108	0.0102
6	7631	120	1.957	13.7	0.084	0.013
7	7618	111	1.607	13.5	0.145	0.0158
8	7435	120	2.031	14.3	0.080	0.0122
9	6954	120	1.885	13.1	0.061	0.0123
Average	7189	105	1.886	13.6	0.090	0.013
COV (%)	4.87	17.7	13.7	2.95	29.6	13.2

Test Number	Specific Gravity	MOE (x 1,000,000-psi)	% Late Wood	Rings per inch	Grain Orientation	Failure Mode
2	0.43	1.67	15	6	Flat	Tooth Withdrawal
3	0.48	1.59	15	6	Flat	Tooth Withdrawal
4	0.47	1.99	10	6	Flat	Tooth Withdrawal
5	0.44	1.67	20	6	Flat	Tooth Withdrawal
6	0.53	1.88	25	6	Flat	Tooth Withdrawal
7	0.53	1.88	20	7	Flat	Tooth Withdrawal
8	0.54	1.82	15	7	Both	Tooth Withdrawal
9	0.56	1.88	25	6	Flat	Tooth Withdrawal
Average	0.50	1.80	18	6	--	--
COV (%)	9.59	7.68	29	7	--	--

NA: Not Available

Flat: Flat-Sawn Lumber (Growth Rings Parallel to Wide Face of Lumber)

Quarter: Quarter-Sawn Lumber (Growth Rings Perpendicular to Wide Face of Lumber)

Both: Combination of Flat and Quarter-Sawn

Tension-Splice Joint
Artificial Earthquake Simulation (Batch-2)

Test Number	Strength (lb)	Stiffness (x 100,000-lb/in)	Moisture Content (%)	Deflection at Maximum Load (in.)	Yield Displacement (in.)	Failure Mode
1	6349	3.428	13.3	0.078	0.006	Tooth Withdrawal
2	6902	3.787	13.8	0.089	0.006	Tooth Withdrawal
3	5081	2.619	13.8	0.074	0.006	Tooth Withdrawal
4	5307	3.282	13.7	0.065	0.005	Tooth Withdrawal
5	7419	4.589	13.7	0.108	0.005	Tooth Withdrawal
6	6764	3.335	13.8	0.107	0.007	Tooth Withdrawal
7	7351	3.334	13.0	0.112	0.007	Tooth Withdrawal
8	6612	3.308	13.6	0.104	0.007	Tooth Withdrawal
9	6549	3.481	12.1	0.089	0.006	Tooth Withdrawal
Average	6482	3.462	13.4	0.092	0.006	--
COV (%)	12.52	15.1	4.24	18.4	10.1	--

Test Number	Specific Gravity	MOE (x 1,000,000-psi)	% Late Wood	Rings per inch	Grain Orientation
1	0.47	NA	20	5	Flat
2	0.47	1.73	25	6	Flat
3	0.48	1.97	15	7	Flat
4	0.50	1.88	20	6	Flat
5	0.47	1.83	20	6	Flat
6	0.45	1.71	20	6	Flat
7	0.51	1.73	25	7	Flat
8	0.50	1.60	25	7	Flat
9	0.49	1.86	25	7	Flat
Average	0.48	1.79	22	6	--
COV (%)	3.85	6.57	16	11	--

NA: Not Available
Flat: Flat-Sawn Lumber
Quarter: Quarter-Sawn Lumber
Both: Combination of Flat and Quarter-Sawn

Tension-Splice Joints

Cyclic Loading (Batch-2)

Test Number	Cyclic Amplitude (%)	Post Cyclic Strength (lb)	Specific Gravity	Moisture Content (%)	MOE (x 1,000,000-psi)	% Late Wood	Rings per inch	Grain Orientation	Failure Mode
1	8.22	5837	0.44	13.4	1.82	25	6	Flat	Tooth Withdrawal
2	8.22	7930	0.44	13.2	1.73	25	5	Flat	Tooth Withdrawal
3	8.22	4246	0.49	13.5	1.83	40	8	Flat	Tooth Withdrawal
4	12.33	4208	0.52	13.7	1.88	35	7	Flat	Tooth Withdrawal
5	12.33	3520	0.40	14.3	1.67	20	5	Flat	Tooth Withdrawal
6	12.33	7549	0.49	13.5	1.83	35	9	Flat	Tooth Withdrawal
7	14.80	7272	0.47	13.9	1.57	40	4	Both	Tooth Withdrawal
8	15.62	4479	0.45	13.6	1.9	25	8	Both	Tooth Withdrawal
9	16.44	6895	0.49	14.9	1.6	20	6	Flat	Tooth Withdrawal
10	16.44	4647	0.42	14.1	1.82	25	6	Flat	Tooth Withdrawal
11	18.08	0	0.45	5.6	1.73	30	7	Both	Tooth Withdrawal
12	18.08	0	0.45	14.4	1.82	40	8	Flat	Tooth Withdrawal
13	18.08	6786	0.45	14.3	NA	NA	NA	NA	Tooth Withdrawal
14	19.73	6660	0.47	0.137	1.83	25	8	Flat	Tooth Withdrawal
15	19.73	0	NA	NA	NA	NA	NA	NA	Tooth Withdrawal
16	19.73	0	NA	NA	NA	NA	NA	NA	Tooth Withdrawal
17	20.55	0	0.45	13.5	1.83	20	4	Flat	Tooth Withdrawal
18	20.55	0	0.44	12.8	1.67	15	5	Flat	Tooth Withdrawal
19	20.55	0	0.45	13.5	1.57	25	6	Flat	Tooth Withdrawal
20	24.66	0	0.4	14.2	1.8	20	8	Flat	Tooth Withdrawal
Average	--	--	0.45	12.6	1.76	27	6	--	--
COV	--	--	6.63	29.4	6.06	29	24	--	--

NA: Not Available

Flat: Flat-Sawn Lumber (Growth Rings Parallel to Wide Face of Lumber)

Quarter: Quarter-Sawn Lumber (Growth Rings Perpendicular to Wide Face of Lumber)

Both: Combination of Flat and Quarter-Sawn

Appendix E

Deflection-Time Curves for the Artificial Earthquake Simulation on Tension-Splice Joints

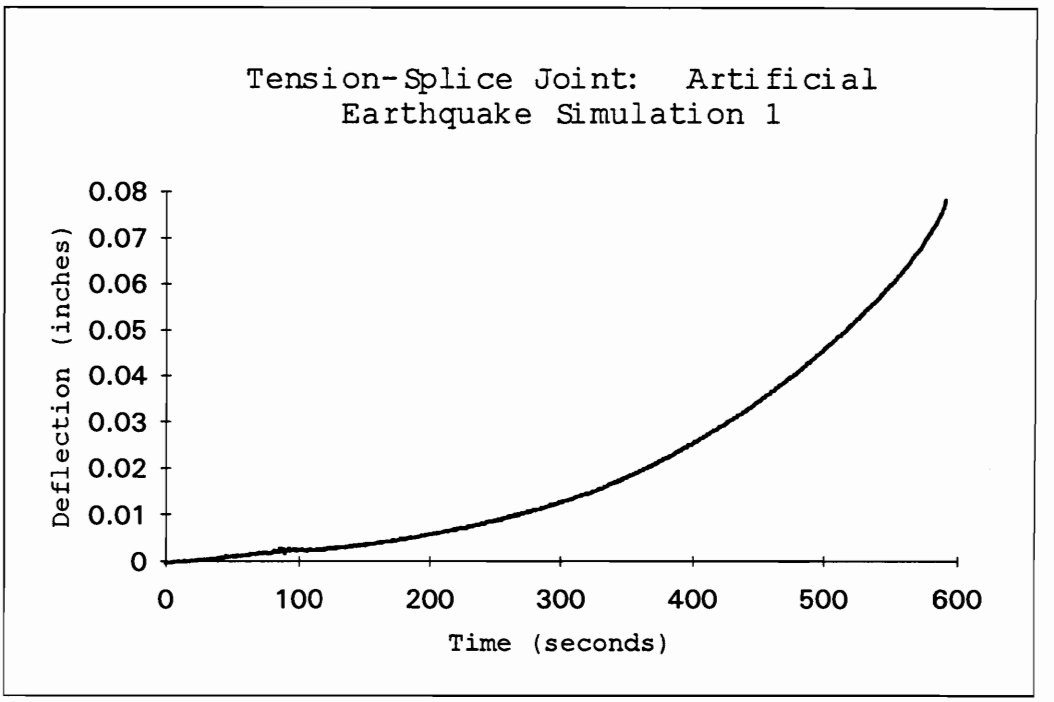
Tension-Splice Joint: Artificial Earthquake Simulation 1
Deflection (inches)
0.08
0.07
0.06
0.05
0.04
0.03
0.02
0.01
0
0
100
200
300
400
500
600
Time (seconds)

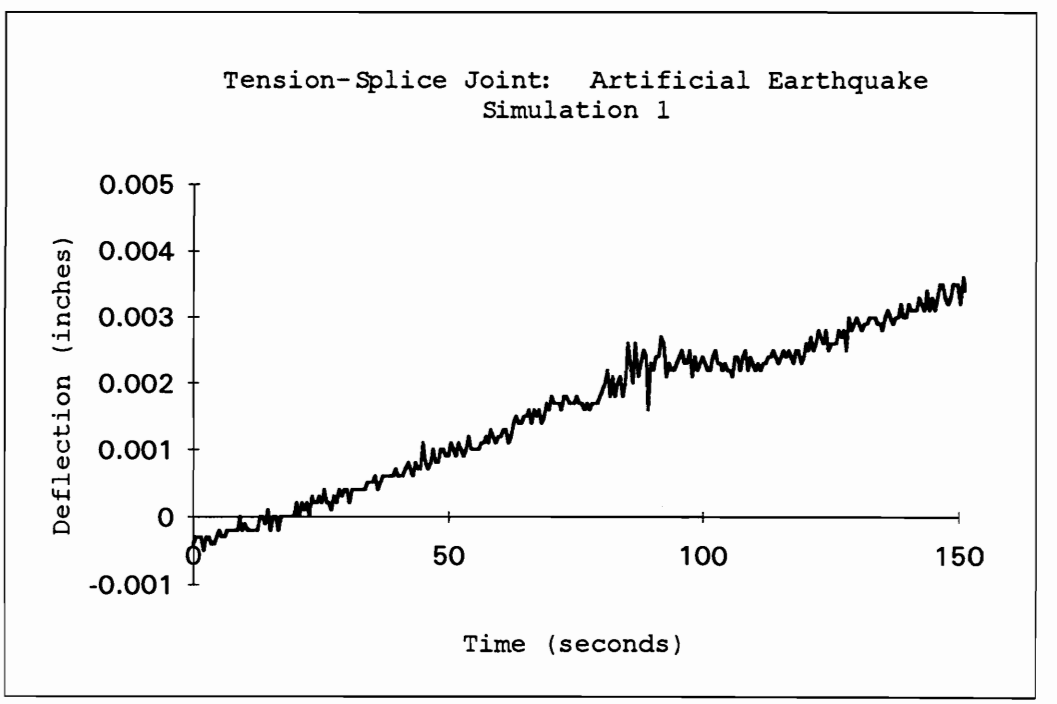
Tension-Splice Joint: Artificial Earthquake Simulation 1
Deflection (inches)
0.005
0.004
0.003
0.002
0.001
0
-0.001
0
50
100
150
Time (seconds)

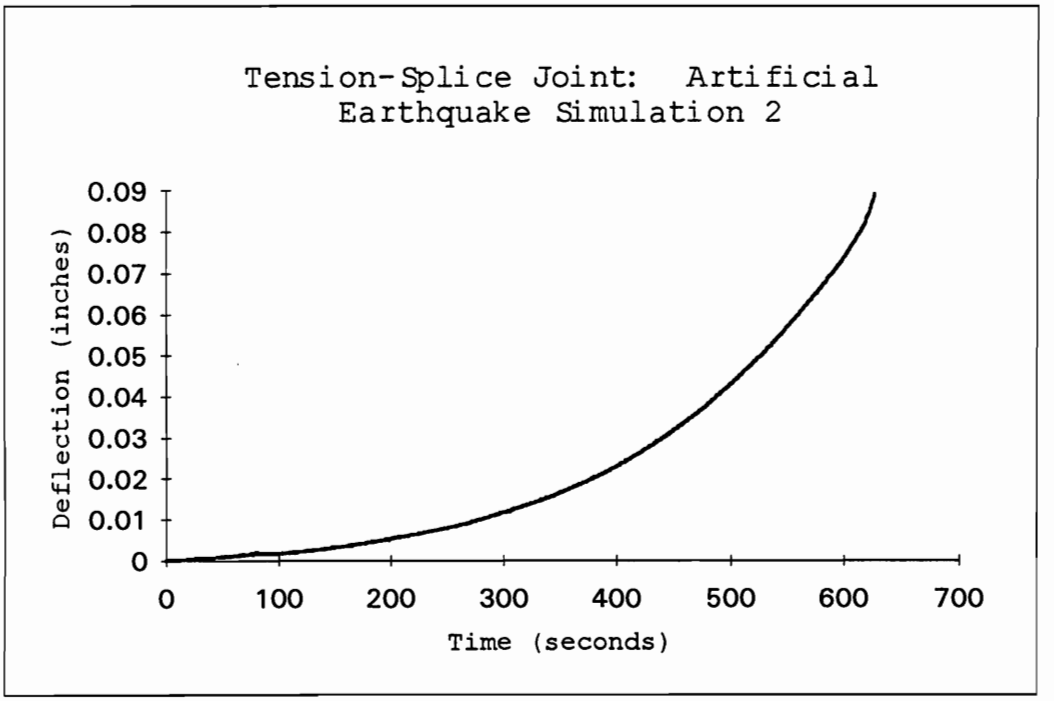
Tension-Splice Joint: Artificial Earthquake Simulation 2
Deflection (inches)
0.09
0.08
0.07
0.06
0.05
0.04
0.03
0.02
0.01
0
0
100
200
300
400
500
600
700
Time (seconds)

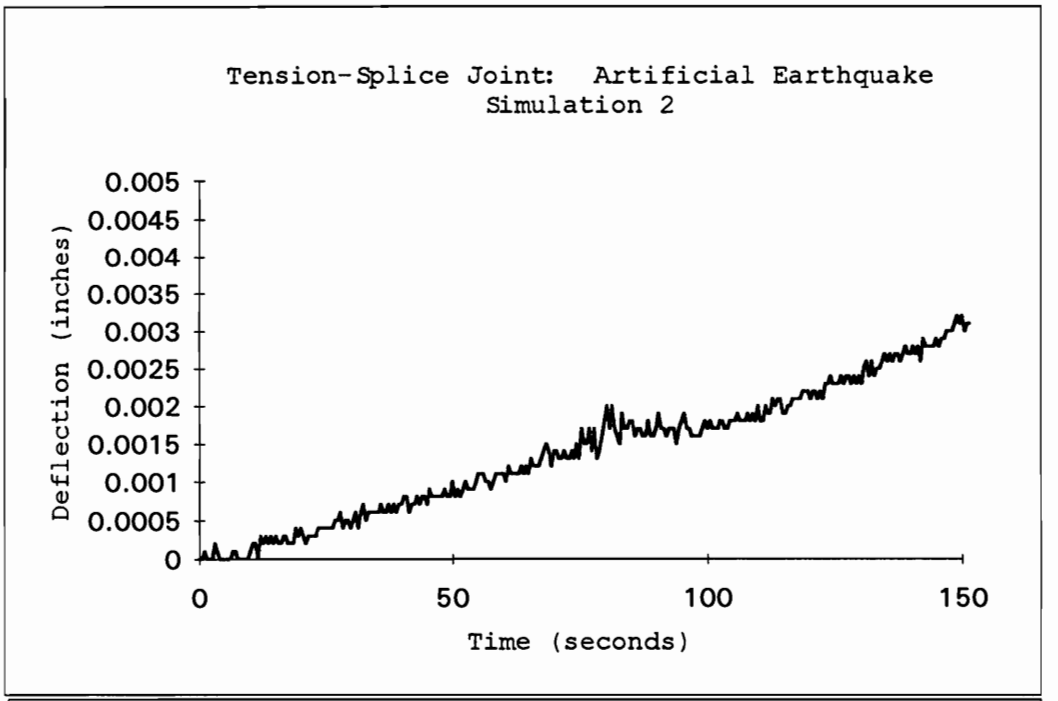
Tension-Splice Joint: Artificial Earthquake Simulation 2
Deflection (inches)
0.005
0.0045
0.004
0.0035
0.003
0.0025
0.002
0.0015
0.001
0.0005
0
0
50
100
150
Time (seconds)

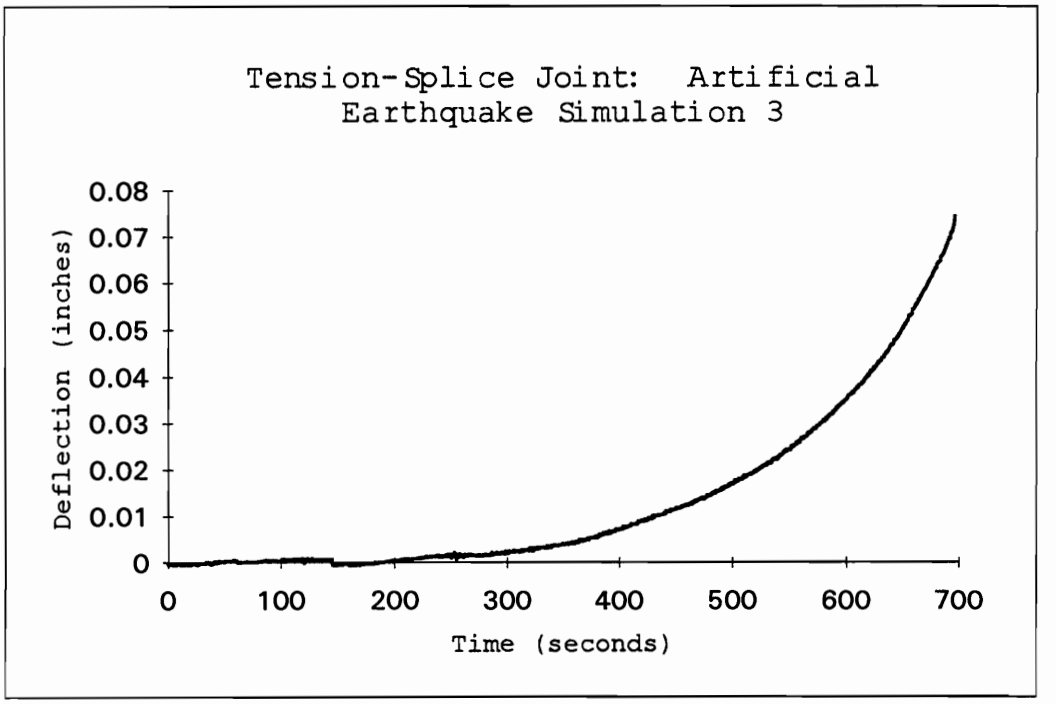
Tension-Splice Joint: Artificial Earthquake Simulation 3
Deflection (inches)
0.08
0.07
0.06
0.05
0.04
0.03
0.02
0.01
0
0
100
200
300
400
500
600
700
Time (seconds)

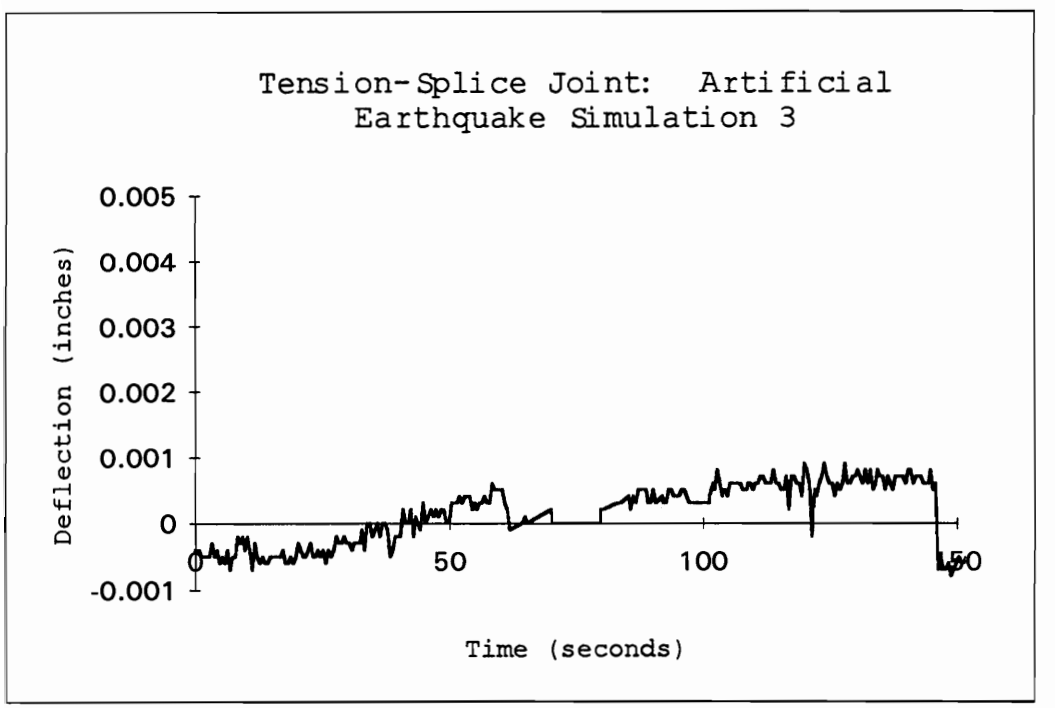
Tension-Splice Joint: Artificial Earthquake Simulation 3
Deflection (inches)
0.005
0.004
0.003
0.002
0.001
0
-0.001
0
50
100
150
Time (seconds)

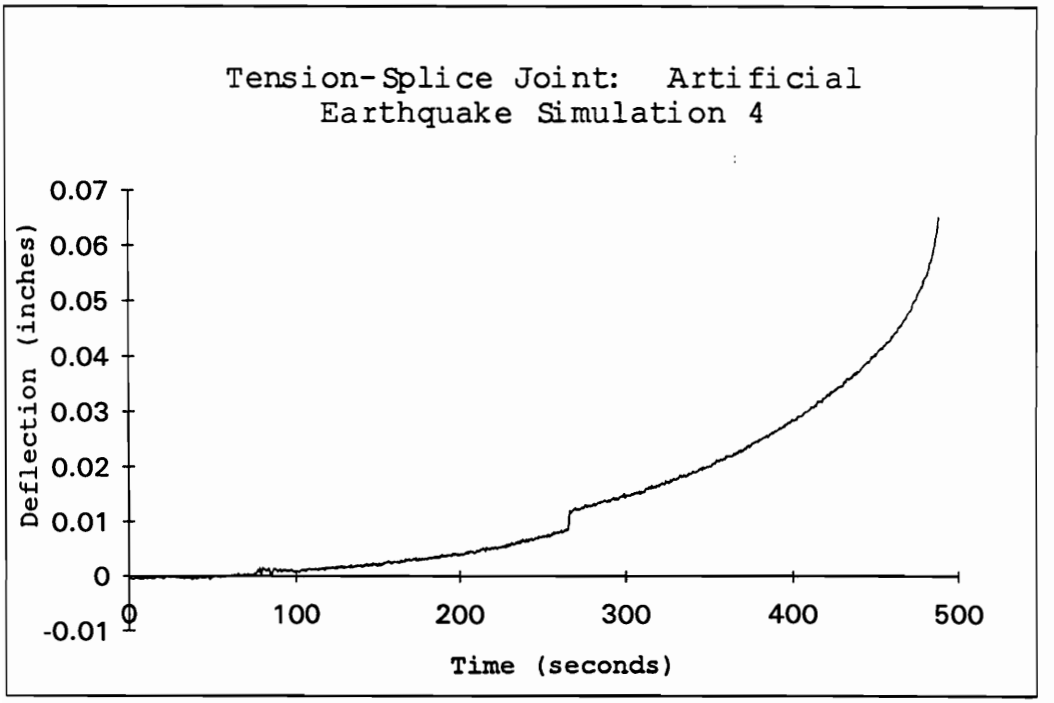
Tension-Splice Joint: Artificial
Earthquake Simulation 4
Deflection (inches)
0.07
0.06
0.05
0.04
0.03
0.02
0.01
0
-0.01
0
100
200
300
400
500
Time (seconds)

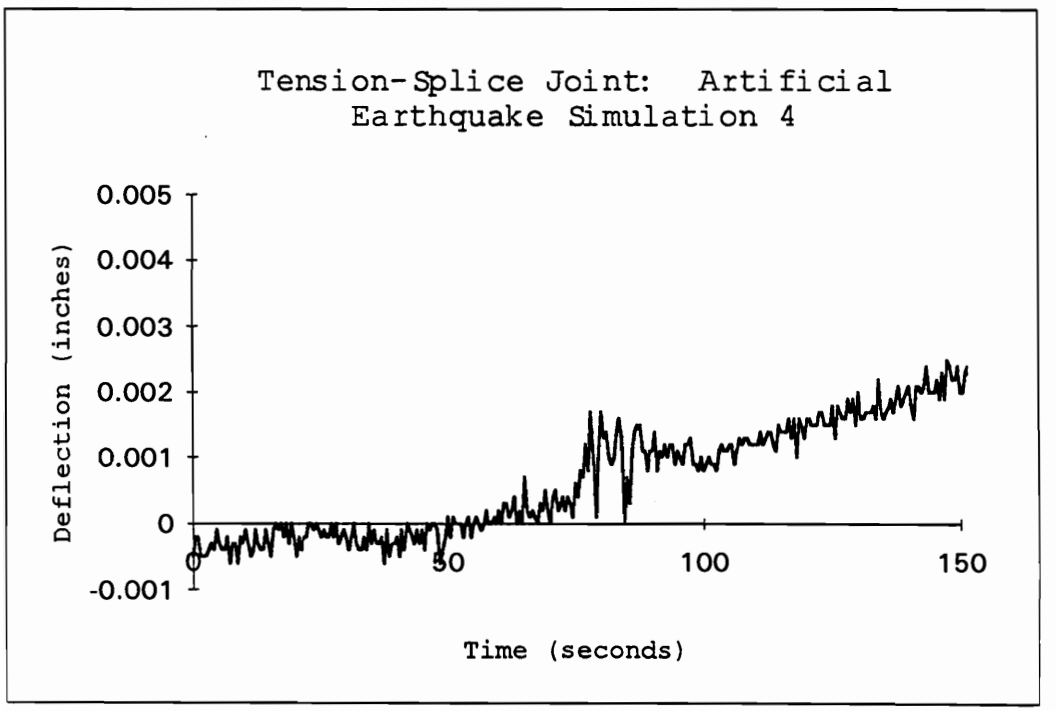
Tension-Splice Joint: Artificial
Earthquake Simulation 4
Deflection (inches)
0.005
0.004
0.003
0.002
0.001
0
-0.001
0
50
100
150
Time (seconds)

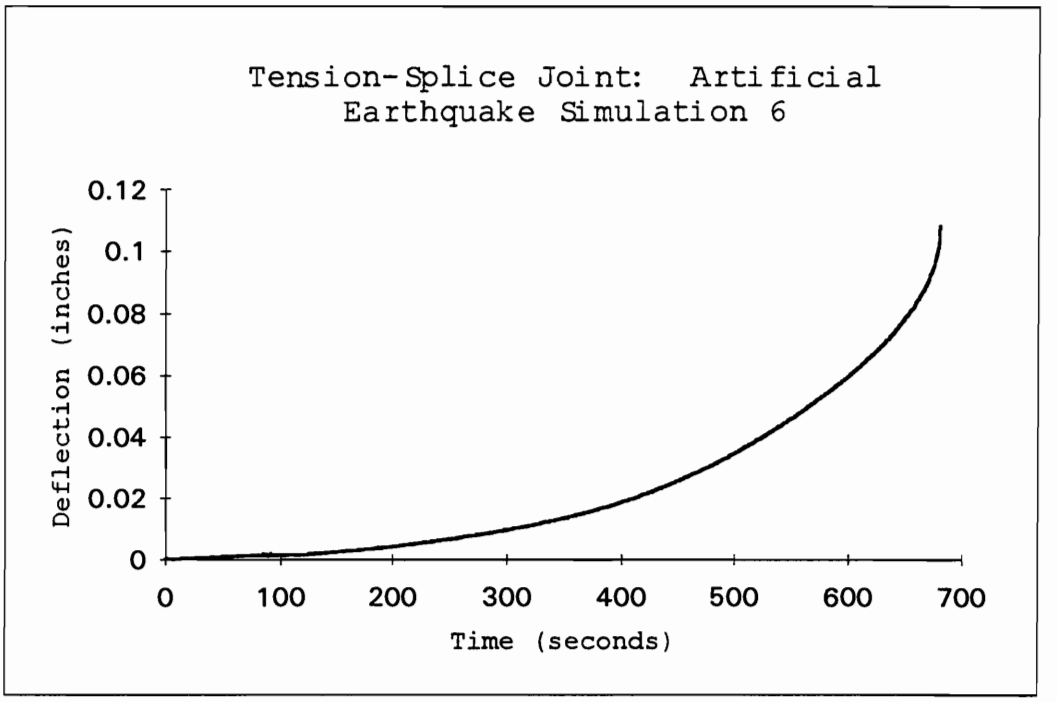
Tension-Splice Joint: Artificial Earthquake Simulation 6
Deflection (inches)
0.12
0.1
0.08
0.06
0.04
0.02
0
0
100
200
300
400
500
600
700
Time (seconds)

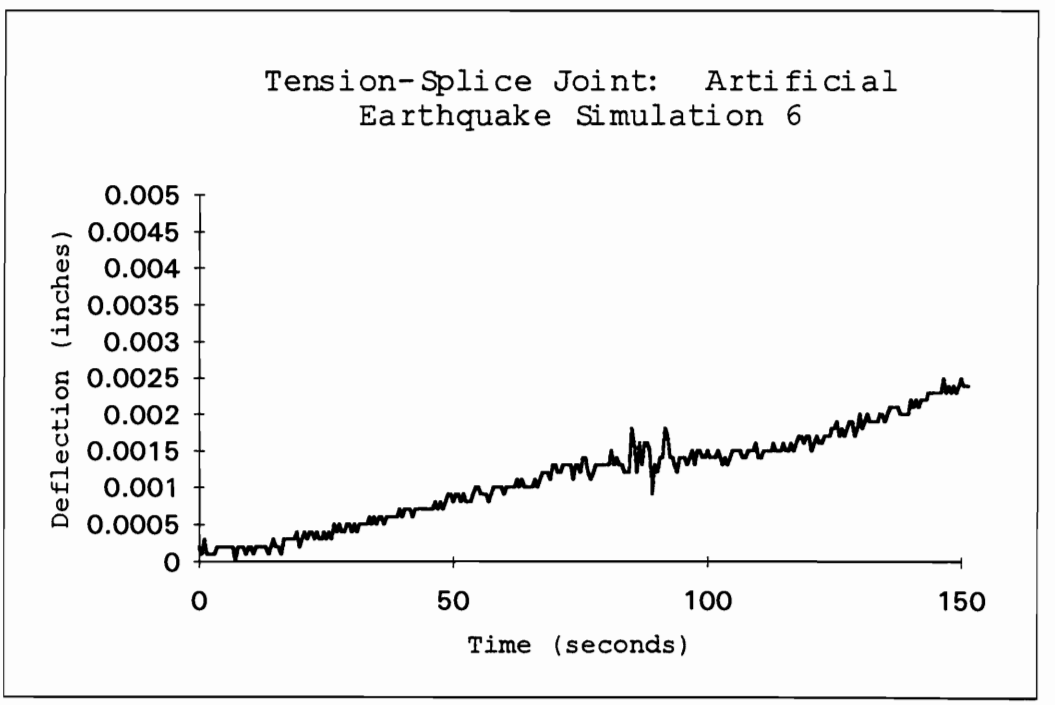
Tension-Splice Joint: Artificial Earthquake Simulation 6
Deflection (inches)
0.005
0.0045
0.004
0.0035
0.003
0.0025
0.002
0.0015
0.001
0.0005
0
0
50
100
150
Time (seconds)

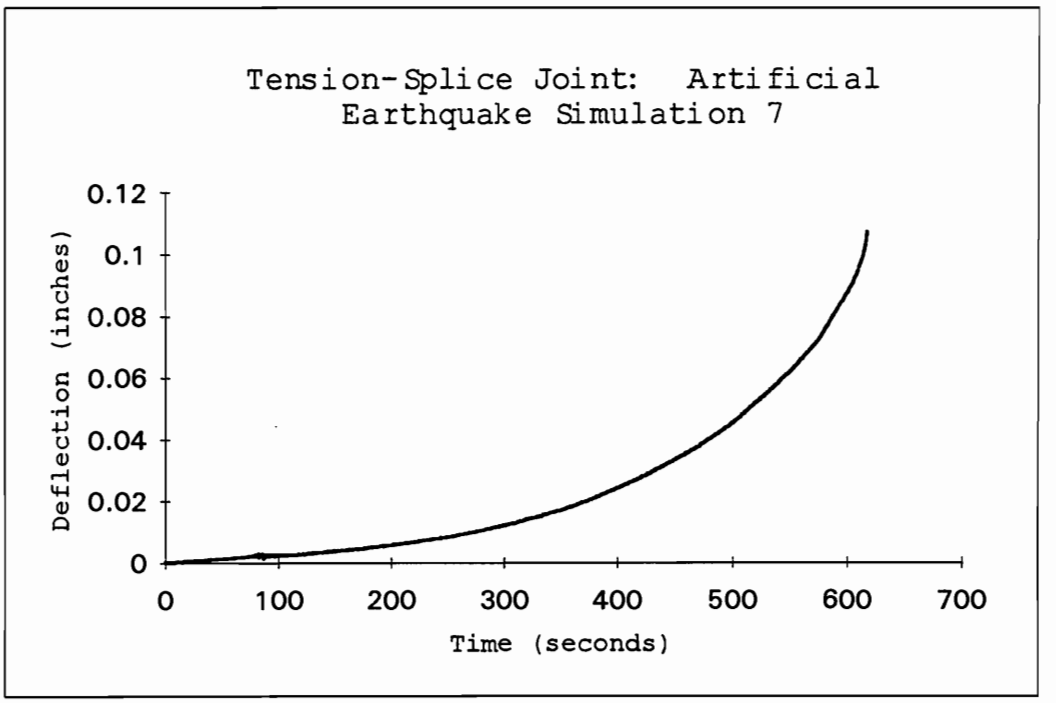
Tension-Splice Joint: Artificial Earthquake Simulation 7
Deflection (inches)
0.12
0.1
0.08
0.06
0.04
0.02
0
0
100
200
300
400
500
600
700
Time (seconds)

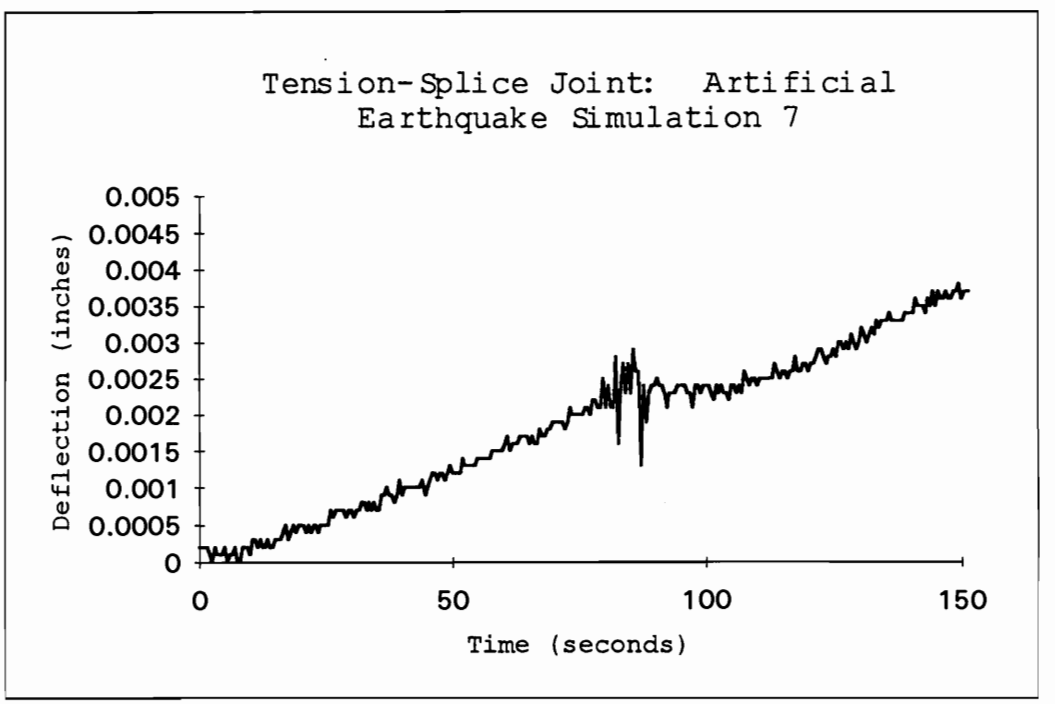
Tension-Splice Joint: Artificial Earthquake Simulation 7
Deflection (inches)
0.005
0.0045
0.004
0.0035
0.003
0.0025
0.002
0.0015
0.001
0.0005
0
0
50
100
150
Time (seconds)

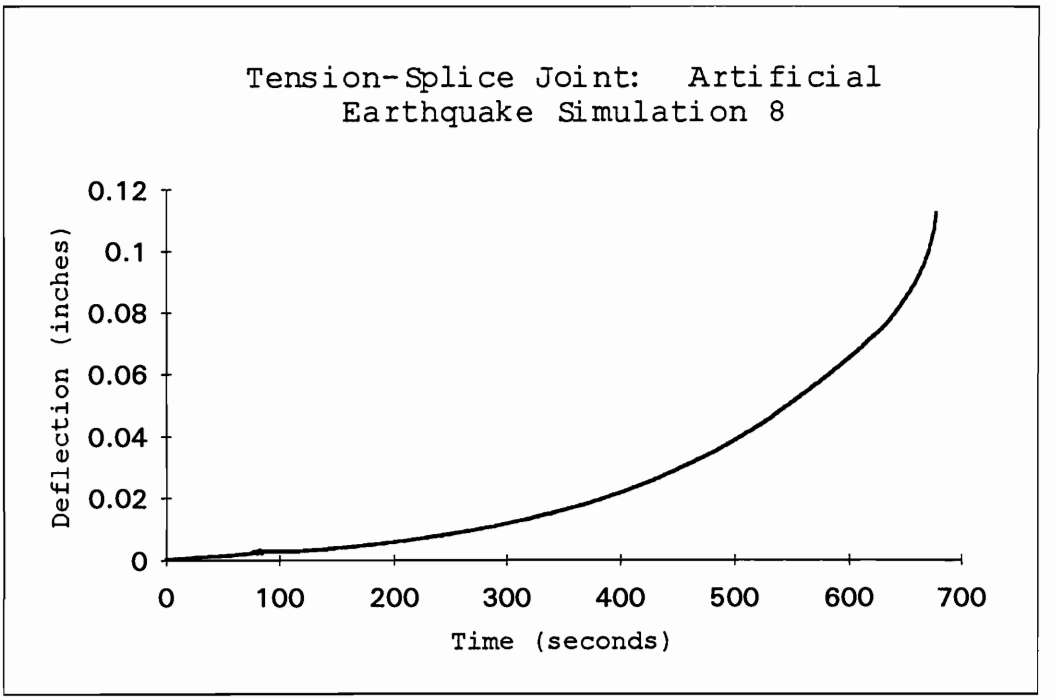
Tension-Splice Joint: Artificial Earthquake Simulation 8
Deflection (inches)
0.12
0.1
0.08
0.06
0.04
0.02
0
0
100
200
300
400
500
600
700
Time (seconds)

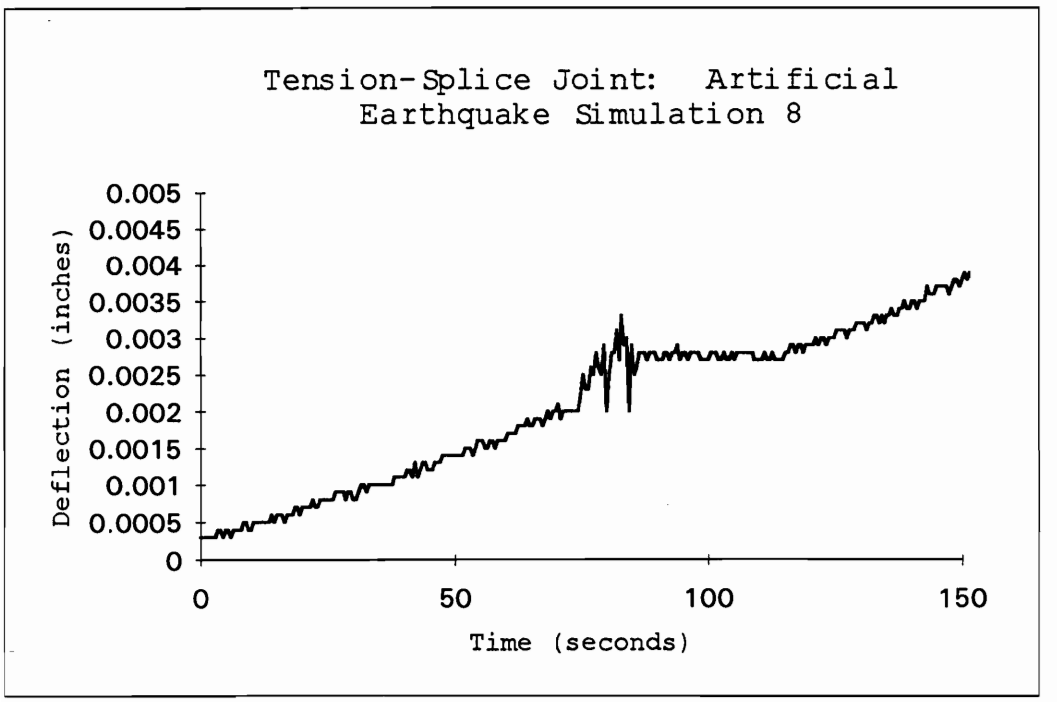
Tension-Splice Joint: Artificial Earthquake Simulation 8
Deflection (inches)
0.005
0.0045
0.004
0.0035
0.003
0.0025
0.002
0.0015
0.001
0.0005
0
0
50
100
150
Time (seconds)

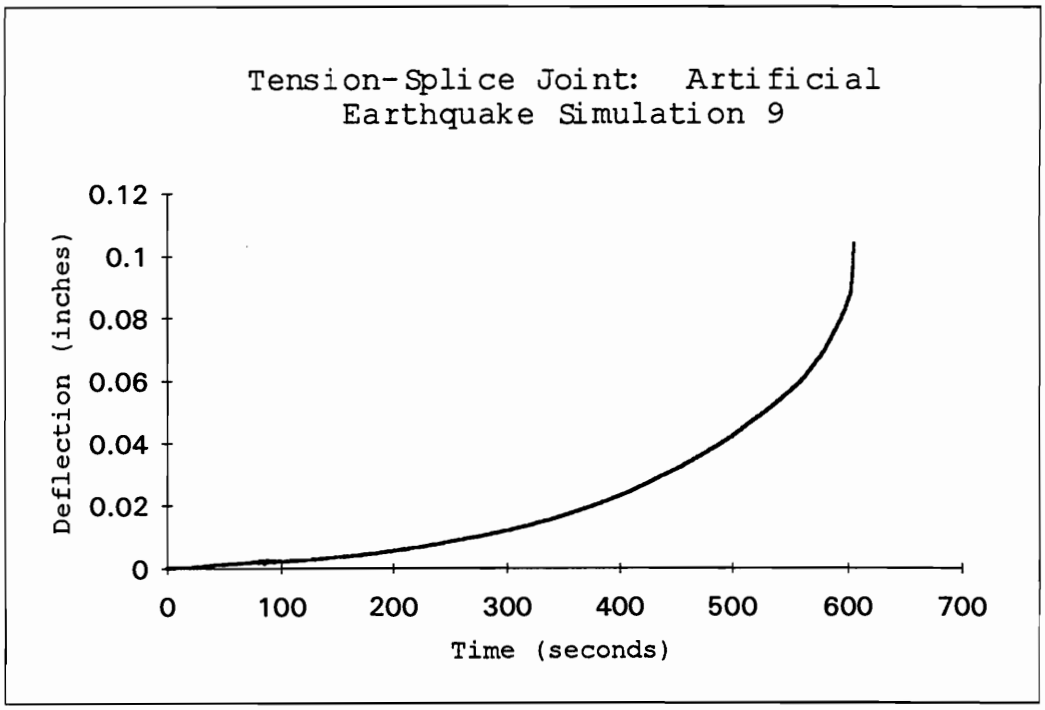
Tension-Splice Joint: Artificial Earthquake Simulation 9
Deflection (inches)
0.12
0.1
0.08
0.06
0.04
0.02
0
0
100
200
300
400
500
600
700
Time (seconds)

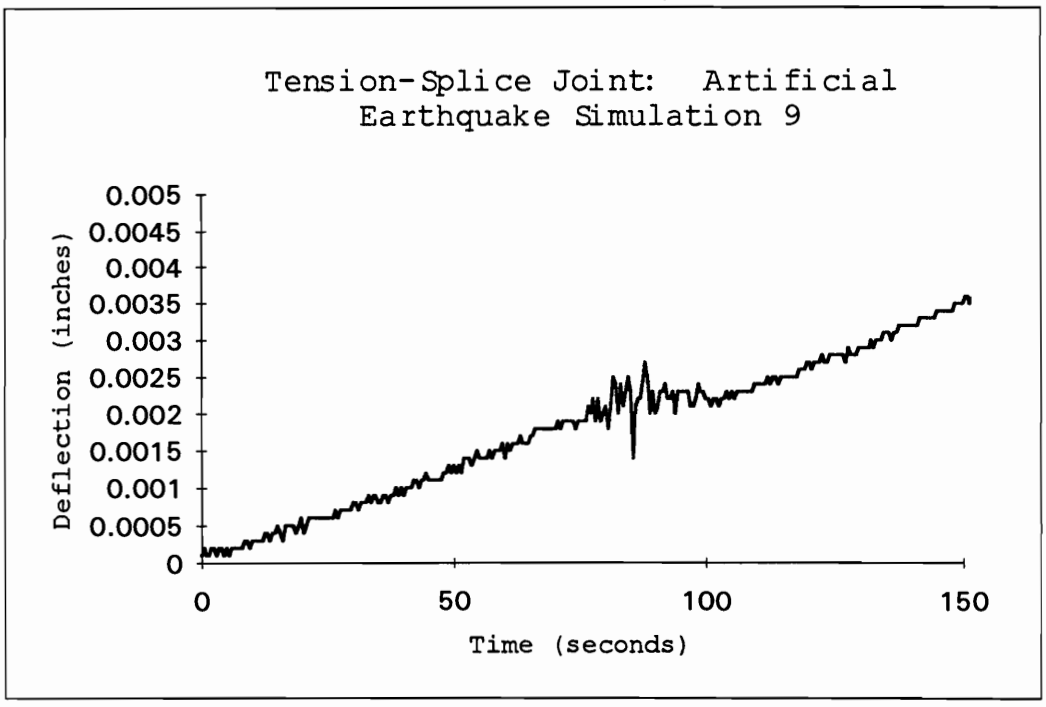
Tension-Splice Joint: Artificial Earthquake Simulation 9
Deflection (inches)
0.005
0.0045
0.004
0.0035
0.003
0.0025
0.002
0.0015
0.001
0.0005
0
0
50
100
150
Time (seconds)

Appendix F

Load and Deflection vs. Time Curves for the Sequential Phased Displacement Loading on Tension-Splice Joints

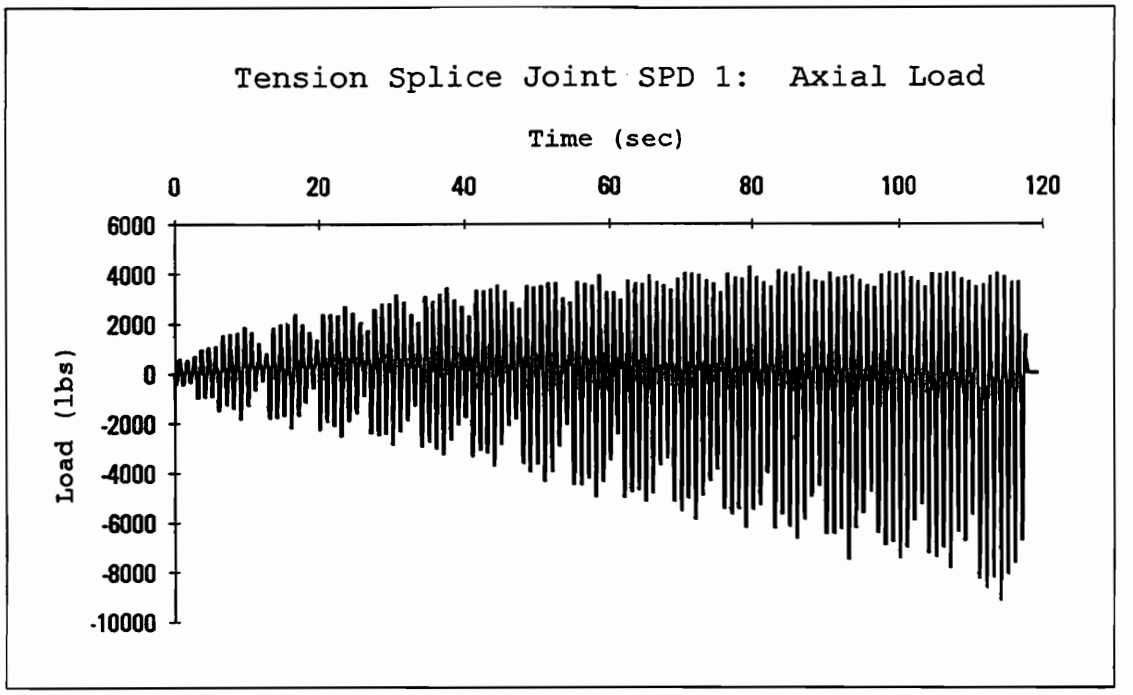
Tension Splice Joint SPD 1: Axial Load
Time (sec)
0
20
40
60
80
100
120
6000
4000
2000
0
-2000
-4000
-6000
-8000
-10000
Load (lbs)

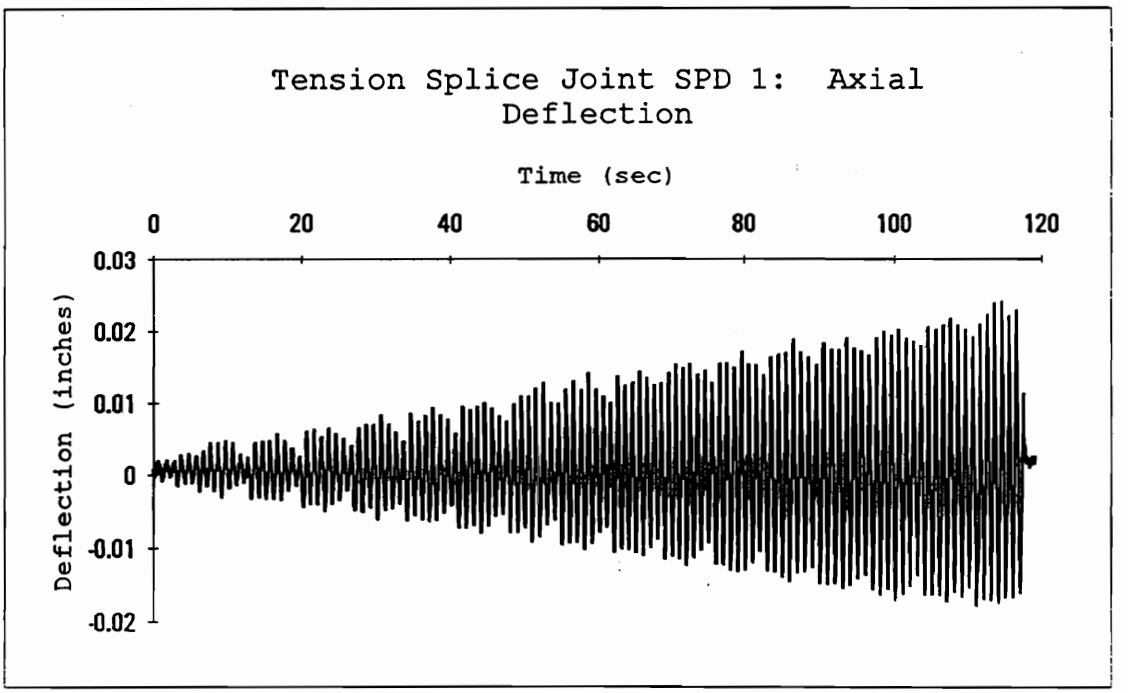
Tension Splice Joint SPD 1: Axial Deflection
Time (sec)
0
20
40
60
80
100
120
0.03
0.02
0.01
0
-0.01
-0.02
Deflection (inches)

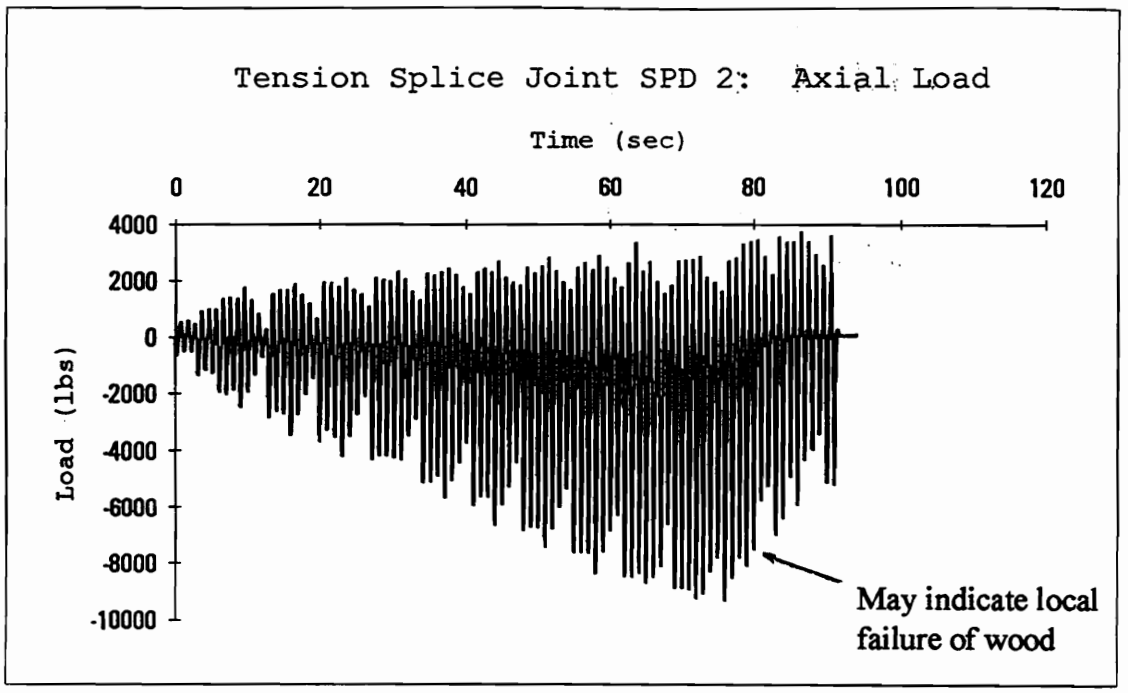
Tension Splice Joint SPD 2: Axial Load
Time (sec)
0
20
40
60
80
100
120
4000
2000
0
-2000
-4000
-6000
-8000
-10000
Load (lbs)
May indicate local failure of wood

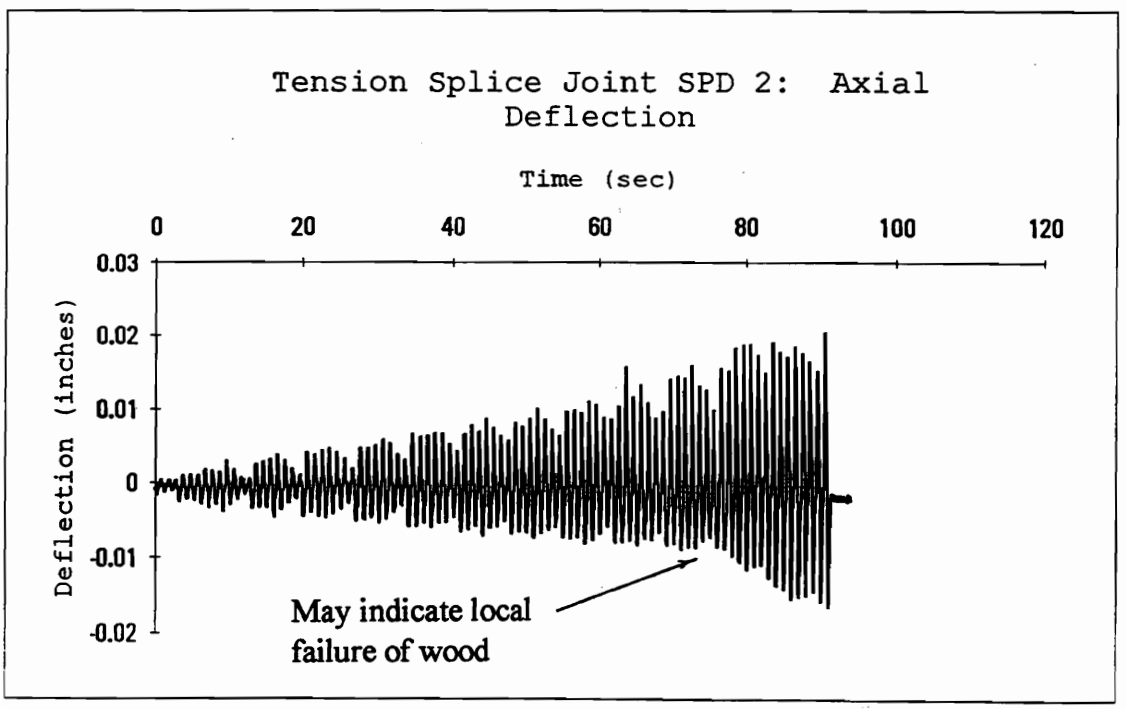
Tension Splice Joint SPD 2: Axial Deflection
Time (sec)
0
20
40
60
80
100
120
0.03
0.02
0.01
0
-0.01
-0.02
Deflection (inches)
May indicate local failure of wood

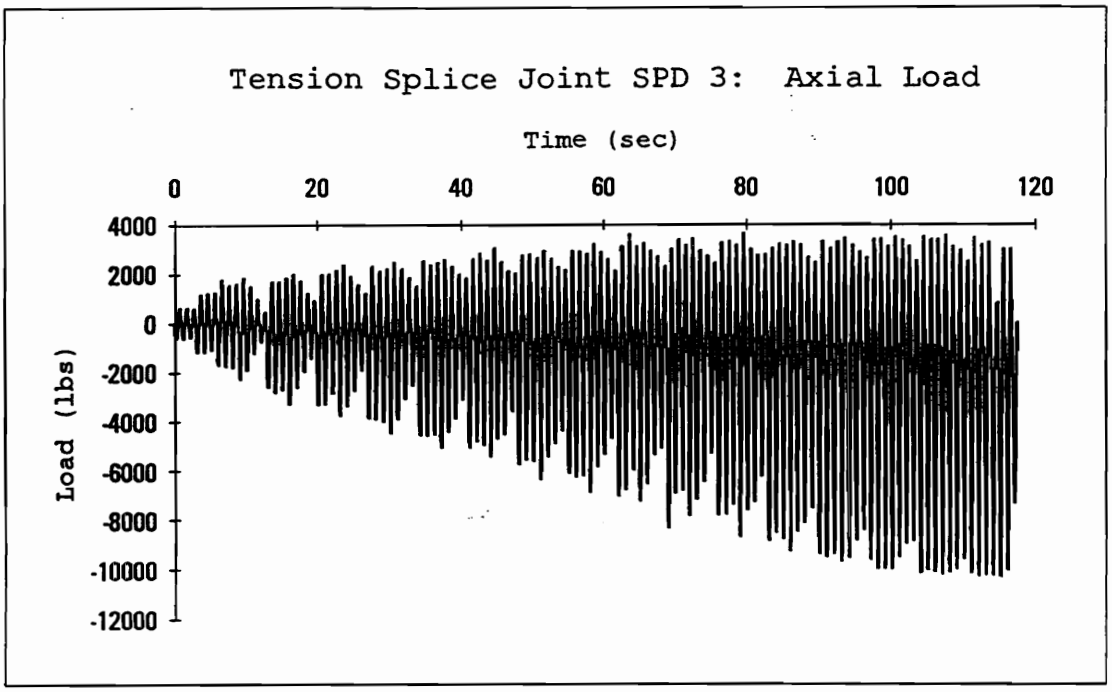
Tension Splice Joint SPD 3: Axial Load
Time (sec)
0
20
40
60
80
100
120
4000
2000
0
-2000
-4000
-6000
-8000
-10000
-12000
Load (lbs)

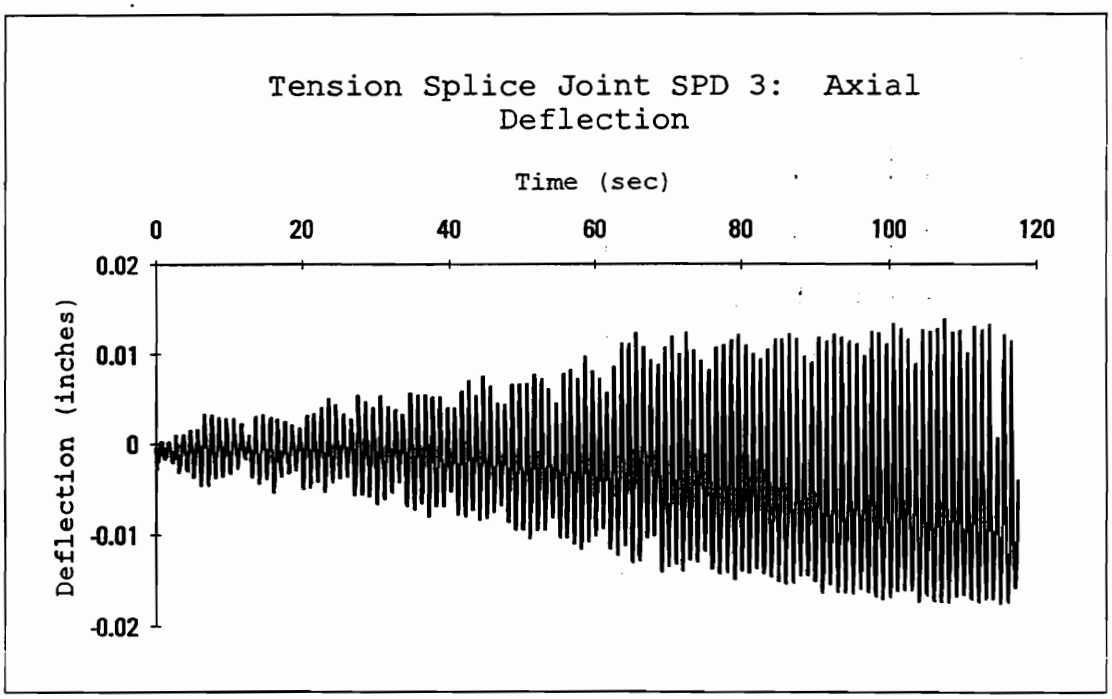
Tension Splice Joint SPD 3: Axial Deflection
Time (sec)
0
20
40
60
80
100
120
0.02
0.01
0
-0.01
-0.02
Deflection (inches)

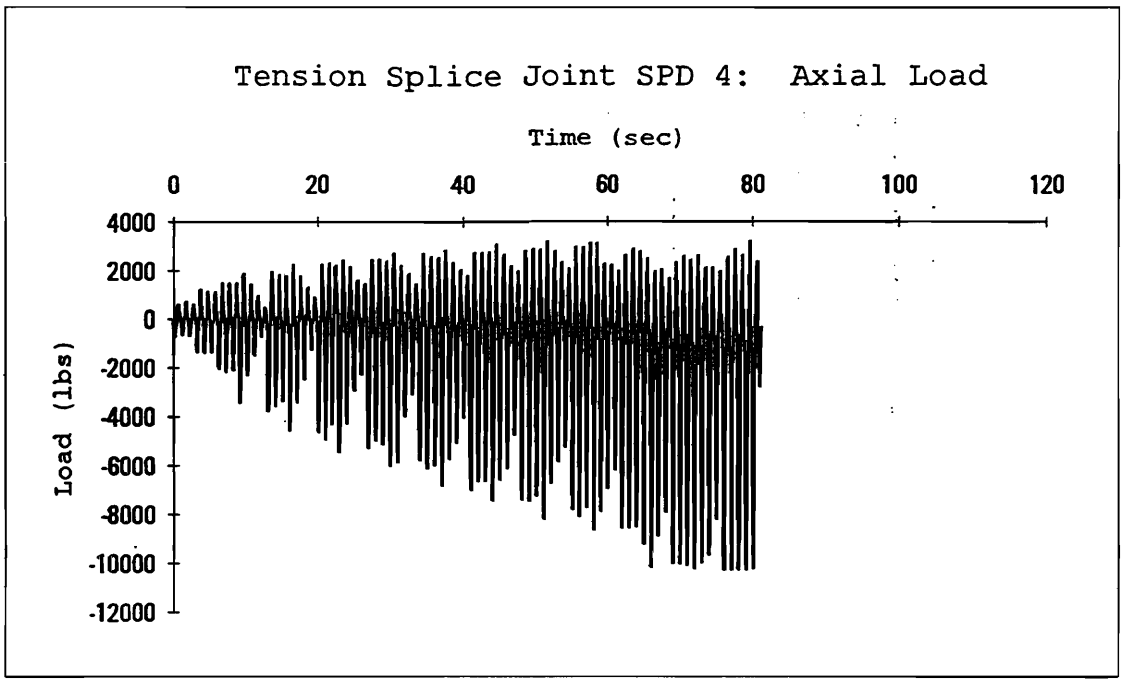
Tension Splice Joint SPD 4: Axial Load
Time (sec)
0
20
40
60
80
100
120
4000
2000
0
-2000
-4000
-6000
-8000
-10000
-12000
Load (lbs)

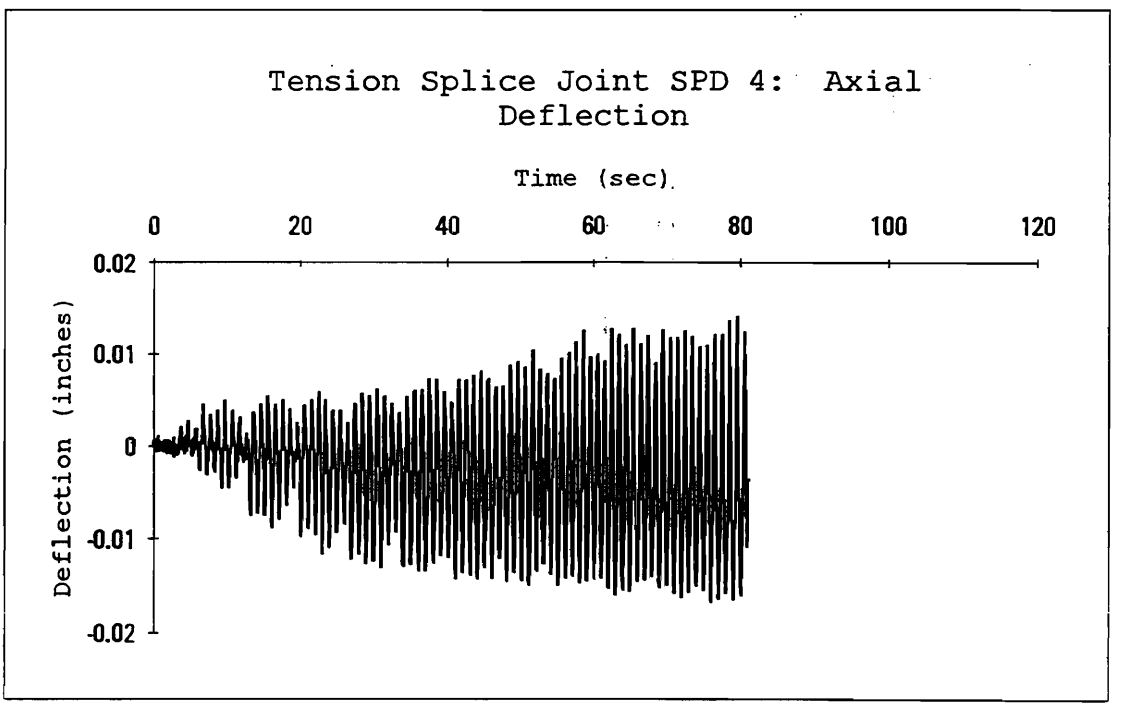
Tension Splice Joint SPD 4: Axial Deflection
Time (sec)
0
20
40
60
80
100
120
0.02
0.01
0
-0.01
-0.02
Deflection (inches)

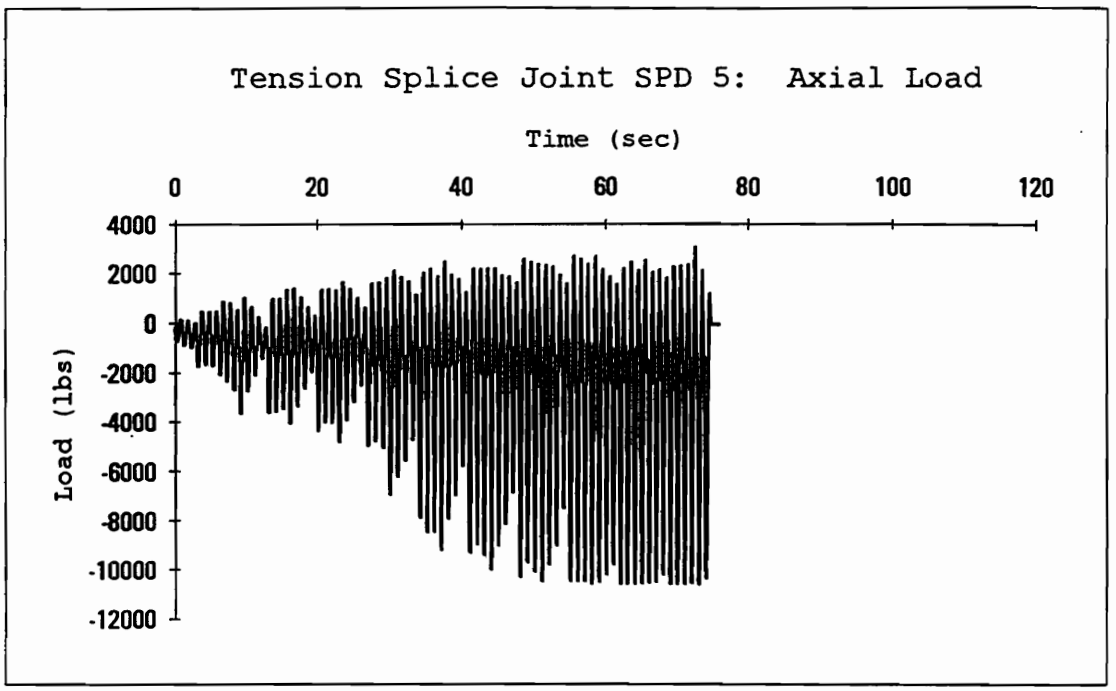
Tension Splice Joint SPD 5: Axial Load
Time (sec)
0
20
40
60
80
100
120
4000
2000
0
-2000
-4000
-6000
-8000
-10000
-12000
Load (lbs)

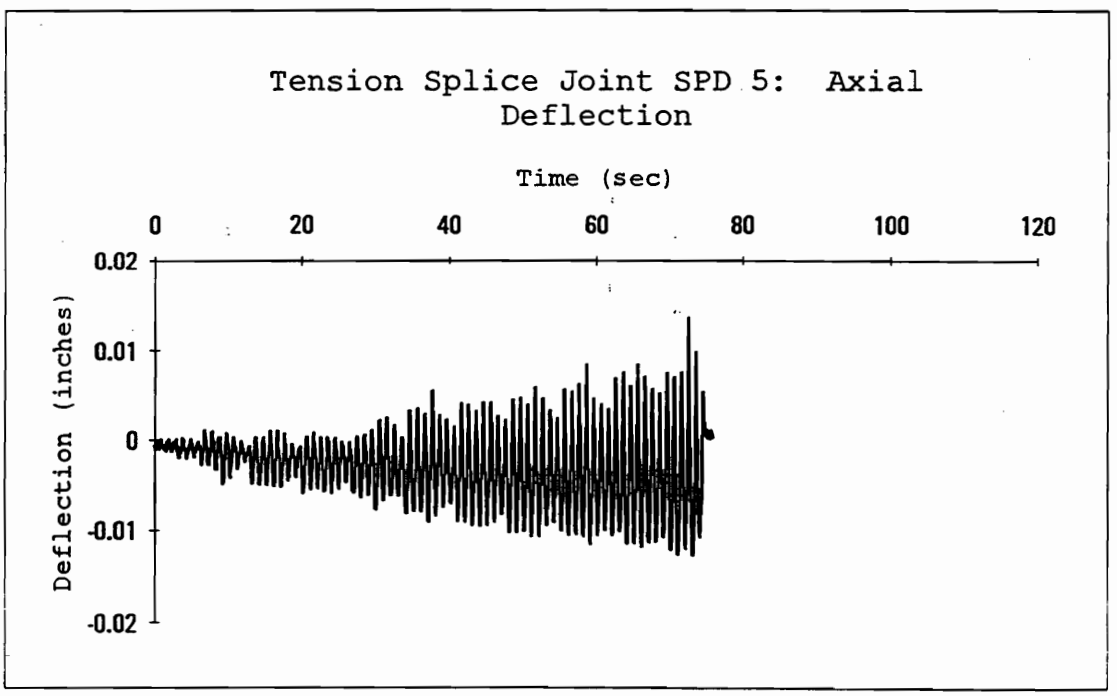
Tension Splice Joint SPD 5: Axial Deflection
Time (sec)
0
20
40
60
80
100
120
0.02
0.01
0
-0.01
-0.02
Deflection (inches)

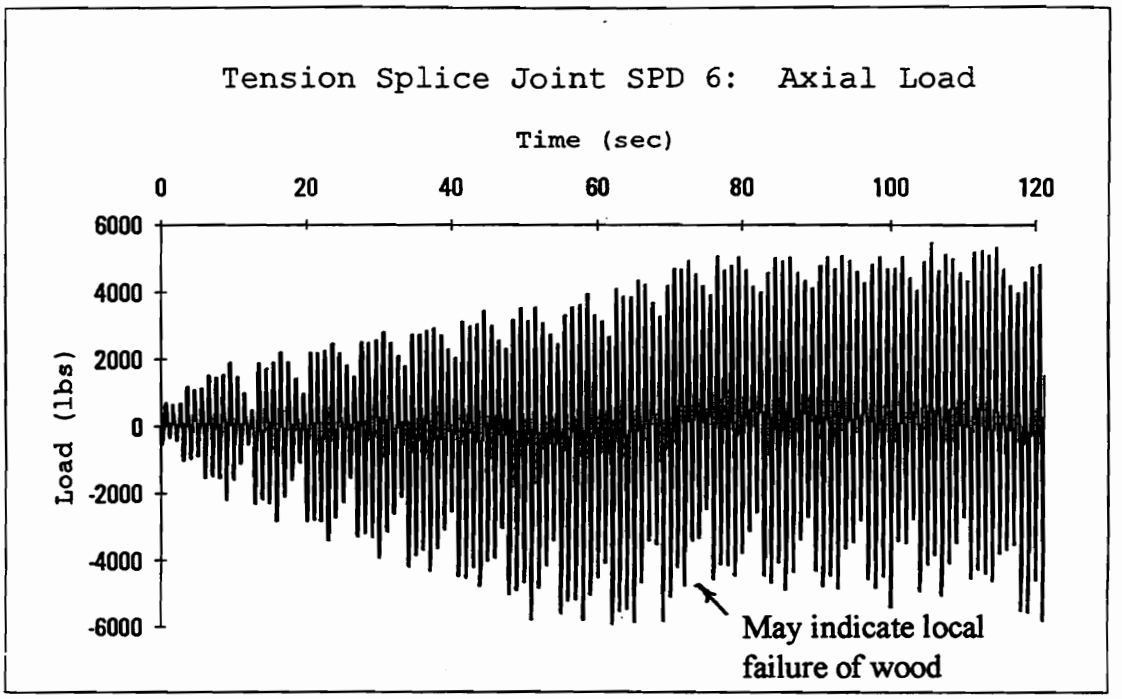
Tension Splice Joint SPD 6: Axial Load
Time (sec)
0
20
40
60
80
100
120
6000
4000
2000
0
-2000
-4000
-6000
Load (lbs)
May indicate local failure of wood

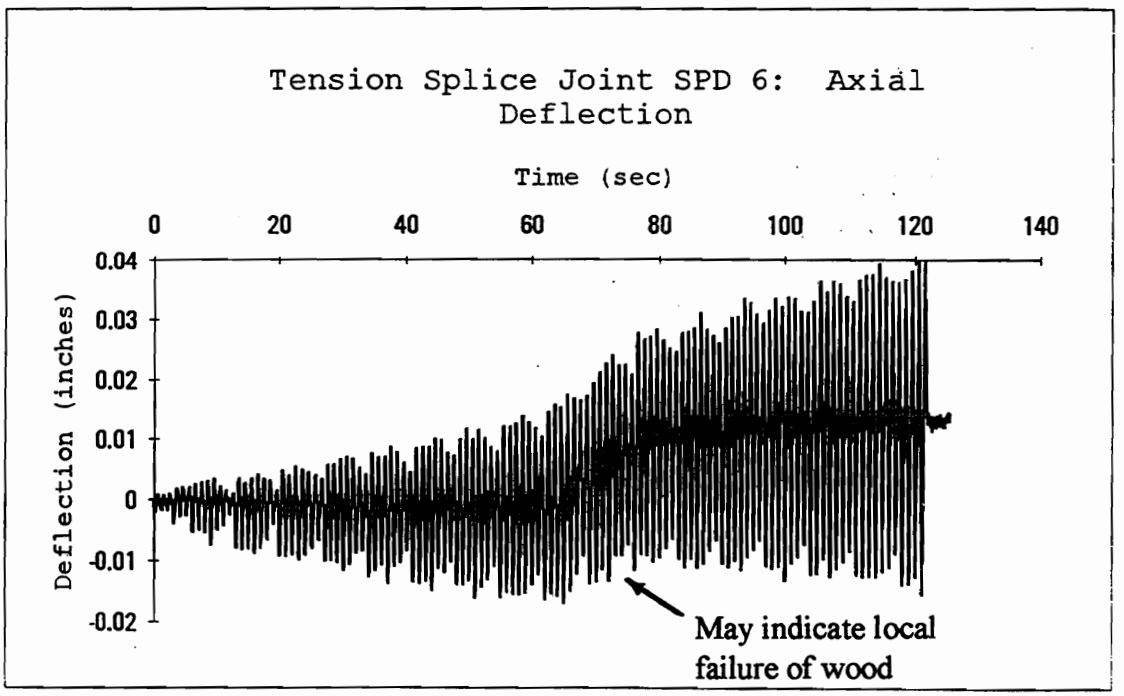
Tension Splice Joint SPD 6: Axial Deflection
Time (sec)
0
20
40
60
80
100
120
140
0.04
0.03
0.02
0.01
0
-0.01
-0.02
Deflection (inches)
May indicate local failure of wood

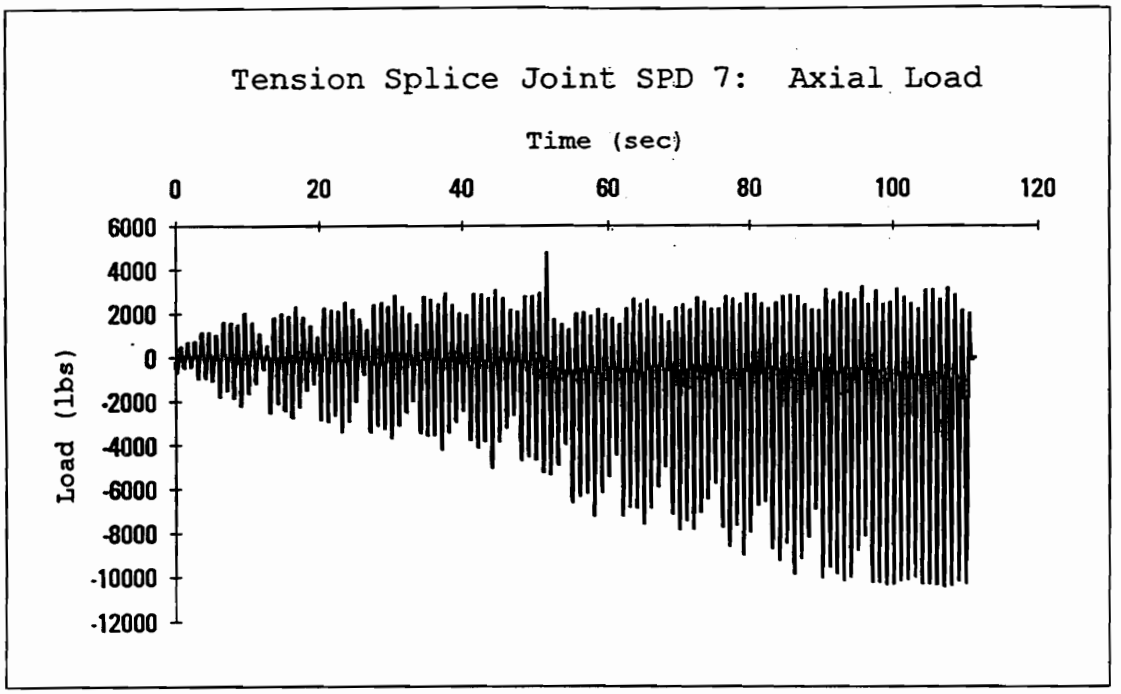
Tension Splice Joint SPD 7: Axial Load
Time (sec)
0
20
40
60
80
100
120
6000
4000
2000
0
-2000
-4000
-6000
-8000
-10000
-12000
Load (lbs)

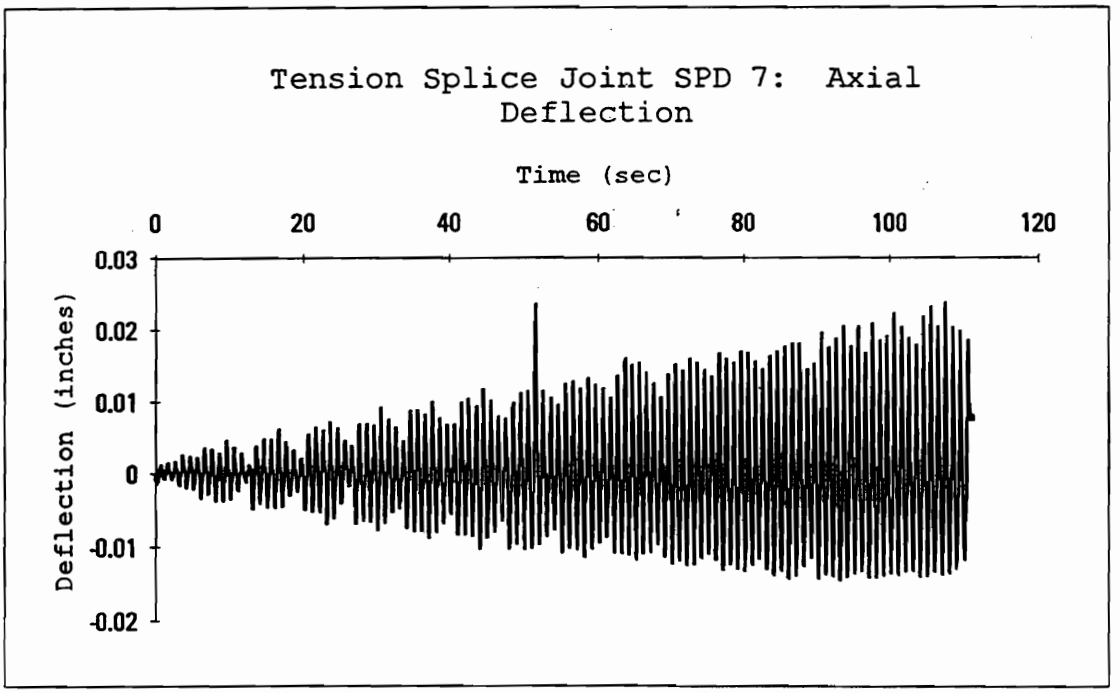
Tension Splice Joint SPD 7: Axial Deflection
Time (sec)
0
20
40
60
80
100
120
0.03
0.02
0.01
0
-0.01
-0.02
Deflection (inches)

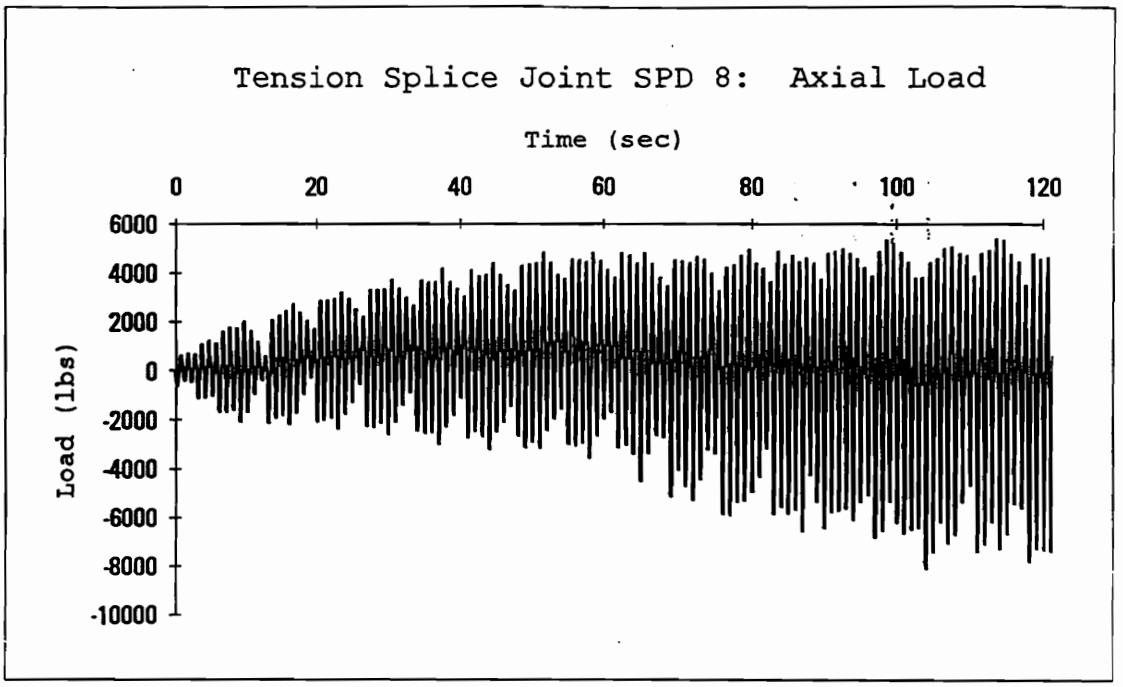
Tension Splice Joint SPD 8: Axial Load
Time (sec)
0
20
40
60
80
100
120
6000
4000
2000
0
-2000
-4000
-6000
-8000
-10000
Load (lbs)

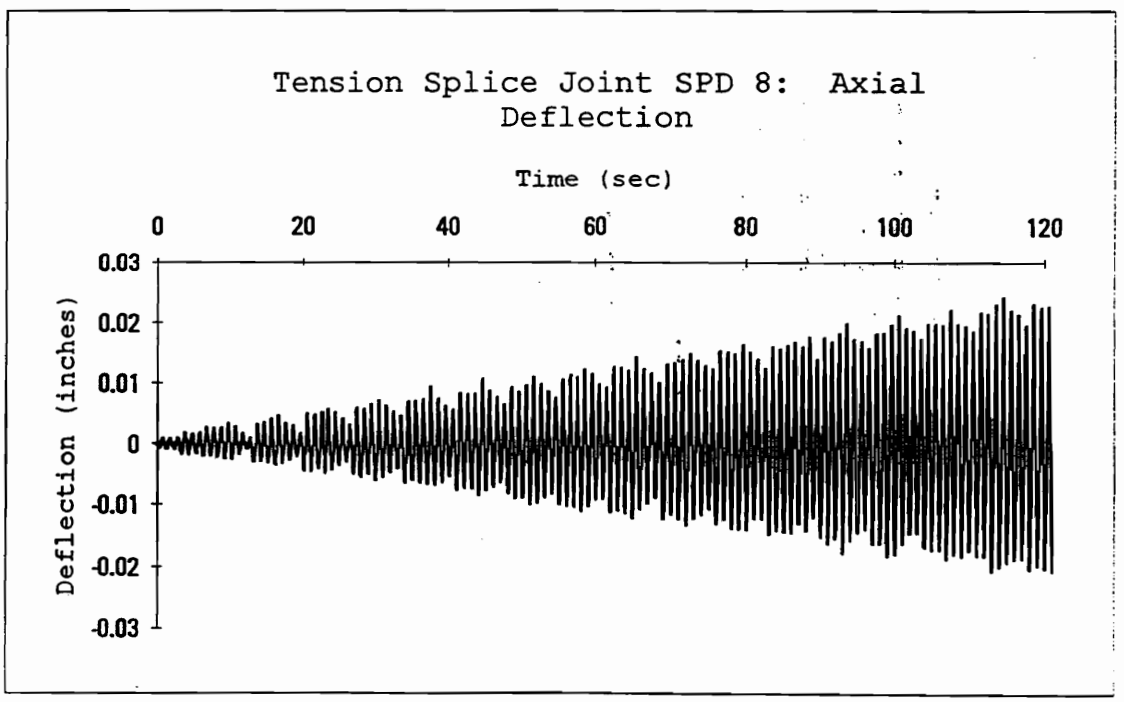
Tension Splice Joint SPD 8: Axial Deflection
Time (sec)
0
20
40
60
80
100
120
0.03
0.02
0.01
0
-0.01
-0.02
-0.03
Deflection (inches)

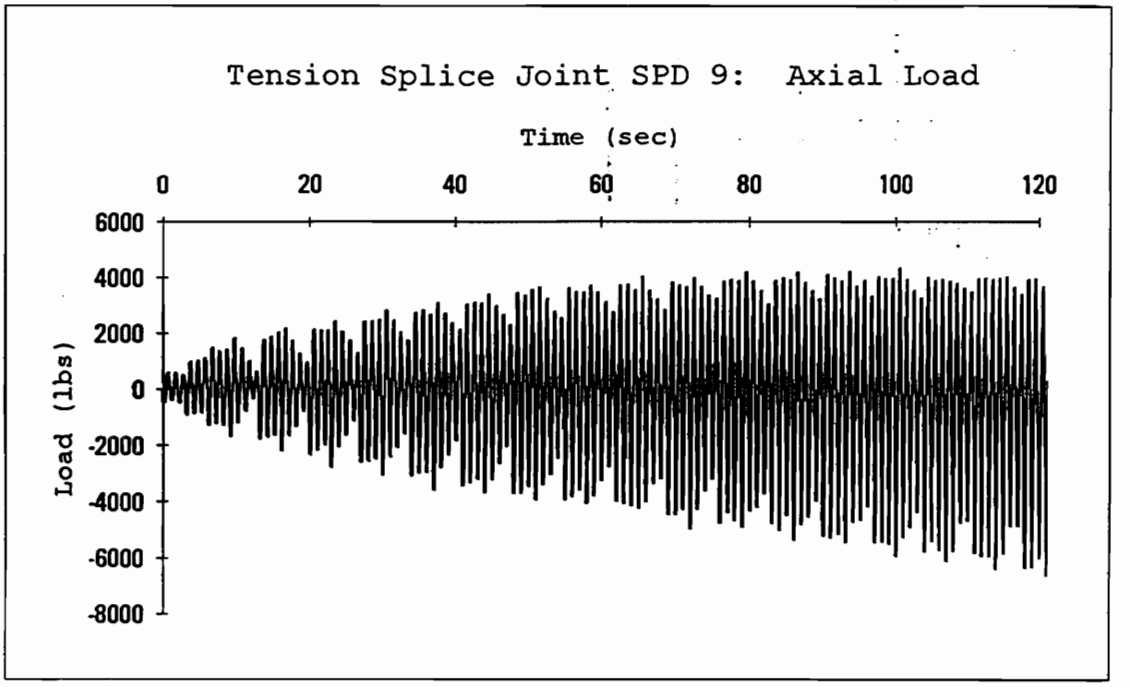
Tension Splice Joint SPD 9: Axial Load
Time (sec)
0
20
40
60
80
100
120
6000
4000
2000
0
-2000
-4000
-6000
-8000
Load (lbs)

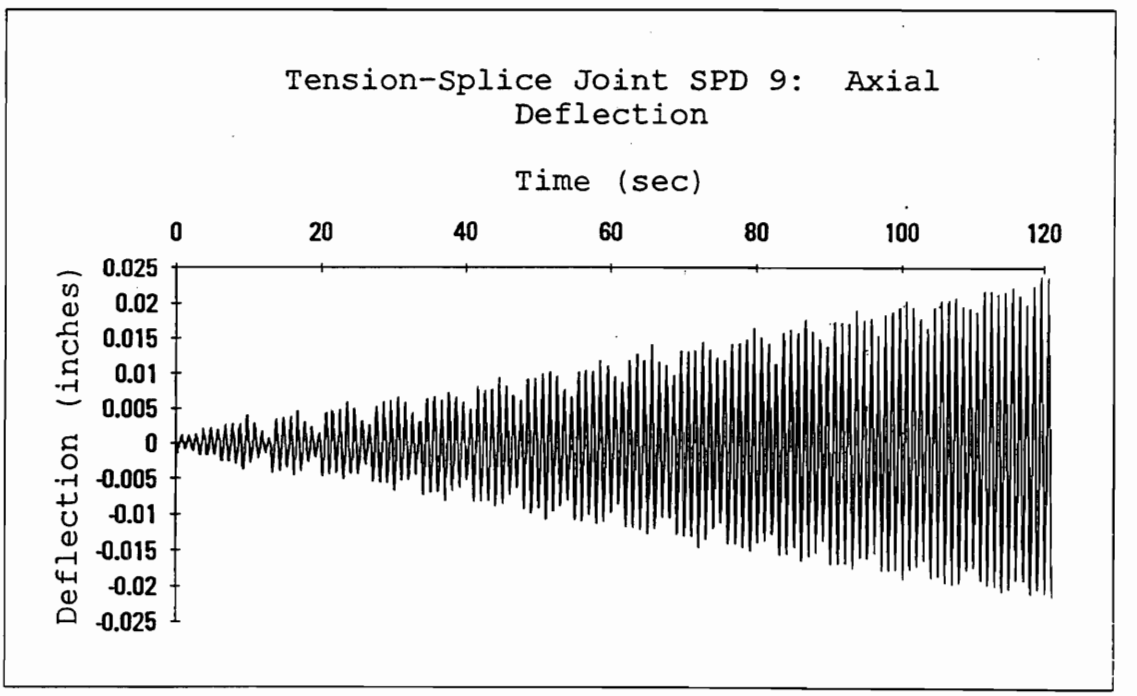
Tension-Splice Joint SPD 9: Axial Deflection
Time (sec)
0
20
40
60
80
100
120
0.025
0.02
0.015
0.01
0.005
0
-0.005
-0.01
-0.015
-0.02
-0.025
Deflection (inches)

Appendix G

Example Calculations to Determine the Dynamic Properties from the SPD Loading for Tension-Splice Joints

This appendix presents the sample calculations to determine the half-cycle cyclic stiffness, half-cycle energy dissipation, and the half-cycle damping ratio of the tension-splice joint during the sequential phased displacement loading (Dolan 1994). A digitizer (Calcomp Digitizer Products Division, Model No. 33120) was used to determine the area confined by the hysteresis curve. A scale factor of 0.667 lb-in. of energy per Calcomp Unit is used.

Given:

- Digitized area confined by the triangle CABC is 15 Calcomp Units which corresponds to the Energy Input

  (15 Calcomp Units)(0.667) = 10.0 lb-in. (Energy Input)

- Digitized area confined by the hysteresis trace is 5.17 Calcomp Units which corresponds to the Energy Dissipation

  (5.17 Calcomp Units)(0.667) = 3.45 lb-in. (Energy Dissipation)

- Maximum tensile load in the tension-splice joint during the sequential phased displacement cycle 50 is 2636 lb

- Maximum tensile deflection in the tension-splice joint during the sequential phased displacement cycle 50 is 0.0076 in.

Calculations:

1) Cyclic Stiffness = $\frac{2636 \text{ lb}}{0.0076 \text{ in.}} = 3.47 \times 10^5$ lb/in.

2) Energy Input = 0.5(2636 lb)(0.0076 in.) = 10.0 lb/in.

3) Damping Ratio = $\frac{\text{Energy Dissipation}}{2\pi(\text{Energy Input})} = \frac{3.45 \text{ lb-in}}{2\pi(10.0 \text{ lb/in.})} = 0.0549$

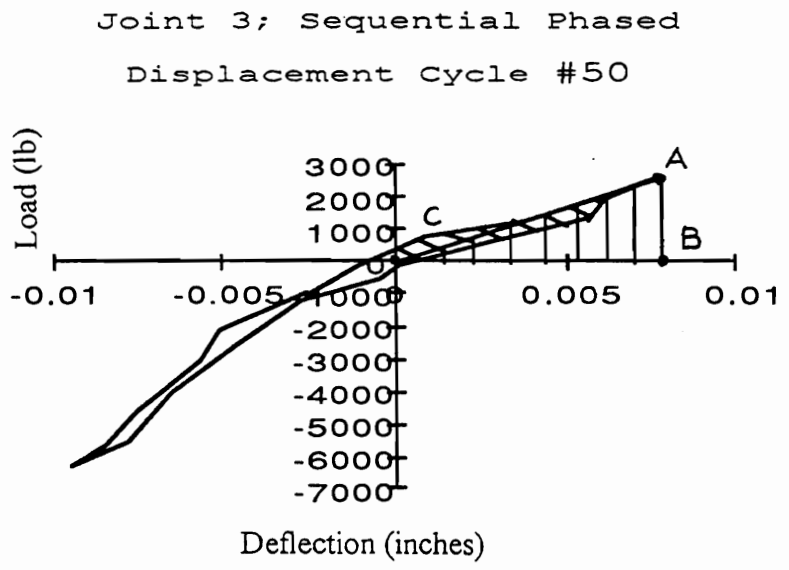

Appendix H

Finite Element Model (SAP 90) Input File for Heel Joints

```
SAP90 Input file used for the dynamic analysis.  Acceleration time-
history data in  a text file named motion.txt.  Linear Model.



C SAO90 Input File
C Fink Truss, 4/12 pitch, 30-ft span
C 20 lbs/ft dead load on top and bottom
C chords.  Includes dead weight of web
C members.  Using 2x4 truss members
C E=1.6e6-psi
C Units are KIP INCHES
SYSTEM
 R=0  L=2  C=0  V=5  T=0.0001  P=0  W=0  Z=0
GRID
 XN=31    YN=3    ZN=14    OG=0                    // Defines the x,y, & z
 0 12 24 36 48 60 72 84                            // grid
96 108 120 132 144 156 168 180
 192 204 216 228 240 252 264 276
 288 300 312 324 336 348 360
 0 12 24
 0 12 24 36 48 60 72 84
 96 108 120 132 144 156
JOINTS                                             // Defines the location
 8    X=24 Y=12 Z=96                               // of the joints
 16   X=384 Y=12 Z=96
 100  X=114 Y=12 Z=126
 101  X=204 Y=12 Z=156
 102  X=294 Y=12 Z=126
 103  X=144 Y=12 Z=96
 104  X=264 Y=12 Z=96
 105  X=24 Y=12 Z=0
 106  X=384 Y=12 Z=0
 200  X=408 Y=12 Z=96
 201  X=0 Y=12 Z=96
 108  X=174 Y=12 Z=96

                                                   // Defines properties of
FRAME                                              // the materials
 NM=5 NL=0 NSEC=0 Z=-1
 1   A=8.25 J=0 I=20700,20700 AS=0,0 E=1600.1 G=0 W=0.00065001
M=1.6822E-006\
     TC=0
 2   A=5.256 J=0 I=5.34989,0.98496 AS=0,0 E=1600.07 G=0 W=0.001667\
     M=4.31333E-006 TC=0
 3   A=5.256 J=0 I=5.34989,0.98496 AS=0,0 E=1600.07 G=0 W=0.001667\
     M=4.31333E-006 TC=0
 4   A=5.256 J=0 I=5.34989,0.98496 AS=0,0 E=1600.07 G=0 W=9.479E-005\
     M=2.45319E-007 TC=0
 5   A=0.012 J=0 I=999999,999999 AS=0,0 E=1600.1 G=0 W=0 M=0 TC=0

                                                   // Places member between
                                                   // the joints

 1    8    100  M=2,2,1 LP=2,0 LR=1,0,0,1,0,1
 2    100  101  M=2,2,1 LP=2,0 LR=0,1,0,0,1,1
```

```
 3     101   102   M=2,2,1 LP=2,0 LR=1,0,0,1,0,1
 8     104   16    M=3,3,1 LP=2,0 LR=0,1,0,0,1,1
 9     100   103   M=4,4,1 LP=2,0 LR=1,1,0,1,1,1
 10    103   101   M=4,4,1 LP=2,0 LR=1,1,0,1,1,1
 11    101   104   M=4,4,1 LP=2,0 LR=1,1,0,1,1,1
 12    104   102   M=4,4,1 LP=2,0 LR=1,1,0,1,1,1
 13    201   8     M=5,5,1 LP=2,0 LR=1,1,0,1,1,1
 14    16    200   M=5,5,1 LP=2,0 LR=1,1,0,1,1,1
 4     102   16    M=2,2,1 LP=2,0 LR=0,1,0,0,1,0
 5     8     103   M=3,3,1 LP=2,0 LR=1,0,0,1,0,0
 6     103   108   M=3,3,1 LP=2,0 LR=0,1,0,0,1,0
 7     108   104   M=3,3,1 LP=2,0 LR=1,0,0,1,0,0
 20    8     105   M=1,1,1 LP=2,0 LR=1,1,0,1,1,1
 21    16    106   M=1,1,1 LP=2,0 LR=1,1,0,1,1,1

                                                  // Defines the location
                                                  // of the restraints
RESTRAINTS
 105   105   1     R=1,1,1,1,0,1
 106   106   1     R=1,1,1,1,0,1
 100   100   1     R=0,1,0,1,0,1
 103   103   1     R=0,1,0,1,0,1
 101   101   1     R=0,1,0,1,0,1
 104   104   1     R=0,1,0,1,0,1
 102   102   1     R=0,1,0,1,0,1
 200   200   1     R=1,1,1,1,1,1
 201   201   1     R=1,1,1,1,1,1
 108   108   1     R=0,1,0,1,0,1
 8     8     1     R=0,1,0,1,0,1
 16    16    1     R=0,1,0,1,0,1

TIMEH
 ATYPE=0 NSTEP=1500 DT=0.02 NF=1 NV=5 D=0.1
 NF=1 PRIN=0 NPL=1 NAM=motion.txt
 LC=-3 NF=1 S=483.4 AT=0 ANGLE=0


COMBO
 1     C=1,1
```

Appendix I

WES-RASCAL Input File for Heel Joints

WES-RASCAL input file used to create an artificial earthquake using the UBC (ICBO 1994) design response spectrum and the Northridge earthquake horizontal accelerations for the phase characteristics (NRINPUT.TXT).

Description	Real RASCAL input file
title	"WES : WUS : HALF-SPACE (M7, 5 % DAMPING, IV25VERT) : KEY5 = -1"
output file name	scotty8
site condition parameters	50.0 2.7 00.0 10.0 3.2
"	300.0 0.0 0.0 7
"	5.0 15.0 4 0.0
keys	0 1 0 0 -1 0
number of near-site amplification factors	5
frequency, amplification factors	0.1 1.023
"	.316 1.096
"	1.0 1.349
"	3.162 2.188
"	10.0 2.344
input time-history file name	NRINPUT.TXT
input time-history file format	3000 1 0.02 (1F9.6)
output time-history normalizing factors	-1.0 0.00 0.00
number of iterations	10 10
number of input response spectrum points	7
input response spectrum points (frequency, pseudo acceleration)	0.33 0.36
"	.5 0.48
"	.67 0.62
"	1 0.96
"	1.11 1
"	10 1
"	30 0.4
output time-history filtering parameters	23.0 5 0.10 -5

Appendix J

Heel Joint Test Results

Heel Joint: Static Load

Joint	Maximum Top Chord Load (lb)	Maximum Moment (in.-lb)	Deflection at Maximum Top Chord Load (in.)	Rotation at Maximum Rotation (rad)	Axial Stiffness (x10^5-lb/in)	Rotational Stiffness x10^5 (in.-lb/rad)	Top Chord Yield Displacement (in.)
1	5619	9833	0.180	0.005	3.41	81.7	0.006
2	6436	11263	0.211	0.011	8.94	28.9	0.002
3	6161	10782	0.276	0.013	1.80	26.4	0.011
4	5865	10264	0.238	0.010	2.38	57.2	0.008
5	6540	11445	0.228	0.013	4.74	24.1	0.005
6	6369	11146	0.290	0.020	2.08	42.3	0.010
7	7001	12252	0.241	0.017	3.07	52.1	0.008
9	5773	10103	0.198	0.007	3.10	110.4	0.006
10	6134	10735	0.143	0.008	2.73	45.6	0.008
Average	6211	10869	0.223	0.012	3.58	52.1	0.007
COV(%)	6.92	32.3	20.6	40.2	60.9	54.4	39.2

Joint	Specific Gravity	Moisture Content (%)	MOE (x1,000,000-psi)	% Late Wood	Rings per inch	Grain Orientation	Yield Rotation (radians)
1	0.53	14.9	1.59	20	9	Both	0.0004
2	0.55	14.3	2.32	30	6	Both	0.0013
3	0.50	12.5	2.16	30	7	Flat	0.0014
4	0.50	16.5	1.73	20	7	Flat	0.0006
5	NA	NA	NA	30	6	Flat	0.0016
6	0.46	NA	1.73	30	8	Both	0.0009
7	0.49	NA	2.61	25	7	Both	0.0008
9	NA	NA	1.78	35	6	Flat	0.0003
10	0.53	13.4	2.16	20	10	Flat	0.0008
Average	0.51	14.3	2.01	27	7	--	0.0009
COV(%)	5.81	10.7	17.7	21	19	--	49.7

NA: Not Available
Flat: Flat-Sawn Lumber
Quarter: Quarter-Sawn Lumber
Both: Combination of Flat and Quarter-Sawn
Failure mode for all tests was Tooth Withdrawal
Moment, Deflection, and Yield Points are Defined in Section 4.3.1

Heel Joint: Simulated Earthquake

Joint	Maximum Top Chord Load (lb)	Maximum Moment (in.-lb)	Deflection at Maximum Top Chord Load (in.)	Rotation at Maximum Rotation (rad)	Axial Stiffness (x10^5-lb/in)	Rotational Stiffness x10^5 (in.-lb/rad)	Yield Displacement (in.)
1	6599	11548	0.383	0.013	2.97	56.4	0.007
2	5944	10402	0.325	0.010	1.54	68.8	0.013
3	5290	9258	0.239	0.017	0.83	22.3	0.021
4	5954	10420	0.303	0.015	0.95	27.5	0.021
5	6531	11429	0.338	0.014	1.16	27.6	0.019
6	6202	10854	0.203	0.014	1.26	15.9	0.016
7	6010	10518	0.332	0.014	0.95	17.4	0.021
8	5620	9835	NA	NA	NA	NA	NA
9	6724	11767	0.318	0.012	2.58	52.5	0.009
10	5698	9972	0.283	0.015	0.84	22.5	0.023
Average	6057	10600	0.303	0.014	1.45	32.3	0.017
COV(%)	7.62	7.62	18.0	13.9	54.3	68.0	34.3

Joint	Specific Gravity	Moisture Content (%)	MOE (x1,000,000-psi)	% Late Wood	Rings per inch	Grain Orientation	Yield Rotation (radians)
1	0.48	12.5	1.77	25	8	Flat	0.0007
2	0.49	13.2	2.00	30	8	Flat	0.0005
3	0.48	13.5	2.00	30	9	Flat	0.0014
4	0.48	13.6	2.01	25	5	Flat	0.0013
5	0.66	12.8	2.21	20	10	Flat	0.0014
6	0.50	13.0	2.04	20	5	Flat	0.0023
7	0.46	11.7	NA	20	9	Flat	0.0020
8	0.50	12.8	2.01	30	6	Flat	NA
9	0.67	13.2	2.20	30	9	Flat	0.0007
10	0.54	13.4	1.78	35	5	Both	0.0015
Average	0.53	13.0	2.00	27	7	--	0.0013
COV(%)	14.3	4.33	7.64	20	26	--	45.6

NA: Not Available

Flat: Flat-Sawn Lumber

Quarter: Quarter-Sawn Lumber

Both: Combination of Flat and Quarter-Sawn

Failure mode for all tests was Tooth Withdrawal

Moment, Deflection, and Yield Points are Defined in Section 4.3.1

Heel Joint: Sequential Phased Displacement

Joint	Maximum Top Chord Load (lb)	Maximum Moment (in.-lb)	Deflection at Maximum Top Chord Load (in.)	Rotation at Maximum Rotation (rad)	Axial Stiffness (x10^5-lb/in)	Rotational Stiffness x10^5(in.-lb/rad)	Yield Displacement (in.)
2†	3657	6400	NA	NA	NA	NA	NA
3††	4625	8094	NA	NA	NA	NA	NA
4	4397	7695	0.074	0.0068	1.33	25.0	0.011
5	4421	7737	0.145	0.0131	2.34	37.8	0.006
6	4306	7536	0.186	0.0071	0.81	NA	0.018
7†	NA	NA	NA	NA	NA	NA	NA
8	4205	7359	0.197	0.0064	0.68	163.5	0.021
9	5085	8899	0.216	0.0061	0.74	122.1	0.023
10	2740	4795	0.075	0.0019	2.54	NA	0.004
11	4227	7397	0.159	0.0043	1.06	71.5	0.013
Average	4185	7323	0.150	0.0065	1.36	84.0	0.014
COV(%)	15.8	15.8	37.8	52.1	56.9	69.3	52.9

Joint	Specific Gravity	Moisture Content (%)	MOE (x1,000,000-psi)	% Late Wood	Rings per inch	Grain Orientation	Yield Rotation (radians)
2	0.52	12.8	2.19	25	8	Quarter	NA
3	NA	NA	NA	NA	NA	NA	NA
4	0.50	13.8	2.04	25	6	Flat	0.0010
5	NA	NA	NA	NA	NA	NA	0.0007
6	0.46	13.6	1.99	25	7	Flat	NA
7†	0.51	13.1	1.99	20	7	Flat	NA
8	0.43	12.0	1.82	20	10	Flat	0.0002
9	0.47	12.2	1.76	20	12	Flat	0.0002
10	0.42	11.9	2.00	20	6	Flat	NA
11	0.56	13.6	1.78	30	9	Flat	0.0003
Average	0.48	12.9	1.95	23	8	--	0.0005
COV(%)	9.39	6.0	7.60	16	26	--	73.9

NA: Not Available
Flat: Flat-Sawn Lumber
Quarter: Quarter-Sawn Lumber
Both: Combination of Flat and Quarter-Sawn
Failure mode for all tests was Tooth Withdrawal
† Joints 2 and 7 Failed in Tension Perpendicular to Grain in the Bottom Chord During the Sequential Phased Displacement Loading
†† Missing Data for the Static Loading Portion
Moment, Deflection, and Yield Points are Defined in Section 4.3.1

Heel: Cyclic Tests

Test Number	Cyclic Amplitude	Maximum Top Chord Load (lb)	Strength Ratio (1)	Specific Gravity	Moisture Content (%)	MOE (x1,000,000-psi)	% Late Wood	Rings per inch	Grain Orientation
1	5	5059	0.82	0.47	NA	NA	25	14	Flat
2	5	5520	0.89	0.50	NA	2.44	25	10	Flat
3	5	6459	1.04	0.45	10.1	1.72	20	7	Flat
4	10	4681	0.76	0.48	13.7	1.73	25	7	Flat
5	10	6426	1.04	0.52	NA	2.61	25	8	Both
6	10	6722	1.09	0.52	NA	2.00	15	4	Flat
7	15	5363	0.87	0.47	10.7	2.29	25	10	Flat
8	15	5983	0.97	NA	NA	NA	NA	NA	NA
9	15	5362	0.87	0.45	NA	2.59	20	10	Both
10	20	6617	1.07	0.48	14.3	1.73	20	7	Quarter
11	20	5710	0.92	0.55	NA	NA	30	7	Both
12	25	5750	0.93	0.58	NA	2.63	35	5	Both
13	25	6502	1.05	0.51	NA	1.77	NA	NA	Both
14	30	4095	0.66	NA	NA	1.99	25	7	Both
15	30	4731	0.76	0.53	NA	NA	30	11	Both
16	30	6705	1.08	0.48	NA	1.77	20	5	Flat
17	33	5208	0.84	0.51	11.8	1.99	30	8	Flat
18	33	5599	0.90	NA	12.9	1.98	35	4	Both
19	33	6200	1.00	0.53	NA	2.00	NA	NA	NA
20	35	5307	0.86	NA	13.6	2.12	30	7	Both
21	35	0	0.00	0.59	NA	1.85	NA	NA	NA
22	35	0	0.00	NA	13.4	2.96	35	12	Flat
23	40	0	0.00	0.58	NA	1.76	NA	NA	NA
24	40	0	0.00	NA	13.9	1.76	40	5	Flat
25	40	0	0.00	NA	NA	2.29	25	6	Both
Average	--	--	--	0.51	12.7	2.09	27	8	--
COV (%)	--	--	--	8.55	11.8	17.5	24	35	--

(1): Ratio of the strength of the heel-joints under the static ramp load portion
after completion of the 200-cycles to the average strength of the control group (6211 lb)
NA: Not Available
Flat: Flat-Sawn Lumber
Quarter: Quarter-Sawn Lumber
Both: Combination of Flat and Quarter-Sawn
Failure mode for all tests was Tooth Withdrawal

Appendix K

Load-Deflection and Moment-Rotation Curves for the Static Loading Control Group for Heel Joints

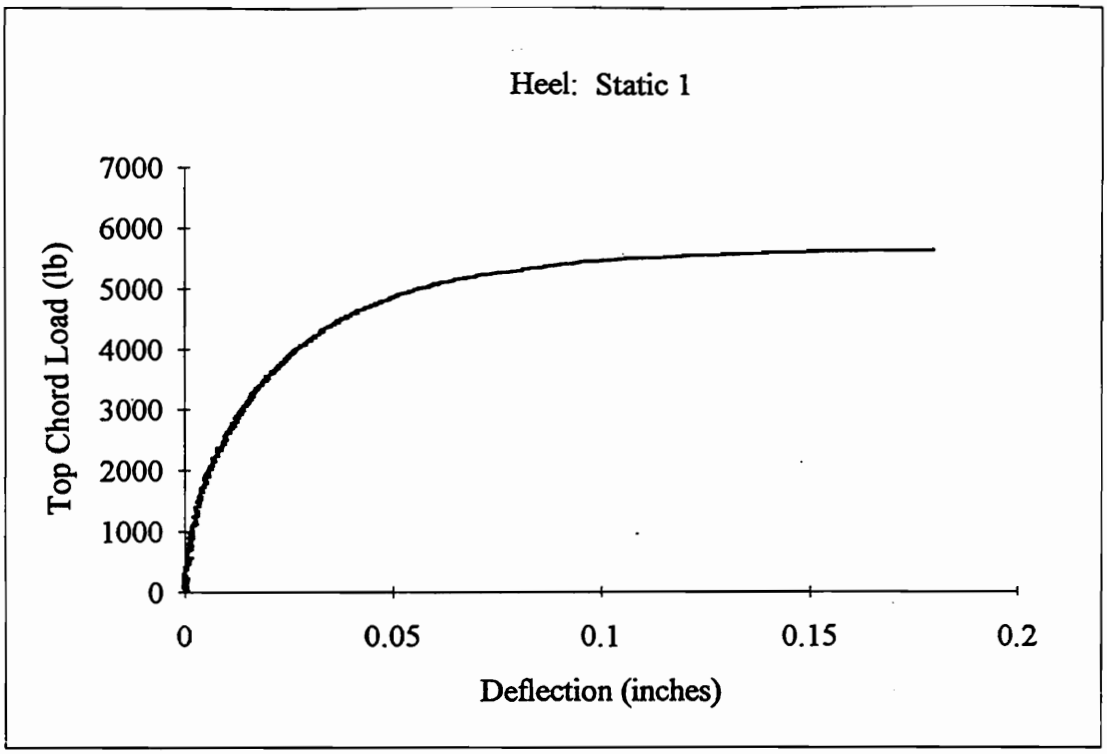
Heel: Static 1
Top Chord Load (lb)
7000
6000
5000
4000
3000
2000
1000
0
0
0.05
0.1
0.15
0.2
Deflection (inches)

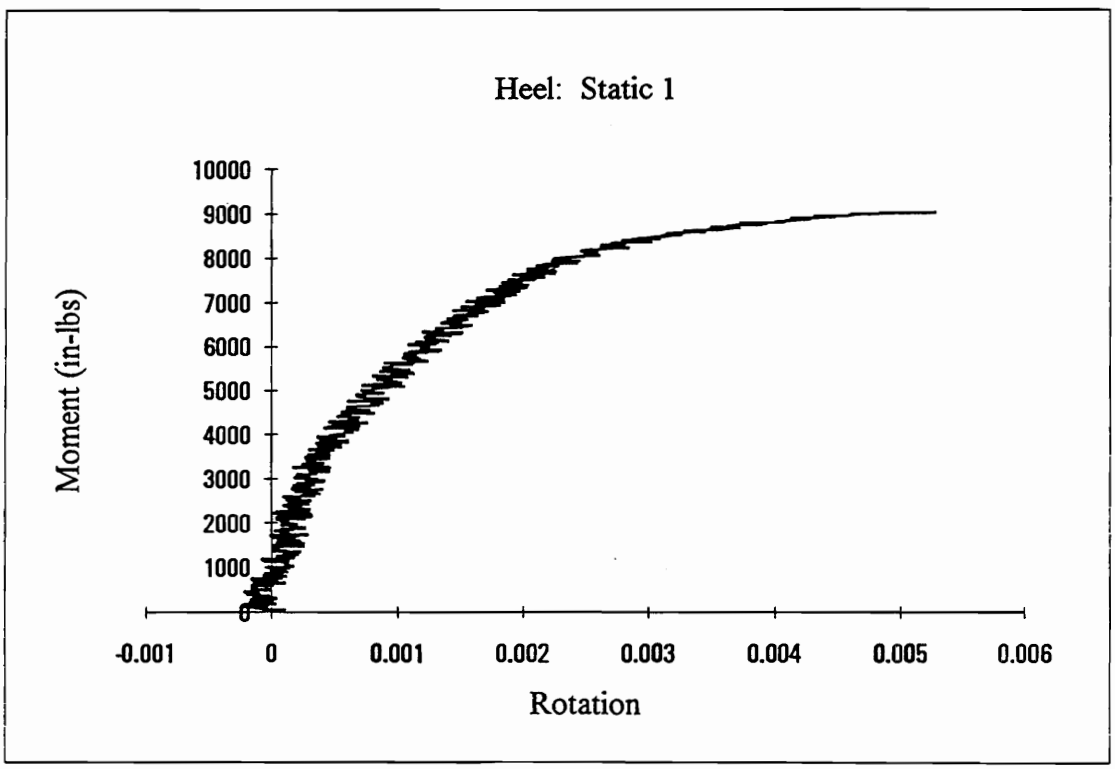
Heel: Static 1
Moment (in-lbs)
10000
9000
8000
7000
6000
5000
4000
3000
2000
1000
0
-0.001
0
0.001
0.002
0.003
0.004
0.005
0.006
Rotation

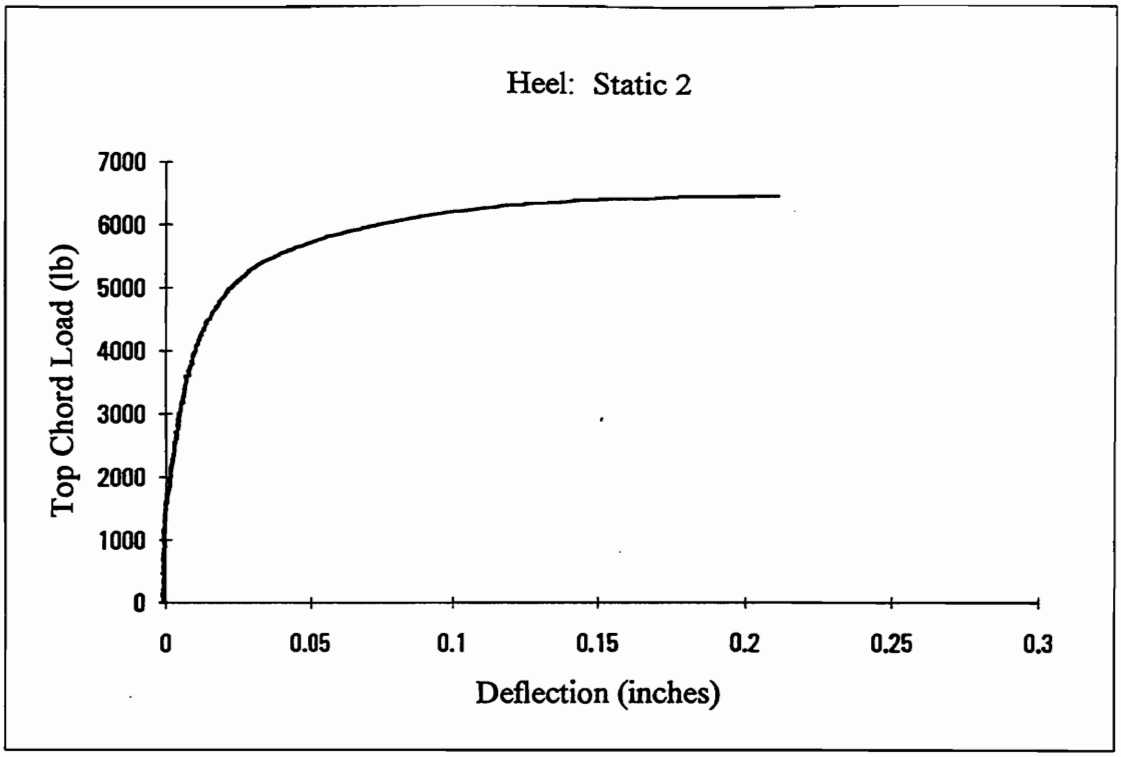
Heel: Static 2
Top Chord Load (lb)
7000
6000
5000
4000
3000
2000
1000
0
0
0.05
0.1
0.15
0.2
0.25
0.3
Deflection (inches)

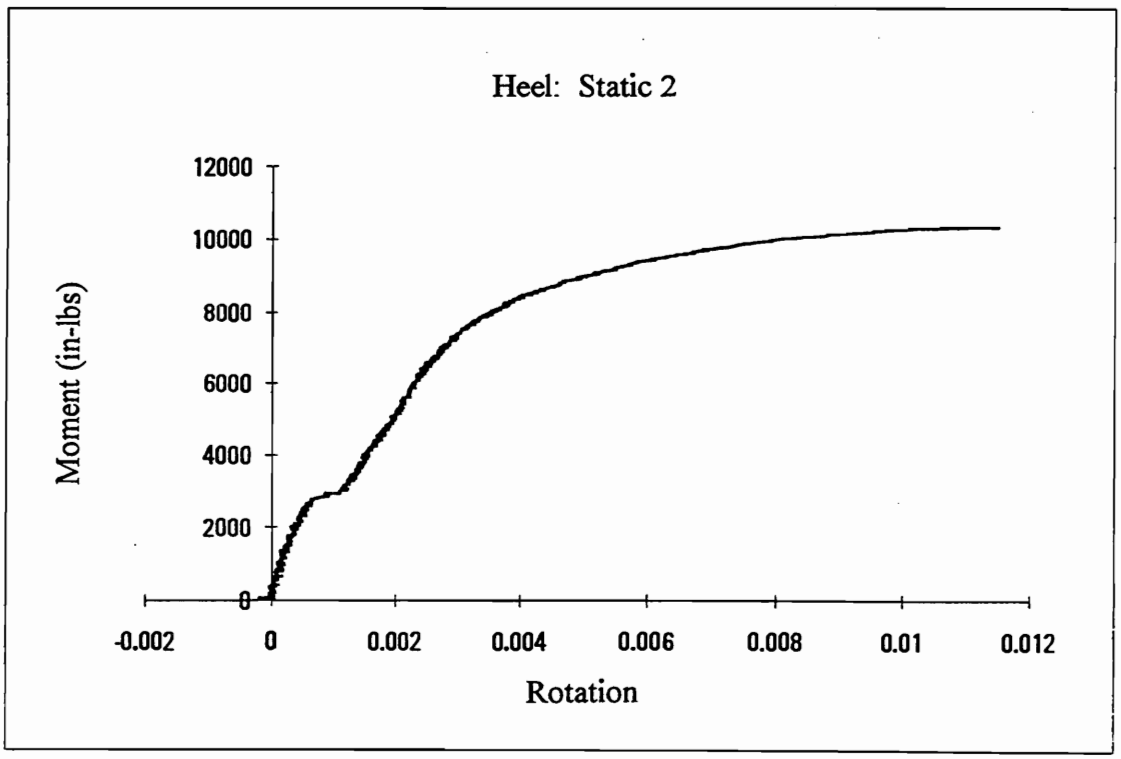
Heel: Static 2
Moment (in-lbs)
12000
10000
8000
6000
4000
2000
0
-0.002
0
0.002
0.004
0.006
0.008
0.01
0.012
Rotation

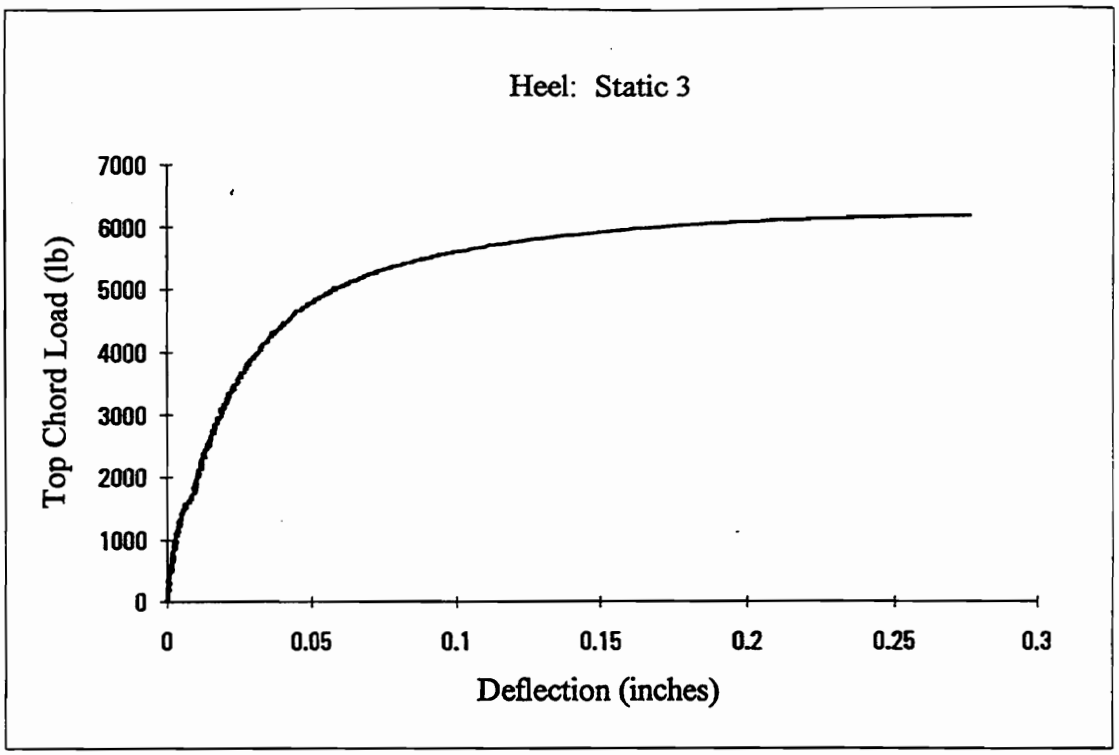
Heel: Static 3
Top Chord Load (lb)
7000
6000
5000
4000
3000
2000
1000
0
0
0.05
0.1
0.15
0.2
0.25
0.3
Deflection (inches)

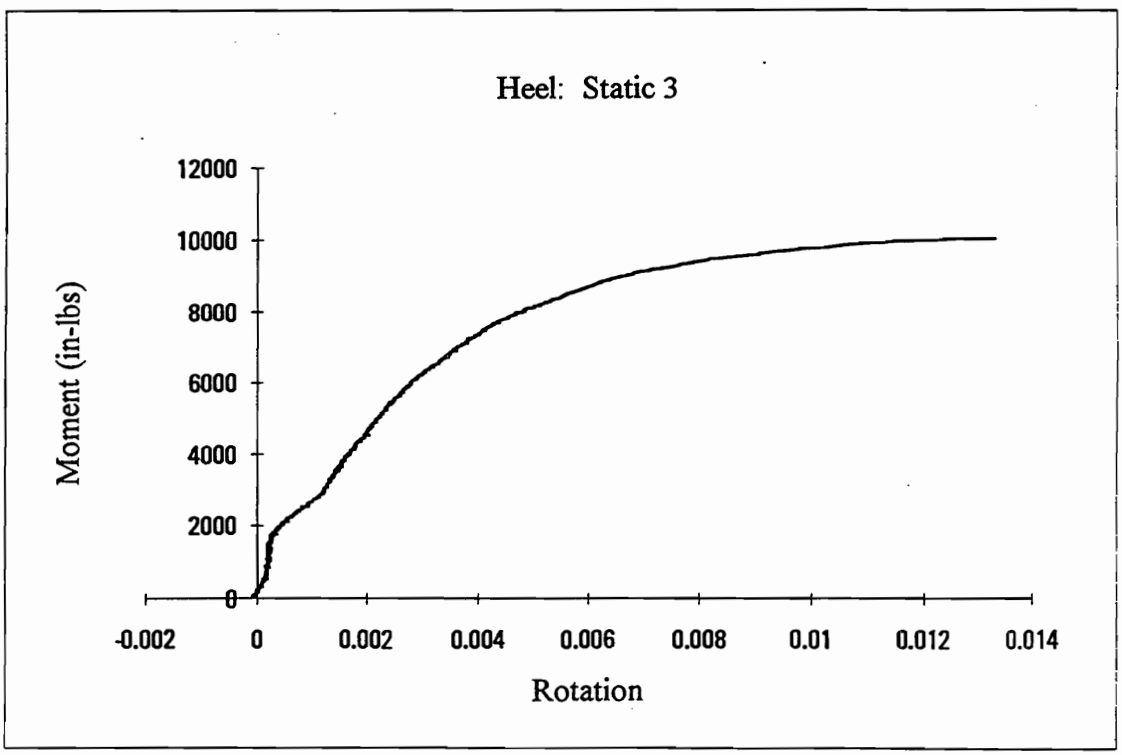
Heel: Static 3
Moment (in-lbs)
12000
10000
8000
6000
4000
2000
0
-0.002
0
0.002
0.004
0.006
0.008
0.01
0.012
0.014
Rotation

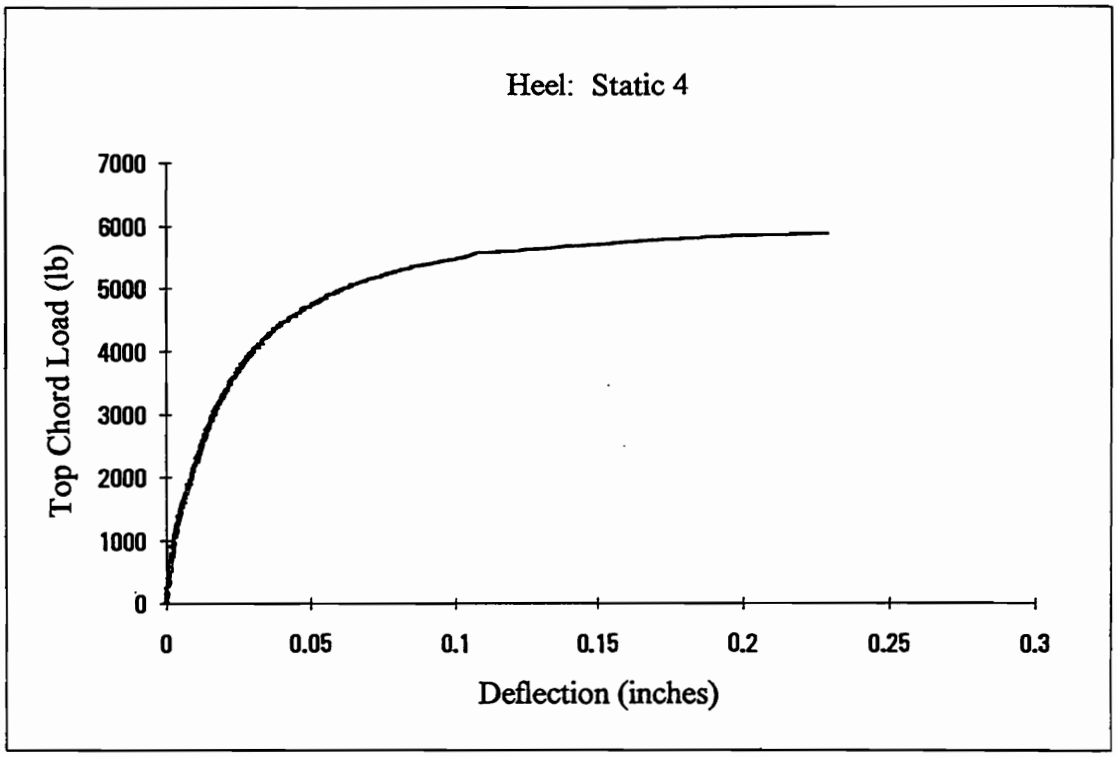
Heel: Static 4
Top Chord Load (lb)
7000
6000
5000
4000
3000
2000
1000
0
0
0.05
0.1
0.15
0.2
0.25
0.3
Deflection (inches)

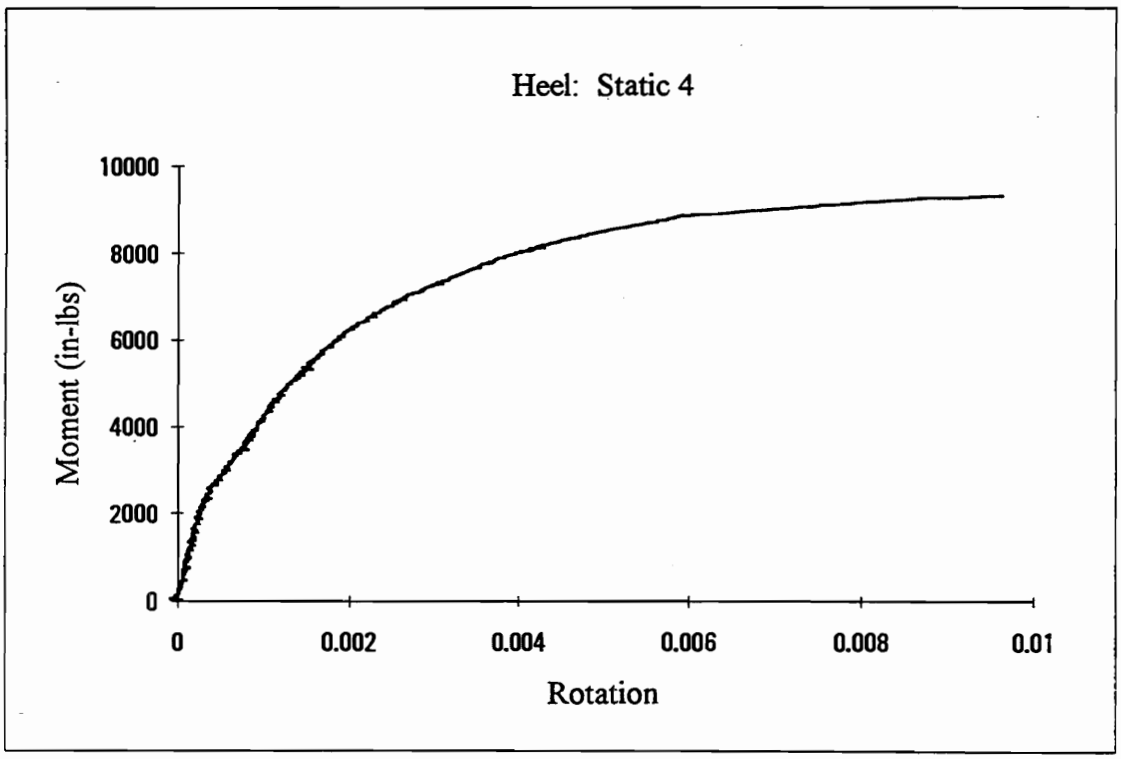
Heel: Static 4
Moment (in-lbs)
10000
8000
6000
4000
2000
0
0
0.002
0.004
0.006
0.008
0.01
Rotation

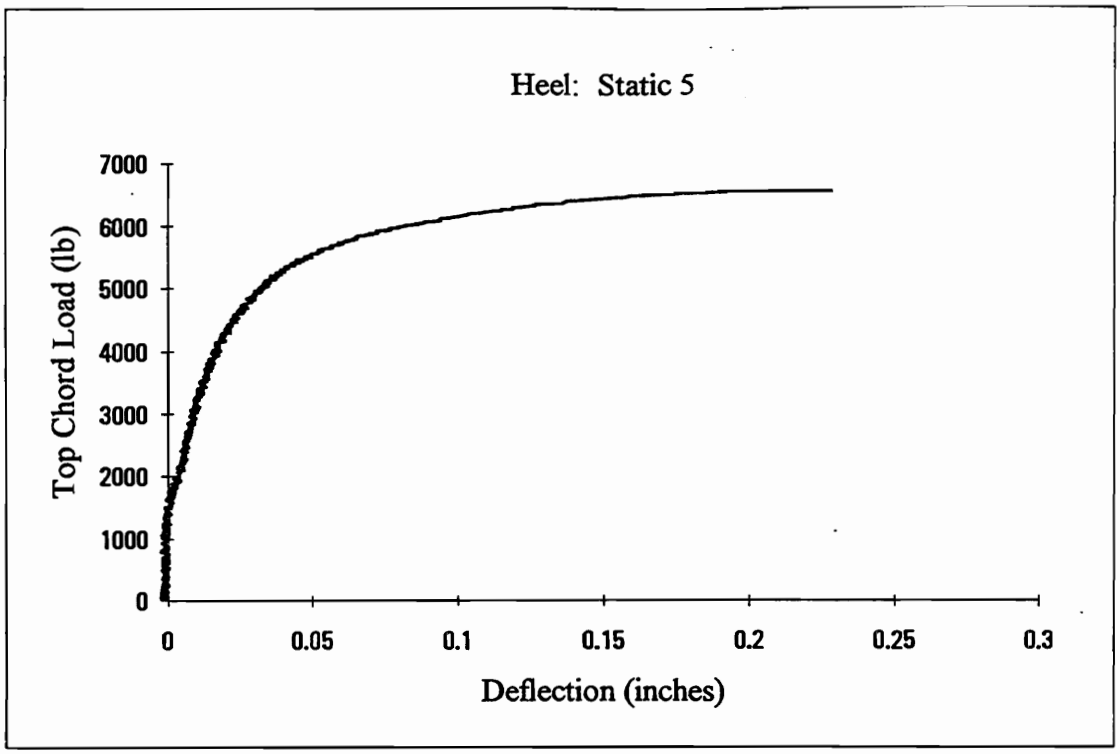
Heel: Static 5
Top Chord Load (lb)
7000
6000
5000
4000
3000
2000
1000
0
0
0.05
0.1
0.15
0.2
0.25
0.3
Deflection (inches)

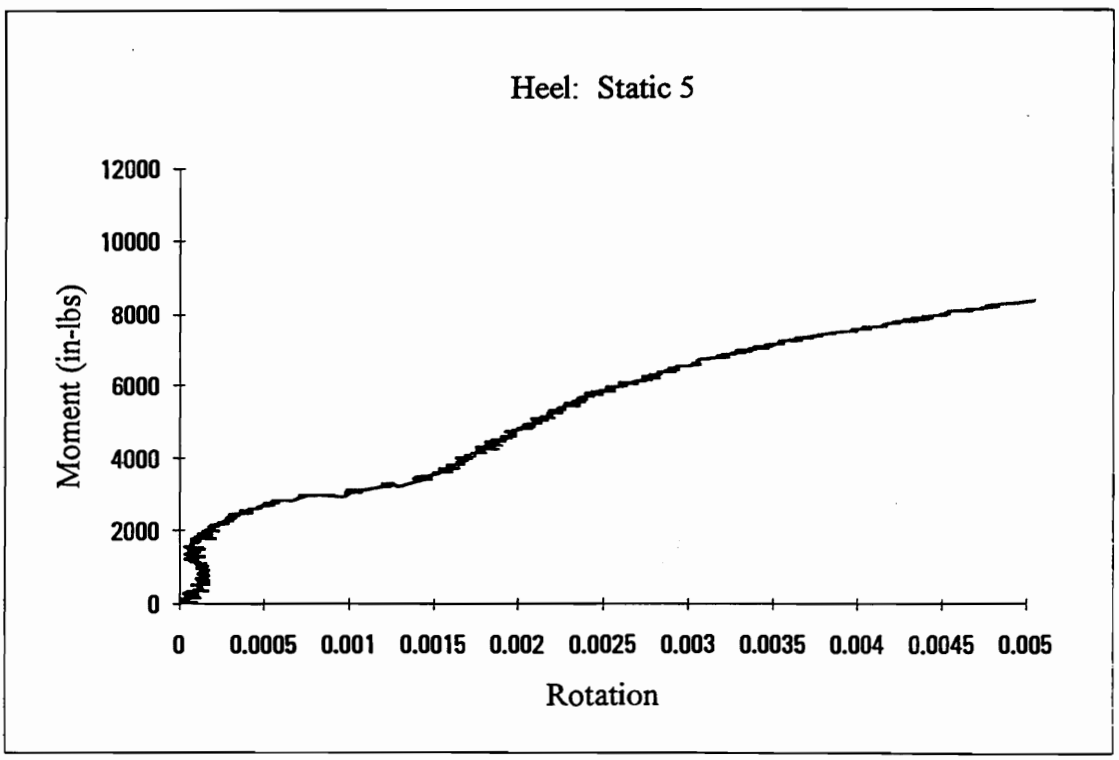
Heel: Static 5
Moment (in-lbs)
12000
10000
8000
6000
4000
2000
0
0
0.0005
0.001
0.0015
0.002
0.0025
0.003
0.0035
0.004
0.0045
0.005
Rotation

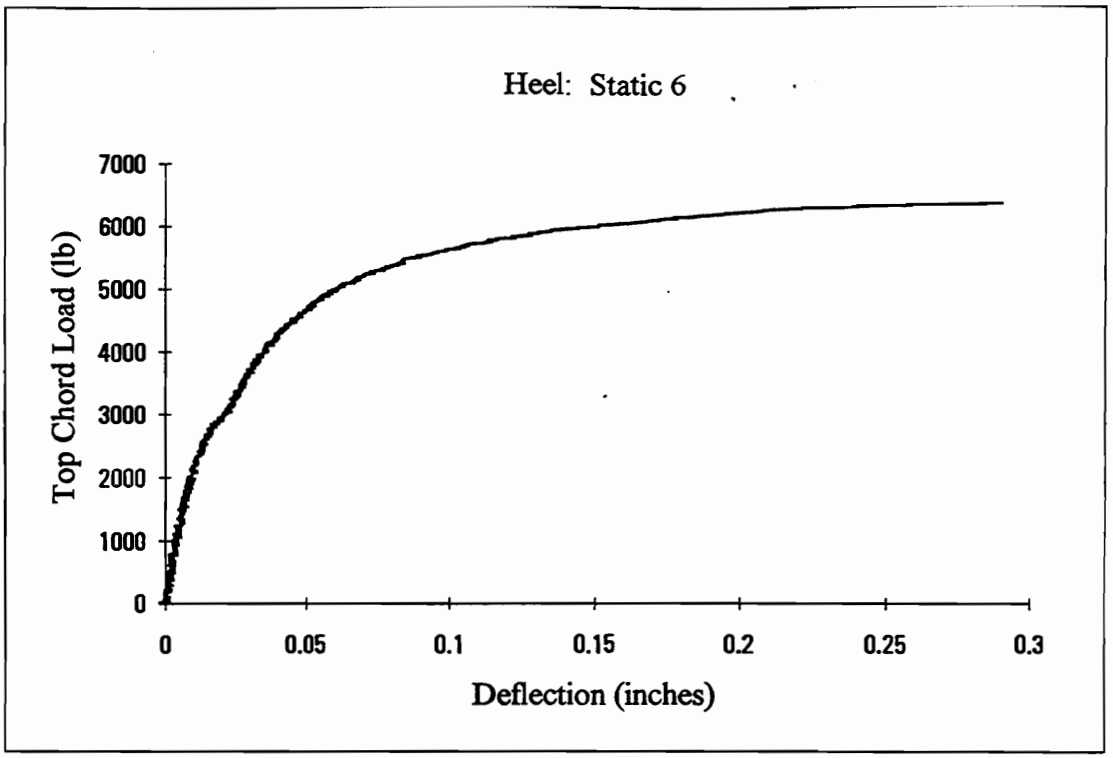
Heel: Static 6
Top Chord Load (lb)
7000
6000
5000
4000
3000
2000
1000
0
0
0.05
0.1
0.15
0.2
0.25
0.3
Deflection (inches)

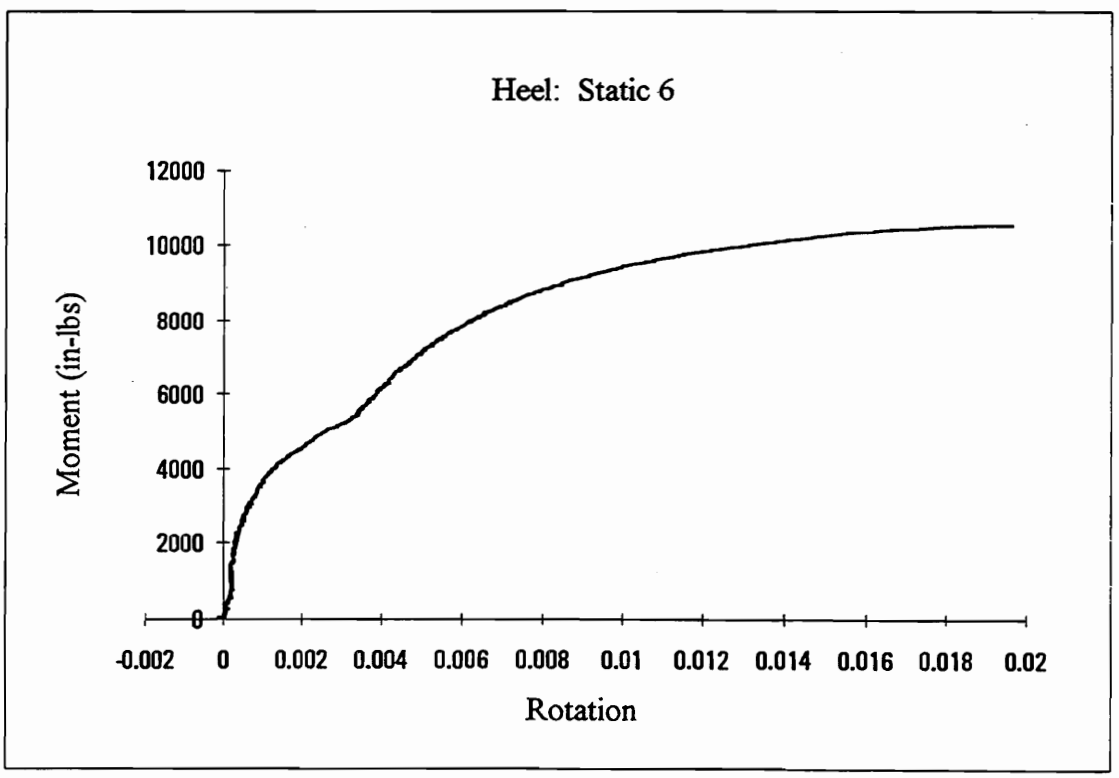
Heel: Static 6
Moment (in-lbs)
12000
10000
8000
6000
4000
2000
0
-0.002
0
0.002
0.004
0.006
0.008
0.01
0.012
0.014
0.016
0.018
0.02
Rotation

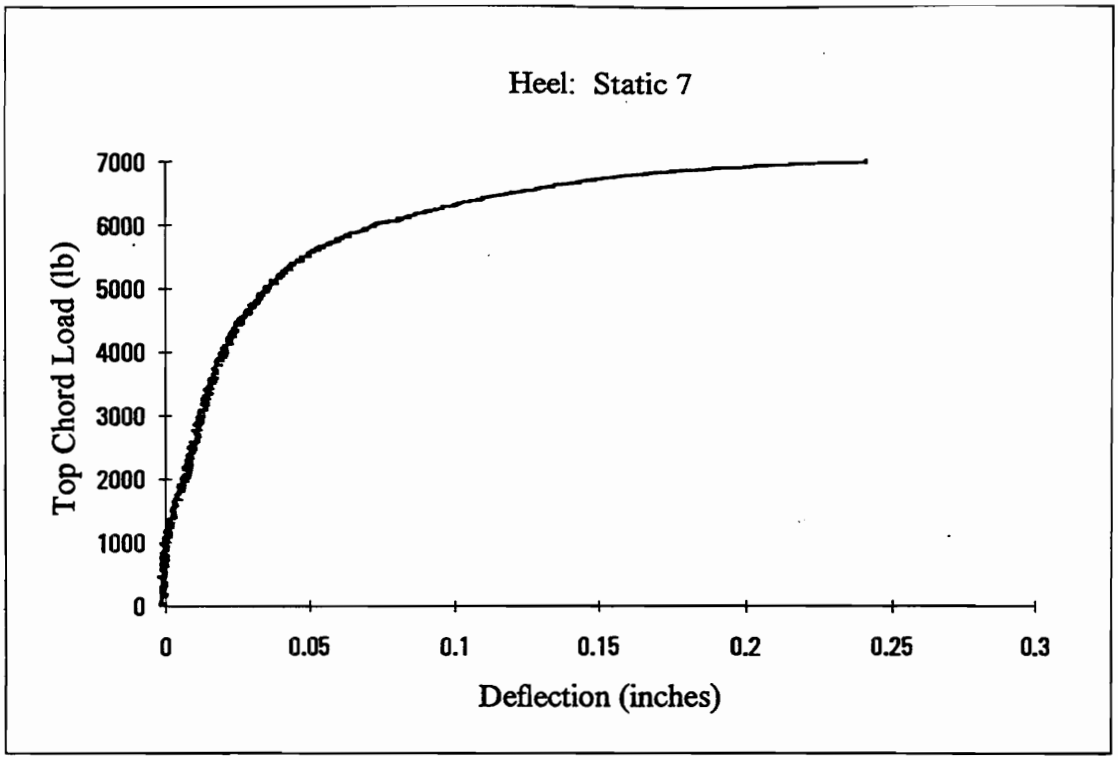
Heel: Static 7
Top Chord Load (lb)
7000
6000
5000
4000
3000
2000
1000
0
0
0.05
0.1
0.15
0.2
0.25
0.3
Deflection (inches)

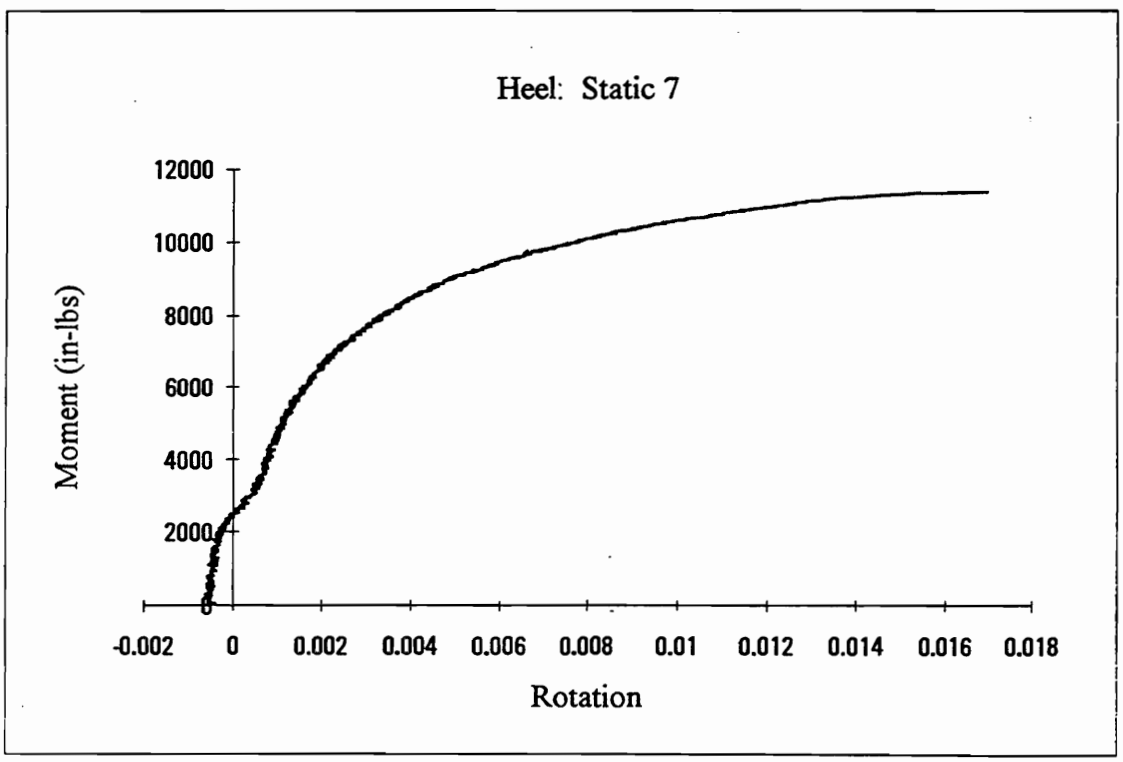
Heel: Static 7
Moment (in-lbs)
12000
10000
8000
6000
4000
2000
0
-0.002
0
0.002
0.004
0.006
0.008
0.01
0.012
0.014
0.016
0.018
Rotation

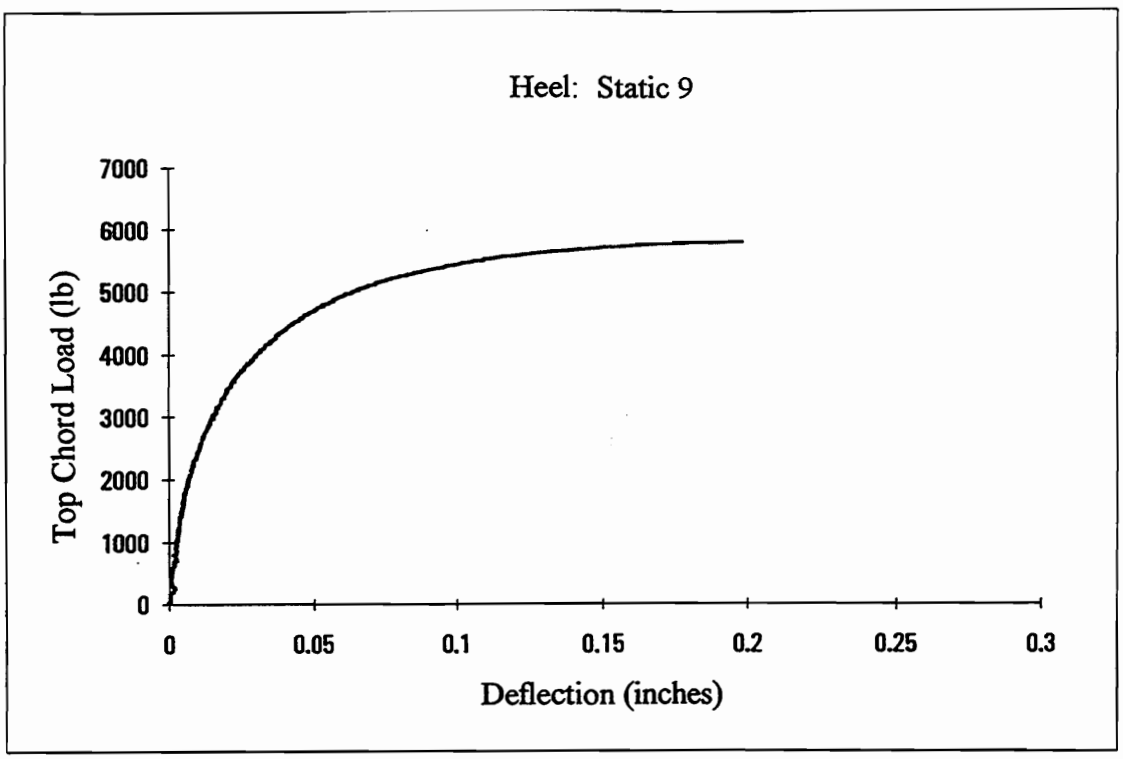
Heel: Static 9
Top Chord Load (lb)
7000
6000
5000
4000
3000
2000
1000
0
0
0.05
0.1
0.15
0.2
0.25
0.3
Deflection (inches)

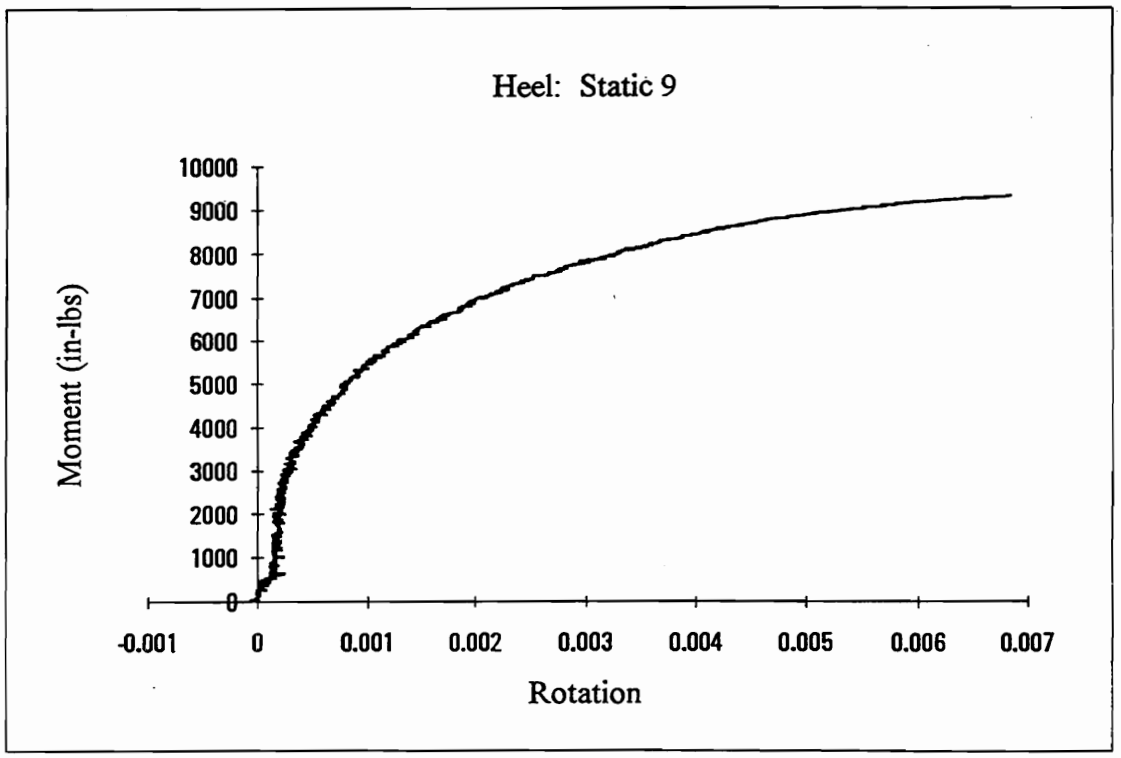
Heel: Static 9
Moment (in-lbs)
10000
9000
8000
7000
6000
5000
4000
3000
2000
1000
0
-0.001
0
0.001
0.002
0.003
0.004
0.005
0.006
0.007
Rotation

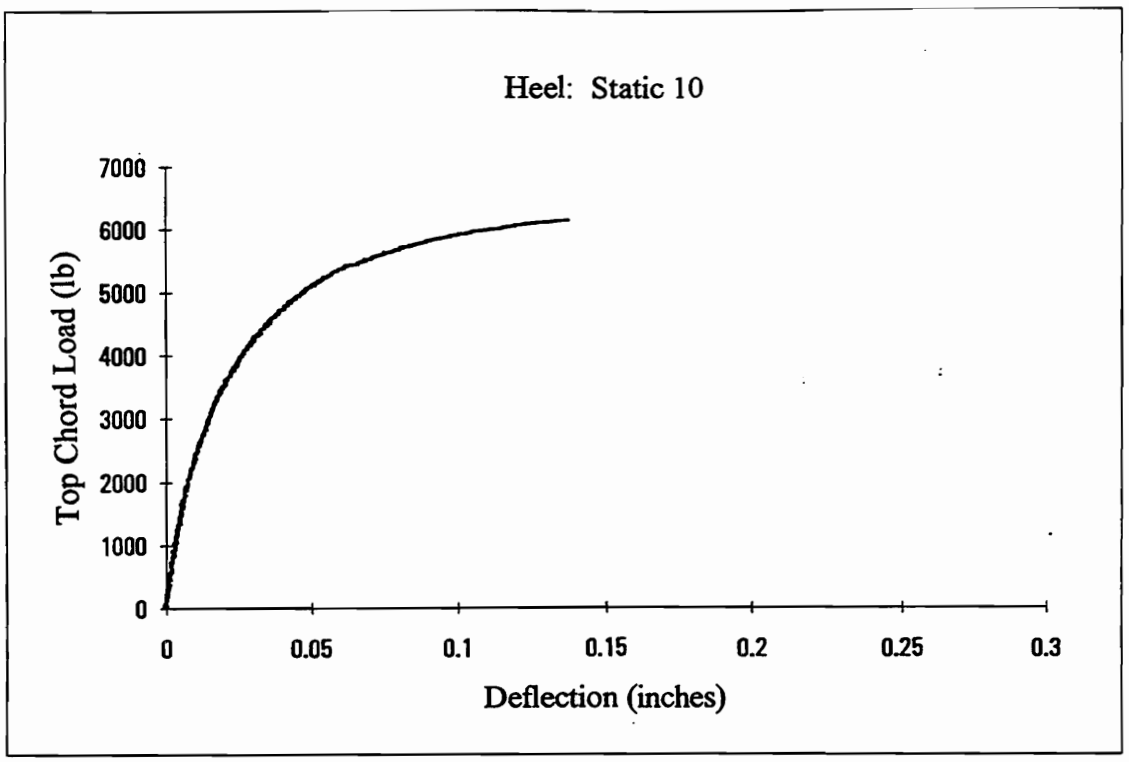
Heel: Static 10
Top Chord Load (lb)
7000
6000
5000
4000
3000
2000
1000
0
0
0.05
0.1
0.15
0.2
0.25
0.3
Deflection (inches)

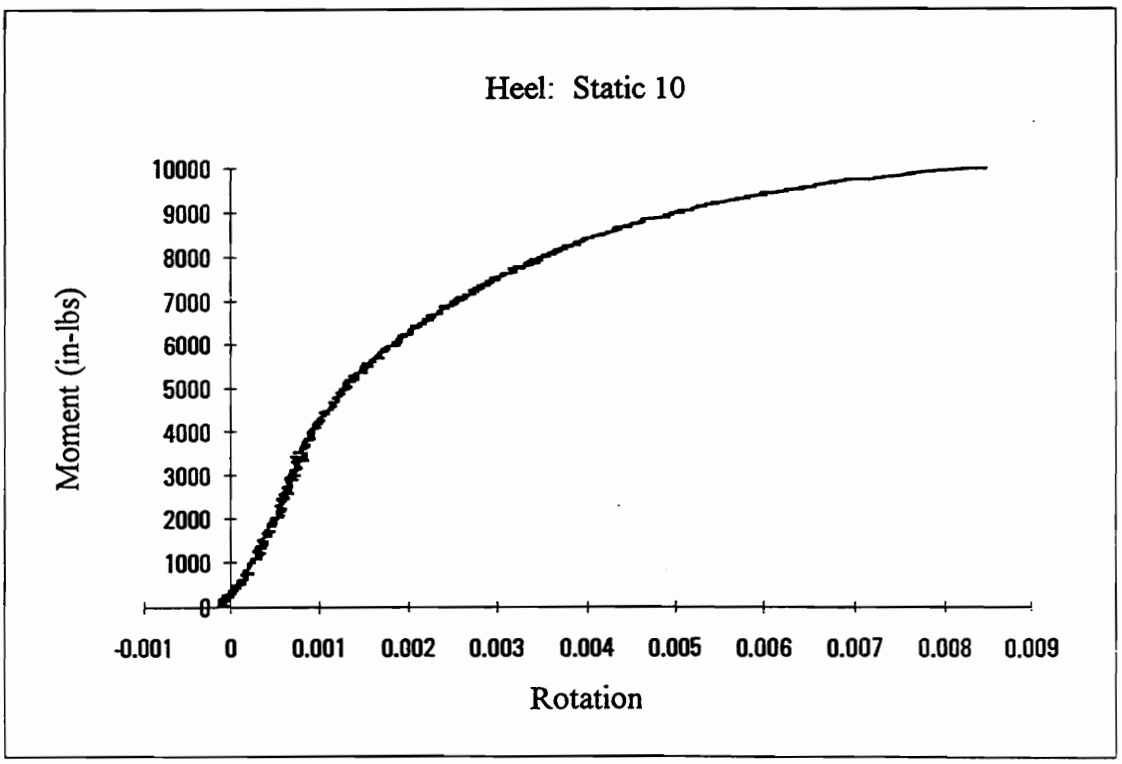
Heel: Static 10
Moment (in-lbs)
10000
9000
8000
7000
6000
5000
4000
3000
2000
1000
0
-0.001
0
0.001
0.002
0.003
0.004
0.005
0.006
0.007
0.008
0.009
Rotation

Appendix L

Axial Deflection-Time Curves for the Artificial Earthquake Simulation on Heel Joints

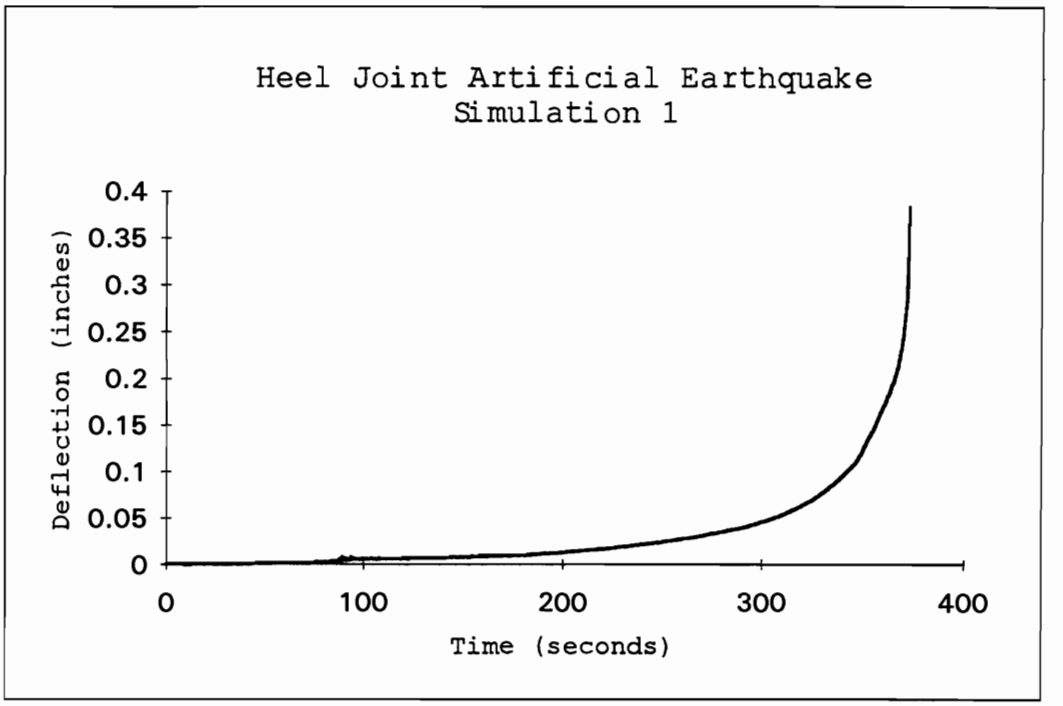
Heel Joint Artificial Earthquake
Simulation 1
Deflection (inches)
0.4
0.35
0.3
0.25
0.2
0.15
0.1
0.05
0
0
100
200
300
400
Time (seconds)

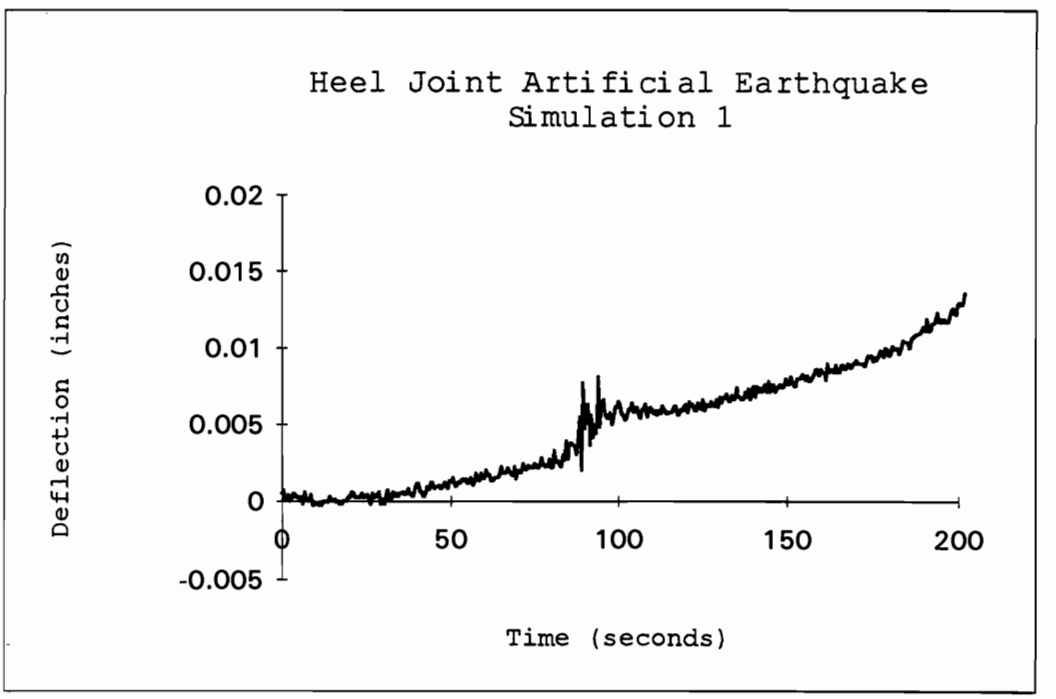
Heel Joint Artificial Earthquake
Simulation 1
Deflection (inches)
0.02
0.015
0.01
0.005
0
-0.005
0
50
100
150
200
Time (seconds)

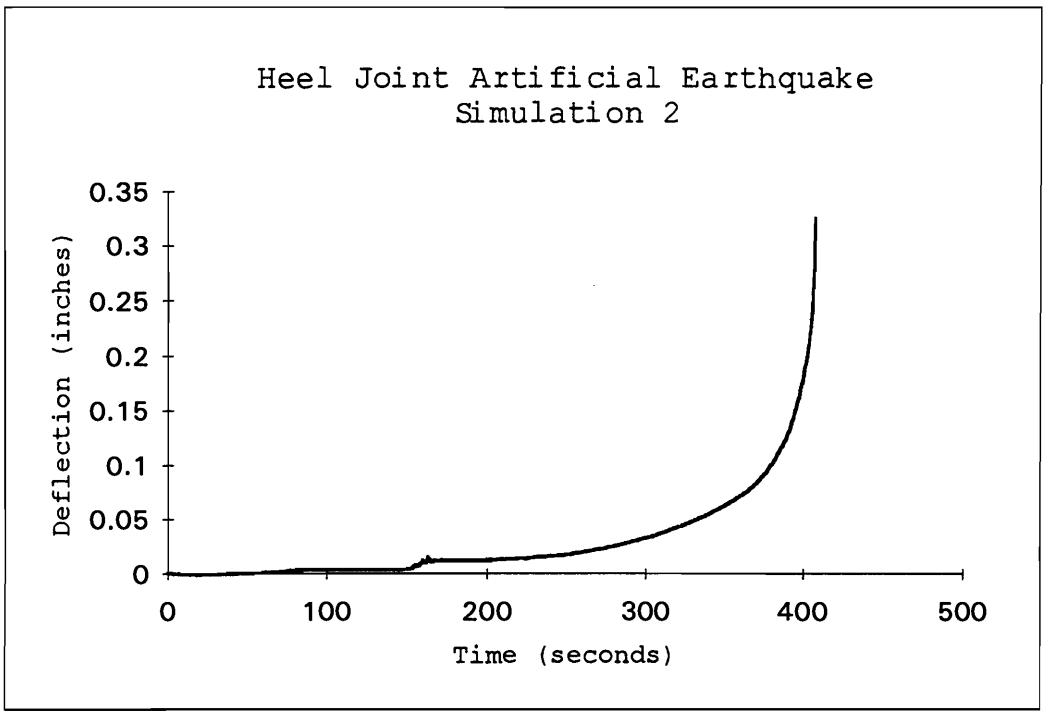
Heel Joint Artificial Earthquake
Simulation 2
Deflection (inches)
0.35
0.3
0.25
0.2
0.15
0.1
0.05
0
0
100
200
300
400
500
Time (seconds)

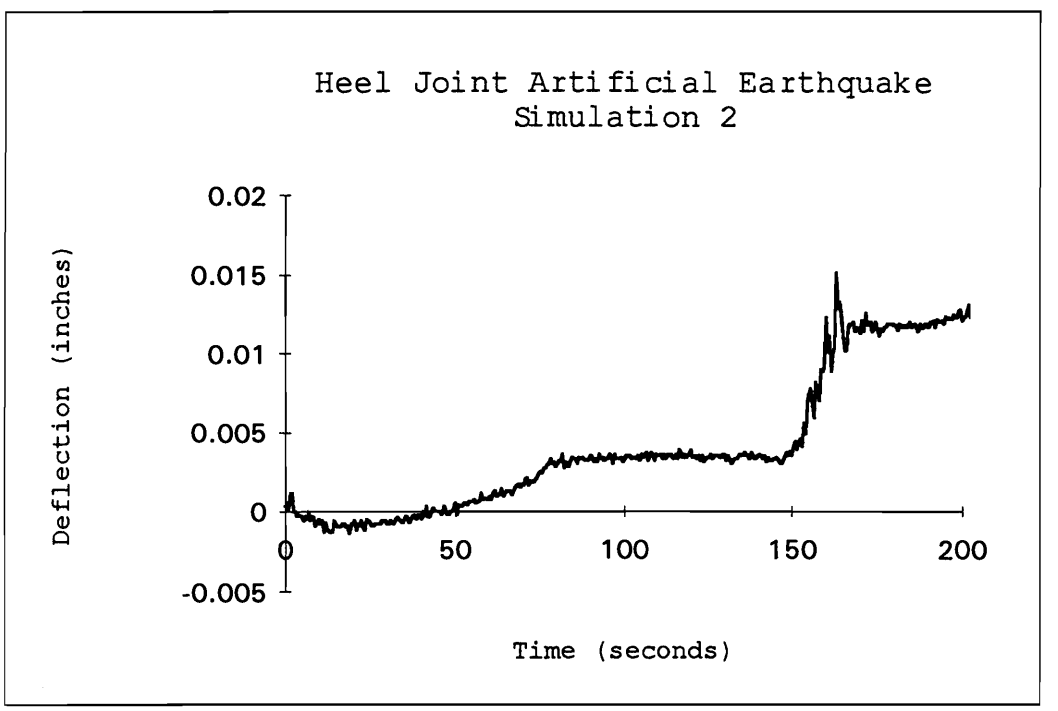
Heel Joint Artificial Earthquake
Simulation 2
Deflection (inches)
0.02
0.015
0.01
0.005
0
-0.005
0
50
100
150
200
Time (seconds)

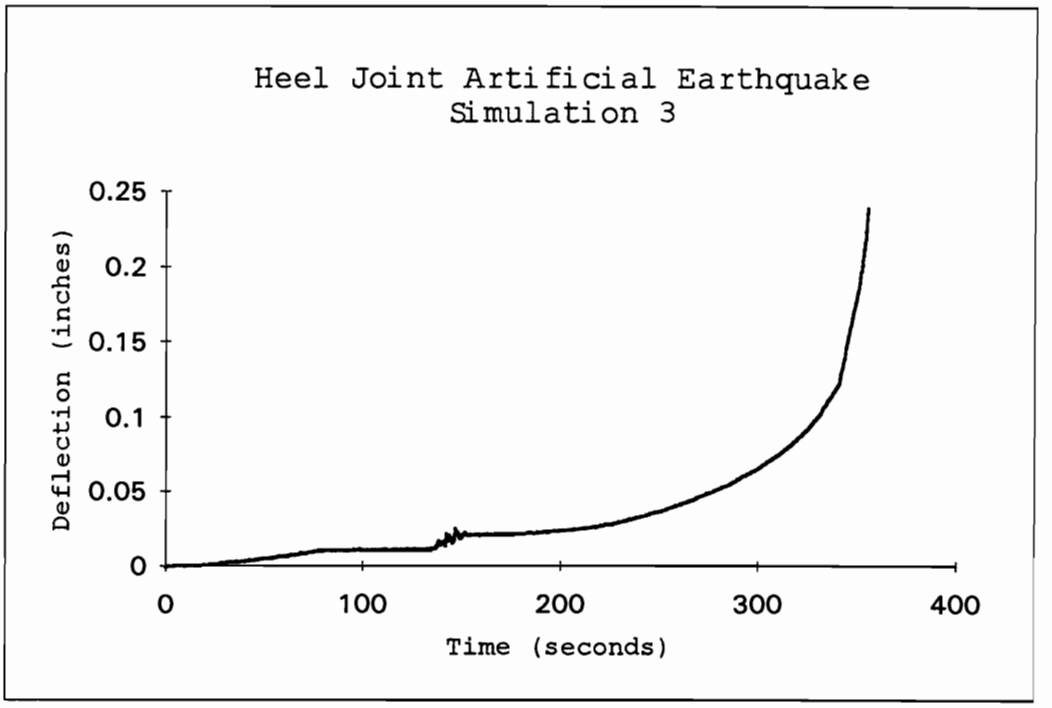
Heel Joint Artificial Earthquake
Simulation 3
Deflection (inches)
0.25
0.2
0.15
0.1
0.05
0
0
100
200
300
400
Time (seconds)

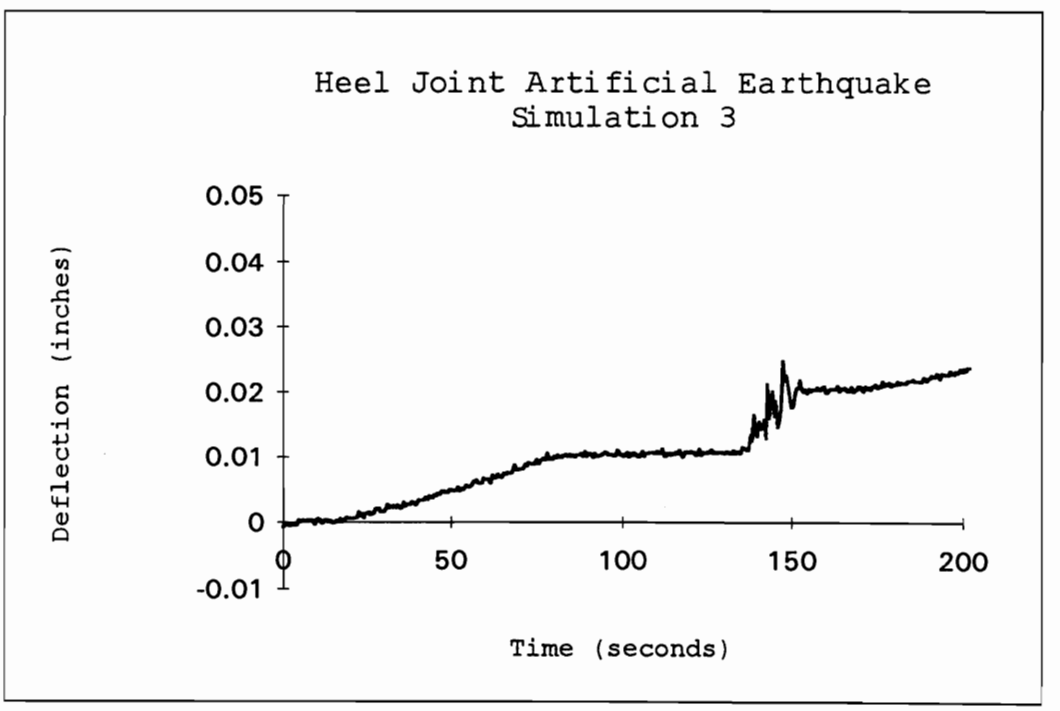
Heel Joint Artificial Earthquake
Simulation 3
Deflection (inches)
0.05
0.04
0.03
0.02
0.01
0
-0.01
0
50
100
150
200
Time (seconds)

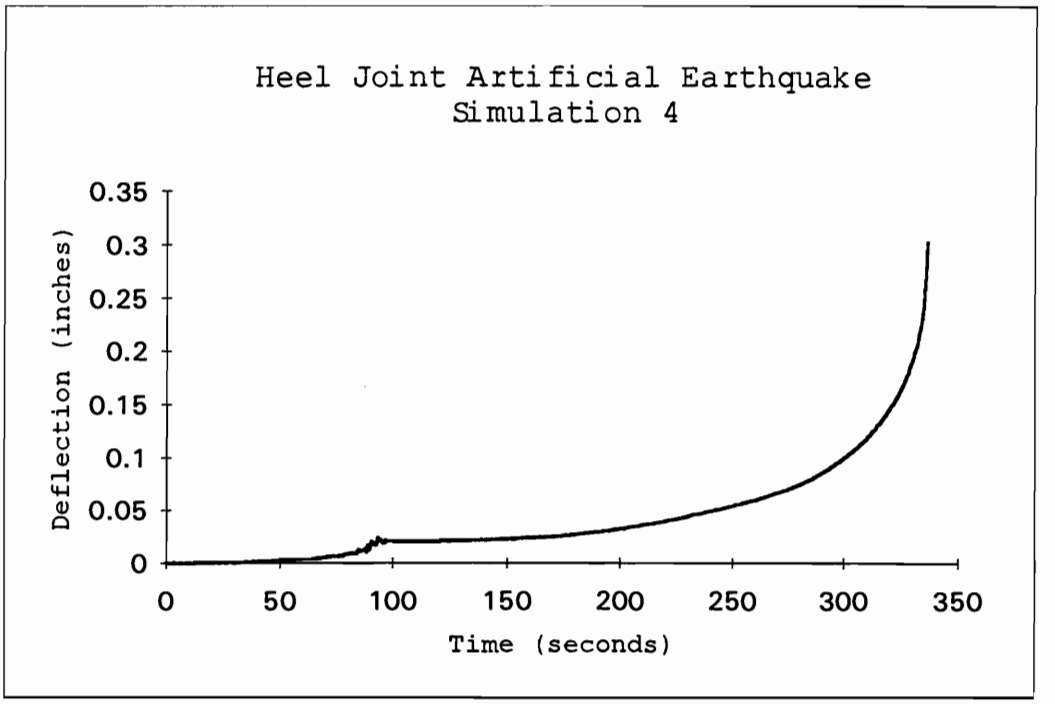
Heel Joint Artificial Earthquake
Simulation 4
Deflection (inches)
0.35
0.3
0.25
0.2
0.15
0.1
0.05
0
0
50
100
150
200
250
300
350
Time (seconds)

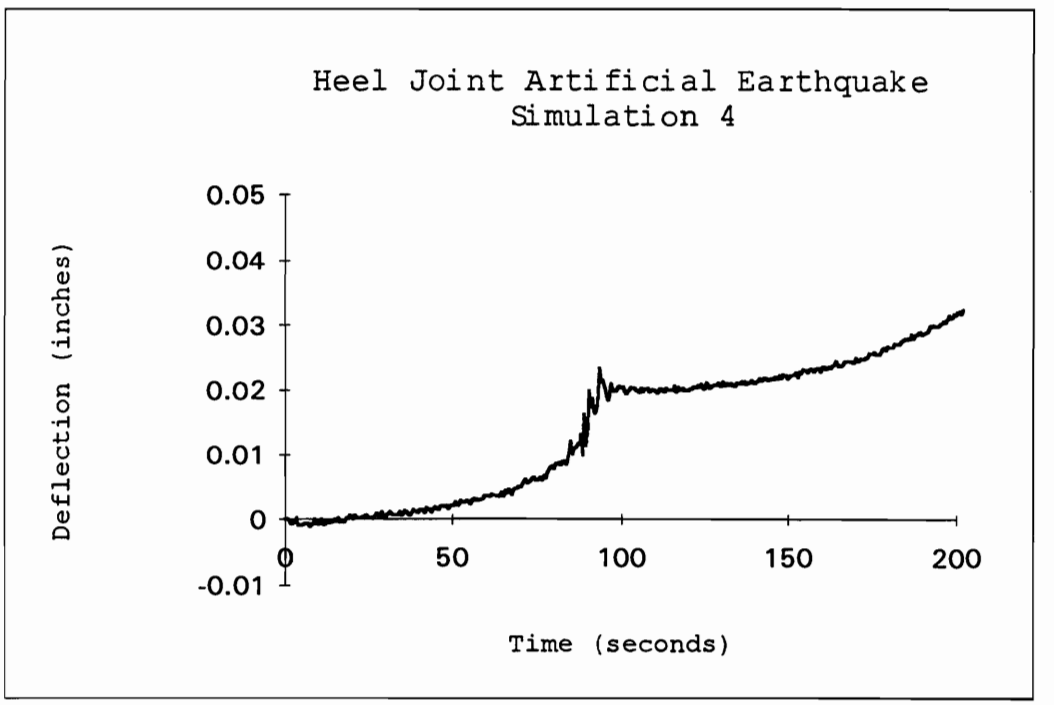
Heel Joint Artificial Earthquake
Simulation 4
Deflection (inches)
0.05
0.04
0.03
0.02
0.01
0
-0.01
0
50
100
150
200
Time (seconds)

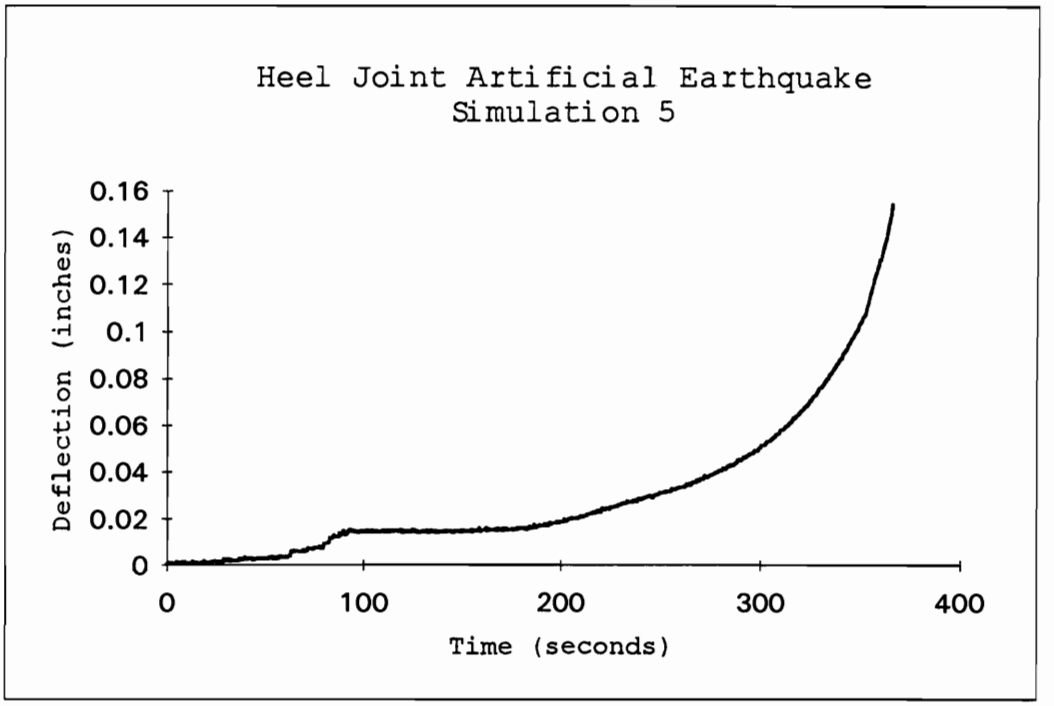
Heel Joint Artificial Earthquake
Simulation 5
Deflection (inches)
0.16
0.14
0.12
0.1
0.08
0.06
0.04
0.02
0
0
100
200
300
400
Time (seconds)

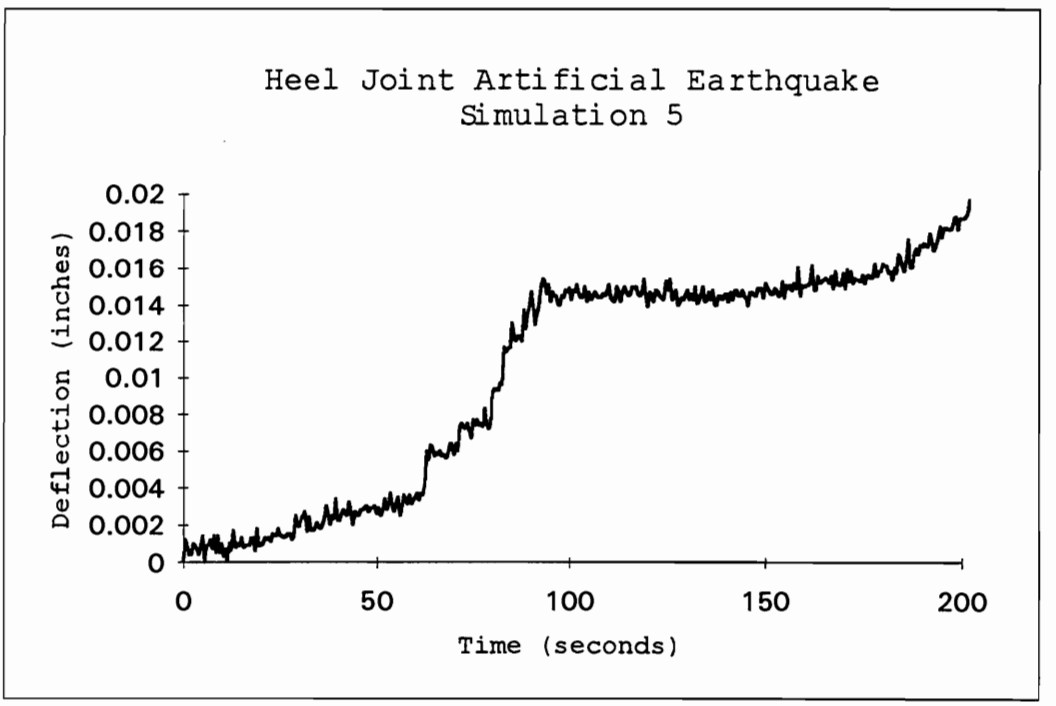
Heel Joint Artificial Earthquake
Simulation 5
Deflection (inches)
0.02
0.018
0.016
0.014
0.012
0.01
0.008
0.006
0.004
0.002
0
0
50
100
150
200
Time (seconds)

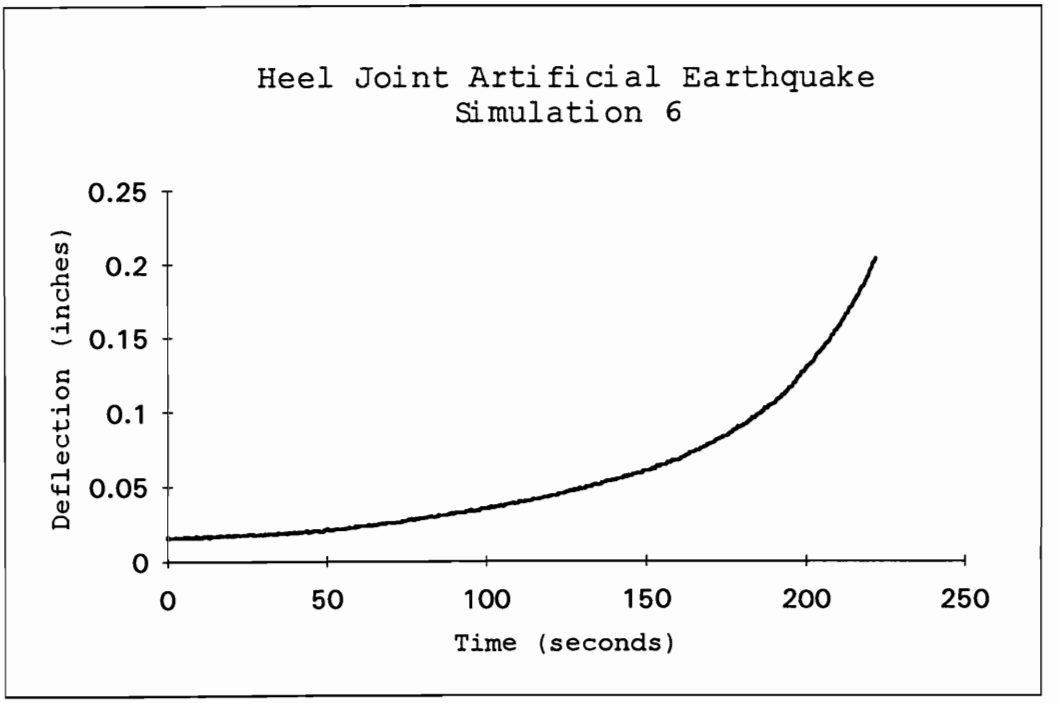
Heel Joint Artificial Earthquake
Simulation 6
Deflection (inches)
0.25
0.2
0.15
0.1
0.05
0
0
50
100
150
200
250
Time (seconds)

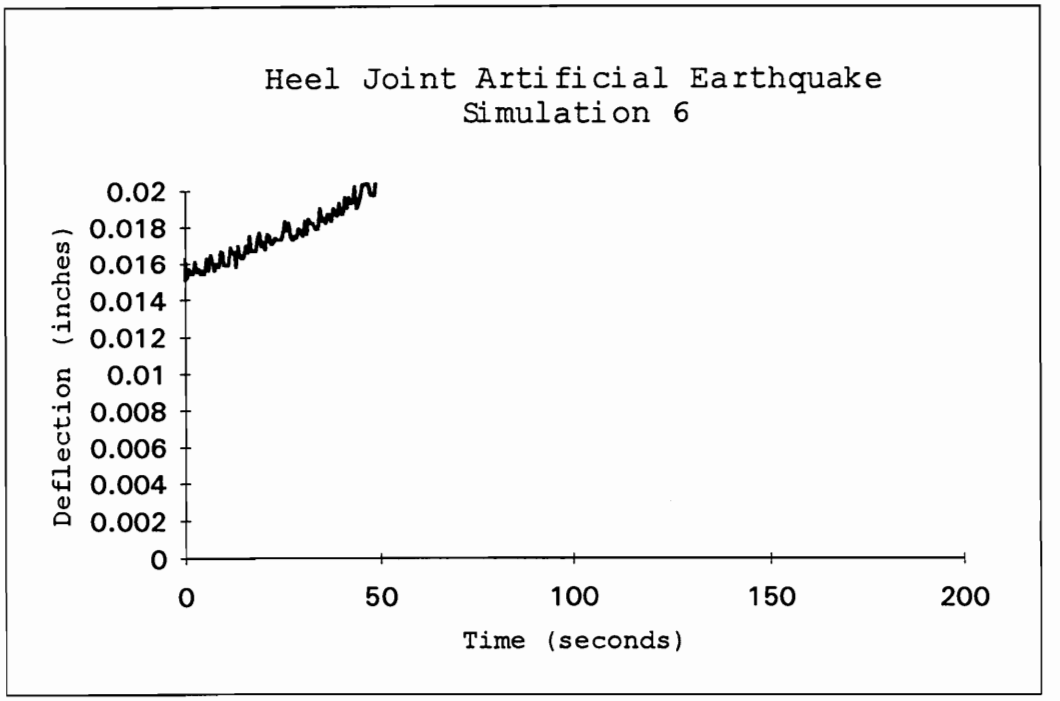
Heel Joint Artificial Earthquake
Simulation 6
Deflection (inches)
0.02
0.018
0.016
0.014
0.012
0.01
0.008
0.006
0.004
0.002
0
0
50
100
150
200
Time (seconds)

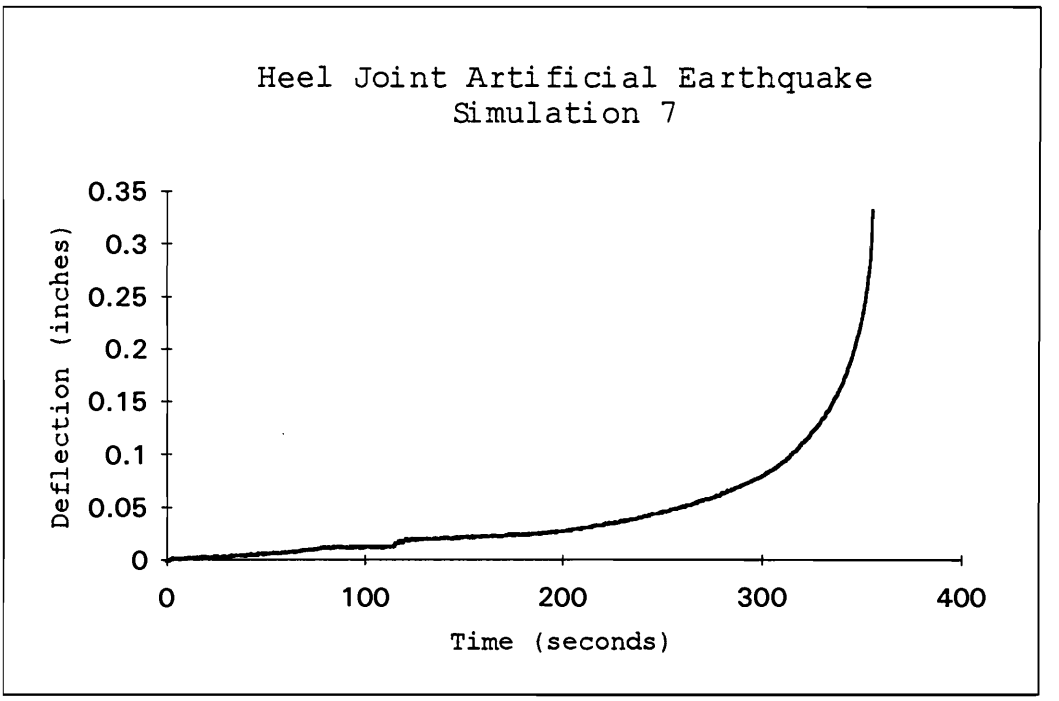
Heel Joint Artificial Earthquake
Simulation 7
Deflection (inches)
0.35
0.3
0.25
0.2
0.15
0.1
0.05
0
0
100
200
300
400
Time (seconds)

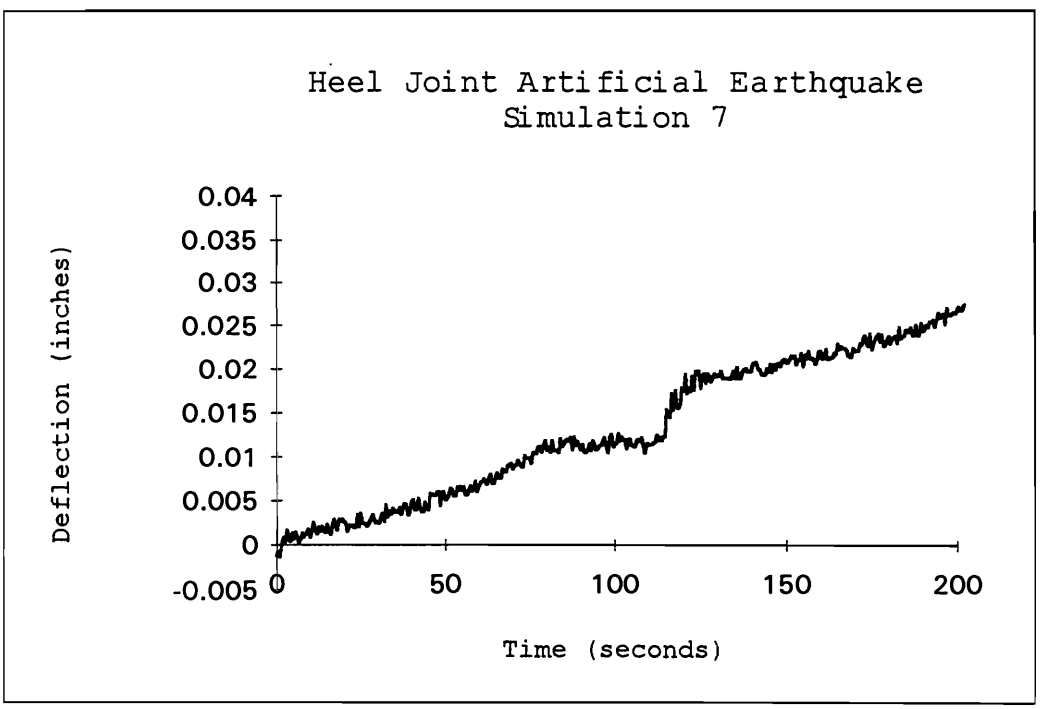
Heel Joint Artificial Earthquake
Simulation 7
Deflection (inches)
0.04
0.035
0.03
0.025
0.02
0.015
0.01
0.005
0
-0.005
0
50
100
150
200
Time (seconds)

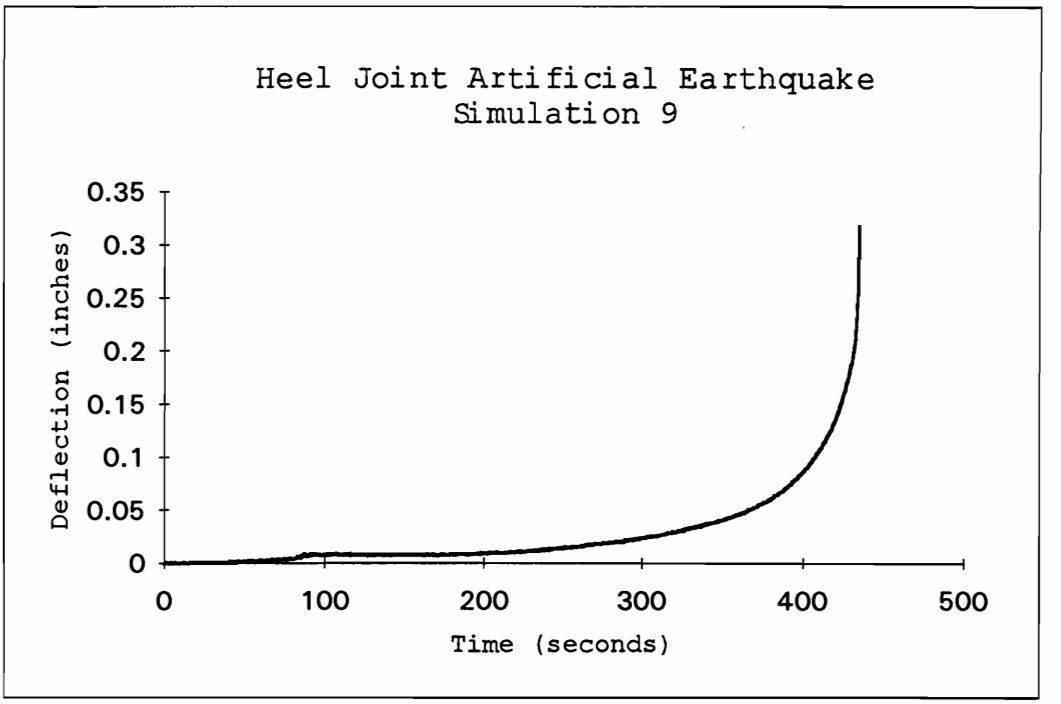
Heel Joint Artificial Earthquake
Simulation 9
Deflection (inches)
0.35
0.3
0.25
0.2
0.15
0.1
0.05
0
0
100
200
300
400
500
Time (seconds)

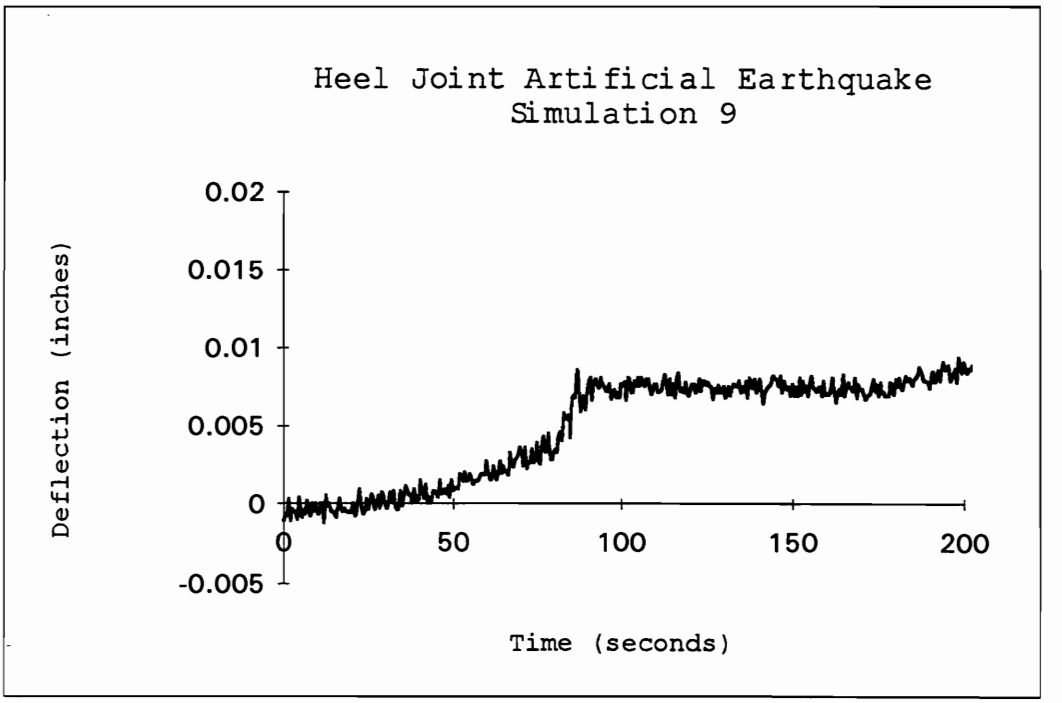
Heel Joint Artificial Earthquake
Simulation 9
Deflection (inches)
0.02
0.015
0.01
0.005
0
-0.005
0
50
100
150
200
Time (seconds)

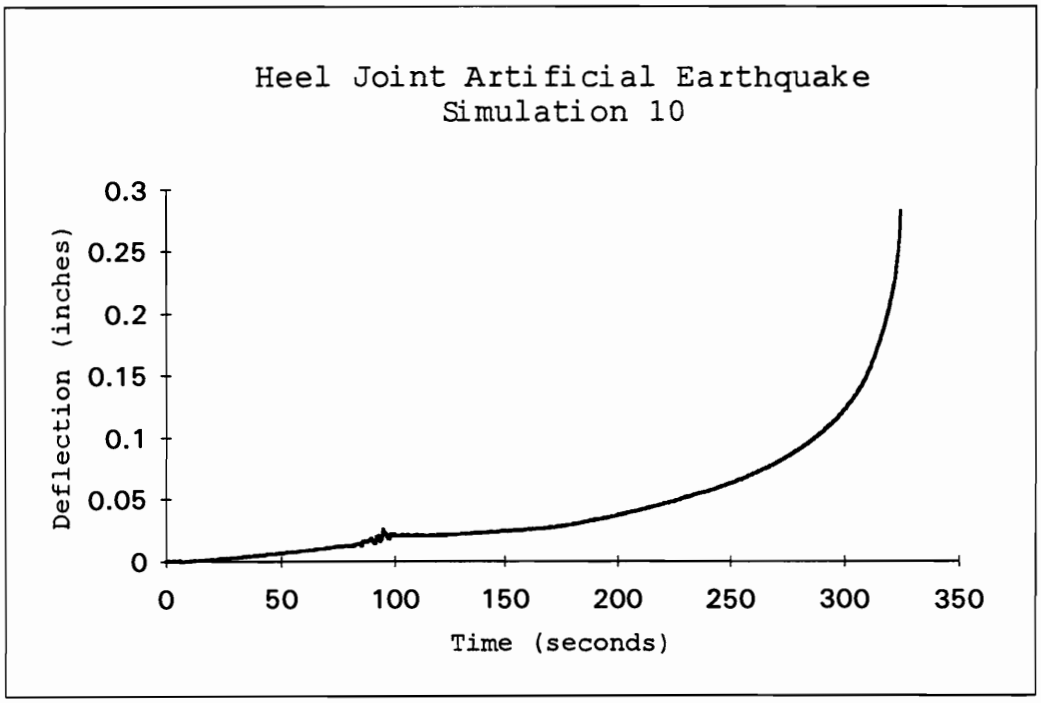
Heel Joint Artificial Earthquake
Simulation 10
Deflection (inches)
0.3
0.25
0.2
0.15
0.1
0.05
0
0
50
100
150
200
250
300
350
Time (seconds)

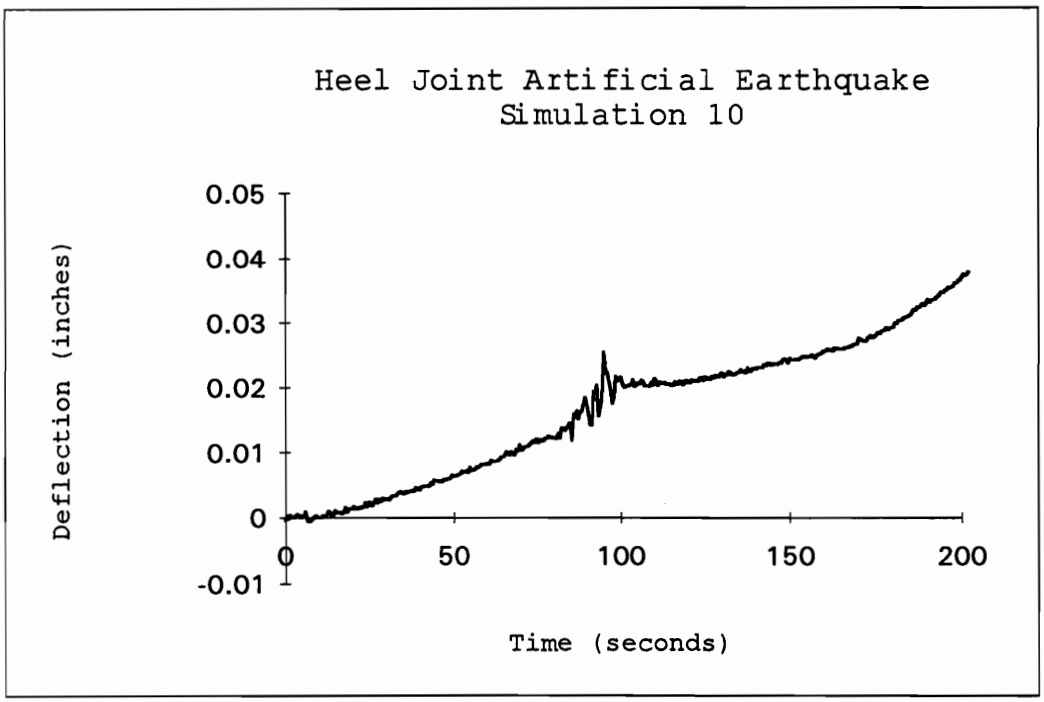
Heel Joint Artificial Earthquake
Simulation 10
Deflection (inches)
0.05
0.04
0.03
0.02
0.01
0
-0.01
0
50
100
150
200
Time (seconds)

Appendix M

Example Calculations to Determine the Dynamic Properties from the SPD Loading for Heel Joints

This appendix presents the sample calculations to determine the half-cycle cyclic stiffness, half-cycle energy dissipation, and the half-cycle damping ratio of the heel joint during the sequential phased displacement loading (Dolan 1994). A digitizer (Calcomp Digitizer Products Division, Model No. 33120) was used to determine the area confined by the hysteresis curve. A scale factor of 1.30 lb-in. of energy per Calcomp Units is used.

Given:

- Digitized area confined by the triangle CABC is 21.8 Calcomp Units which corresponds to the Energy Input

  (21.8 Calcomp Units)(1.30) = 28.3 lb-in. (Energy Input)

- Digitized area confined by the hysteresis trace is 4.2 Calcomp Units which corresponds to the Energy Dissipation

  (4.2 Calcomp Units)(1.30) = 5.46 lb-in. (Energy Dissipation)

- Maximum compressive load in the top chord of the heel joint during the sequential phased displacement cycle 85 is 2074 lb

- Maximum axial deflection in the top chord of the heel joint during the sequential phased displacement cycle 85 is 0.0273 in.

Calculations:

1) Cyclic Stiffness = $\frac{2074 \text{ lb}}{0.0273 \text{ in.}} = 0.760 \times 10^5$ lb/in.

2) Energy Input = 0.5(2074 lb)(0.0273 in.) = 28.3 lb-in.

3) Damping Ratio = $\frac{\text{Energy Dissipation}}{2\pi(\text{Energy Input})} = \frac{5.46 \text{ lb-in}}{2\pi(28.3 \text{ lb/in.})} = 0.0307$

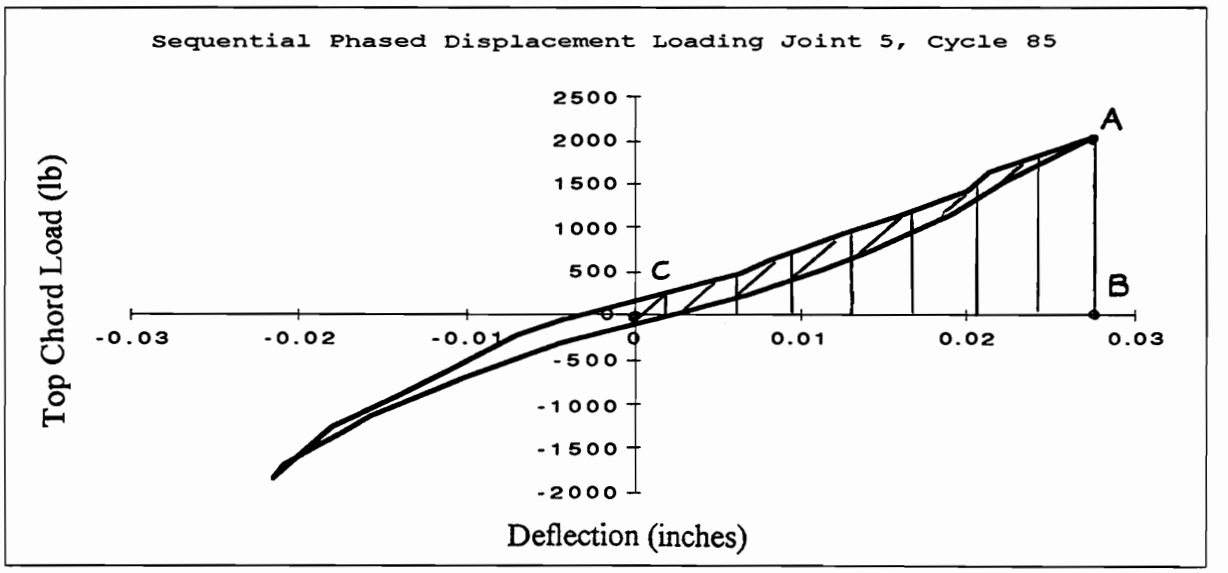

Appendix N

Load and Deflection vs. Time Curves for the Sequential Phased Displacement Loading on Heel Joints

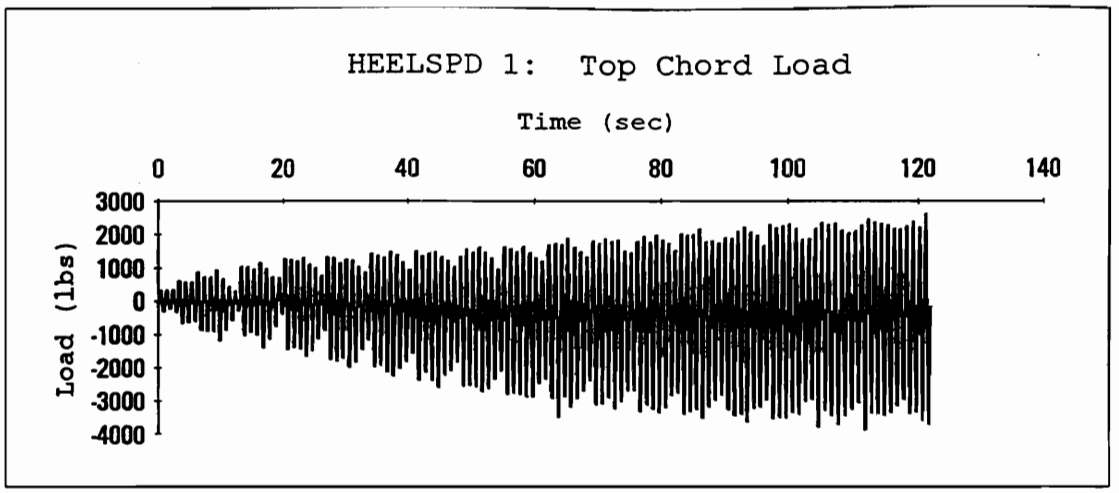
HEELSPD 1: Top Chord Load
Time (sec)
0
20
40
60
80
100
120
140
Load (lbs)
3000
2000
1000
0
-1000
-2000
-3000
-4000

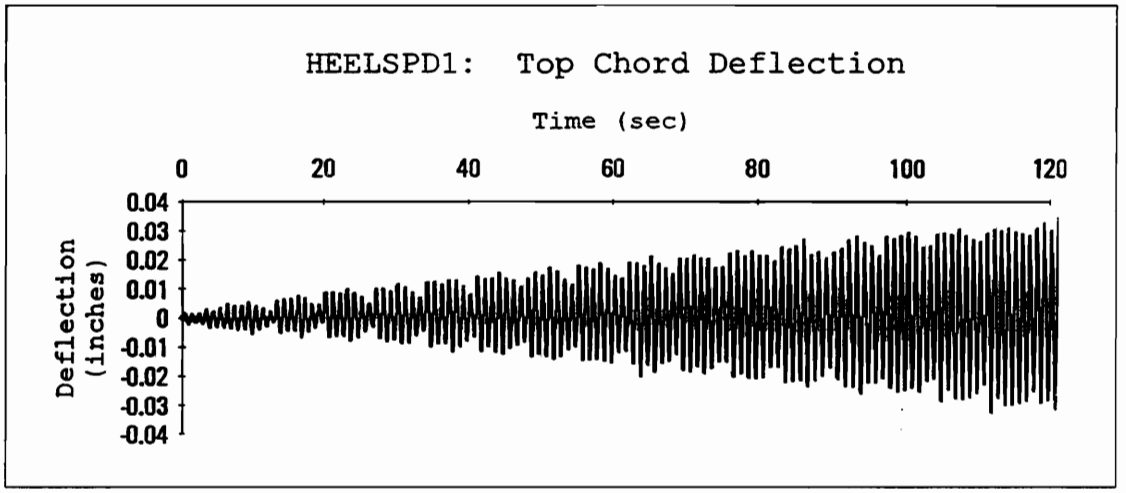
HEELSPD1: Top Chord Deflection
Time (sec)
0
20
40
60
80
100
120
Deflection (inches)
0.04
0.03
0.02
0.01
0
-0.01
-0.02
-0.03
-0.04

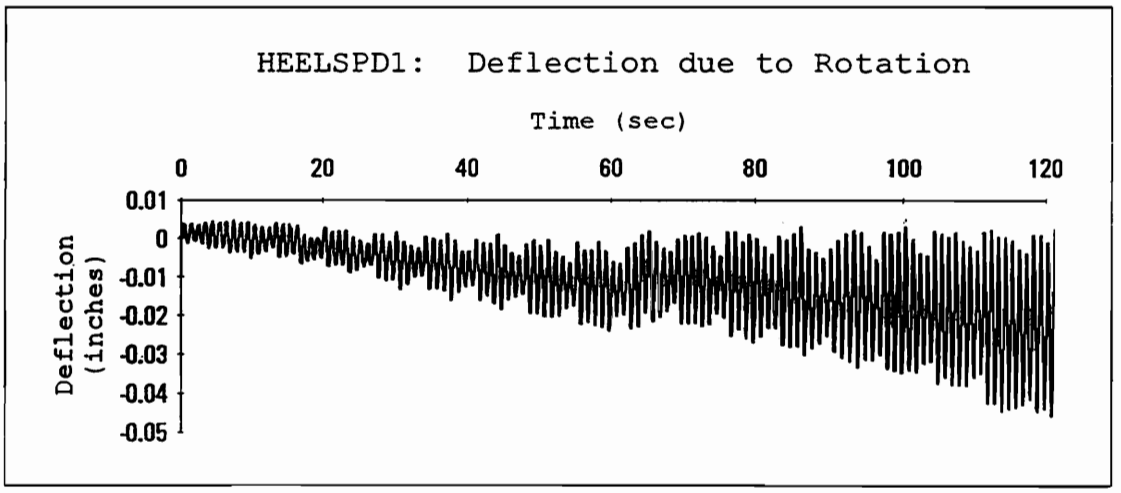
HEELSPD1: Deflection due to Rotation
Time (sec)
0
20
40
60
80
100
120
Deflection (inches)
0.01
0
-0.01
-0.02
-0.03
-0.04
-0.05

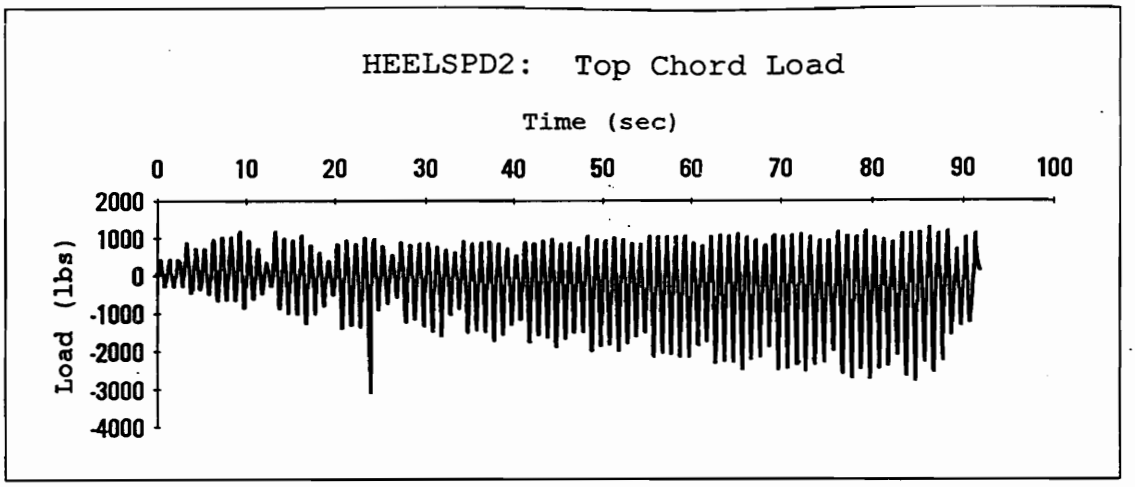
HEELSPD2: Top Chord Load
Time (sec)
0 10 20 30 40 50 60 70 80 90 100
Load (lbs)
2000
1000
0
-1000
-2000
-3000
-4000

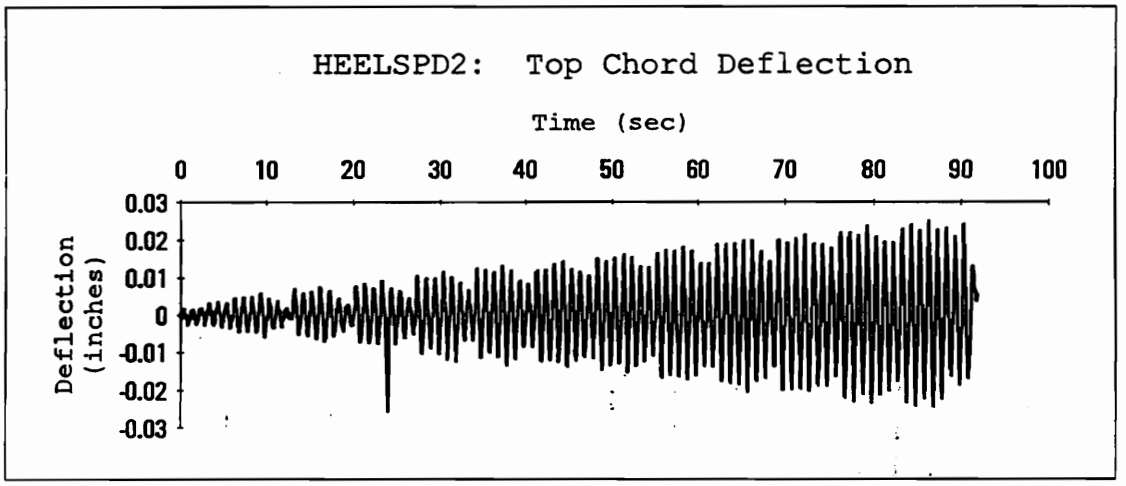
HEELSPD2: Top Chord Deflection
Time (sec)
0 10 20 30 40 50 60 70 80 90 100
Deflection (inches)
0.03
0.02
0.01
0
-0.01
-0.02
-0.03

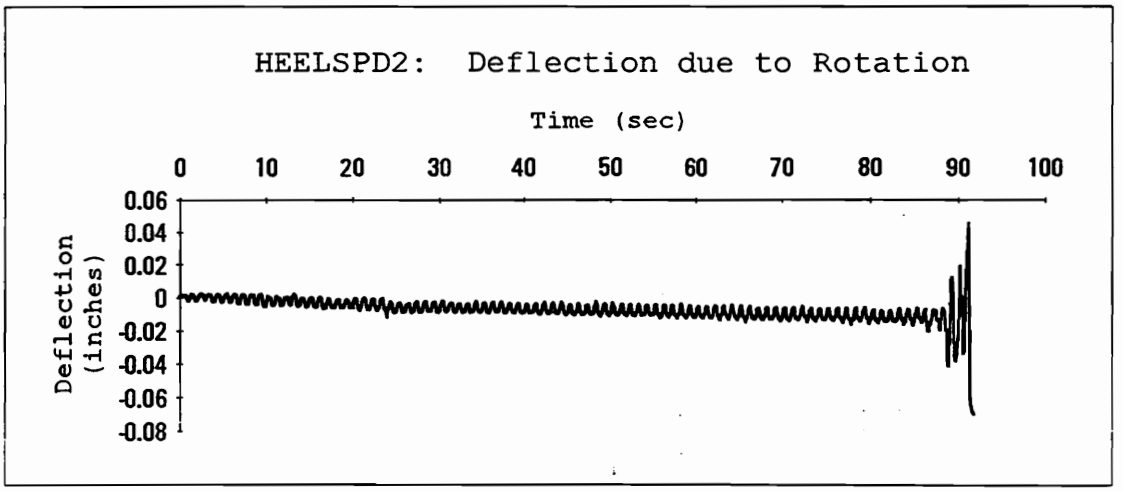
HEELSPD2: Deflection due to Rotation
Time (sec)
0 10 20 30 40 50 60 70 80 90 100
Deflection (inches)
0.06
0.04
0.02
0
-0.02
-0.04
-0.06
-0.08

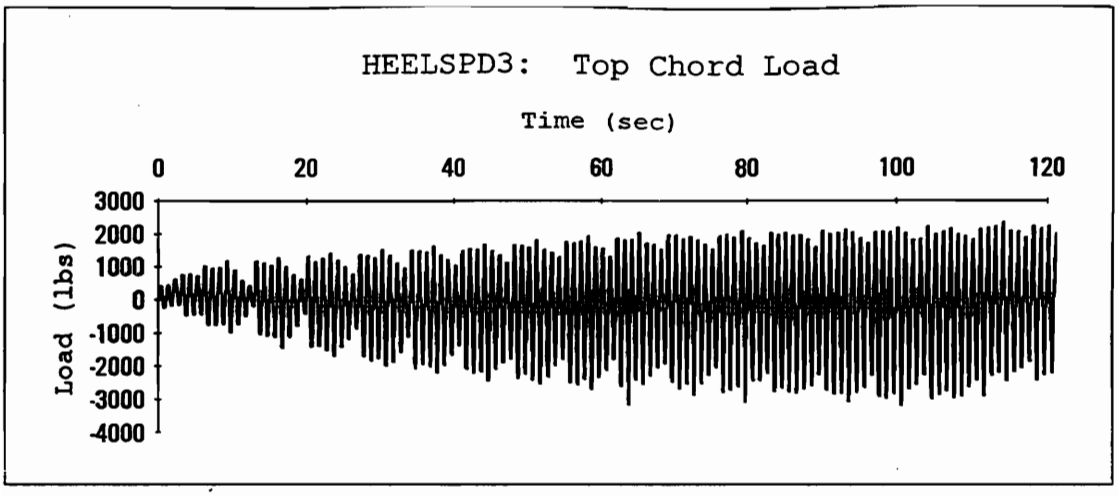
HEELSPD3: Top Chord Load
Time (sec)
0
20
40
60
80
100
120
Load (lbs)
3000
2000
1000
0
-1000
-2000
-3000
-4000

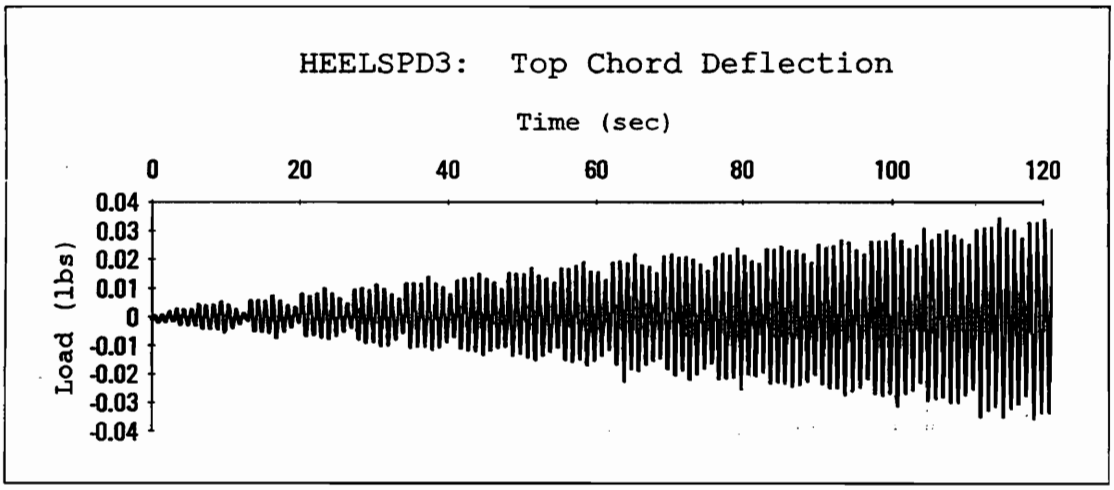
HEELSPD3: Top Chord Deflection
Time (sec)
0
20
40
60
80
100
120
Load (lbs)
0.04
0.03
0.02
0.01
0
-0.01
-0.02
-0.03
-0.04

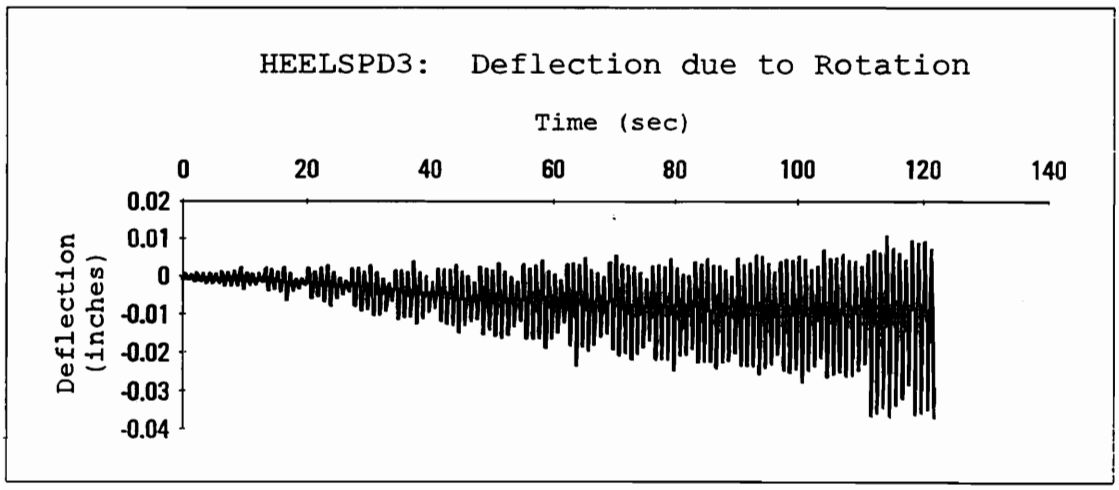
HEELSPD3: Deflection due to Rotation
Time (sec)
0
20
40
60
80
100
120
140
Deflection (inches)
0.02
0.01
0
-0.01
-0.02
-0.03
-0.04

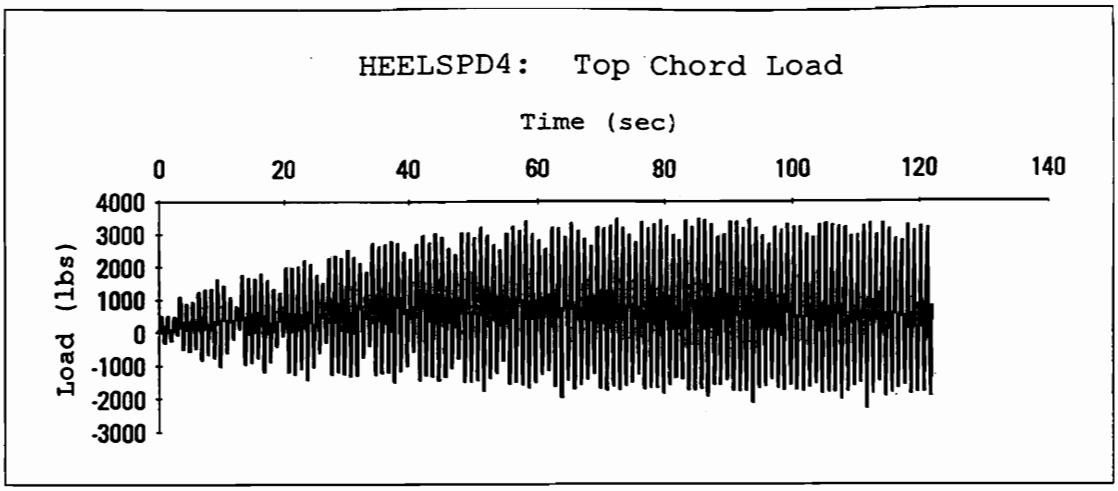
HEELSPD4: Top Chord Load
Time (sec)
0
20
40
60
80
100
120
140
Load (lbs)
4000
3000
2000
1000
0
-1000
-2000
-3000

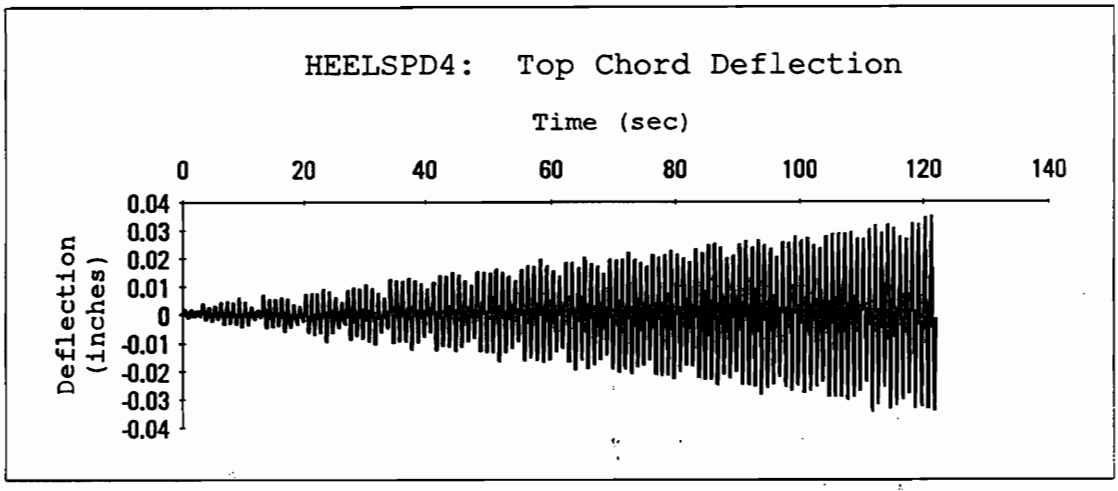
HEELSPD4: Top Chord Deflection
Time (sec)
0
20
40
60
80
100
120
140
Deflection (inches)
0.04
0.03
0.02
0.01
0
-0.01
-0.02
-0.03
-0.04

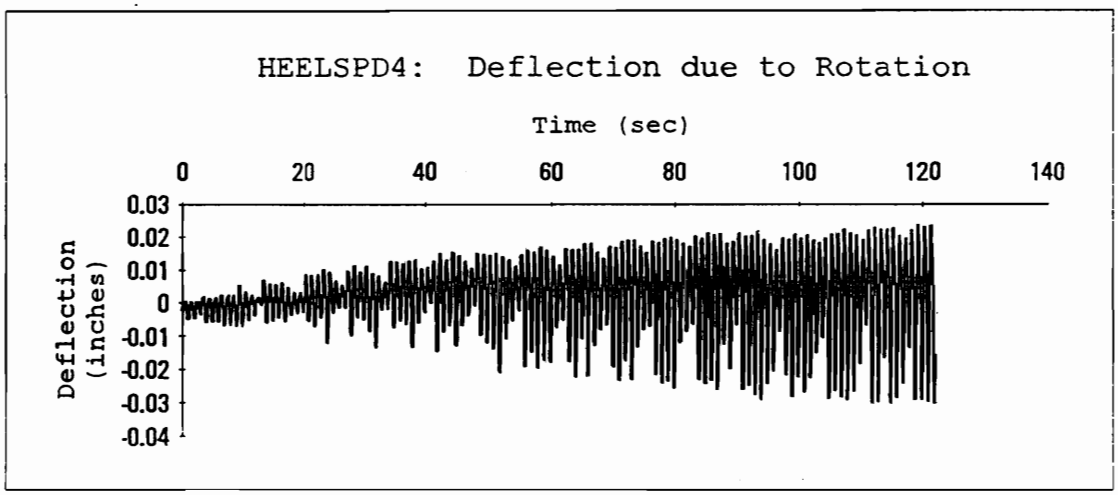
HEELSPD4: Deflection due to Rotation
Time (sec)
0
20
40
60
80
100
120
140
Deflection (inches)
0.03
0.02
0.01
0
-0.01
-0.02
-0.03
-0.04

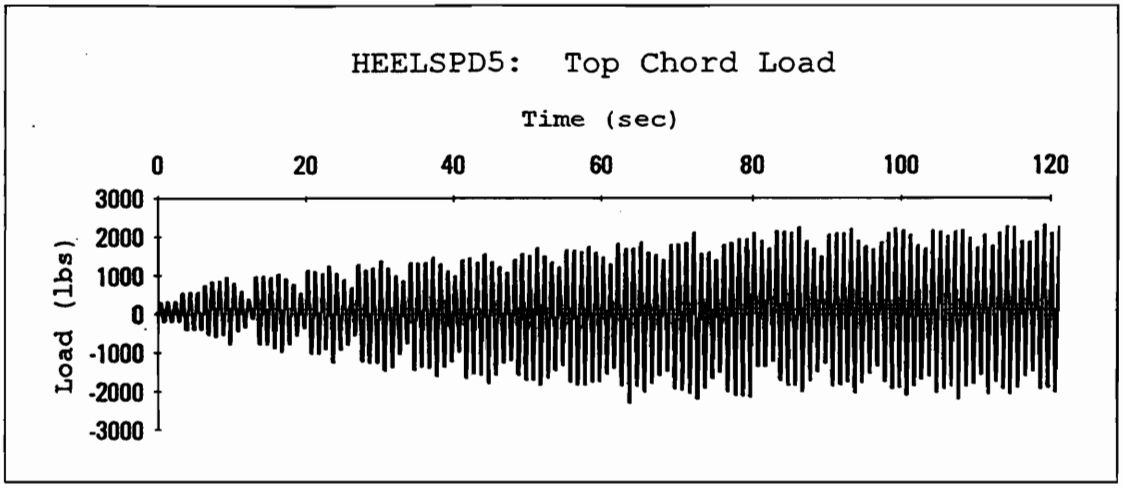
HEELSPD5: Top Chord Load
Time (sec)
0
20
40
60
80
100
120
Load (lbs)
3000
2000
1000
0
-1000
-2000
-3000

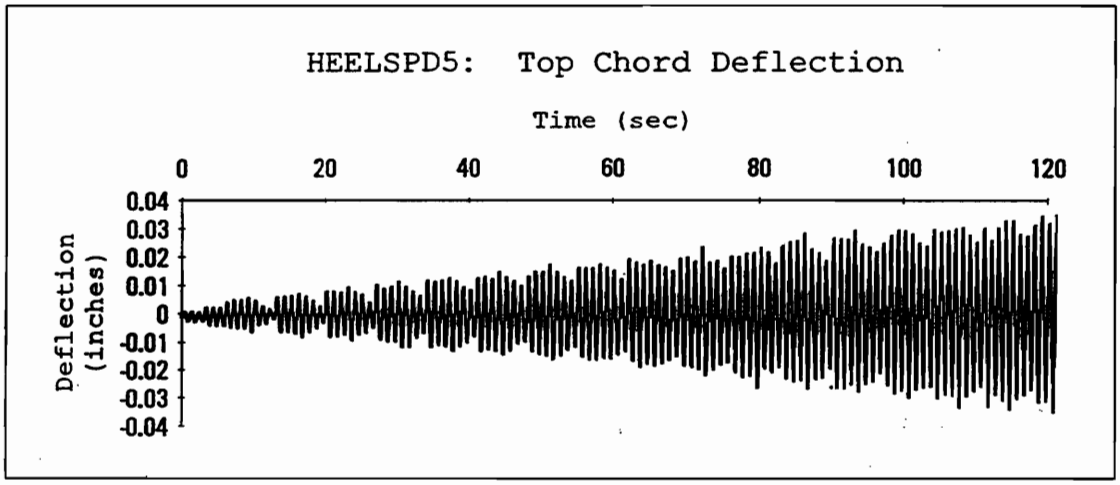
HEELSPD5: Top Chord Deflection
Time (sec)
0
20
40
60
80
100
120
Deflection (inches)
0.04
0.03
0.02
0.01
0
-0.01
-0.02
-0.03
-0.04

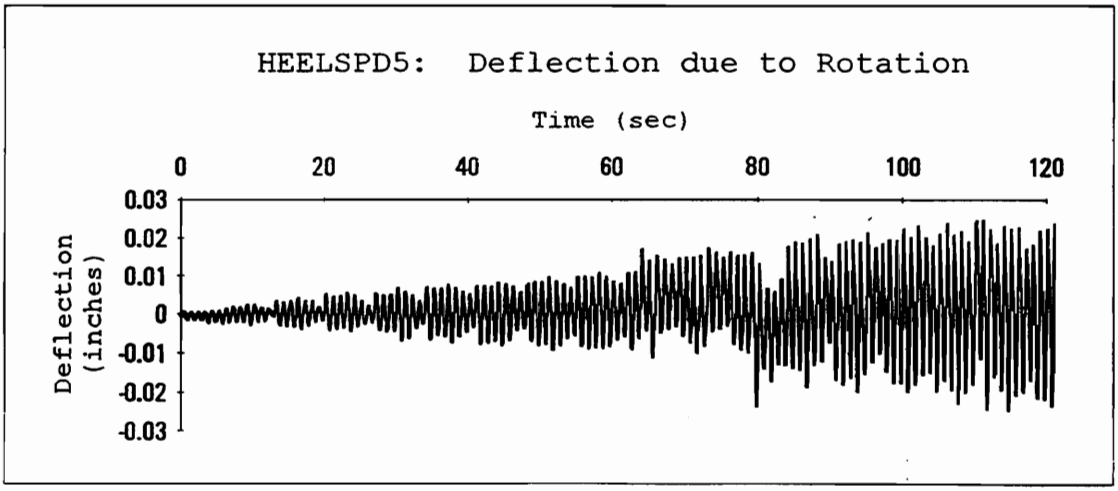
HEELSPD5: Deflection due to Rotation
Time (sec)
0
20
40
60
80
100
120
Deflection (inches)
0.03
0.02
0.01
0
-0.01
-0.02
-0.03

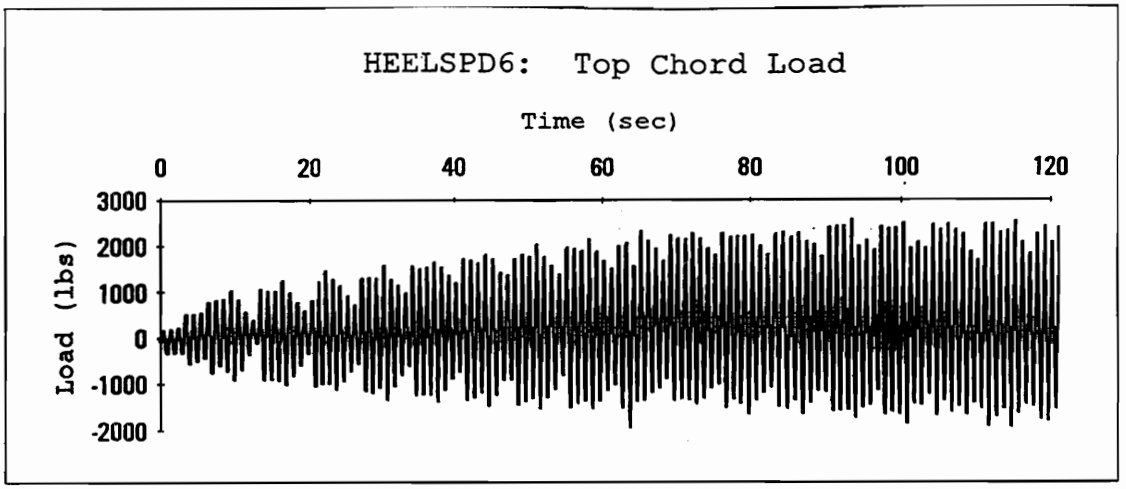
HEELSPD6: Top Chord Load
Time (sec)
0
20
40
60
80
100
120
Load (lbs)
3000
2000
1000
0
-1000
-2000

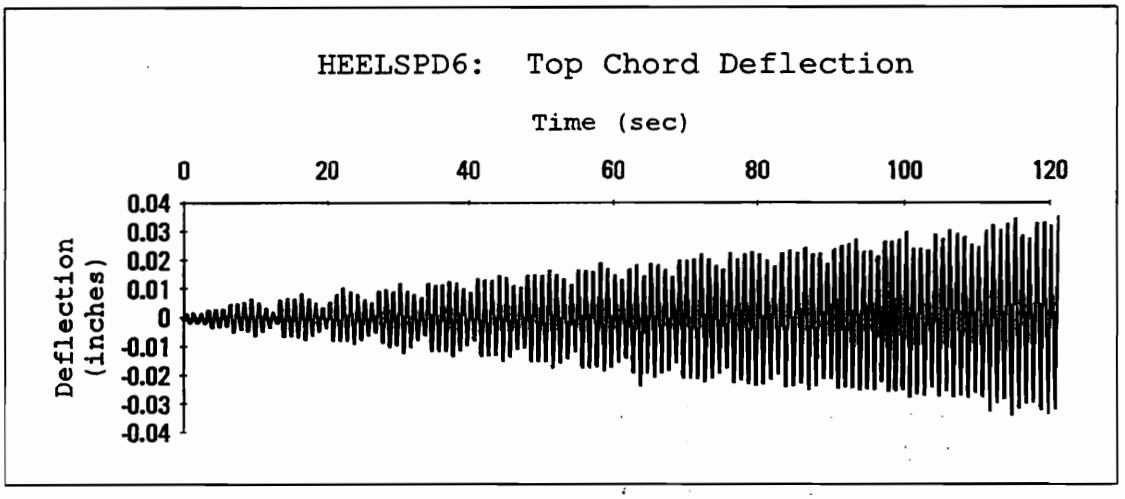
HEELSPD6: Top Chord Deflection
Time (sec)
0
20
40
60
80
100
120
Deflection (inches)
0.04
0.03
0.02
0.01
0
-0.01
-0.02
-0.03
-0.04

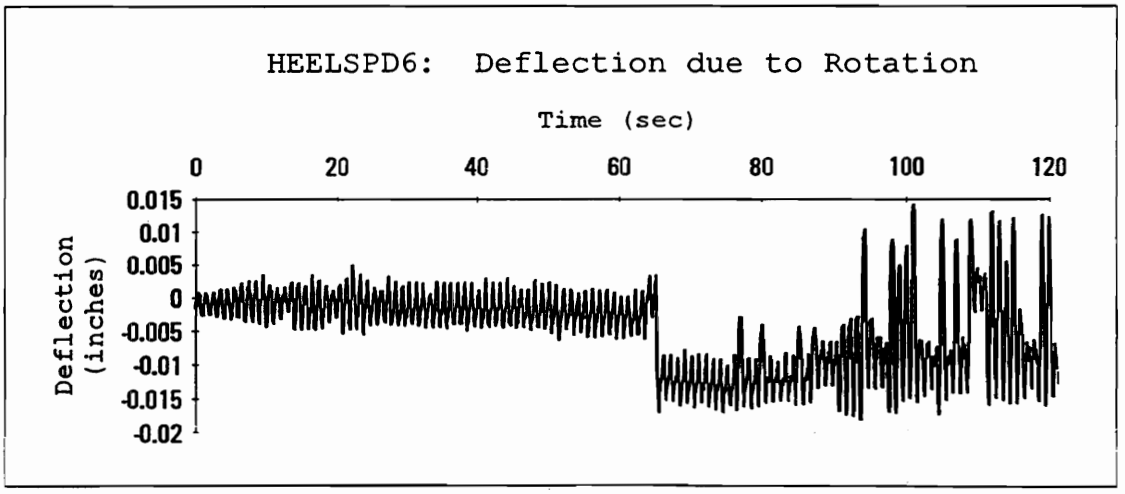
HEELSPD6: Deflection due to Rotation
Time (sec)
0
20
40
60
80
100
120
Deflection (inches)
0.015
0.01
0.005
0
-0.005
-0.01
-0.015
-0.02

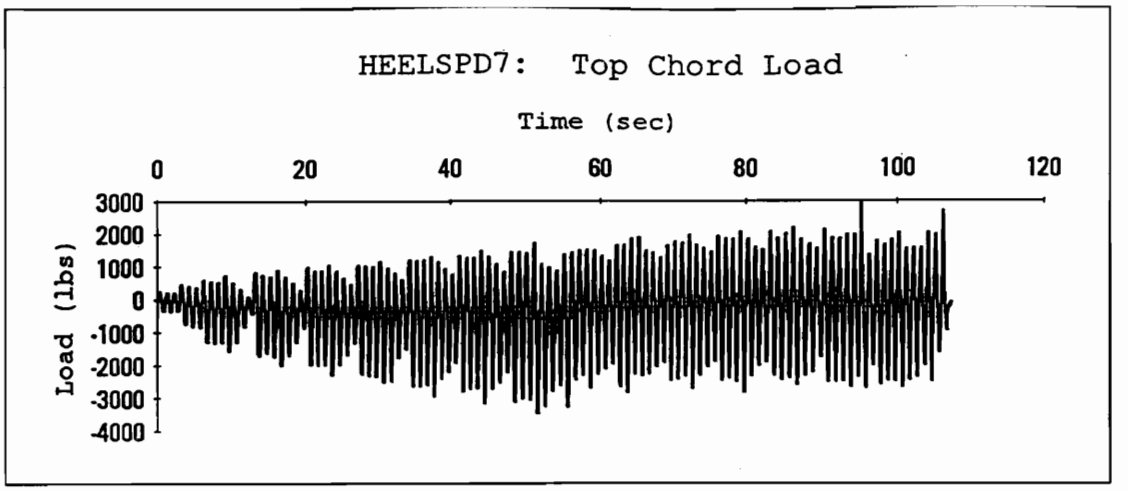
HEELSPD7: Top Chord Load
Time (sec)
0
20
40
60
80
100
120
Load (lbs)
3000
2000
1000
0
-1000
-2000
-3000
-4000

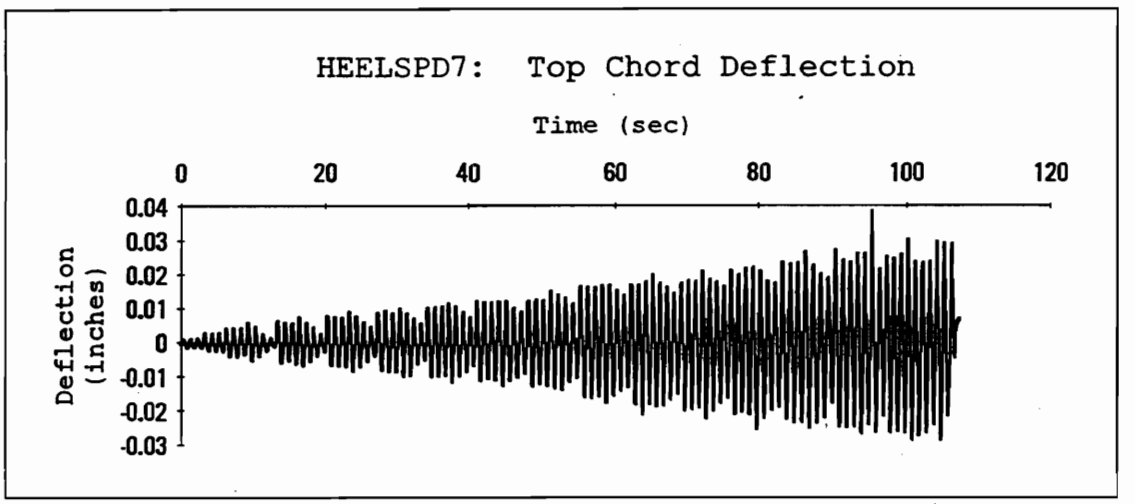
HEELSPD7: Top Chord Deflection
Time (sec)
0
20
40
60
80
100
120
Deflection (inches)
0.04
0.03
0.02
0.01
0
-0.01
-0.02
-0.03

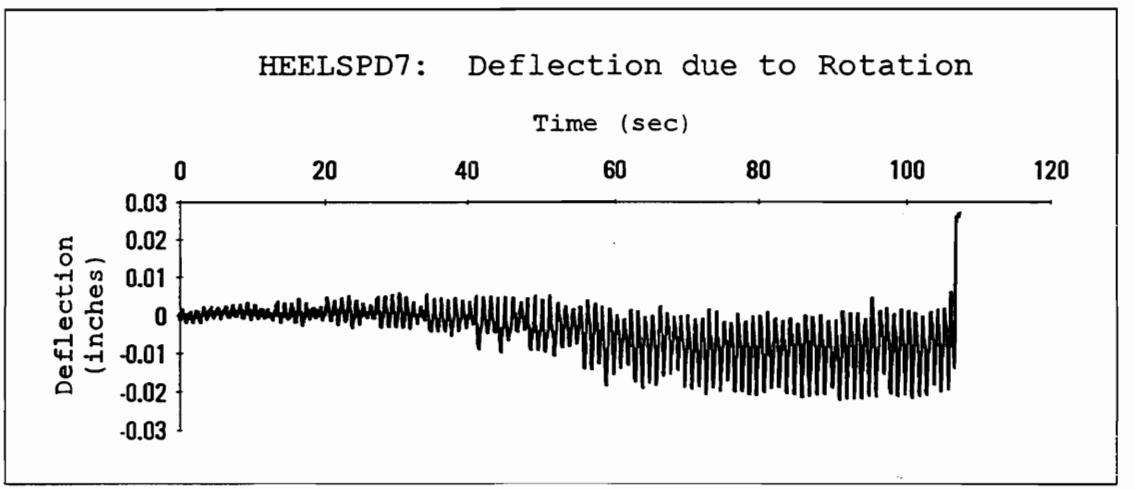
HEELSPD7: Deflection due to Rotation
Time (sec)
0
20
40
60
80
100
120
Deflection (inches)
0.03
0.02
0.01
0
-0.01
-0.02
-0.03

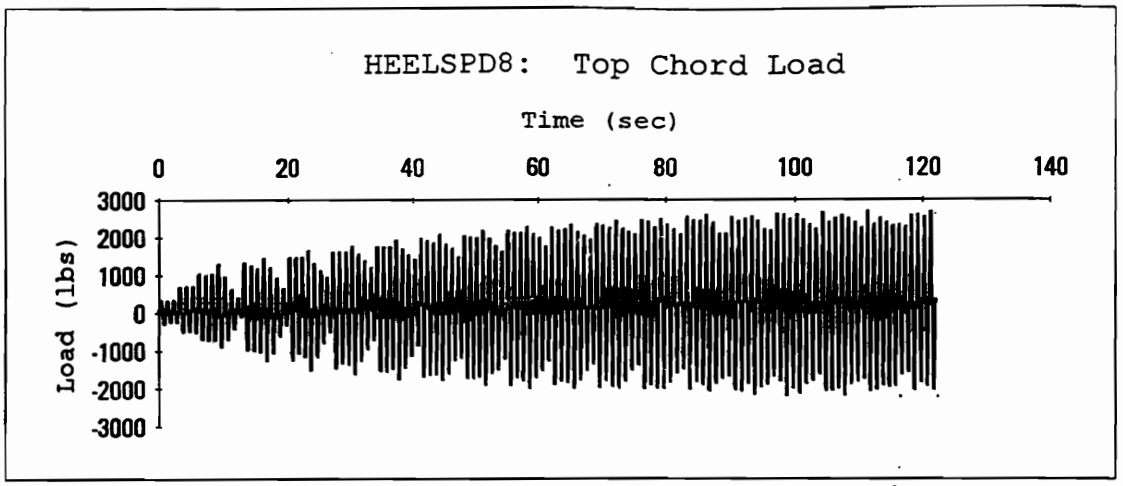
HEELSPD8: Top Chord Load
Time (sec)
0
20
40
60
80
100
120
140
Load (lbs)
3000
2000
1000
0
-1000
-2000
-3000

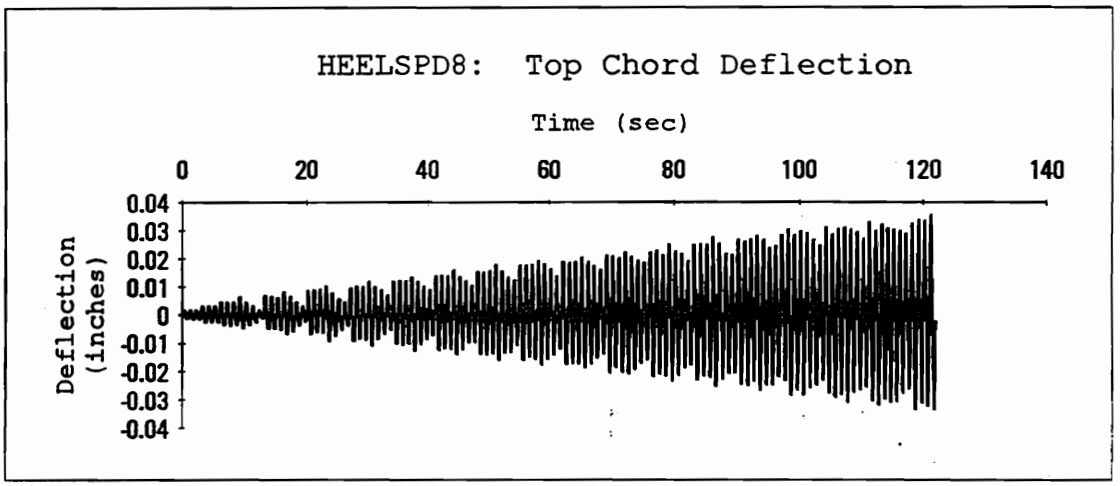
HEELSPD8: Top Chord Deflection
Time (sec)
0
20
40
60
80
100
120
140
Deflection (inches)
0.04
0.03
0.02
0.01
0
-0.01
-0.02
-0.03
-0.04

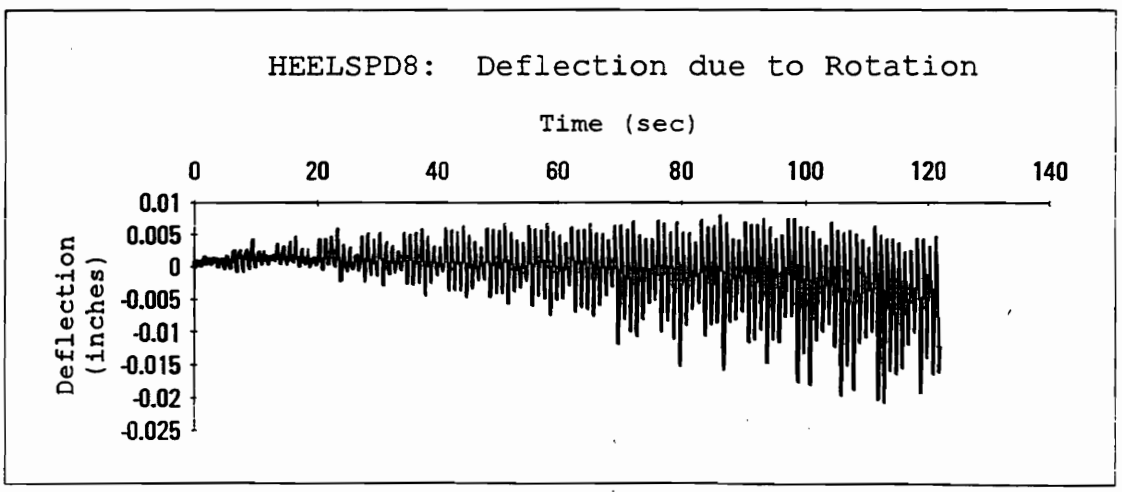
HEELSPD8: Deflection due to Rotation
Time (sec)
0
20
40
60
80
100
120
140
Deflection (inches)
0.01
0.005
0
-0.005
-0.01
-0.015
-0.02
-0.025

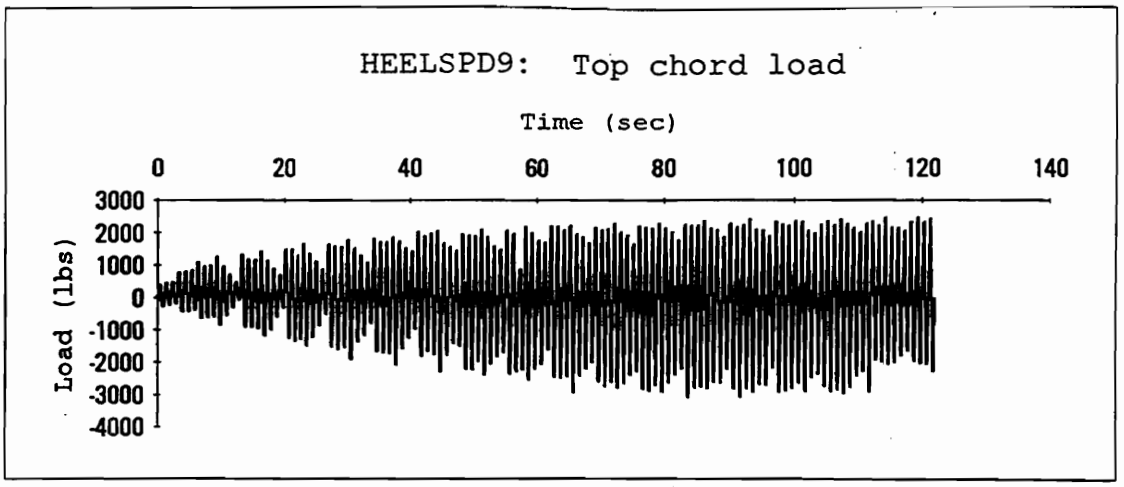
HEELSPD9: Top chord load
Time (sec)
0
20
40
60
80
100
120
140
Load (lbs)
3000
2000
1000
0
-1000
-2000
-3000
-4000

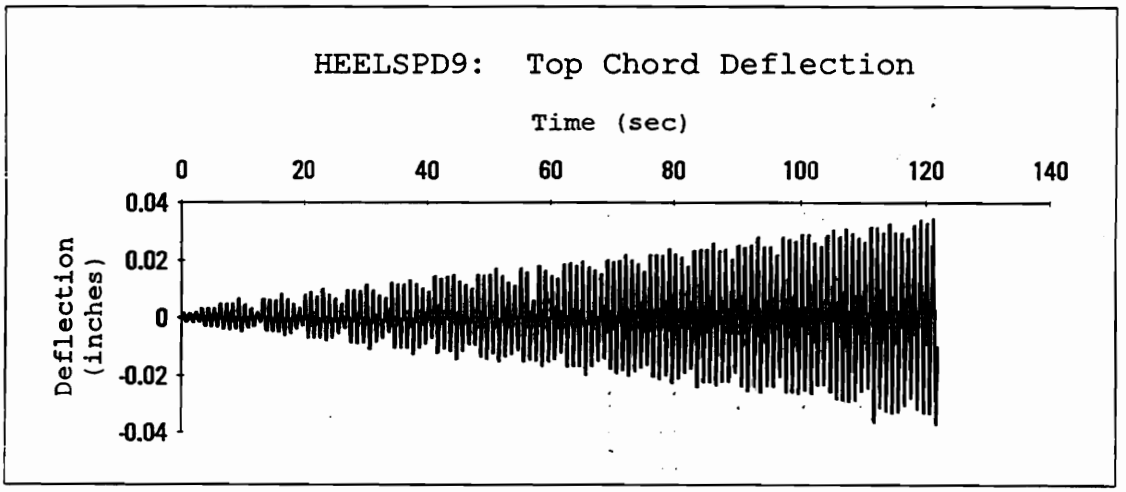
HEELSPD9: Top Chord Deflection
Time (sec)
0
20
40
60
80
100
120
140
Deflection (inches)
0.04
0.02
0
-0.02
-0.04

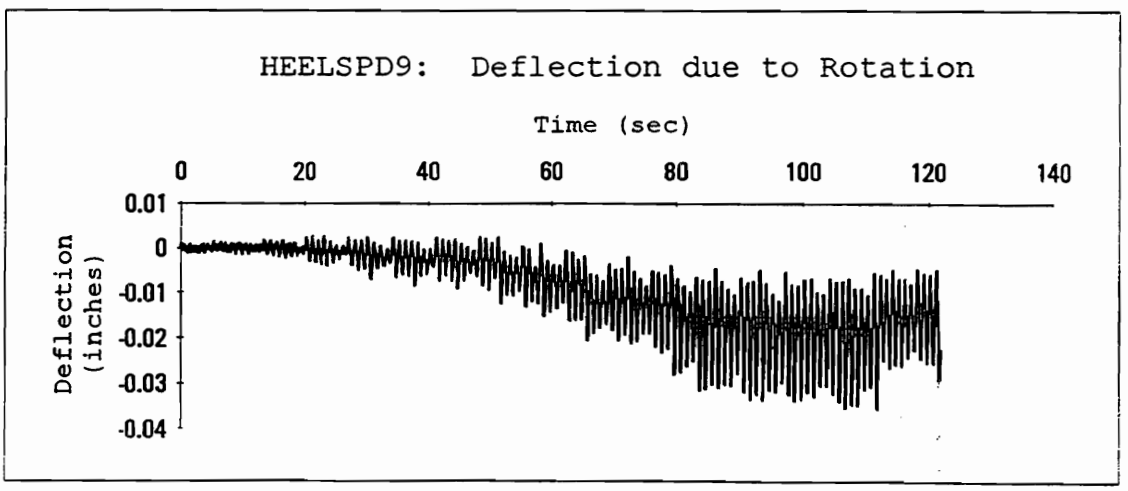
HEELSPD9: Deflection due to Rotation
Time (sec)
0
20
40
60
80
100
120
140
Deflection (inches)
0.01
0
-0.01
-0.02
-0.03
-0.04

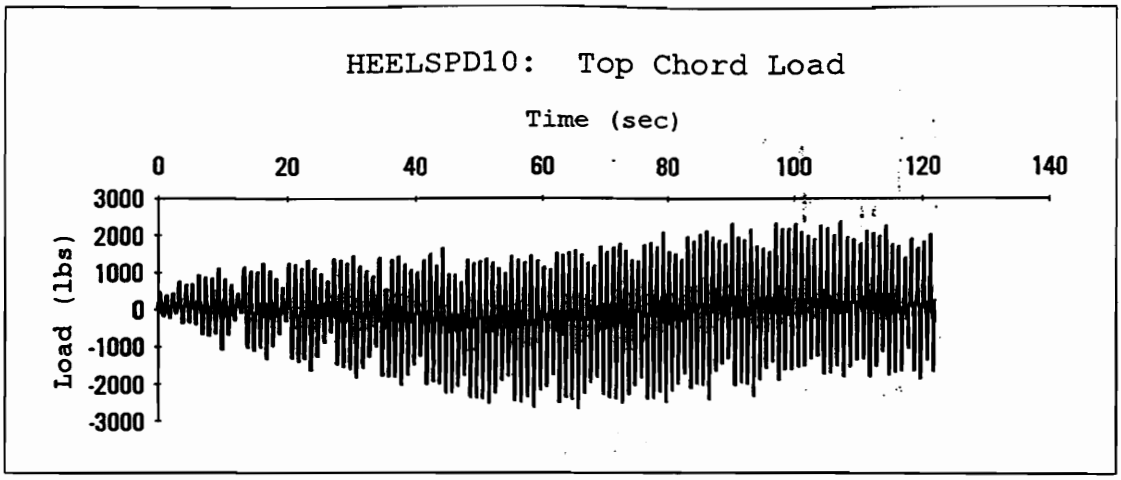
HEELSPD10: Top Chord Load
Time (sec)
0
20
40
60
80
100
120
140
Load (lbs)
3000
2000
1000
0
-1000
-2000
-3000

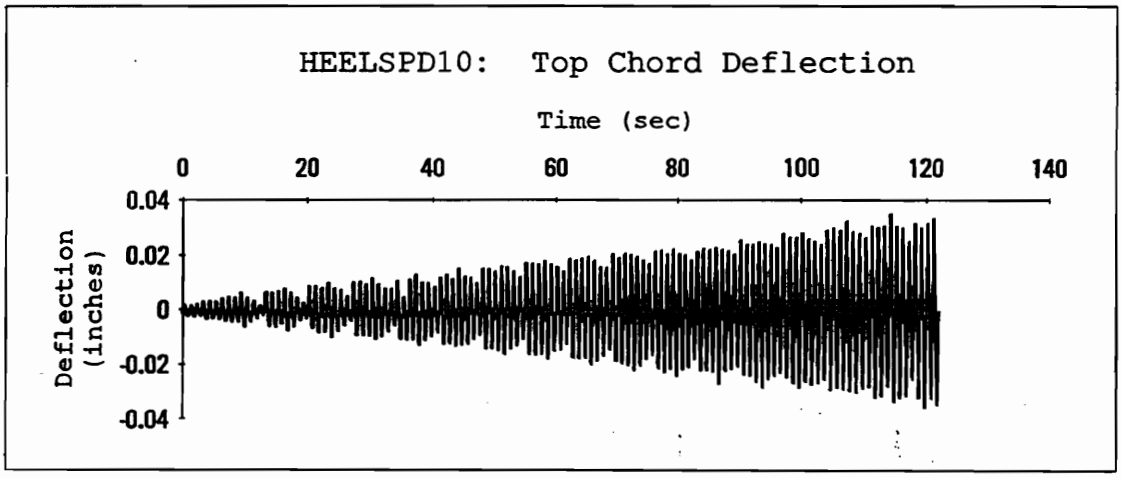
HEELSPD10: Top Chord Deflection
Time (sec)
0
20
40
60
80
100
120
140
Deflection (inches)
0.04
0.02
0
-0.02
-0.04

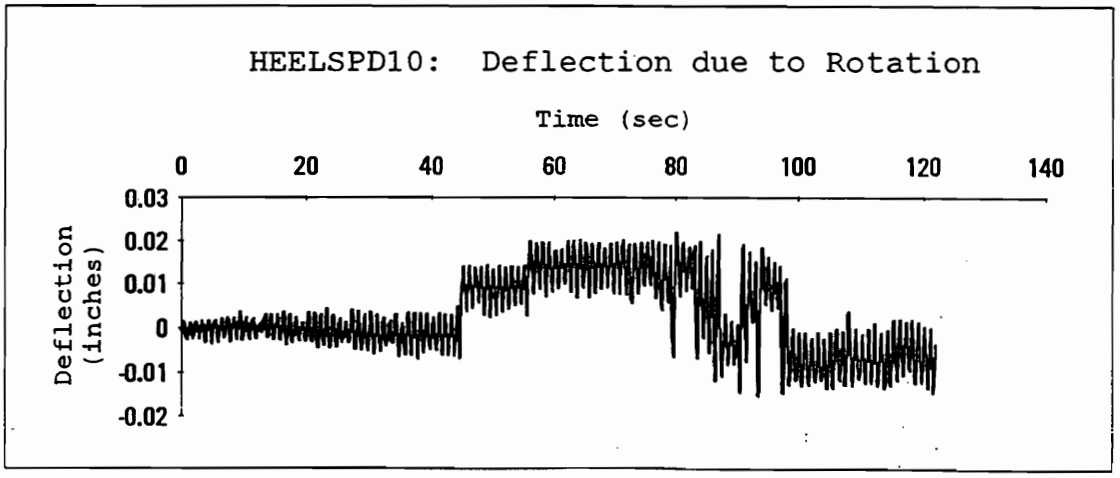
HEELSPD10: Deflection due to Rotation
Time (sec)
0
20
40
60
80
100
120
140
Deflection (inches)
0.03
0.02
0.01
0
-0.01
-0.02

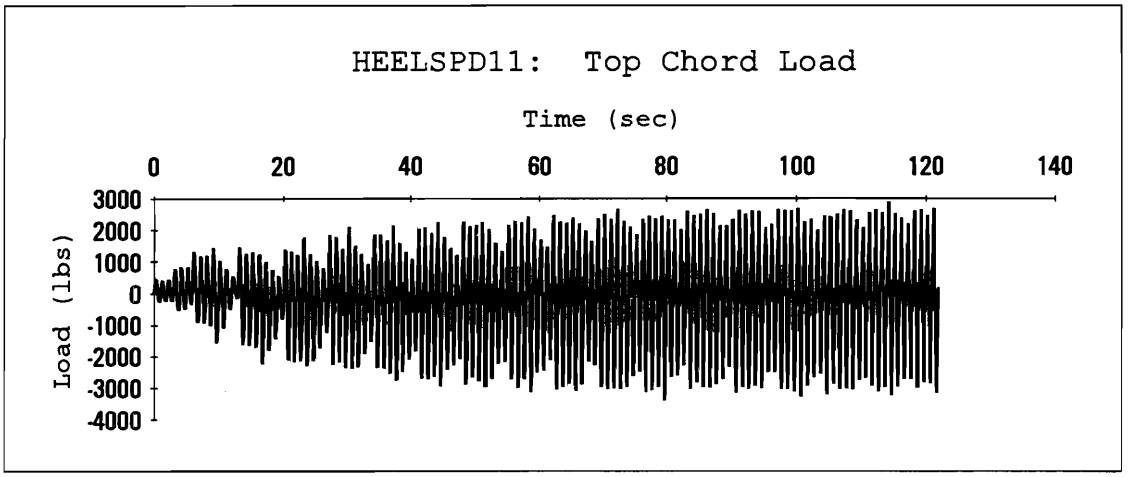
HEELSPD11: Top Chord Load
Time (sec)
0
20
40
60
80
100
120
140
Load (lbs)
3000
2000
1000
0
-1000
-2000
-3000
-4000

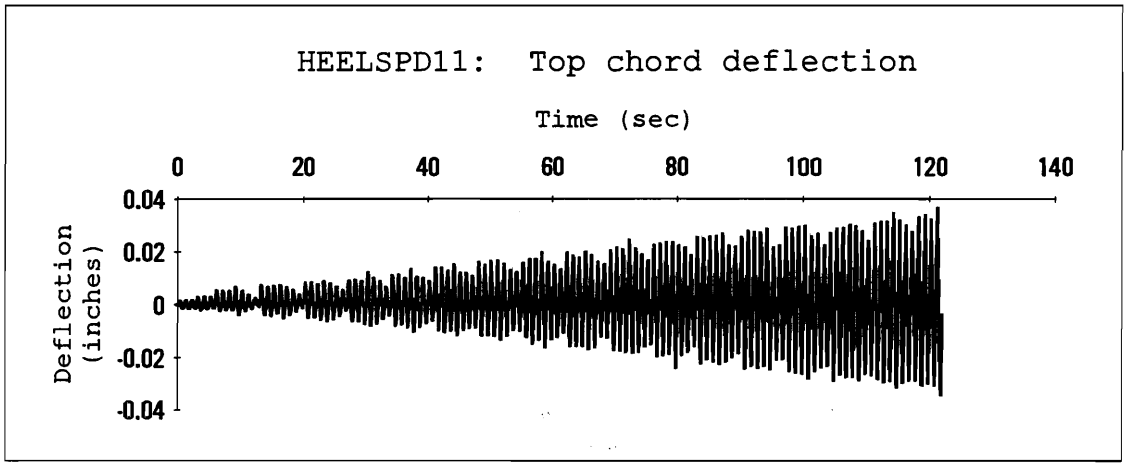
HEELSPD11: Top chord deflection
Time (sec)
0
20
40
60
80
100
120
140
Deflection (inches)
0.04
0.02
0
-0.02
-0.04

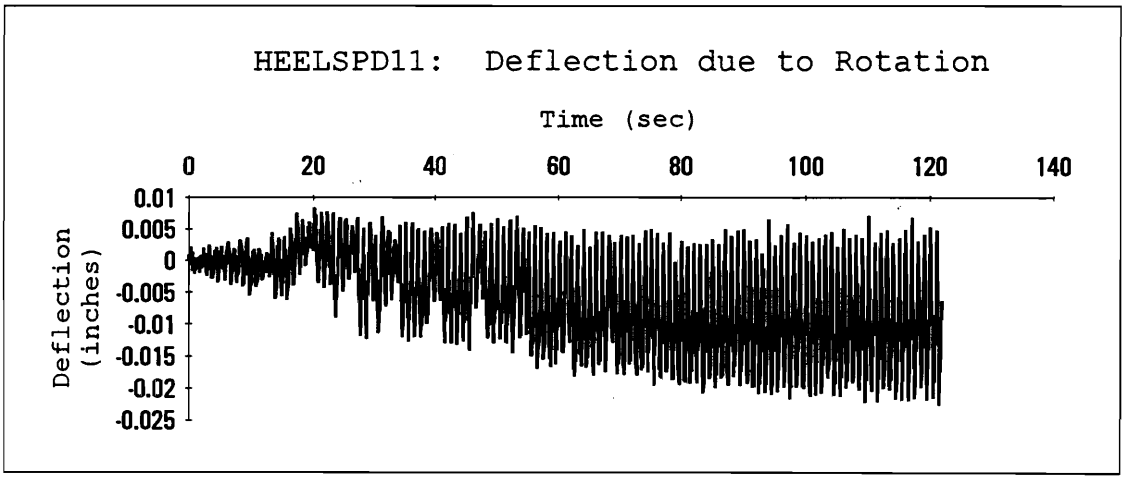
HEELSPD11: Deflection due to Rotation
Time (sec)
0
20
40
60
80
100
120
140
Deflection (inches)
0.01
0.005
0
-0.005
-0.01
-0.015
-0.02
-0.025